HETEROGENEOUS NUCLEAR RIBONUCLEOPROTEIN A2/B1 REGULATES THE ABUNDANCE OF THE COPPER-TRANSPORTER ATP7A, AND ITS LOCALIZATION DEPENDS ON CELLULAR COPPER LEVELS

by
Courtney McCann

A dissertation submitted to Johns Hopkins University in conformity with the requirements for the degree of Doctor of Philosophy

Baltimore, Maryland

November 2021

Abstract

Copper (Cu) is an essential micronutrient that plays roles in mammalian growth and development. Imbalance of Cu is implicated in several human diseases; thus, cellular Cu levels are tightly regulated by Cu-binding and -transporting proteins that act in concert. While the main Cu homeostasis proteins and their post-translational regulation have been well-characterized, their regulation at the mRNA-level is incompletely understood. Heterogeneous nuclear ribonucleoprotein (hnRNP) A2/B1, an RNA-binding protein, was found to regulate Cu levels: its knockdown via small interfering RNA (siRNA) induced a significant decrease in cellular Cu. In this study, we investigated this phenomenon and found that the knockdown of hnRNP A2/B1 decreased Cu levels through increasing the abundance of the Cu-transporter ATP7A, likely through a mechanism involving the 3' untranslated region (UTR) of the ATP7A transcript. Moreover, downregulation of just the exon 2-containing B-isoforms of hnRNP A2/B1 was sufficient to produce this effect, indicating that they may play a specific role in Cu regulation. This link between hnRNP A2/B1 and ATP7A was found to be true in reverse: increasing the expression of individual hnRNP A2/B1 isoforms lead to a decrease in ATP7A abundance, further suggesting that ATP7A expression is negatively regulated by hnRNP A2/B1. An increase in ATP7A abundance and decrease in hnRNP A2/B1 abundance and Cu levels was also observed in SH-SY5Y neuronal cells during retinoic acid-induced differentiation, highlighting an inverse relationship between hnRNP A2/B1 and ATP7A abundance that may play a role during neuronal differentiation. We also explored the effects of Cu accumulation on hnRNP A2/B1 and found that Cu elevation results in a rapid, dose-dependent increase in the amount of cytoplasmic hnRNP A2/B1. Interestingly, cytoplasmic hnRNP A2/B1 clustered into granules that did not stain for markers of common cytoplasmic granules, suggesting that they form as a unique response to Cu elevation. It is yet unclear whether the Cu-induced cytoplasmic accumulation of hnRNP A2/B1 is related to the hnRNP A2/B1-mediated regulation of ATP7A. However, our data show that there is

a link between Cu homeostasis and RNA processing via hnRNP A2/B1 that could potentially be involved in a rapid and specific response to changing Cu levels.

Primary Reader and Advisor: Dr. Svetlana Lutsenko

Secondary Reader: Dr. Dax Fu

Acknowledgements

I would like to extend my sincerest thanks to my advisor, Dr. Svetlana Lutsenko, for supporting me these past seven years as I've completed my PhD research. Under her mentorship, I learned what it is to be a research scientist and to hold myself to rigorous scientific standards. She always encouraged me to ask questions and assisted me in my pursuit of answers. In Dr. Lutsenko's lab, I was given the opportunity to work alongside many incredible scientists, and those experiences allowed me to develop my own skills and grow not only as a research scientist, but also as a person. For her guidance, motivation, and support I will always be grateful.

I would also like to express my gratitude to Drs. Dax Fu, Valeria Culotta, and Jiou Wang for serving on my thesis committee. Their combined expertise enriched my studies and allowed me to approach my research from new perspectives I wouldn't have considered on my own. I would also like to extend additional thanks to Dr. Fu, who has supported my research and career in so many ways and whose lab was the first I rotated in when I started my graduate studies, helping make Johns Hopkins feel like home even at that early junction.

Over the years I have had the privilege of working with many amazing people to whom I owe a debt of gratitude for the myriad ways in which they've supported me and my work. I would like to thank my lab mates, past and present, from the bottom of my heart: Dr. Hannah Pierson, Dr. Abigael Muchenditsi, Alex Zak, Ekaterina Kabin, Dr. Samuel Jayakanthan, Dr. Haojun Yang, Dr. Katharina Schmidt, Xuechun Zhang, Dr. Shubhrajit Roy, Dr. Aline Gottlieb, Dr. Dawn Hayward, Masha Osipova, Dr. Nan Yang, Dr. Som Dev, Dr. Clorissa Washington-Hughes, Dr. Li Wang, Dr. Yu Wang, Dr. Jenifer Calvo, Dr. Kelly Summers, and Dr. Benjamin Devenney. I would also like to thank Dr. Nesrin Hasan in particular for her initial experiments on hnRNP A2/B1 that paved the way for the studies in my thesis.

I am deeply grateful for the support of my long-time friend and mentor, Dr. Teresita Padilla-Benavides. She encouraged my interest in research—and in Cu homeostasis in particular—and was the biggest supporter of my decision to pursue a PhD. I am excited to be able to work with her once again as a postdoctoral researcher.

Finally, I would like to give all of my thanks and love to my friends and family. To my parents, Deb Bevilacqua Ela, Kevin McCann, Jeremy Ela, and Jasmin McCann, and my sisters, Taylor McCann, Mia McCann, and Lori Yanni, who have shown me nothing but love and support as I've worked towards my personal and professional goals. To my friends—especially Tony Cavalieri, Leto Lynch, Kristen Shannon, and Samantha Jiminez—who have always been there for me, through every up and down. And to my partner, Chris Caporaso, whose support and encouragement have meant the world to me, and without whom I wouldn't be the person I am today.

Table of Contents

List of Tables

List of Figures

1 Introduction

Copper (Cu) is a trace metal crucial to mammalian growth and development. Due to its redox activity, Cu serves as a cofactor and activator of a variety of enzymes involved in key cellular processes, such as respiration, antioxidant defense, iron utilization, myelination, and neurotransmitter production (1-5). Because of its essentiality, as well as its toxicity in excess, cellular Cu balance must be maintained, and imbalance of Cu is implicated in several human diseases (6,7). As such, Cu levels are tightly regulated through a network of Cu-binding and Cu-transporting proteins (8). While post-translational regulation of Cu homeostasis is well-understood, comparatively little has yet been described about the mechanisms by which Cu homeostasis is regulated on the mRNA-level. This work discusses the importance of regulating Cu balance, describes the protein machinery that act in concert to maintain Cu levels, and considers a new role for heterogeneous nuclear ribonucleoprotein (hnRNP) A2/B1 in the regulation of Cu transporters at the messenger RNA (mRNA) level.

1.1 Cu in human health and disease

Cu is an essential micronutrient. Humans get Cu in their diets, and a daily dietary intake of 0.9 mg/day is recommended for adults (9). Failure to meet Cu intake needs is linked to poor health outcomes: studies in rodents linked dietary Cu deficiency to hepatic steatosis and insulin resistance (10,11). Cu imbalance is also linked to human diseases, with Menkes and Wilson diseases being the classical examples of Cu deficiency and excess, respectively (12). However, even milder perturbations in Cu balance have been associated with pathologies. Changes in Cu homeostasis have been observed in patients with cancer, Alzheimer's disease, Parkinson's disease, and non-alcoholic fatty liver disease (6,7,13). Thus, to maintain normal human physiology, cellular Cu levels are kept under close control through a system of proteins that

manage the journey of Cu through the cell, from influx to storage and transport to efflux (**Figure 1.1**).

1.1.1 Cu importers

The current model of Cu homeostasis describes the import of Cu via Ctr1, a high-affinity Cu transporter (8,12,14,15). In humans, Ctr1 is responsible for the uptake of dietary Cu, wherein the Cu is distributed to proteins involved in Cu trafficking in the cell (12,16,17). Ctr1 consists of monomers with three transmembrane domains that assemble into a homotrimer to form a pore through which Cu passes into the cell (1,14,18-22). Under basal conditions, Ctr1 largely localizes to the plasma membrane, with a smaller amount present in cytoplasmic vesicles. When Cu levels are low, Ctr1 mobilizes from these pools to the plasma membrane, where it facilitates the import of Cu; when Cu levels are high, Ctr1 internalizes via endocytosis and localizes once again to these vesicles, eventually degrading if Cu concentrations are sufficiently high (1,4,19,23,24).

Ctr1 function is essential to normal mammalian development and physiology. While there is no specific disease attributed to loss of Ctr1 function or expression, inactivation of Ctr1 results in severe physiological consequences. Whole body *Ctr1* knockout mice have impaired growth and developmental defects *in embryo*, which eventually result in embryonic death (14,16,17,25). Organ-specific knockout mice present with various perturbations in Cu balance (17). Heart-specific deletion of *Ctr1* results in cardiac pathologies arising from Cu deficiency, while liver-specific deletion results in a significant decrease in hepatic Cu but no marked changes in liver function (26-28). Intestinal inactivation of *Ctr1* does not prevent Cu import into enterocytes; instead, it reduces the availability of Cu to other Cu machinery proteins, resulting in intestinal accumulation of Cu and subsequent systemic Cu deficiency (8,27).

Humans also express a second Cu-uptake transporter, Ctr2 (4,15). Comparatively less is known about Ctr2 function. It was previously thought that Ctr2 could serve as a lower-affinity Cu importer in lieu of Ctr1, though perhaps in a less bioavailable state (27,29). This was supported by the observation of partial localization of overexpressed Ctr2 to the plasma membrane (4,30). However, more recent studies indicate that Ctr2 largely localizes to intracellular vesicles and co-localizes with markers of late endosomes and lysosomes, suggesting a role for Ctr2 in the mobilization of Cu stored in these organelles (1,4,14,29,31).

The physiological impact of *Ctr2* inactivation in mammals is not well-understood. Deletion in yeast yields cells with higher Cu tolerance, and yeast lacking Ctr1 but overexpressing Ctr2 are less affected by Cu depletion (30,32). In COS-7 cells, overexpression of Ctr2 results in massive intracellular Cu accumulation, whereas depletion of Ctr2 results in a decrease in cellular Cu content (14,30). Interestingly, Ctr2 expression has been linked to cisplatin resistance, which could result in poorer cancer prognoses (14,33).

1.1.2 Cu-chaperones and Cu-binding proteins

Cu in its unbound form, known as free Cu, is toxic to the cell if allowed to accumulate. Free Cu can trigger the formation of hydroxyl radicals, causing oxidative damage in the cell, and can compete with other metal cofactors in binding metalloenzymes (1,34-36). Thus, once inside the cell, Cu must be bound by either Cu-chaperones, which mediate its transfer to or incorporation into other proteins, or Cu-binding proteins, which sequester excess Cu in the cell (4,37).

1.1.2.1 Cu-chaperones

Atox1 is a soluble cytosolic protein whose main known function is as a Cu-chaperone (4,38). It is involved in the delivery of imported Cu to the secretory pathway via direct interaction with and subsequent transfer of Cu to the Cu-transporters ATP7A and ATP7B (4,38-42). This process is

key to the maturation of enzymes that require Cu as a cofactor for their activity (38). While Atox1 may receive Cu directly from Ctr1 *in vitro* (4), downregulation of Atox1 does not affect Cu entry into the cell, suggesting that it is not the main—or not the only—way in which Cu transfers from Ctr1 to its end locations (38). Interestingly, Atox1 has also been identified as a Cu-dependent transcription factor, and has been shown to translocate into the nucleus to perform this role (4,43).

Atox1 plays an important role in Cu trafficking during development in newborn mice (17,43,44). Knockout of *Atox1* in mouse embryonic fibroblasts results in the accumulation of Cu in the cytosol, and whole-body deletion of *Atox1* in mice impedes Cu transport across the placenta (38,44). This impacts the activity of key cuproenzymes, such as cytochrome *c* oxidase (CCO), and ultimately results in mice that have growth impairments and skin defects and fail to thrive, which may lead to death (17,43,44).

The Cu chaperone for superoxide dismutase 1 (CCS) is a cytosolic protein involved in the maturation of the cuproenzyme Cu, Zn superoxide dismutase 1 (SOD1) (37,45). CCS directly interacts with SOD1 to coordinate the incorporation of Cu as well as facilitate the formation of a disulfide bond in SOD1 crucial for its activity (38,46). CCS has also been implicated in the regulation of the intracellular localization of SOD1 (4,45).

CCS expression is required for the maturation of SOD1, ensuring its proper function and activity. Inactivation of the *CCS* gene in mice results in normal expression of SOD1 but impaired SOD1 activity due to the markedly reduced incorporation of Cu into SOD1 (47,48). As such, these mice present similarly to SOD1 knockout mice (47). Crossbreeding between *CCS* knockout mice and mouse models of familial amyotrophic lateral sclerosis (ALS) bearing disease-linked SOD1 mutations show that *CCS* deletion does not prevent the development of disease (47-49). However, *CCS* inactivation results in increased motor neuron death in mice, though it doesn’t impact disease onset (49).

At least four Cu-chaperones deliver Cu to the mitochondria and facilitate Cu inclusion into CCO: Cox17, Cox11, Sco1, and Sco2 (4,37,50). Cox17, Cox11, and Sco1 are thought to form a Cu relay to CCO, with the soluble Cox17 delivering Cu to the inner mitochondrial membrane proteins, Sco1 and Cox11, which go on to participate in the transfer of Cu into the two binding sites in CCO: Cu_A in the Cox2 subunit and Cu_B, in the Cox1 subunit, respectively (1,37,50-54). Cox17, which can shuttle between the cytosol and the mitochondrial intermembrane space, also supplies Cu to the inner mitochondrial membrane protein Sco2, which functions in the biogenesis of the Cu_A Cu-binding site and oxidizes Cu-coordinating Cys residues in Sco1 (55-57).

Loss of function of any of these four mitochondrial Cu chaperones negatively impacts CCO assembly and activity. Deletion of *Cox17* in mice results in severely impaired CCO activity and is embryonic lethal (17,58). RNA interference-mediated knockdown of *Cox11* in HEK293 cells causes a decrease in both CCO assembly and activity (59), and Cox11 is one of several proteins involved in Cu homeostasis upregulated in colorectal cancer (60). Mutations in both Sco1 and Sco2 are associated with decreased Cu content and CCO activity, leading to hypertrophic cardiomyopathy, encephalopathy, and liver failure. (17,61-66).

1.1.2.2 Cu-binding proteins

SOD1, the cuproenzyme to which CCS delivers Cu, is a dismutase that catalyzes the conversion of superoxide radicals formed during cellular respiration into oxygen and hydrogen peroxide, neutralizing their toxic effects (67-69). The mature enzyme is a homodimer consisting of two hydrophobically-linked subunits that each contain a disulfide bond, as well as a Cu and a zinc (Zn) ion that are key for enzymatic activity (68,70-75). SOD1 receives the majority of its Cu cofactor from CCS, which transfers Cu through direct protein-protein interaction, and this interaction is also responsible for the formation of the key disulfide bond in each of the monomers (38,68).

Mutations in SOD1 have long been recognized as causative factors in the development of familial ALS (76,77). Up to 25% of all cases of hereditary ALS can be linked to SOD1 mutations—roughly 2% of all diagnosed cases (2,78,79). Expression of ALS-associated SOD1 mutants in mice results in decreased SOD1 protein stability, reduced Zn-binding affinity, and, with the expression of some mutants, significantly decreased SOD1 activity (80,81). These mice present with symptoms of motor neuron disease, such as muscular atrophy and weakness and motor neuron death (79,82-84). Moreover, ALS-associated SOD1 mutations result in the formation of cytoplasmic aggregates of misfolded SOD1 protein, and these aggregates are associated with cellular toxicity independent from SOD1 loss of activity (84-87). While these effects were not ameliorated by expression of wild type (WT) SOD1, CRISPR-mediated deletion of mutant *SOD1* in mice partially alleviates the toxic effects, indicating the presence of mutant SOD1 and not simply loss of SOD1 activity induces disease (79,85).

Metallothioneins (MTs) are small, Cys-rich proteins that bind metals such as Cu, Zn, and cadmium (Cd) with high affinity (88-90). Due to this property, their main function in cells is to serve as regulators of intracellular metal availability and to protect against oxidative stress. As such, MTs play a key role in sequestering Cu to prevent the accumulation of free Cu in the cytosol (38,88,91-93). Mammals express four isoforms in a tissue-specific manner: MT-1, MT-2, MT-3, and MT-4 (88,91). MT-1 and MT-2 are ubiquitously expressed, and they respond to increases in cellular metal concentrations. In the case of Cu, MT-1 and MT-2 regulate the pool of Cu available for transport by the Cu-transporter ATP7A, described below (36,89,91,94). MT-3 is expressed mainly in the brain, and acts as a growth inhibitory factor in neurons (89,91,94,95). While the function of MT-4 in mammals is poorly understood, it is known to be largely expressed in stratified epithelial tissue (89,91,94).

Aberrations in the expression and function of MTs is associated with several diseases. Mice with deletions of *MT-1* and *MT-2* show normal growth but have lower Zn levels and are highly sensitive

to Cd toxicity (90). Crossbreeding mice in which *MT-1* and *MT-2* have been deleted with Cu-deficient mice lacking *ATP7A* results in embryonic lethality (17,96,97). Moreover, polymorphisms in the *MT-1* and *MT-2* genes are linked to type 2 diabetes risk (98). Though mice with *MT-3* deletion do not present with any neuropathy (99,100), MT-3 expression is decreased in the brains of patients with Alzheimer's disease, Creutzfeldt-Jakob disease, Parkinson's disease and Down's syndrome (101,102).

1.1.3 Cu exporters

Central to Cu metabolism in humans are the Cu-exporters, the ATPases ATP7A and ATP7B. These proteins receive Cu from the cytosolic chaperone Atox1 and transport it across membranes using the energy released during ATP hydrolysis. This activity facilitates the transport of Cu into the secretory pathway, wherein it is incorporated into various cuproenzymes, or the efflux of Cu from the cell when Cu concentrations exceed cellular needs (4,8). This dual function is enabled by Cu-responsive trafficking of ATP7A and ATP7B. Under basal and low Cu conditions, ATP7A and ATP7B are localized to the *trans*-Golgi network (TGN), where they pump Cu into the lumen of the TGN to be incorporated into Cu-dependent enzymes; under high Cu conditions, ATP7A and ATP7B traffic into vesicles and translocate to the plasma membrane, where they excrete Cu from the cell (7,8,37,103,104).

ATP7A is ubiquitously expressed in tissues, and it is involved in the dietary uptake of Cu and the activation of Cu-dependent enzymes within the secretory pathway (24,105). In mammals, ATP7A is responsible for transporting Cu across the basolateral membrane of intestinal enterocytes so that Cu can enter portal circulation and ultimately make its way to other organs (7,12,103,106,107). ATP7A also plays a key role in the transport of Cu across the blood-brain barrier and the placenta (12).

Mutations that impact the activity and expression of ATP7A are detrimental to human health. Inactivation of ATP7A is associated with Menkes disease, while milder mutations in ATP7A result in occipital horn syndrome or motor neuropathy (7). In Menkes disease, failure of Cu to enter into the circulation from the intestine results in systemic Cu deficiency (7,8,12). On a cellular level, Cu deficiency causes reductions in the activities of Cu-dependent enzymes, defects in collagen synthesis, inhibition of mitochondrial function, diminished cellular antioxidant defense, and impaired lipid metabolism (11,108-111). As a result, Menkes patients present with impaired growth, seizures, skeletal and neurological defects, and connective tissue disorders, and the disease often leads to childhood mortality (12,37,112-115).

Cu deficiency is also linked to metabolic disorders. Rodents fed a high fat diet develop hepatic Cu deficiency, even if their livers had elevated Cu levels prior to high-fat feeding, and a Cu-deficient diet alone is sufficient to cause non-alcoholic fatty liver disease (NAFLD)-like hepatic steatosis and lipid accumulation in mice (10,11,116-118). Studies in humans have repeatedly found that NAFLD patients have lower hepatic Cu levels compared to healthy controls (10).

ATP7B has a more tissue-specific expression pattern than ATP7A, with the highest level of expression occurring in the liver and more modest levels of expression in the brain, kidney, heart, and placenta (104,119,120). In mammalian hepatocytes, ATP7B facilitates the incorporation of Cu into ceruloplasmin, the main Cu-containing protein the blood, as well as the excretion of excess Cu into the bile (12,119). When cellular Cu levels increase, ATP7B traffics from the TGN to vesicles that cluster and pool in the cytoplasm until the Cu concentration reaches a threshold at which vesicles fuse with the apical membrane to release excess Cu into the bile for subsequent excretion from the body (37,104,112,119,121-126).

Inactivating mutations in ATP7B lead to the development of Wilson disease, in which there is Cu accumulation in the liver (112,123,126). Loss of ATP7B function results in impaired Cu excretion,

increased hepatic and neuronal Cu concentrations, reduced loading of Cu into ceruloplasmin, increased levels of free Cu in the blood serum, and changes in nuclear size (5,12,127,128). These disruptions in Cu balance lead to the development of liver disease, which may progress to liver failure; neurological problems, such as ataxia; and behavioral and mood disorders (12,37,114,129). Mouse models of Wilson disease with whole-body *ATP7B* deletion present with hepatic Cu accumulation and liver dysfunction and inflammation, while mice with hepatocyte-specific deletion of *ATP7B* present with hepatic Cu accumulation but lack liver dysfunction and inflammation, instead developing mild obesity and hepatic steatosis (130,131). Moreover, certain single nucleotide polymorphisms in ATP7B that alter the cellular properties of the protein are enriched in patients with AD (119).

While mammalian cells have an incredible capacity to buffer and compensate for changes in Cu concentrations, perturbations in Cu balance can have significant, far-reaching effects. As such, it is essential that proteins involved in maintaining Cu homeostasis are tightly regulated in order to respond to changes in cellular Cu status.

1.2 Regulation of Cu homeostasis

It is well-established that Cu regulates its own homeostasis in cells, with changes in cellular Cu levels modulating the expression and trafficking of Cu-responsive proteins in order to maintain Cu balance (4,125). Cu-dependent regulation of these proteins occurs on three levels: (i) transcriptionally, at the DNA-level; (ii) post-transcriptionally, at the RNA-level; and (iii) post-translationally, at the protein-level. The method of regulation and the extent to which it occurs varies depending on such factors as cell-type, stage of development, and cell cycle (4,132-134).

1.2.1 Transcriptional regulation

Much of what is known about the transcriptional regulation of Cu homeostasis has been established in yeast, which express many homologs of mammalian Cu homeostatic machinery proteins (135). By comparison, and contrary to what one might expect, changes in intracellular Cu levels do not appear to significantly change the expression of most Cu homeostasis genes at the transcription-level in mammals (17,135). However, transcriptional regulation of Cu machinery has been described, and some transcription factors (TFs) involved in this regulation have been identified.

Perhaps the best characterized TF involved in Cu regulation is metal-responsive transcription factor-1 (MTF-1) (12,37). MTF-1 is a Zn finger protein that is highly conserved in eukaryotes, and it is activated by the accumulation of heavy metals, including Cu, which MTF-1 has been shown to bind (136,137). Once activated, MTF-1 translocates from the cytoplasm to the nucleus where it binds genes containing a metal response element (MRE) and promotes their transcription (37,137-142).

The TF specificity protein 1 (Sp1) plays a role in regulation of Cu homeostasis through modulating both Cu import and cellular response to intracellular Cu elevation (4,15,143,144). Sp1 mediates transcriptional regulation via binding target promoters and recruiting transcriptional machinery (145). Like MTF-1, Sp1 is a Zn finger protein that is able to bind, and therefore “sense”, Cu in the cell and respond to changes in Cu levels accordingly (15,146). Interestingly, Sp1 is itself regulated by Cu concentration—it binds to its own promoter and upregulates or downregulates transcription in response to high and low Cu levels, respectively (147).

In addition to its role as a Cu-chaperone, Atox1 has also been identified as a Cu-dependent TF (38,43). While it appears that Atox1 does not regulate the transcription of known Cu machinery

genes, Cu triggers the activation of Atox1 as a TF (43,148). Atox1 contains a putative nuclear localization signal at its C-terminus and has been observed to translocate to the nucleus in response to changes in Cu levels (43).

The import of Cu into the cell is largely mediated by Ctr1. Ctr1 expression is generally unaffected by changes in cellular Cu levels—with the exception of one study showing that Ctr1 mRNA and protein expression were increased in the intestines of rat pups on a high Cu diet (149,150). However, transcriptional induction of Ctr1 does occur under different stimuli (135,151-153). Placental cells stimulated with estrogen and progesterone showed an increase in Ctr1 expression, indicating its transcription is susceptible to hormonal signaling (151). Ctr1 expression levels were also shown to increase under hypoxic conditions, mediated by the hypoxia-inducible factor 2α (HIF-2α) TF (154,155). Basal-level maintenance of Ctr1 levels is thought to be largely controlled by Sp1, which has been identified as a positive regulator of *Ctr1* transcription under normal Cu conditions (8,15,156).

SOD1 transcription is regulated by a number of different TFs, some of which work in concert. Like Ctr1, SOD1 expression is regulated by Sp1, which binds to the *SOD1* promoter in a GC-rich region to activate transcription (69,157-159). CCAAT/enhancer-binding protein (C/EBP) α and β both bind *SOD1* at the CCAAT box in its proximal promoter to activate the basal transcription of SOD1 (69,157), and early growth response-1 (Egr1) binds *SOD1* at a noncanonical consensus sequence in response to a variety of cellular stimuli to induce SOD1 transcription in response (157,159-161). Activator protein-1 (AP-1), by contrast, does not directly bind the *SOD1* gene, instead exerting transcriptional control via binding and sequestering other TFs, such as Sp1, and preventing them from acting on *SOD1* (157,158).

MT transcription is directly induced by elevated Cu (and other heavy metals) via the Cu-induced binding of MTF-1 at their MREs (36,138,162). Of the four MTs, *MT-1* and *MT-2* are most

susceptible to heavy metal-induced transcriptional control, while transcription of *MT-3* and *MT-4* appear to largely be regulated by alternative factors (163). *MT-1*, *MT-2*, and *MT-3* all possess at least one MRE to which MTF-1 binds (164-166), facilitating the MTF-1-mediated activation of transcription in response to increases in cellular Cu levels (12), and *MT-2* and *MT-3* both contain binding sites for Sp1 (164-166). MREs also facilitate the basal transcription of MTs in the absence of extra- or intracellular stimuli (162,167).

As of yet, there exists virtually no evidence that either of the Cu-exporters, ATP7A and ATP7B, are directly transcriptionally regulated by Cu in mammals (111,135). The sole incidence of Cu-mediated regulation was reported by Bauerly, et al., wherein they observed a minor increase in ATP7A expression in the intestines of rat pups on a high Cu diet (149), though other studies reported no change in ATP7A expression under similar conditions (135,150,168). Basal-levels of transcription for *ATP7A* are regulated by TAp73, an isoform of the p73 TF that modulates the expression of genes in response to cellular stress in order to maintain homeostasis (169-172). *ATP7A* expression is modulated by changes in cellular iron (Fe), with an increase in expression observed in the intestines of Fe-deficient rats (173,174), and upregulation of *ATP7A* transcription occurs concurrently with Fe homeostasis genes under hypoxic conditions, mediated by the TFs HIF-2α and Sp1 (154,175,176). Hormone and hormone-like signaling can also impact transcription levels, with *ATP7A* expression upregulated by retinoic acid (RA) (177) and both *ATP7A* and *ATP7B* expression upregulated by estrogen and insulin (151,178). While MTF-1 doesn't regulate either ATP7A or ATP7B on the transcriptional-level in response to Cu, it does enhance basal-level transcription of *ATP7B* via binding an MRE in its promoter region (179).

Though there are many conditions and stimuli that induce the transcription of genes involved in Cu homeostasis, very few of these genes are transcriptionally regulated in response to cellular Cu levels. The majority of Cu-driven regulation of the Cu machinery takes place post-

translationally through factors that modulate protein stability, activity, and trafficking (105,135,151,180-182).

1.2.2 Post-translational regulation

The post-translational regulation of proteins involved in Cu homeostasis in eukaryotes is well-characterized (20,37,104,183,184). Cu levels directly or indirectly influence Cu handling proteins by impacting their activity, stability, and abundance, as well as their localization and trafficking, typically through modulating protein-protein interactions between these proteins and other factors that induce conformational changes and chemical modifications, e.g., phosphorylation (4,17,151,155).

The uptake of Cu into cells is largely regulated via the manipulation of Ctr1 localization and abundance at the plasma membrane (17,24,151,185). Low extracellular Cu concentrations result in the mobilization of Ctr1 from intracellular vesicles to the plasma membrane in order to facilitate the import of Cu, while high extracellular Cu concentrations lead to the rapid endocytosis of the membrane-localized Ctr1, returning them to the vesicles to mitigate excess uptake of Cu (4,17,20,24,152,185). Prolonged exposure to high Cu concentrations leads to the degradation of Ctr1 protein, potentially to prevent the inappropriate recycling of Ctr1 between the surface membrane and the intracellular pools (24,151,152,155,186). In addition to Cu, cellular hypoxia also affects the abundance and localization of Ctr1 protein (14). Moreover, insulin, progesterone, and estrogen were all found to promote the formation of the function Ctr1 trimer in Jeg-3 placental cells, suggesting a role for hormonally-mediated Ctr1 maturation during gestation (187). Glycosylation also serves an important function in the regulation of Ctr1 protein: N-linked glycosylation at Asn15 is required for full Cu-transport activity, and O-linked glycosylation at Thr27 has been shown to have a protective effect against proteolytic cleavage (14,188). In contrast to

Ctr1, Ctr2 localization is not Cu-responsive, and its localization is mostly restricted to endosomes and lysosomes (29,151). The post-translational regulation of Ctr2 is yet poorly understood (14).

Abundance of CCS is directly affected by intracellular Cu concentration (184,189,190). In rodents fed a Cu-deficient diet and in cells treated with a Cu chelator, CCS protein levels were found to increase as Cu concentration decreased, demonstrating an inverse relationship between CCS protein levels and cellular Cu levels (189,191). Increasing Cu levels did not affect CCS mRNA abundance, and further investigation revealed that Cu mediates the regulation of CCS protein via inducing the degradation of CCS via the 26 S proteasome—i.e., higher levels of Cu result in higher levels of degradation and, therefore, lower levels of CCS (17,189,192,193). Moreover, the rate of CCS degradation was found to be faster under higher Cu conditions, indicating that lower Cu concentrations may stabilize CCS protein (189). Interestingly, CCS was found to bind and deliver Cu to the X-linked inhibitor of apoptosis (XIAP), a protein whose abundance is markedly decreased in diseases of Cu accumulation such as Wilson disease (194,195). Under high Cu conditions, XIAP receives Cu from CCS, resulting in its destabilization. In turn, XIAP ubiquitinates CCS, and rather than promoting the degradation of CCS, this ubiquitination enhances the CCS-mediated delivery of Cu to SOD1 (195,196). These findings highlight the role of CCS as a rapid and sensitive Cu responder, which could explain why CCS is regulated almost entirely post-translationally.

The most well-known method of post-translational regulation of SOD1 is via its chaperone, CCS, which delivers a Cu ion to SOD1 that is essential to its activity (47,48). While CCS expression doesn't affect the abundance of SOD1, the activity of SOD1 is dependent on CCS, and insufficient levels of CCS lead to decreased SOD1 activity (17,45,47). SOD1 is also heavily post-translationally modified. SOD1 has at least a dozen phosphorylation sites which are thought to influence its localization and stability (197-201). Lys modification is also common in SOD1: acylation of key Lys residues attenuates the formation of SOD1 aggregates (202) and impacts

localization (203), enzyme maturation (201,204), and function (205-207); SUMOylation of Lys promotes SOD1 protein stability and aggregation propensity (201,208-210). SOD1 is also susceptible to several redox modifications, among them oxidation of Cys, which affects protein folding and stability (201,211), and glutathionylation of Cys, which is linked to SOD1 destabilization and aggregation (212-215).

The switch between the flow of Cu into the secretory pathway to metallate Cu-dependent enzymes and the excretion of excess Cu from the cell, is facilitated by the ability of the two Cu-ATPases, ATP7A and ATP7B, to traffic between the TGN, cytoplasmic vesicles, and the plasma membrane in response to cellular Cu levels (4,8,105,151,216). This concerted movement is largely due to post-translational modifications, which also regulate protein abundance, stability, and activity, and chief among them is phosphorylation (4,151). Cellular Cu accumulation stimulates the kinase-mediated phosphorylation of ATP7A and ATP7B at multiple Ser residues, a process that is both rapid and reversible (4,125,155,217-220). Phosphorylation induces protein movement from the TGN to cytoplasmic vesicles; in non-polarized cells, these ATP7A- and ATP7B-vesicles traffic to the plasma membrane, whereas in polarized cells, ATP7A-vesicles traffic to the basolateral membrane and ATP7B-containing vesicles to the apical membrane (4,125,151,155,218). A return to basal Cu levels coincides with the dephosphorylation of ATP7A and ATP7B and subsequent retrograde trafficking to the TGN (125,151). While both ATP7A and ATP7B undergo phosphorylation—though ATP7A to a lesser degree than ATP7B (54,221)—and glutathionylation (222), only ATP7A undergoes glycosylation, which is thought to enhance its localization to the plasma membrane (54,221,223). Though there is evidence to suggest that ATP7B protein abundance may be regulated by ubiquitination, this modification has not been characterized in ATP7B and putative sites have yet to be identified (151,224). By contrast, ATP7A ubiquitination leads to its proteasomal degradation, a fate that is attenuated by interaction with Caveolin-1 (Cav-1) and Akt2 in response to insulin (225,226).

In addition to mediating ATP7A and ATP7B phosphorylation, protein-protein interactions between the two Cu-transporters and binding partners can regulate their function and stability (103). The Cu chaperone Atox1 has been shown to directly interact with both ATP7A and ATP7B at their metal binding domains (MBDs) in order to transfer over Cu, and the conformational change in these proteins induced by this interaction is necessary for their activation and Cu-responsive trafficking (41,103,222,227,228). Cu metabolism MURR1 domain protein 1 (COMMD1), a protein involved in proinflammatory signaling and hypoxic response (229-231), and clusterin, a protein implicated in lipid transport and oxidative stress response (232), have both been identified as regulatory binding partners of ATP7A and ATP7B (233). Both COMMD1 and clusterin facilitate the degradation of ATP7A and ATP7B, though they differ in the way they do so: COMMD1 promotes proteasomal degradation, whereas clusterin promotes lysosomal degradation (103,233). COMMD1 has also been shown to modulate ATP7B trafficking in response to Cu elevation (234).

Though changes in Cu are the main influencing factor regulating the trafficking of ATP7A and ATP7B, other cellular stimuli can impact trafficking as well. In addition to activating the Akt2-dependent stabilization of ubiquitinated ATP7A (225,226), insulin has been found to affect the localization of ATP7A and ATP7B during gestation. It, as well as estrogen, induce the trafficking of ATP7A to the basolateral membrane and the retention of ATP7B in the TGN to maintain adequate Cu levels in developing fetal tissue (151,178). NMDA receptor activation stimulates the trafficking of ATP7A to neuronal processes in hippocampal neurons (235). Hypoxic conditions, which upregulate ATP7A transcription (154,175,176), also induce the trafficking of ATP7A protein from the TGN (151,236).

Protein-level regulation allows for rapid, and oftentimes reversible, responses to various intracellular stimuli. This versatility is invaluable to proteins such as those involved in Cu homeostasis, which must work in concert to prevent the cytoplasmic accumulation of free Cu and

ensure that adequate Cu concentrations are maintained. Post-transcriptional regulation, or the regulation of mRNA transcripts, is an intermediary step between transcriptional and post-translational regulation that allows for additional versatility in the cellular response to changes in Cu.

1.2.3 Post-transcriptional regulation

Relatively little is yet known about the mechanisms by which Cu homeostasis is regulated post-transcriptionally in mammals. As is the case with transcriptional regulation, most studies have been carried out in non-mammalian systems, whose modes of regulation may differ from those of mammals (237). Nevertheless, several instances of post-transcriptional regulation of the Cu machinery have been described, encompassing the modulation of transcript length, alternative splicing, mRNA stability, and translation initiation (238-240).

As described above, Cu uptake is mainly regulated on the transcriptional level via the TFs Sp1 and HIF-2α in a Cu-independent manner (8,15,154-156). The mRNA levels of Ctr1 have not been observed to change in response to cellular Cu levels, with one recorded exception (149,150,184). However, Ctr1 has multiple distinct transcripts: a 2 kb transcript, a 5.5 kb transcript, and a less abundant 8.5 kb transcript (1,241). The functional significance of these different transcripts is unknown. Similarly, SOD1 has two known transcripts—one 0.7 kb in length and a second 0.9 kb in length—that have different length 3' untranslated regions (UTRs) and multiple 5'-UTRs (242-244). While the transcript with the longer 3' UTR is four times less abundant than the transcript with the shorter 3' UTR (157), the longer 3' UTR transcript results in the translation of more SOD1 protein (243). The 3' UTR of SOD1 contains multiple AU-rich elements (AREs), which serve as binding sites for ELAV proteins that positively regulate the stability and translation of SOD1 mRNA (245). MTs are also post-transcriptionally regulated via modulation of transcript levels in a manner that is both metal- and isoform-specific (246,247). Treatment of rats with Cd or Cu and hepatic

HepG2 cells with Zn or Cu showed that these metal treatments differently affected hepatic levels of MT-1 and MT-2 mRNA by either preferentially enhancing polyribosome association, thus increasing translation, or activating mRNA turnover pathways, resulting in decreased transcript abundance (247,248).

Compared to other Cu machinery, the proteins involved in Cu export have the most characterized post-transcriptional regulation. ATP7B undergoes alternative splicing of exon 2 in response to P-coumaric acid (249). ATP7A is known to be post-transcriptionally regulated in several ways, largely via mechanisms involving the 3' UTR, which is nearly as long as its coding region (250). Alternative polyadenylation results in transcripts with different 3' UTR lengths due to differences in the size of their poly(A) tails, despite having arisen from the same target gene. This process is driven by the presence of multiple polyadenylation sites (PAS) in the mRNA, to which poly(A) polymerase binds to generate the poly(A) tail (251). Through the inclusion or exclusion of other regulatory elements downstream of the PAS into the transcript, alternative polyadenylation can greatly impact transcript stability and translation (251-254). ATP7A transcripts undergo alternative polyadenylation during myogenic differentiation. During differentiation, the abundance of a transcript with a shorter, more stable 3' UTR increases, which correlates well with the increase in ATP7A protein abundance observed in differentiating myotubes (250). Moreover, studies by Reddy, et al. have identified a short, alternatively spliced ATP7A transcript lacking exons 3–15 that produces a truncated version of the ATP7A protein, indicating that several transcripts that generate ATP7A proteins of different properties exist (255,256). In addition to transcript-based changes, several proteins that bind the ATP7A 3' UTR and potentially modulate transcript stability or translation have been identified, indicating the presence of machinery to participate in the post-transcriptional regulation of ATP7A (250,257-259).

More recently, some of the Cu machinery were shown to be subject to microRNA (miRNA)-mediated regulation at the transcript-level. miRNAs, which are small RNAs that target and bind

mRNA to silence its expression, serve as a means of post-transcriptional regulation whose significance in Cu regulation has thus far mostly been characterized in plants (3,260-263). SOD1 is a target of miR-377, the binding of which results in a decrease in SOD1 protein abundance (157,264). Studies by Xiao, et al. demonstrate that miR-139 downregulates ATP7A expression in mice and both ATP7A and ATP7B expression in cisplatin-resistant ovarian cancer cells, which they suggest is via the direct binding of miR-139 to the 3' UTRs of the transcripts (265,266). ATP7A is also a target of miR-148a-3p, which induces a downregulation in ATP7A expression in the breast cancer cell line MDA-MD-231 (267).

Cu itself may play a role in the post-transcriptional regulation of Cu machinery. A study by Burkhead, et al. found that the accumulation of Cu in hepatic nuclei of mice resulted in surprising changes in protein abundance within the nuclei as well as the post-translational modifications of those proteins (268). Interestingly, the classes of proteins most changed in the Cu overloaded nuclei compared to the control were proteins involved in different aspects of mRNA processing, such as alternative splicing and RNA transport (268). Among the proteins most affected were heterogeneous nuclear ribonucleoproteins (hnRNPs), and one in particular, hnRNP A2/B1, showed an increase in the abundance of one of its four isoforms in the nuclei, suggesting a Cu-driven shift in the splicing of hnRNP A2/B1 (268). A later study by Malinouski, et al. identified hnRNP A2/B1 in a screen for potential novel regulators of Cu levels in cells (269), providing further evidence for the existence of a link between Cu and RNA regulation via hnRNPs.

1.3 Heterogeneous nuclear ribonucleoproteins

The journey from gene to mature transcript is a multi-step one. It begins with the RNA polymerase II (RNA Pol II)-driven transcription of the gene, yielding a pre-mRNA which must undergo processing before leaving the nucleus. This processing includes the addition of a 5' 7-methylguanosine cap, the splicing out of introns and ligation of included exons, and the formation

of a 3’ poly(A) tail. Once done, the now mature mRNA can be packaged for translocation into the cytoplasm, where it will be translated into protein (270-275). hnRNPs, which are abundant, ubiquitously expressed proteins with a steady-state localization in the nucleus of the cell, mediate this journey at every step, binding to nascent transcripts to facilitate their maturation and translation (273-280). There are over 20 members in the hnRNP family, ranging in size from approximately 30 kDa to 120 kDa, and while they share many core features, their exact structures, the functions they carry out, and their cellular expression levels are distinct and specific (273,281-284).

1.3.1 Structure

The molecular structure of the hnRNPs includes several distinct functional domains; the presence or absence of these domains affect the specific function of the hnRNP protein (276). The functional domains include (i) RNA-recognition and binding sites, (ii) regulatory Arg-Gly-Gly (RGG) boxes, (iii) auxiliary domains that facilitate a variety of functions, and (iv) nuclear import/export signals (273,276,277,285). The domain composition varies among the different hnRNPs, resulting in a high level of functional diversity among the members of this protein family (276).

As RNA processing proteins, all hnRNPs possess some means by which to bind transcripts (276). The most common RNA-binding domains (RBDs) found in the hnRNPs are RNA recognition motifs (RRMs), also known as the ribonucleoprotein (RNP) domain (274,286,287). The RRM consists of two RNP consensus sequences, RNP-1 and RNP-2, approximately 30 residues apart from each other and arranged in a βαββαβ structure, which allows the hnRNPs to bind single-stranded nucleic acids in both a specific and non-specific manner (273,274,288,289). Alternative RBDs include the K-homology (KH) domain, a 50-nucleotide (nt) sequence that arranges into a βααββα structure and binds RNA based largely on hydrogen-bonding and electrostatic

interactions (276), and quasi-RRMs (qRRMs), RRM-like domains that lack RNP consensus sequences and bind RNA in a different manner than do RRMs (276,290). Many hnRNPs contain multiple RBDs, which allows the protein to bind and interact with longer transcripts, if the RBDs work in concert, or bring different transcripts in close proximity of each other, if the RBDs work independently (273,289). The RGG boxes of hnRNPs have also been shown to bind RNA, and in fact, the RGG box is the primary RNA binding site in hnRNP U (291).

RGG boxes are Arg/Gly-rich stretches that contain repeats of RGG, GRG, or RRG that confer RNA-binding activity on proteins (292,293). These domains also serve as potential sites for the post-translational methylation of Arg residues, an important mode of regulation of the hnRNP proteins (273,292,293). Many hnRNPs contain auxiliary domains consisting of mostly one type of amino acid (AA), such as Gly-rich and acidic (Asp/Glu) stretches (276), while other hnRNPs possess low complexity, prion-like domains (PrLDs) (294,295).

Most hnRNPs contain nuclear localization signals (NLSs), as these proteins are largely nuclear at steady state (279,296). While some contain more classical NLSs—especially those that are exclusively nuclear—some hnRNPs that shuttle between the nucleus and the cytoplasm contain non-canonical NLSs, called M9 domains, that facilitate both their nuclear import and their nuclear export (281,297-299).

In addition to these functional domains, most hnRNPs undergo alternative splicing, yielding one or more splice variants that could differentially carry out protein functions (273,276). Post-translational modifications are common among hnRNPs and add another dimension of functional variety to the proteins (273,279,300). Several hnRNPs are phosphorylated at Ser and Thr residues, and these modifications impact RNA binding, subcellular localization, translational activation ability, protein stability, protein binding, and even post-translational modification of the hnRNPs (279,300-310). Methylation of Arg residues can modulate RNA binding at the RGG box,

transcriptional activation ability, protein-binding, and subcellular localization (273,276,277,279,311-316). hnRNPs also undergo SUMOylation of Lys residues, which affects protein stability, protein binding, RNA binding, mRNA export, and miRNA binding (317-322).

1.3.2 Roles and functions

The main, overall function of hnRNPs is to facilitate the maturation of a nascent pre-mRNA into a transcript prepared to be translated (323). This is achieved through the participation of hnRNPs in several mRNA processing steps, such as alternative splicing, 3'-end processing, mRNA transport and localization, and regulation of mRNA stability (279,324-329). The known functions of the different hnRNPs are described below.

Alternative splicing, the process by which exons are preferentially excluded from the pre-mRNA, allows for the generation of many different transcripts from a single gene, greatly increasing the complexity of gene expression (294,330). Many hnRNPs participate in the splicing process, forming a part of the splicing machinery that binds target mRNAs to modulate interaction between the transcript and the spliceosome (330). As largely negative regulators of alternative splicing, hnRNPs bind to exonic and intronic splicing silencers within the mRNA to inhibit spliceosome assembly on the transcript (330-333). hnRNPs A1, A2/B1, E1, F, G, H, I, K, L, M, Q, and U are involved in the alternative splicing of many transcripts involved in a wide variety of cellular functions and processes, such as cellular stress response, proliferation and differentiation, splicing, cellular signaling, and apoptosis (276,287,323,324,333-347).

Nearly all mRNAs undergo 3'-end processing, which involves the endonucleolytic cleavage of the mRNA and the addition of a poly(A) tail to the cleaved transcript at PASs (348-351). Both of these steps are regulated in part by different hnRNPs. hnRNPs K and I are known to recruit 3' end processing factors and stabilize their interactions with the target transcripts (348,352-356).

Several hnRNPs are involved in PAS selection and activation, including hnRNPs F, H, I, and L (276,343,357-361), and hnRNP H is also known to directly participate in the endonucleolytic cleavage of mRNA (359).

Transcript abundance is regulated by hnRNPs on the mRNA-level via modulation of mRNA stability, mRNA silencing, and miRNA activity (323). hnRNPs A1, A2/B1, and D have been implicated in the regulation of mRNA stability through binding to regulatory elements in the 3' UTR of transcripts, such as AU-rich elements (AREs), and promoting transcript destabilization and decay (362-368). By contrast, hnRNPs C, E, and K increase mRNA stability through interaction with other RBPs (369-372). hnRNP K has also been found to participate in mRNA silencing (373-375), while hnRNPs A1, C, I, and L play roles in miRNA-mediated gene regulation (321,323,376).

hnRNPs play a large role in mRNA localization, with involvement in mRNA packaging and intracellular trafficking (276). This role has been best characterized for hnRNP A2/B1 in neurons and oligodendrocytes (377) and will described in more detail further in this chapter. hnRNP A1 has been found to accumulate in the cytoplasm in response to cellular stress, acting as one of several component RBPs in stress granules that bind and regulate the translation of mRNAs whose expression during times of stress isn't crucial (378,379). Similarly, hnRNP E1 is recruited by hnRNP A2/B1 to RNA granules where it acts to inhibit translation until trafficking of the mRNAs is complete (276,380). Packaging of mRNAs into cytoplasmic granules is also mediated by hnRNPs C1 and C2, which sort transcripts by length for proper packaging (381-383).

hnRNPs are not limited to these mRNA processing functions—they are also known to participate in the regulation of both transcription and translation (279,302,323,384). hnRNP U, which is solely localized to the nucleus, is a key player in RNA Pol II-mediated transcription (385). hnRNP K also regulates transcription via binding RNA Pol II and enhancing the transcription of its targets (386,387). Likewise, hnRNPs D, E, and R serve as transcriptional activators of target genes

through interacting with other proteins involved in the transcriptional process (279,323,388,389). A variety of hnRNPs—including hnRNPs A, A2/B1, C, E, I, J, K, and R—are involved in the regulation of translation through their roles as internal ribosomal entry site (IRES)-transactivating factors, or ITAFs (295,390). As ITAFs, these hnRNPs bind IRESs in target transcripts and enhance their translation via the recruitment of ribosomes (276,295,302,304,323,390-395). As of yet, hnRNPs J, N, O, P, S, and T are not well-characterized and their roles in mRNA processing and regulation are poorly understood (276).

The roles that the hnRNPs play in cellular processes largely depend on their subcellular localization (276). For example, an hnRNP localized entirely to the nucleus, such as hnRNP U, will be unable to perform functions that occur in the cytoplasm, such as translational regulation. The ability of some of the hnRNPs to move between the nucleus and cytoplasm—called nucleocytoplasmic shuttling—is crucial to the ways in which they interact with and regulate mRNA (276,323).

1.3.3 Nucleocytoplasmic shuttling

At steady state, the majority of the hnRNPs localize to the nucleus, in which a large portion of their functions—e.g., alternative splicing, transcriptional regulation, mRNA processing—are carried out (276,295,396). Several hnRNPs have been observed to shuttle rapidly between the nucleus and cytoplasm, and this movement is facilitated by the presence of one or more NLSs or nuclear import/export signals (279,296,299,302,397-402).

The movement of hnRNPs between the nucleus and cytoplasm is facilitated by two classes of nuclear transport receptors: importins, which recognize NLS, and exportins, which recognize nuclear export signals (403,404). Both nuclear import and export are RanGTP-dependent; the release of imported hnRNPs into the nucleus requires the exchange of RanGDP for RanGTP,

and the release of exported hnRNPs into the nucleus requires the hydrolysis of RanGTP to RanGDP (403,405). Nucleocytoplasmic shuttling is often induced by post-translational modification of the hnRNPs. Different modifications have different effects on hnRNP shuttling: Lys acylation and SUMOylation appear to be associated with the nuclear return of hnRNPs, while Ser/Thr phosphorylation and Arg methylation are thought to inhibit nuclear return (302,315,378,390,406-413).

One of the main benefits of nucleocytoplasmic shuttling is that it confers upon hnRNPs the ability to export mRNA from the nucleus and to participate in modes of mRNA regulation that occur in the cytoplasm (273,377,401,414,415). In the cytoplasm, hnRNPs can exert control over translation by binding IRESs of target transcripts (276,295). hnRNPs can also form RNA-containing granules in the cytoplasm, creating concentrated microenvironments of RBPs to enact specific effects on bound transcripts, such as stalling translation (276,294,328,416).

RNA granules are membraneless cytoplasmic assemblies of RNA and RBPs wherein regulation of mRNA occurs (417,418). Cellular signals drive the formation of these granules, and their components dictate the functions they carry out. Stress granules (SG), a common type of RNA granule, form in response to many types of cellular stress (419). SGs serve to collect translationally-stalled mRNAs while the cell is undergoing stress, and these transcripts either resume translation once cellular conditions return to normal or are degraded as a result of sustained stress (417,420). In addition to hnRNPs, SGs typically include eukaryotic initiation factors (eIFs), poly(A)-binding protein (PABP), Ras-GAP SH3 binding protein (G3BP), and T-cell intracellular antigen (TIA), all of which are involved in various aspects of the regulation of the transcripts, such as mRNA stability/decay and translational initiation/stalling (421,422). Cytoplasmic hnRNPs may also localize to Gly- and Trp-rich cytoplasmic processing bodies (GW/P-bodies), which mainly function to regulate mRNA stability/decay and silencing (417-419,422). GW/P-bodies contain proteins involved in RNA interference (e.g., Dicer, Ago2), mRNA

degradation (e.g., CCR4, Dcp1/2), and RNA processing and transport (various hnRNPs) (417,419,421,422). Other cytoplasmic RNA granules include U-rich small nuclear ribonucleoprotein-containing bodies (U-bodies), which serve to assemble spliceosome components in the cytoplasm prior to nuclear import (417,422,423), and neuronal transport RNP granules, which function to transport translationally-stalled mRNAs to their target sites of translation (417,422).

Nucleocytoplasmic shuttling has been extensively studied for hnRNP A2/B1, especially in oligodendrocytes and neuronal cells. A study by Burkhead, et al. has shown that the localization of hnRNP A2/B1 changes in response to cellular Cu levels—i.e., one or two of the hnRNP A2/B1 isoforms are selectively enriched in the nucleus upon Cu accumulation in mouse hepatocytes (3). This, combined with data by Malinouski, et al. that demonstrate that cellular Cu levels are impacted by hnRNP A2/B1 expression (269), suggest that hnRNP A2/B1 may play a particular, specialized role in Cu homeostasis.

1.4 hnRNP A2/B1

hnRNP A2/B1 is a highly abundant, ubiquitously expressed RBP that participates in myriad functions pertaining to RNA processing and metabolism (424). It is part of the hnRNP A/B family, which also includes hnRNPs A1, A3, and A0, and shares common functions and structural features with these proteins (295,333). Like other hnRNPs, hnRNP A2/B1 has a modular structure that includes two N-terminal RRMs, a central RGG box, and a C-terminal Gly-rich stretch in which there is a low complexity PrLD and an M9 nuclear import/export domain (***Figure 1.2***) (294,295,425-427). The *hnRNP A2/B1* gene consists of 12 exons, and alternative splicing yields four isoforms: B1, B1b, A2, and A2b (428).

1.4.1 Isoforms

While hnRNP A2B1 is an abundant protein and its important physiologic roles are well established, surprisingly little is known about the specific functions of all four individual hnRNP A2B1 isoforms. The different isoforms of hnRNP A2/B1 arise from the alternative splicing of exons 2 and 9; B1 contains all 12 isoforms, B1b lacks exon 9, A2 lacks exon 2, and A2b lacks both exons 2 and 9 (294,429). hnRNP A2 and B1 have been shown to have slightly different selectivity for RNA motifs, indicating that exon inclusion/exclusion may affect the transcripts to which the different isoforms bind (430).

Exon 2 is a 12-AA stretch of largely charged residues, including three Lys residues, as well as a Thr at position 4 that is known to be phosphorylated (431). Inclusion of this exon has been correlated with a decrease in the diffusion rate of the isoforms in the cytoplasm, likely due to an increase in interactions with immobile cytoplasmic binding partners (429). This suggests that the splicing out of exon 2 is associated with freer movement through the cytoplasm, possibly due to a lower binding affinity with cytoplasmic protein targets. Moreover, the exon 1_3 junction of isoforms lacking exon 2 makes up a 4-AA sequence that resembles classical NLSs, further indicating that alternative splicing of exon 2 could impact hnRNP A2/B1 isoform nucleocytoplasmic distribution (429).

Exon 9 is 38-AA long and consists mostly of Gly residues, as it falls partially within the RGG box and Gly-rich domain. It also contains a Ser residue at position 259 that can be phosphorylated, as well as an Arg at position 266 that can be methylated (431,432). The inclusion of this exon has been correlated with a decrease in the diffusion rate of the isoforms in the nucleus, likely due to an increase in interactions with immobile nuclear binding partners (429). This is supported by secondary structure analysis of exon 9, which predicts the formation of Gly loops that could mediate protein-protein interactions (429,433).

1.4.2 Modes of regulation

hnRNP A2/B1 is a versatile, multifunctional RNA processing protein. Its ability to move between the nucleus and the cytoplasm allows it to regulate mRNA at all stages of production and processing, from transcription to translation. In the nucleus, hnRNP A2/B1 acts as a transcriptional activator/repressor of target genes (294). This function is carried out via hnRNP A2/B1 binding to promoter regions in two different ways. In the first, hnRNP A2/B1 directly recognizes and binds G-quadruplex structures in the promoters of genes (434). In the second, the binding of hnRNP A2/B1 to promoters is facilitated by noncoding RNAs, transcribed RNAs that are not translated into proteins but still carry out regulatory functions within the cell, such as modulating mRNA splicing, stability, and translation (294,430,435-438). hnRNP A2/B1 also regulates telomeres; by binding G-quadruplexes within telomeric DNA, hnRNP A2/B1 modulates telomerase activity and protects telomeres from the cell's DNA damage response (439-444). Interestingly, hnRNP A2/B1 also plays a role in the mitochondrial stress response, acting as a coactivator of key TFs to induce the transcriptional activation of genes in response to stress signaling (445,446).

Among the nuclear functions of hnRNP A2/B1 is the regulation of splicing. There are two types of splicing that occurs in cells: (i) constitutive splicing, in which introns are spliced out and exons ligated together, and (ii) alternative splicing, in which exons are also preferentially excluded from the mature transcript, creating variety in the transcripts derived from a single gene (330). During constitutive splicing, hnRNP A2/B1 acts largely as a splicing inhibitor—binding of hnRNP A2/B1 to enhancer sequences for introns and alternative exons prevents their inclusion into the mature transcript via alternative splicing (324,333,447). During alternative splicing, hnRNP A2/B1 promotes both the exclusion of typical exons and the inclusion of alternative exons, which can greatly impact transcript stability (294,448,449).

hnRNP A2/B1 impacts mRNA stability in several ways in addition to alternative splicing. For some transcripts, hnRNP A2/B1 dictates PAS selection, resulting in longer or shorter 3' ends and thereby impacting transcript stability (450). In fact, many of the ways by which hnRNP A2/B1 regulates mRNA stability involve binding to specific sites within the transcript's 3' UTR (294). hnRNP A2/B1 has long been known to bind AU-rich elements in the 3' UTRs of transcripts to inhibit their expression (294,366,451-453). Geissler, et al. described an hnRNP A2/B1 and A1-mediated decay pathway involving the recruitment of the CCR4-NOT deadenylation complex in response to the hnRNPs binding a novel 8-nt motif that is present in the 3' UTRs of roughly 7% of known human transcripts (367,454). hnRNP A2/B1 also regulates transcripts with adenosine N6 nitrogen methylation (m^6A) modifications, recognizing these marks and directly or indirectly binding at these sites to enhance transcript stability (321,427,455-457).

In addition to its many nuclear functions, hnRNP A2/B1 also regulates mRNA in the cytoplasm. hnRNP A2/B1 enhances the translation of mRNAs in both a cap-independent manner, in which hnRNP A2/B1 binds to IRES within transcripts and promotes ribosomal recruitment, and a cap-dependent manner, in which hnRNP A2/B1 binds to specific sites in transcripts with 5' caps (294,295,458-460). One of the best-characterized roles of hnRNP A2/B1 is its involvement in mRNA transport. Largely studied in oligodendrocytes and neurons, hnRNP A2/B1-mediated mRNA transport is facilitated via the binding of hnRNP A2/B1 to mRNAs containing all or at least the core part of a 21-nt sequence called the A2 response element (A2RE) (377,416,461,462). Upon binding the A2RE, hnRNP A2/B1 and its bound transcript are exported to the cytoplasm and organized into RNA granules that subsequently traffic to the intended location of translation through interactions with microtubules (294,328,377,416). This process was originally described for the trafficking of myelin basic protein (MBP) in oligodendrocytes (323,463,464).

Changes in the expression, localization, or function of hnRNP A2/B1 have been implicated in several diseases. Overexpression of one or more hnRNP A2/B1 isoforms has been noted in a

number of different cancers, consistent with the fact that hnRNP A2/B1 is involved in the maintenance of proliferative state in cells (465-472). Cholinergic deficiency in Alzheimer's disease patients induces a decrease in hnRNP A2/B1 expression in the brain, resulting in subsequent abnormal alternative splicing events (294,473,474). Mutations in hnRNP A2/B1's PrLD that induce protein fibrillization and aggregation have been linked to ALS and frontotemporal dementia (475-477). hnRNP A2/B1 expression and localization is also known to be differentially regulated under stress conditions, such as starvation and hypoxia (478), and there is evidence to suggest that this may also occur under conditions of Cu accumulation (268).

1.5 Conclusions: A potential role for hnRNP A2/B1 in Cu homeostasis?

Regulation of Cu homeostasis is a complex process, involving the participation of numerous proteins that both directly and indirectly interact with Cu ions. While our understanding of this regulation on the transcriptional- and translational-levels is robust, our knowledge of how Cu balance is regulated on the post-transcriptional-level is not as well-defined. Post-transcriptional regulation is largely mediated by RBPs such as the hnRNPs, which modulate transcript length, composition, stability, and localization through a variety of means in response to different cellular needs without necessitating additional transcription of target genes. It also provides an additional level of protein diversity stemming from a single gene.

A study by Burkhead, et al. found that inactivation of the Cu-transporter ATP7B in mice and the associated accumulation of Cu in their livers induced the enrichment of RNA-binding and RNA-processing proteins in the nucleus, and hnRNP A2/B1 was among the proteins whose abundance was most notably changed (268). More specifically, Cu accumulation in these cells resulted in the nuclear enrichment of the hnRNP A2/B1 isoforms containing exon 2, which could be due to an increase in exon 2 inclusion during mRNA splicing or due to some mechanism by which exon 2 inclusion promotes nuclear localization (268,429). This link between Cu concentration and hnRNP

A2/B1 is strengthened by the discovery that hnRNP A2/B1 downregulation in HeLa cells results in a significant decrease in cellular Cu levels (269). This observation suggests that hnRNP A2/B1 an important role in the regulation of either or both Cu import (via the importer Ctr1) and Cu export (via the exporters ATP7A and ATP7B). Given these data and the known functions of hnRNP A2/B1, it is tempting to speculate that hnRNP A2/B1 mediates the post-transcriptional regulation of Cu importers and/or exporters and that it might do so in an isoform-specific manner. Further study of this connection and its implications could reveal novel mechanisms by which Cu homeostasis is regulated on the RNA-level as well as define a role for hnRNP A2/B1 in the cellular response to Cu-induced stress.

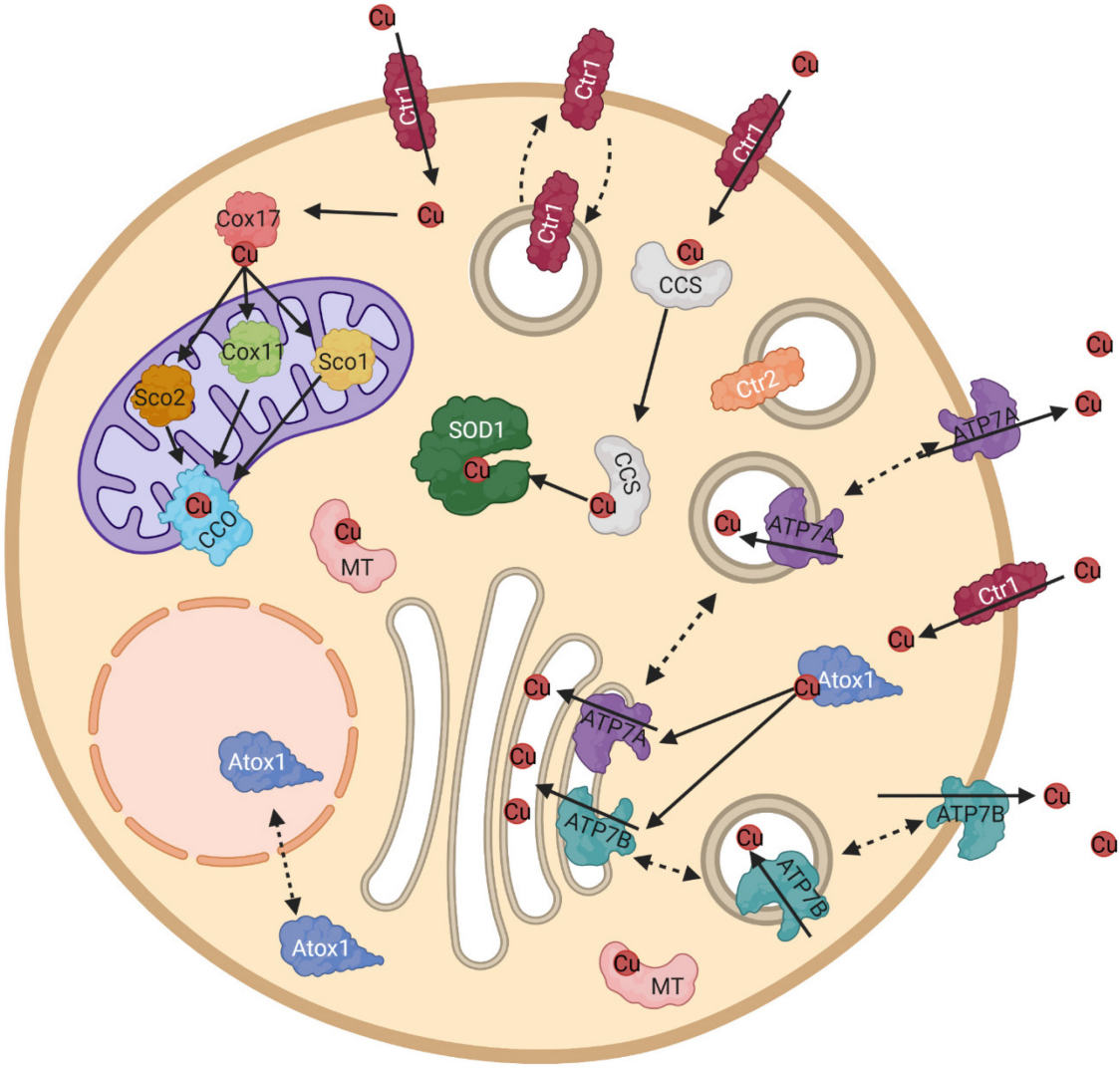

Figure 1.1. Model of mammalian Cu homeostasis.

Schematic of Cu homeostasis in a mammalian cell indicating the localization and functions of the Cu importers (Ctr1, Ctr 2), chaperones and binding proteins (CCS, Atox1, MT, SOD1, CCO, Cox17, Cox 11, Sco1, Sco2), and exporters (ATP7A, ATP7B). Solid lines indicate movement of Cu, dashed lines indicate trafficking of proteins. Cu represented by red circles. Created with BioRender.com.

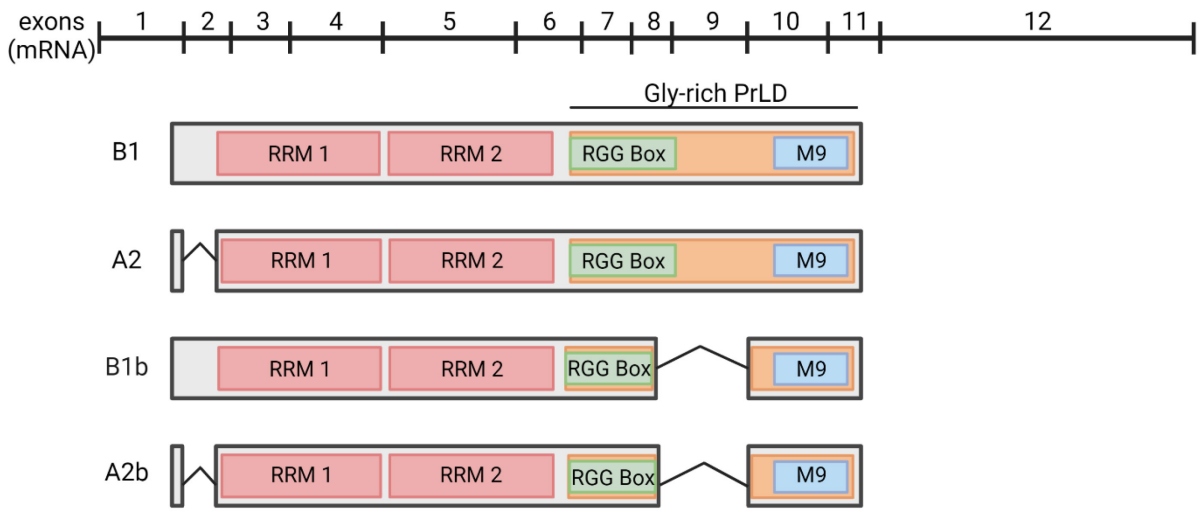

Figure 1.2. Modular domain structure of the hnRNP A2/B2 isoforms.

Schematic of the hnRNP A2/B1 isoforms. *Top*, hnRNP A2/B1 mRNA showing all exons as their relative lengths. *Bottom*, domains present in each hnRNP A2/B1 isoform. B1 contains all isoforms, A2 lacks exon 2, B1b lacks exon 9, and A2b lacks exons 2 and 9. RNA recognition motifs (RRMs) indicated in red, Gly-rich, low complexity prion-like domain (PrLD) in orange, RGG box in green, and M9 nuclear import/export signal in blue. Box length is representative of domain size. Created with BioRender.com.

2 Experimental Procedures

2.1 Cell Lines and Culture Conditions

2.1.1 Cell lines

HeLa cells (ATCC® CCL-2™) were cultured in Dulbecco's modified Eagle's medium (DMEM; Corning) supplemented with 10% heat-inactivated fetal bovine serum (FBS; Corning). Non-differentiated SH-SY5Y cells (ATCC® CRL-2266™) were cultured in complete medium consisting of 1:1 Eagle's Minimum Essential Medium (EMEM; Corning) and F12 Ham's Medium (Corning) supplemented with 10% heat-inactivated FBS. Cells were maintained at 37°C in a humidified incubator with 5% CO_2.

2.1.2 Differentiation of SH-SY5Y cells

SH-SY5Y cells were plated at 20% confluency and treated as described previously (479). Briefly, 24 h after plating the cells (day 0, d0), non-differentiated cells were collected and cells to be differentiated were treated with complete medium containing 10 μM retinoic acid (RA; Sigma). After 48 h of treatment (day 2, d2), the media was replaced with fresh media containing RA and incubated for a further 48 h. On day 4 (d4), the media was replaced with serum-free media containing 50 ng/mL brain-derived neurotrophic factor (BDNF; Shenandoah Biotech) and cells were incubated for 72 h before collection on day 7 (d7).

2.2 Transfection of cells

2.2.1 Transient transfection of DNA plasmids

Cells were grown to approximately 60% confluency in 6-well or 12-well plates, as indicated, and transfected with plasmid DNA using Lipofectamine LTX with PLUS reagent (Invitrogen) following the manufacturer's protocols. For 6-well plates, a total of 2 μg plasmid DNA and 6 μL lipofectamine diluted in Opti-MEM reduced serum media (Gibco) were used per well; for 12-well plates, a total

of 1 µg plasmid DNA and 3 µL lipofectamine were used. DNA-lipofectamine mixtures were incubated at room temperature (RT) for 10 min. Fresh complete media was added to the cells prior to adding the DNA-lipofectamine mixtures dropwise to each well. The transfection was carried out for a total of 20 h.

2.2.2 Transfection of small interfering (si)RNA

siRNA-mediated knockdowns were performed using wet-reverse transfection, a procedure in which cells are plated at the time of transfection, following DharmaFECT manufacturer's protocols. Prior to transfection, all siRNA stocks were diluted to 5 µM in RNase-free water. Samples transfected without siRNA or non-targeting siRNA were used as controls. The sequences of siRNA (Dharmacon) used in this study are listed in **Table 2.1**.

For 6-well plates. Per each well, 4 µL of either siRNA or water were added to 196 µL of Opti-MEM, and 5 µL of DharmaFECT 1 transfection reagent (Dharmacon) were added to 195 µL of Opti-MEM. The two mixtures were added together 1:1 and incubated for 30 min at RT. Cells grown to 40–60% confluency were harvested and plated at a density of 2×10^5 cells per well in complete medium, to which the siRNA-DharmaFECT mixture was added

For 6 cm dishes. Per each plate, 12 µL of either siRNA or water were added to 588 µL of Opti-MEM, and 15 µL of DharmaFECT 1 transfection reagent (Dharmacon) were added to 585 µL of Opti-MEM. The two mixtures were added together 1:1 and incubated for 30 min at RT. Cells grown to 40–60% confluency were harvested and plated at a density of 6×10^5 cells per well in complete medium, to which the siRNA-DharmaFECT mixture was added.

For both 6-well and 6 cm plate experiments, after 48 h of incubation at 37°C, 1 mL of complete medium was added to each well, and the transfection was continued for 24 h more, for a total transfection time of 72 h. The final concentration of siRNA in each well or plate was 10 nmol.

2.3 Generation of pSF-6xHis-GFP-TEV-hnRNP A2/B1 isoform plasmid constructs

His-tagged pET28a bacterial expression plasmids of each hnRNP A2/B1 isoform were kindly gifted by Dr. Max Konig (Johns Hopkins Bayview). To insert the cDNA for each hnRNP A2/B1 isoform into the pSF-6xHis-GFP-TEV mammalian expression vector (Cat. No. OG4716; OXGENE), the plasmids and the vector were digested with EcoRI and XhoI restriction enzymes for 3 h at 37°C and purified from a 0.8% agarose gel using a PureLink Quick Gel Extraction Kit (Invitrogen). hnRNP A2/B1 isoform inserts were ligated into the pSF-6xHis-GFP-TEV vector by incubating with T4 DNA ligase (New England Biolabs) for 2 h at RT. Ligated plasmids were transformed into 5-α competent *E. coli* cells (New England Biolabs) following the manufacturer's protocol. Plasmid DNA was isolated by miniprep using a QIAprep Spin Miniprep Kit (Qiagen). Sequences were confirmed using the primers listed in **Table 2.2**.

2.4 Western blot analysis

Cells were lysed in 1X RIPA buffer (10X: 0.5M tris-HCl, pH 7.0; 1.5M NaCl; 2.5% deoxycholic acid; 10% NP-40; 10mM EDTA; Millipore) for 30 m on ice. Unless otherwise indicated, lysates were then centrifuged at 3000 x*g* for 15 m to pellet cell debris. Protein concentrations in the lysates were determined using BCA assay (Pierce). Twenty micrograms of protein were separated on 15% SDS gels; to achieve good resolution and separation of the individual hnRNP A2/B1 isoforms, gels were run until the 25 kDa ladder marker (PageRuler Plus Prestained Protein Ladder; Thermo Scientific) ran off the bottom of the gel, roughly 3 h. Protein was then transferred to PVDF (Millipore) membranes using 1X N-cyclohexyl-3-aminopropanesulfonic acid (CAPS) running buffer containing 10% methanol for 2 h at 90 V. Membranes were blocked for 1 h at RT in 5% milk in phosphate-buffered saline (PBS) and then incubated overnight (16 h) in the indicated primary antibodies (**Table 2.3**) diluted in PBS containing 0.2% Tween 20 (PBST) and 0.05% sodium azide. Membranes were washed three times in PBST and then incubated for 1 h at RT in

the indicated secondary antibodies (**Table 2.3**) diluted in 1% milk in PBST. Following two washes in PBST and one wash in PBS, membranes were treated with horseradish peroxidase (HRP) substrate for enhanced chemiluminescence (ECL; Pierce), and then imaged on an AlphaImager (ProteinSimple). The raw intensity of each band was quantified with Image-J (NIH) and normalized to indicated loading controls. At least three biological replicates (*n*=3) were performed for each condition. Relative protein abundances for the experimental samples were calculated by normalizing to loading controls and then to experimental controls, as indicated.

2.5 Analysis of cellular Cu content by atomic absorption spectrometry

HeLa cells following siRNA-mediated knockdown of hnRNP A2/B1 in 6 cm dishes and SH-SY5Y cells following differentiation in 6 cm dishes were collected, washed three times in PBS, and split into two aliquots: one containing 10% of the cells and another containing 90% of the cells. The cells in the 10% aliquot were lysed in 1X RIPA buffer for 30 m on ice, centrifuged at 3000 x*g* for 15 m, and the supernatant used to quantify total protein content by BCA assay. The cells in the 90% aliquot were digested in 200 µL of 70% nitric acid at 65°C for 2 h and, after cooling to RT, the sample volumes were adjusted to 500 µL using HPLC-grade water. Samples were stored at 4°C until analysis.

Prior to measurement, samples were diluted 1:10 in HPLC-grade water and a standard Cu curve of 0, 10, and 100 parts per billion (ppb) Cu was constructed. Measurements were taken on a PinAAcle 900T atomic absorption spectrometer (Perkin Elmer). At least three biological replicates (*n*=3) and three technical replicates were performed for each condition. Cu content values were normalized to total protein content, and results are reported as pmol Cu/mg protein.

2.6 Quantitative real-time polymerase chain reaction (qRT-PCR)

Total RNA was isolated from cells using an RNeasy kit (Qiagen) following the manufacturer's protocols. qRT-PCR was performed using a Power SYBR Green RNA-to-C_T 1-Step Kit (Thermo Fisher) following the manufacturer's instructions and 50 ng RNA per reaction on a QuantStudio 7 Flex Real-Time PCR machine (Applied Biosystems). At least three technical and biological replicates (*n*=3) were performed for each condition: exon 2 *n*=15, exon 9 *n*=9, exon 1_3 *n*=9, ATP7A *n*=21, ATP7B *n*=6, Ctr1 *n*=9, SOD1 *n*=6. Primers used (268) are listed in **Table 2.4**. Fold-changes for the experimental samples were calculated by normalizing to hS18 loading control and then to experimental controls, as indicated.

2.7 Immunofluorescence analysis

Cells grown on glass coverslips were washed twice in PBS and then fixed in 4% paraformaldehyde (PFA; Electron Microscopy Sciences). Fixed cells were permeabilized in 0.1% Triton X-100 (Thermo Fisher) for 15 min at RT and then blocked in 5% bovine serum albumin (BSA; Gemini Bio-Products) for 40 min at RT. Coverslips were incubated in the indicated primary antibodies (**Table 2.5**) diluted in 1% BSA for 1 h at RT and then washed twice in PBST and once in PBS. Coverslips were then incubated in the indicated secondary antibodies (**Table 2.5**) diluted in 1% BSA for 1 h at RT. Coverslips were washed twice in PBST and once in PBS before being quickly rinsed in deionized water. Coverslips were mounted to glass slides with DAPI-Fluoromount (Electron Microscopy Sciences) and cured overnight. Images were taken with a Zeiss LSM800 microscope with a Plan-Apochromat 63x/1.4 NA oil lens and processed with Image-J (NIH).

2.7.1 Analysis of ATP7A trafficking

2.7.1.1 In HeLa cells with hnRNP A2/B1 downregulated

HeLa cells were grown to approximately 80% confluency on untreated 18 mm glass coverslips (Electron Microscopy Sciences) in 12-well plates and treated with media containing 0, 5, 10, or 20 μM $CuCl_2$ for 4 h at 37°C. After treatment, cells were prepared for immunofluorescence analysis as described above. Anti-ATP7A and anti-TGN46 primary antibodies were used and donkey anti-mouse AlexaFluor 488 and donkey anti-sheep AlexaFluor 568 secondary antibodies were used in immunostaining.

2.7.1.2 In differentiating SH-SY5Y cells

SH-SY5Y cells were plated on collagen-coated 18 mm glass coverslips (Neuvitro) and differentiated in 12-well plates as described above. Cells were prepared for immunofluorescence analysis as described above. Anti-ATP7A and anti-TGN46 primary antibodies and donkey anti-mouse AlexaFluor 488 and donkey anti-sheep AlexaFluor 647 secondary antibodies were used in immunostaining.

2.7.2 Analysis of hnRNP A2/B1 localization

2.7.2.1 In response to changes in Cu

Cells were grown to approximately 80% confluency on either untreated 18 mm glass coverslips (HeLa) or collagen-coated 18 mm glass coverslips (SH-SY5Y) in 12-well plates.

To determine effect of increasing Cu concentration. Cells were treated with media containing 0, 5, 10, 20, 50, or 100 μM $CuCl_2$ for 4 h at 37°C. After treatment, cells were prepared for immunofluorescence analysis as described above. Anti-hnRNP A2/B1 primary and donkey anti-mouse AlexaFluor 488 secondary antibodies were used in immunostaining.

To determine effect of increasing incubation time in presence of Cu. Cells were treated with media containing 20 μM $CuCl_2$ for 0, 1, 2, 3, 4, 6, or 8 h at 37°C. After treatment, cells were prepared for immunofluorescence analysis as described above. Anti-hnRNP A2/B1 primary and donkey anti-mouse AlexaFluor 488 secondary antibodies were used in immunostaining.

The ratio of hnRNP A2/B1 signal inside the nucleus (i.e., co-localized with DAPI staining) to hnRNP A2/B1 signal outside the nucleus (i.e., not co-localizing with DAPI staining, cytoplasmic) was quantified by using the lasso tool in Image-J to select the relevant areas for determination of signal intensity per area. The nucleocytoplasmic (N/C) ratio was calculated by dividing the total normalized nuclear signal by the total normalized cytoplasmic signal. The mean N/C ratio was generated from at least 5 cells per independent experiment and at least 3 independent experiments. Data was normalized to either 0 μM Cu or 0 h treatment controls, as indicated. A larger N/C ratio value indicates less cytoplasmic staining and a smaller N/C ratio value indicates more cytoplasmic staining of hnRNP A2/B1 compared to nuclear staining. In SH-SY5Y cells, hnRNP A1, a homolog of hnRNP A2/B1, was also stained and the N/C ratio calculated to serve as a specificity control.

2.7.2.2 In response to Cu in HeLa cells with hnRNP A2/B1 downregulated

hnRNP A2/B1 was downregulated in HeLa cells as described above, and cells were plated onto untreated 18 mm glass coverslips. After 72 h of transfection, the media was replaced with media containing 0, 5, 10, or 20 μM $CuCl_2$ for 4 h at 37°C. After treatment, cells were prepared for immunofluorescence analysis as described above. Anti-hnRNP A2/B1 primary and donkey anti-mouse AlexaFluor 488 secondary antibodies were used in immunostaining. The N/C ratios were calculated as described above.

2.7.3 Co-localization with markers of cytoplasmic granules

HeLa cells were grown to approximately 80% confluency on untreated 18 mm glass coverslips in 12-well plates and treated with media containing 0, 5, 10, or 20 μM $CuCl_2$ for 4 h at 37°C. Following treatment, cells were prepared for immunofluorescence analysis as described above. Anti-hnRNP A2/B1, anti-G3BP1, anti-Dcp2, anti-DDX20, and anti-LAMP1 primary antibodies and donkey anti-mouse AlexaFluor 488 and donkey anti-rabbit 568 secondary antibodies were used in immunostaining.

2.8 Dual Luciferase assay

For hnRNP A2/B1 knockdown. HeLa cells were transfected non-targeting (NT), hnRNP A2B1-total, or hnRNP A2/B1-exon 2 siRNA in 6-well plates, as described above. After 48 h of transfection with the siRNA, cells were transfected with 1200 ng empty pcDNA plasmid, 600 ng ATP7A 3'UTR-luciferase plasmid (Cat. No. 128100810195; Applied Biological Materials, Inc.), and 200 ng Renilla-luciferase plasmid for a total of 2 μg of DNA transfected.

For hnRNP A2/B1 overexpression. HeLa cells were grown in 12-well plates and transfected with 600 ng of empty pcDNA plasmid, empty pSF-6xHis-GFP-TEV plasmid, or the individual pSF-6xHis-GFP-TEV-hnRNP A2/B1 isoform plasmids; 300 ng ATP7A 3'UTR-luciferase plasmid; and 100 ng Renilla-luciferase plasmid for a total of 1 μg of DNA transfected.

Following 20 h of transfection, cells were prepared for dual luciferase assay (Promega) following the manufacturer's protocol. Briefly, cells were washed once with PBS and then incubated in either 500 μL (6-well) or 250 μL (12-well) 1X Passive Lysis Buffer (PLB) for 15 m at RT with shaking. Lysates were collected and 20 μL of each were dispensed into each well of a black, flat-bottom 96-well plate (Corning). Luminescence was measured on a FLUOStar Omega plate reader (BMG Labtech) using the following workflow: dispense 100 μL Luciferase Assay Buffer II reagent,

wait 1 s, measure firefly luminescence in half-second intervals for 12 s, dispense 100 µL Stop & Glo reagent, wait 1 s, and measure renilla luminescence in half-second intervals for 12 s. Firefly luminescence and renilla luminescence reads over the 12 s measurements were summed up individually, and then total firefly luminescence was normalized to total renilla luminescence. At least three technical and biological replicates (n=3) were performed for each condition. Luminescence values of the experimental samples were normalized to the sample controls, as indicated.

2.9 Statistical analysis

All values are reported as means ± standard deviation (SD) from at least three independent experiments. Statistical analyses were performed using student's t-test, one-way ANOVA, or two-way ANOVA, as indicated, using GraphPad Prism v8 (GraphPad Software, Inc). * p<0.05, ** p<0.01, *** p<0.001 **** p<0.0001.

Table 2.1. siRNA sequences used in hnRNP A2/B1 knockdown experiments.

siRNA	Catalog No.	Sequence
siGENOME non-targeting siRNA pool #1	D-001206-13	5'- UAGCGACUAAACACAUCAA -3'
		5'- UAGCGACUAAACACAUCAA -3'
		5'- AUGUAUUGGCCUGUAUUAG -3'
		5'- AUGAACGUGAAUUGCUCAA -3'
siGENOME hnRNP A2/B1 siRNA pool	M-011690-01	5'- GGAGAGUAGUUGAGCCAAA -3'
		5'- GUUCAGAGUUCUAGGAGUG -3'
		5'- GAACAAUGGGGAAAGCUUA -3'
		5'- GCAAGACCUCAUUCAAUUG -3'
siGENOME hnRNP A2/B1-exon 2 siRNA	Custom	5'- CUUUAGAAACUGUUCCUUUUU -3'

Table 2.2. Primer sequences used in sequencing the pSF-6xHis-GFP-TEV-hnRNP A2/B1 isoform plasmid constructs.

Primers	Sequence
hnRNP A2/B1 R1	5'- AGCCATGGCAGCATCAAC -3'
hnRNP A2/B1 F1	5'- TAATGAGGGATCCTGCAAGC -3'
hnRNP A2/B1 F2	5'- AAAGAAGATACTGAGGAACATCACC -3'
hnRNP A2/B1 F4	5'- CTTTGGTGGTAGCAGGAACA -3'
hnRNP A2/B1 R4	5'- ACCCTGGTTGCCATATCCA -3'

Table 2.3. Antibodies used in Western blotting experiments.

Antibody	Catalog No.	Company	Dilution
hnRNP A2/B1	R4653-200UL	Sigma-Aldrich	1:1000
CTPS2	ab196016	Abcam	1:10,000
ATP7A	sc-376467	Santa Cruz	1:1000
GFP	ab290	Abcam	1:5000
α-Tubulin	T6199	Sigma	1:1000
Sheep anti-mouse IgG-HRP	AC111P	Sigma-Aldrich	1:5000
Goat anti-rabbit IgG-HRP	sc-2004	Santa Cruz	1:5000

Table 2.4. Primer sequences used in qRT-PCR experiments.

Primers	Sequence
hS18 F	5'-CTGCCATTAAGGGTGTGG-3'
hS18 R	5'-TCCATCCTTTACATCCTTCTG-3'
hnRNP A2/B1_exon 2 F	5'-AACTTTAGAAACTGTTCCTTTGG-3'
hnRNP A2/B1_exon 2 R	5'-CAGTCTGTAAGCTTTCCCCAT-3'
hnRNP A2/B1_exon 9 F	5'-CAATTTTGGAGGTAGCCCTG-3'
hnRNP A2/B1_exon 9 R	5'-CTCCATAGTTGTCATAACCACC-3'
hnRNP A2/B1_exon 1_3 F	5'-CGATGGAGAGAGAAAAGGAAC-3'
hnRNP A2/B1_exon 1_3 R	5'-GCTTTCCCCATTGCTCATAG-3'
ATP7A F	5'-ATTGATGACATGGGCTTTGA-3'
ATP7A R	5'-GCAATGTGCTTTGGATATGG-3'
ATP7B F	5'-AGGAGCCCTGTGACATTCTT-3'
ATP7B R	5'-TTGCTCTTTGCCAAGTGTTC-3'
Ctr1 F	5'-GACCAAATGGAACCATCCTT-3'
Ctr1 R	5'-ATGACCACCTGGATGATGTG-3'
SOD1 F	5'-TGAAGAGAGGCATGTTGGAG-3'
SOD1 R	5'-ATGATGCAATGGTCTCCTGA-3'

Table 2.5. Antibodies used in immunofluorescence experiments.

Antibody	Catalog No.	Company	Dilution
ATP7A	sc-376467	Santa Cruz	1:200
GFP	ab290	Abcam	1:200
TGN46	GTX74290	Genetex	1:200
LAMP1	ab25245	Abcam	1:200
G3BP1	A14836	Abclonal	1:200
Dcp2	A8282	Abclonal	1:200
DDX20	A5817	Abclonal	1:200
AlexaFluor 488 donkey anti-mouse	A-21202	Thermo Fisher	1:500
AlexaFluor 488 donkey anti-rabbit	A-21206	Thermo Fisher	1:500
AlexaFluor 568 donkey anti-sheep	A-21099	Thermo Fisher	1:500
AlexaFluor 647 donkey anti-sheep	A-21448	Thermo Fisher	1:500

3 Heterogeneous nuclear ribonucleoprotein A2/B1 regulates the abundance of the copper-transporter ATP7A in an isoform-dependent manner

3.1 Introduction

Copper (Cu) is an essential cofactor of enzymes involved in key physiological processes, including respiration, antioxidant defense, neurotransmitter production, and myelination (2,8,111). Misbalance of Cu is observed in several human diseases. Menkes disease and Wilson disease are classic examples of disorders in which patients have Cu deficiency or accumulation, respectively. Perturbations in Cu balance are also found in patients with cancer and Alzheimer's, Parkinson's, and non-alcoholic fatty liver diseases (7,13,480). In cells, Cu levels are tightly regulated through a network of Cu-binding and Cu-transporting proteins (8). ATP7A is a ubiquitously expressed mammalian Cu-transporting P_{1B}-type ATPase that is central for regulation of cellular Cu levels. It is essential for dietary Cu uptake and activation of most Cu-dependent enzymes within the secretory pathway, and the loss of ATP7A expression or function is associated with Menkes disease (105,481). ATP7A is localized to the *trans*-Golgi network (TGN), and when intracellular Cu levels exceed cellular needs, it traffics to vesicles and then to the basolateral membrane of the cell to excrete the excess Cu from the cell (8).

Cu homeostasis and the associated Cu-handling proteins, including ATP7A, are regulated at several levels. Post-translational regulation of Cu homeostasis has been extensively characterized. One example is the modulation of cellular Cu levels through changes in the intracellular localization of ATP7A, which is controlled via kinase-mediated phosphorylation and depends on various stimuli (151). Much less is known about the mechanisms by which Cu homeostasis is regulated post-transcriptionally and the *trans*-acting factors involved. The 3'

untranslated region (UTR) of ATP7A is 3.8 kb long—nearly as long as the 4.5 kb coding region—and there is evidence to suggest that there are several versions of *ATP7A* transcripts that differ in the length of their 3' UTRs (250). Alternative splicing of the Cu-transporters ATP7A and ATP7B as well as the Cu/Zn superoxide dismutase (SOD1) have been reported, but the mechanisms remain unknown (245,249,255,482). More recent studies have shown that regulation of ATP7A also occurs at the 3' UTR of *ATP7A* transcripts (250,265,483).

Heterogeneous nuclear ribonuclear proteins (hnRNP) are a large family of RNA-binding proteins involved in mRNA splicing, trafficking, and stability. Studies in the mouse model of Wilson disease found that intracellular Cu accumulation increases the abundance of a specific isoform of hnRNP A2/B1 and causes nuclear-cytosolic shuttling of several other RNA-binding proteins (268). Whether any of the hnRNP A2/B1 isoforms in return affect Cu homeostasis and regulate the Cu transport machinery was unknown. In this study, we addressed this question and found that hnRNP A2/B1 modulates ATP7A mRNA and protein abundance in HeLa cells via the *ATP7A* 3' UTR. We characterized the effects of the four known hnRNP A2/B1 isoforms on ATP7A and found that the hnRNP A2/B1-dependent regulation of ATP7A abundance is associated with changes in intracellular Cu levels.

3.2 Downregulation of hnRNP A2/B1 decreases Cu content in HeLa cells

hnRNP A2/B1 has four distinct isoforms that arise from the alternative splicing of exons 2 and 9 and are differentially expressed depending on cell-type and cell cycle stage (429,484). The finding by Burkhead, et al. that one or both of the exon 2-containing B-isoforms of hnRNP A2/B1 were enriched in hepatic nuclei in response to Cu accumulation (268) raised the possibility that these isoforms are Cu-sensitive. Inspection of the amino acid (AA) sequences of the alternatively spliced exons 2 and 9 (**Figure 3.1 A**) showed that neither of the two exons encode AA residues typically found in Cu-binding sites, such as Cys, Met, and His. The 12-AA long exon 2 contains

several charged residues, while the 39-AA long exon 9 consists largely of Gly residues, characteristic of a Gly-rich domain common to hnRNPs. Consequently, to examine whether hnRNP A2/B1 regulates Cu homeostasis, we first took advantage of the dataset generated in our earlier study (269). In this work, genome-wide siRNA-mediated knockdown in HeLa cells followed by inductively coupled plasma mass spectrometry (ICP-MS) analysis of metal content identified proteins specifically involved in the homeostasis of Se, Cu, Fe, or Zn (269). By examining the dataset generated in that study, we found that Cu concentration in cells with hnRNP A2/B1 downregulated was significantly lower than that in the control cells by approximately four standard deviations from the mean (**Figure 3.1 B**). These data, along with the previous work by Burkhead et al., suggested that hnRNP A2/B1 expression and cellular Cu levels are somehow linked.

To verify that downregulation of hnRNP A2/B1 affects cellular Cu content and to determine whether this effect is isoform-specific, we downregulated hnRNP A2/B1 in HeLa cells using siRNA against all four hnRNP A2/B1 isoforms (A2B1-T) or against only the exon 2-containing B isoforms (A2B1-e2). A non-targeting (NT) siRNA was used as a control. Following hnRNP A2/B1 downregulation, atomic absorption spectrometry (AAS) was conducted to measure cellular Cu content. As seen in **Figure 3.2 A**, Cu content was decreased by 38% in A2B1-T cells (26.28 ± 4.47 pmol Cu/mg protein) and by 44% in A2B1-e2 cells (23.94 ± 3.36 pmol Cu/mg protein) compared to the NT control (42.81 ± 10.71 pmol Cu/mg protein). The similar decrease in cellular Cu levels by total and isoform-specific siRNA suggested that the B-isoforms could be primarily responsible for this effect.

To verify that both the A- and B-isoforms were downregulated in the total knockdown, we performed qPCR (**Figure 3.2 B**). The mRNA levels of all the hnRNP A2/B1 isoforms were significantly decreased in the A2B1-T cells, with a 71% decrease for the exon 2 probe, an 86% decrease for the exon 9 probe, and a 90% decrease for the exon 1_3 probe compared to the NT control (0.29 ± 0.15 a.u., 0.13 ± 0.08 a.u., and 0.11 ± 0.08 a.u., respectively). Moreover, in the

A2B1-e2 cells, the mRNA levels of the B-isoforms were 87% lower than in the NT control (0.13 ± 0.04 a.u.), whereas those of the A-isoforms were unchanged as measured by the exon 9 and exon 1_3 probes (0.90 ± 0.14 a.u. and 0.99 ±0.35 a.u., respectively).

Western blot analysis of cell homogenates revealed two distinct hnRNP A2/B1 protein bands, one at approximately 40 kDa, roughly corresponding to isoform B1, and a second at approximately 35 kDa, roughly corresponding to isoform A2 (**Figure 3.2 C**, indicated by black arrows). As seen in **Figure 3.2 D**, both bands are significantly diminished in A2B1-T cells, with the upper band decreased by 84% and the lower by 76% compared to the NT control (0.16 ± 0.12 a.u. and 0.24 ± 0.21 a.u., respectively). A2B1-e2 cells, on the other hand, had a marked decrease in only the upper band (76%, 0.24 ± 0.01 a.u.), while the lower band was unchanged compared to the NT control (1.03 ± 0.16 a.u.). Taken together, these data indicate that the downregulation of the isoforms was successful, and that the B isoforms alone may be sufficient to induce the observed decrease in cellular Cu.

Cellular Cu content depends on Cu uptake, mediated by the high-affinity Cu transporter Ctr1, and Cu efflux carried by the Cu-transporting ATPases ATP7A and ATP7B. In addition, SOD1 is a very abundant Cu-containing protein that contributes to total cellular Cu. To identify which Cu-handling proteins are affected by hnRNP A2/B1 and which could contribute to the decrease in Cu content, mRNA levels of ATP7A, ATP7B, Ctr1, and SOD1 were measured in control cells and in cells with hnRNP A2/B1 downregulated (**Figure 3.2 B**). When compared to control, both A2B1-T and A2B1-e2 cells showed no significant changes in ATP7B mRNA levels (1.13 ± 0.44 a.u. and 1.07 ± 0.33, respectively) or SOD1 mRNA levels (1.26 ± 0.21 a.u. and 0.78 ± 0.26 a.u., respectively). By contrast, both Ctr1 and ATP7A mRNA levels were upregulated in response to hnRNPA2/B1 downregulation. The Ctr1 transcript was upregulated 2.20-fold in A2B1-T cells and 1.67-fold in A2B1-e2 cells (2.19 ± 0.93 a.u. and 1.67 ± 0.44 a.u., respectively) compared to control, while ATP7A mRNA was upregulated 2.42-fold and 1.80-fold (2.42 ± 0.55 a.u. and 1.80 ± 0.67 a.u.,

respectively). To determine whether the increase in ATP7A mRNA carried over to protein levels, Western blot analysis was performed and revealed a 1.88-fold increase in ATP7A protein abundance in A2B1-T cells (1.88 ± 0.27 a.u.) and a 2.13-fold increase in A2B1-e2 cells (2.13 ± 0.35 a.u.) compared to control cells treated with NT. These results demonstrate that hnRNP A2/B1, particularly the B-isoforms, mediate Cu levels in HeLa cells through the regulation of ATP7A and Ctr1 abundance. Given that the total effect was a decrease in cellular Cu content, which would not occur if Ctr1 import activity exceeds ATP7A efflux activity, we surmised that ATP7A plays a larger role in this phenotype and focused our attention on ATP7A.

3.3 hnRNP A2/B1 downregulation in HeLa cells does not affect ATP7A trafficking in response to elevated Cu

One of the ways in which ATP7A maintains cellular Cu homeostasis is through the export of excess Cu, a process in which ATP7A traffics from the TGN to release Cu at the cell surface membrane (8). Under basal or low Cu conditions, ATP7A is mainly localized to the TGN, whereas under high Cu conditions, ATP7A localizes to vesicles. The loss of co-localization between ATP7A and a TGN marker can therefore be used as a means to qualitatively assess ATP7A trafficking in response to Cu.

Since Ctr1 levels—and, presumably, Cu uptake—were upregulated, it is possible that, in addition to the increase in ATP7A abundance, the decrease in Cu content observed upon hnRNP A2/B1 downregulation in HeLa cells could be due in part to enhanced ATP7A trafficking. To test this, the trafficking of ATP7A in response to Cu was monitored in cells in which either total (A2B1-T) or exon 2-containing isoforms (A2B1-e2) of hnRNP A2/B1 were downregulated and compared to that observed in control cells in which either no (no siRNA) or NT siRNA was transfected (**Figure 3.3**). In both controls (no siRNA and NT siRNA), ATP7A trafficked normally: high levels of co-localization (as evidenced by white signal) between ATP7A (green signal) and the TGN marker,

TGN46 (magenta signal), was observed at basal levels of Cu. The co-localization gradually decreases as time of exposure to elevated Cu increased, with the punctate ATP7A staining indicative of vesicular localization at higher Cu conditions. This was also the case in both the A2B1-T and A2B1-e2 cells, in which ATP7A localized largely to the TGN at basal Cu levels in the medium and moved into vesicles as Cu increased. These data show that hnRNP A2/B1 downregulation in HeLa cells does not impact ATP7A targeting to the TGN in basal medium nor significantly alter trafficking in response to Cu. Thus, the observed decrease in cellular Cu upon downregulation is predominantly due to the increase in ATP7A abundance.

3.4 hnRNP A2/B1-mediated regulation of ATP7A involves the ATP7A 3' UTR

A recent study showed that hnRNP A2/B1 was involved in the regulation of a large number of transcripts through interaction with an 8-nucleotide (nt) motif present in their 3' UTRs (367). Notably, hnRNP A2/B1 binding at this site resulted in the eventual decay of the target transcripts, whereas downregulation of hnRNP A2/B1 increased transcript levels. Since, in our studies, the downregulation of hnRNP A2/B1 increases ATP7A mRNA abundance, we examined whether the ATP7A transcript has a predicted binding site for hnRNP A2/B1. Analysis of the mRNA sequence of ATP7A revealed the presence of one copy of this motif near the proximal end of its 3' UTR (**Figure 3.4**).

To test whether the 3' UTR is in fact involved in the hnRNP A2/B1-mediated regulation of ATP7A in HeLa cells, control cells (transfected with NT siRNA) and cells with downregulated hnRNP A2/B1 (both A2B1-T and A2B1-e2 cells) were subsequently transfected with a plasmid containing firefly luciferase-tagged ATP7A 3' UTR and a plasmid encoding Renilla-luciferase. The abundance of the ATP7A 3'-UTR transcript was quantified through firefly luciferase luminescence and was normalized to Renilla luciferase luminescence used as a control. We predicted that luminescence would increase in cells with hnRNP A2/B1 downregulation compared to the control

if the 3' UTR is involved in hnRNP A2/B1-mediated regulation of ATP7A. If the 3' UTR is not involved, luminescence would not differ between the cells with hnRNP A2/B1 downregulated and the control. As seen in **Figure 3.5**, firefly luminescence increases in cells with total hnRNP A2/B1 downregulation and in cells with exon 2-specific hnRNP A2/B1 downregulation. A2B1-T cells had a 2.40-fold increase in ATP7A 3'UTR abundance (2.40 ± 0.15 a.u.) and A2B1-e2 cells had a 3.19-fold increase in abundance (3.19 ± 0.62 a.u.) compared to NT. These results indicate that the 3' UTR of ATP7A mRNA plays a role in the hnRNP A2/B1-mediated regulation of ATP7A abundance, and that the B-isoforms are likely to be the main isoforms involved in this process.

3.5 Overexpression of hnRNP A2/B1 isoforms results in a decrease in ATP7A 3'UTR expression

To test whether hnRNP A2/B1 overexpression would have an opposite effect, i.e., would *decrease* ATP7A expression, expression constructs for each of the four hnRNP A2/B1 were generated. The isoforms were inserted into a vector containing a 6x His-tag, a GFP tag, and a TEV cleavage site at the N-terminus (HGT vector) to allow for a broader range of future experimental applications. Expression of these constructs in HeLa cells was confirmed by the presence of green GFP signal in transfected cells (**Figure 3.6 A)** and the absence of the signal in non-transfected cells. Despite identical transfection/expression conditions, the relative abundance and localization of hnRNP A2/B1 differed. A2b and B1 isoforms were targeted primarily to the nucleus, whereas A2 and B1b isoform were seen mostly in the cytosol.

Western blot analysis of cell lysates (**Figure 3.6 B**) revealed at least five distinct bands that stained with anti-GFP antibody. No GFP signal was seen in control mock-transfected cells, as expected. The expected sizes of the HGT-hnRNP A2/B1 isoform proteins range from 60–65 kDa, and the bands in each lane most closely corresponding to this size are indicated by black arrow. These bands were used for quantification (**Figure 3.6 C**). The B1 isoform was expressed at the

lowest level, with only a modest increase (1.57 ± 0.21 a.u.) compared to the control (neg). The A2, A2b, and B1b isoform expression levels were all 3–4-fold higher compared to the control (3.97 ± 1.02 a.u., 3.85 ± 0.97 a.u., and 3.43 ± 1.12 a.u., respectively.) Analysis of ATP7A protein abundance showed that overexpression of the A2 and A2b isoforms resulted in a significant decrease of ATP7A (0.60 ± 0.13 a.u. and 0.64 ± 0.30 a.u., respectively), whereas overexpression of the B1b isoform resulted in a more modest decrease (0.85 ±0.35 a.u.) and the B1 isoform in no change (1.04 ± 0.19 a.u.) compared to the control.

We then tested how hnRNP A2/B1 isoform overexpression in cells impacts the abundance of ATP7A 3' UTR. Dual-luciferase assay (**Figure 3.7**) showed that overexpression of any of the hnRNP A2/B1 isoforms resulted in a significant decrease in ATP7A 3'UTR abundance: overexpression of A2 resulted in a 47% luminescence intensity (0.47 ± 0.07 a.u.), A2b in a 40% intensity (0.40 ± 0.07 a.u.), B1 in a 47% intensity (0.47 ± 0.05), and B1b in a 33% intensity (0.33 ± 0.02 a.u.) compared to luciferase signal in cells expressing the empty HGT vector. These results indicate that the overexpression of the hnRNP A2/B1 isoforms results in a decrease of the ATP7A 3'UTR transcript. The lack of a strong correlation between changes in the abundance of ATP7A 3'UTR and the abundance of the ATP7A protein suggests a role for the ATP7A coding portion of the transcript in the hnRNP A2/B1-dependent regulation of ATP7A mRNA and/or the presence of additional factors.

3.6 ATP7A increases as hnRNP A2/B1 decreases during the differentiation of SH-SY5Y neuronal cells

While the data thus far made it clear that hnRNP A2/B1 directly or indirectly affects the ATP7A transcript in HeLa cells, it was less clear whether this regulatory relationship would occur in other cellular contexts or whether it plays a role in key cellular processes. Published reports indicate that expression of both ATP7A and hnRNP A2/B1 are responsive to retinoic acid (RA), with

ATP7A expression increasing in response to RA treatment and hnRNP A2/B1 expression decreasing in response to RA treatment (177,479,485). Moreover, RA is known to induce neuronal differentiation (479). To determine whether hnRNP A2/B1-mediated regulation of ATP7A occurred during neuronal differentiation, SH-SY5Y neuronal cells were fully differentiated via RA and brain-derived neurotrophic factor (BDNF) treatments (**Figure 3.8 A**). Cells were collected at four different points along the differentiation process: before differentiation (ND), after 2-days of RA treatment (D2), after 4-days of RA treatment with the growth medium changed every 2 days (D4), and after 4 days of RA treatment plus one 3-day of BDNF treatment (D7). During this process the SH-SY5Y cells undergo morphological changes, with branched neurites starting to form at D2 and having fully developed at D7 (**Figure 3.8 B**).

As in HeLa cells, qRT-PCR and Western blotting were used to quantify mRNA and protein levels of both ATP7A and hnRNP A2/B1. The mRNA levels of the exon 2-containing hnRNP A2/B1 isoforms decrease significantly over the course of differentiation (**Figure 3.9 A**), with an approximately 30–40% decrease at D2 and D4 (0.73 ± 0.11 a.u. and 0.62 ± 0.02 a.u., respectively) and an 80% decrease at D7 (0.80 ± 0.04 a.u.) compared to NT control values, taken as 1. The mRNA levels of the exon 9-containing isoforms also decreased at D2 and D4 compared to the ND control, although more modestly (0.81 ± 0.03 a.u. for D2, 0.71 ± 0.06 a.u. for D4). Unlike the exon 2-containing isoforms, the abundance of mRNA for exon 9-containing isoform was elevated at D7 (1.27 ± 0.22 a.u. compared to the ND control). The protein abundance of hnRNP A2/B1 showed partial agreement with the mRNA changes. Specifically, Western blotting detected two distinct hnRNP A2/B1 bands (**Figure 3.9 B**, indicated in black arrows). Quantification using densitometry (**Figure 3.9 C**) revealed that the upper band decreased significantly over the course of differentiation compared to ND (0.44 ± 0.09 a.u. at D2, 0.60 ± 0.26 a.u. at D4, and 0.12 ± 0.04 a.u. at D7), while the lower band was unchanged compared to ND at D2 and D4 (1.02 ± 0.37 a.u. and 1.00 ± 0.41 a.u., respectively) and decreased at D7 (0.12 ± 0.39 a.u.). These data indicate

that hnRNP A2/B1 expression does change over the course of differentiation, and that these changes are well in line with previous studies showing that hnRNP A2/B1 is a RA-responsive gene.

ATP7A mRNA levels, by contrast, significantly increase over the course of differentiation (**Figure 3.9 A**). This increase corresponded to RA treatment, with ATP7A mRNA levels at D2 7.61-fold higher and levels at D4 7.87-fold higher than control (7.61 ± 2.11 a.u. and 7.87 ± 2.45 a.u., respectively), and unchanged compared to control at D7 (1.11 ± 0.28 a.u.) ATP7A protein levels (**Figure 3.9 B, C**) followed suit, with an 8.51-fold increase (8.51 ± 0.74 a.u.) at D2, an 8.39-fold increase (8.39 ± 3.51 a.u.) at D4, and a 4.96-fold increase (4.96 ± 0.91 a.u.) at D7, all compared to ND control. These data show that ATP7A expression increases over the course of neuronal differentiation, concurrent with hnRNP A2/B1 decrease.

To determine whether cellular Cu content also decreased in cells over the course of differentiation, AAS was used to measure Cu at each collected point (**Figure 3.10 A**). Cu levels dropped significantly over the course of differentiation, decreasing by 65% at D2 (6.60 ± 2.77 pmol Cu/mg protein), 81% at D4 (3.55 ± 2.37 pmol Cu/mg protein), and 53% at D7 (8.80 ± 3.15 pmol Cu/mg protein) compared to ND control (18.79 ± 9.01 pmol Cu/mg protein). Analysis of ATP7A trafficking at each of these points (**Figure 3.10 B**) revealed trafficking patterns consistent with Cu levels: more vesicular staining of ATP7A (in green) when Cu is higher in ND cells and more co-localization with TGN46 (in pink, co-localization in white) when Cu is lower at D2, D4, and D7. Taken together, these data show that hnRNP A2/B1 decreases and ATP7A increases during the course of neuronal differentiation, and these changes correspond to a decrease in available cellular Cu in SH-SY5Y cells.

In summary, the observed decrease in Cu levels upon hnRNP A2/B1 downregulation in HeLa cells is due to the consequent upregulation of ATP7A, one of the functions of which is to traffic

Cu out of cells. This upregulation of ATP7A is induced in full by the downregulation of only the exon 2-containing B1-isoforms, and this hnRNP A2/B1-mediated regulation involves the 3' UTR of ATP7A. Both ATP7A and hnRNP A2/B1 are RA-responsive genes whose expression levels change in opposite ways during neuronal differentiation—i.e., ATP7A expression increases concurrently with hnRNP A2/B1 decrease, resulting in lower cellular Cu levels.

3.7 Discussion

Cu balance is crucial to mammalian health and development, and to ensure that Cu homeostasis is maintained, highly-coordinated and tightly-regulated cellular mechanisms have evolved. While the post-translational regulation of key Cu machinery proteins is well-understood, the full scope of regulatory mechanisms governing cellular Cu homeostasis remains unknown, with relatively few studies investigating the post-transcriptional regulation of Cu. Here, a novel regulator of cellular Cu content, hnRNP A2/B1, was identified and shown to impact Cu levels in HeLa cells through regulation of the expression of the Cu-transporter ATP7A.

hnRNP A2/B1 is a well-characterized RNA-binding protein with four distinct isoforms that arise from the alternative splicing of exons 2 and 9. These isoforms are differentially expressed according to a number of factors, including tissue-type and cell cycle stage (429,484). Despite the abundance of research regarding hnRNP A2/B1, most studies do not consider these four isoforms separately and so do not explore the possibility of isoform-specific functions or effects. The finding by Burkhead, et al. that one or both of the exon 2-containing B-isoforms of hnRNP A2/B1 were specifically enriched in hepatic nuclei in response to Cu accumulation raised the possibility that these isoforms were Cu-sensitive by virtue of exon 2 inclusion (268). We show that downregulation of these two isoforms was sufficient to induce the decrease in cellular Cu, suggesting that the B-isoforms are largely responsible for this result. Moreover, downregulation of the B-isoforms alone produced the same magnitude of upregulation of ATP7A mRNA and

protein abundance as did the total downregulation, providing further proof that the inclusion of exon 2 in these isoforms leads to their Cu-responsiveness.

hnRNP A2/B1-mediated regulation of mRNA occurs in many forms—e.g., expression of different isoforms via alternative splicing, localization-dependent translation via mRNA trafficking, and maintenance of mRNA abundance via transcript stabilization/degradation (367,380,429,447,448,464,486). Geissler, et al. characterized an hnRNP A2/B1-mediated regulatory mechanism in which hnRNP A2/B1 binds to a specific 8-nt motif (UAA[G/C]UUAU) in the 3' UTR of transcripts, leading to their destabilization via CCR4-NOT-directed deadenylation and subsequent decay (367). ATP7A mRNA has a long 3' UTR, the functional significance of which is incompletely understood, although recent studies have identified mechanisms by which changes in the length of the 3' UTR may be involved in the regulation of ATP7A abundance (250,483). Our work provides additional information about the role of this region. Sequence analysis of the ATP7A 3' UTR revealed one copy of the UAAGUUAU motif at the proximal end of the UTR. Expression of a luciferase-tagged ATP7A 3' UTR construct in cells in which either all or only the B-isoforms of hnRNP A2/B1 were downregulated demonstrated that not only is the 3' UTR of ATP7A involved in hnRNP A2/B1-mediated regulation, but also that the B-isoforms likely play the main role in this regulation.

The data show that there is an inverse relationship between hnRNP A2/B1 and ATP7A abundance—in this case, when hnRNP A2/B1 levels decrease, ATP7A levels increase. However, when hnRNP A2/B1 abundance increased, ATP7A abundance decreased only slightly, and only in cells overexpressing the A-isoforms, which showed the highest expression. This discrepancy could be due, at least in part, to the tendency of hnRNP A2/B1 to form aggregates in response to certain cellular stressors. hnRNP A2/B1 contains a prion-like low complexity domain (LCD), and previous studies have demonstrated the propensity of LCD-containing RBPs to aggregate when protein concentrations reach saturating levels or when cellular redox status changes (487,488).

This aggregation could also explain the multiple bands observed on the Western blot, as aggregates could not only decrease protein mobility but also be broken down into smaller degradation products (489). Nevertheless, there are bands at the expected size for each of the four overexpressed isoforms, and the analysis of the luciferase-tagged ATP7A 3' UTR construct revealed a marked decrease in the abundance of the ATP7A transcript. Taken together, these results indicate that hnRNP A2/B1-mediated regulation of ATP7A expression is a negative regulation (i.e., hnRNP A2/B1 and ATP7A abundances are inversely correlated) and involves the 3' UTR of the ATP7A transcript. The lack of direct correlation between the abundance of the 3' UTR and the ATP7A protein upon hnRNP A2/B1 overexpression could indicate a role for additional factors that remain to be identified.

It is well-known that hnRNP A2/B1 plays a role in cellular differentiation. Previous studies have shown that hnRNP A2/B1 is involved in the maintenance of an undifferentiated phenotype in human embryonic stem cells, and downregulation of hnRNP A2/B1 is observed during the differentiation process in several cell types (486,490). Moreover, retinoic acid (RA) induction of differentiation in human neuroblastoma SK-N-SH cells causes a significant decrease in hnRNP A2/B1 abundance, and RA treatment results in the downregulation of hnRNP A2/B1 in lung cancer cell lines (485,491). ATP7A is also a RA-responsive gene, though the effect on its expression is opposite: RA-induced differentiation in SH-SY5Y neuroblastoma cells results in an upregulation of ATP7A expression (177,479). In the developing brain, the demand for Cu increases, especially within the secretory pathway where ATP7A operates (23). Taken together, these data suggest a possible connection between the increased need for available Cu in the secretory pathway and the regulation of hnRNP A2/B1 expression levels during neuronal differentiation.

While previous studies have compared the changes in Cu levels and ATP7A expression in nondifferentiated (ND) and fully differentiated neuronal cells (479), this study takes a comparative look at four different points along the differentiation process: before differentiation (ND), after one

RA treatment (D2), after 2 RA treatments (D4), and after full differentiation (D7). It was found that ATP7A expression increased significantly at D2 and D4, which corresponds well to RA treatment, and returns to levels closer to ND by D7, which is in agreement with previous results (479). Cu levels also decreased over the course of differentiation, with the lowest levels occurring post-RA treatment, and ATP7A localization reflected these changes in Cu with higher levels of co-localization with the TGN at D4 and D4.

Monitoring of hnRNP A2/B1 mRNA shows that abundance of exon 2-containing transcripts decreases significantly over the course of differentiation, continuing to decrease even beyond RA treatment to a minimum at D7. Exon 9-containing isoforms, by contrast, decreased more modestly in response to RA treatment, and by D7 were even present at slightly higher levels compared to ND. hnRNP A2/B1 protein levels followed a similar pattern, with one higher molecular weight band decreasing significantly over the entire course of differentiation and a second lower molecular weight band remaining unchanged until D7, when it decreased compared to ND. These data show that the inverse relationship between hnRNP A2/B1 and ATP7A expression occurs during neuronal differentiation, as well as support the idea that B-isoforms are the ones mainly involved in the regulation of ATP7A expression, and subsequently, cellular Cu levels.

This study has demonstrated that hnRNP A2/B1 modulates cellular Cu levels through regulation of ATP7A expression. This process is both isoform-specific and 3’ UTR-dependent: the exon 2-containing B-isoforms of hnRNP A2/B1 drive the negative regulation of ATP7A abundance, and the ATP7A 3’ UTR is involved in the mechanism. Concurrent decrease in hnRNP A2/B1 expression and increase in ATP7A expression occurs during neuronal differentiation, and this could lead to an influx of Cu into the secretory pathway when cellular Cu needs are greatest. These results provide a basis for future studies into the finer details of the post-transcriptional regulation of Cu homeostasis, especially in the context of neuronal differentiation.

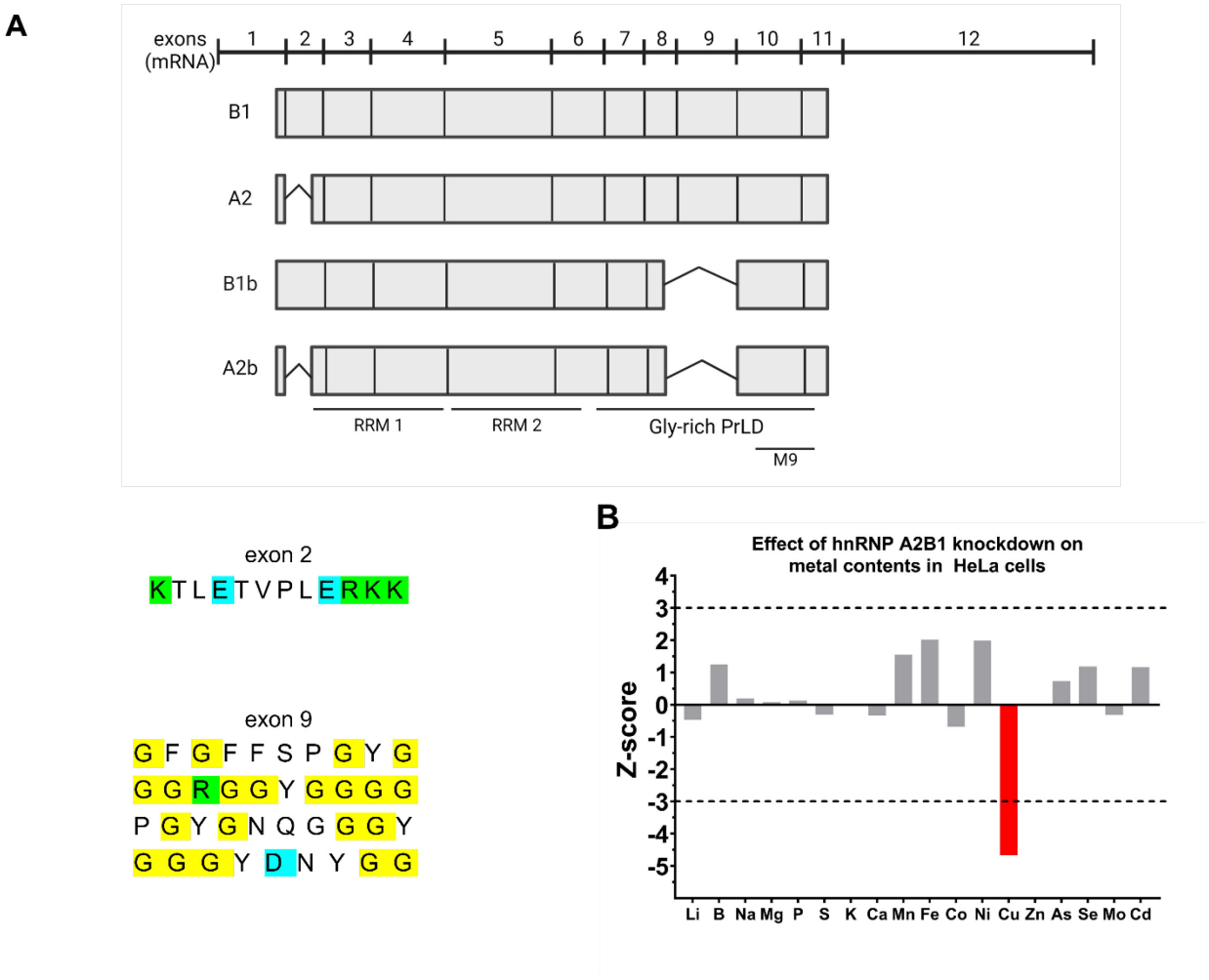

Figure 3.1. Downregulation of RNA-binding protein hnRNP A2/B1 decreases Cu content in HeLa cells.

(A) hnRNP A2/B1 has four distinct isoforms that arise from the alternative splicing of exons 2 and 9. *Top*, *domain* organization of the four hnRNP A2/B1 isoforms at the transcript-level. Alternative splicing yields four isoforms: B1, A2, B1b, and A2b. Box length is indicative of the relative size of the exon within the transcript Created with BioRender.com. *Bottom*, amino acid sequences of exons 2 and 9. Positively charged amino acids are indicated in green, negatively charged amino acids in blue, and glycines in purple. **(B)** Knockdown of hnRNP A2/B1 in HeLa cells results in a specific and significant decrease in Cu levels. hnRNP A2/B1 expression was downregulated in HeLa cells via siRNA-mediated knockdown, and inductively coupled plasma mass spectrometry (ICP-MS) was used to measure the abundance of trace metals in these cells. Z-score was calculated as the number of standard deviations from the mean signal value. A positive z-score indicates an increase in the metal content and a negative z-score a decrease (269).

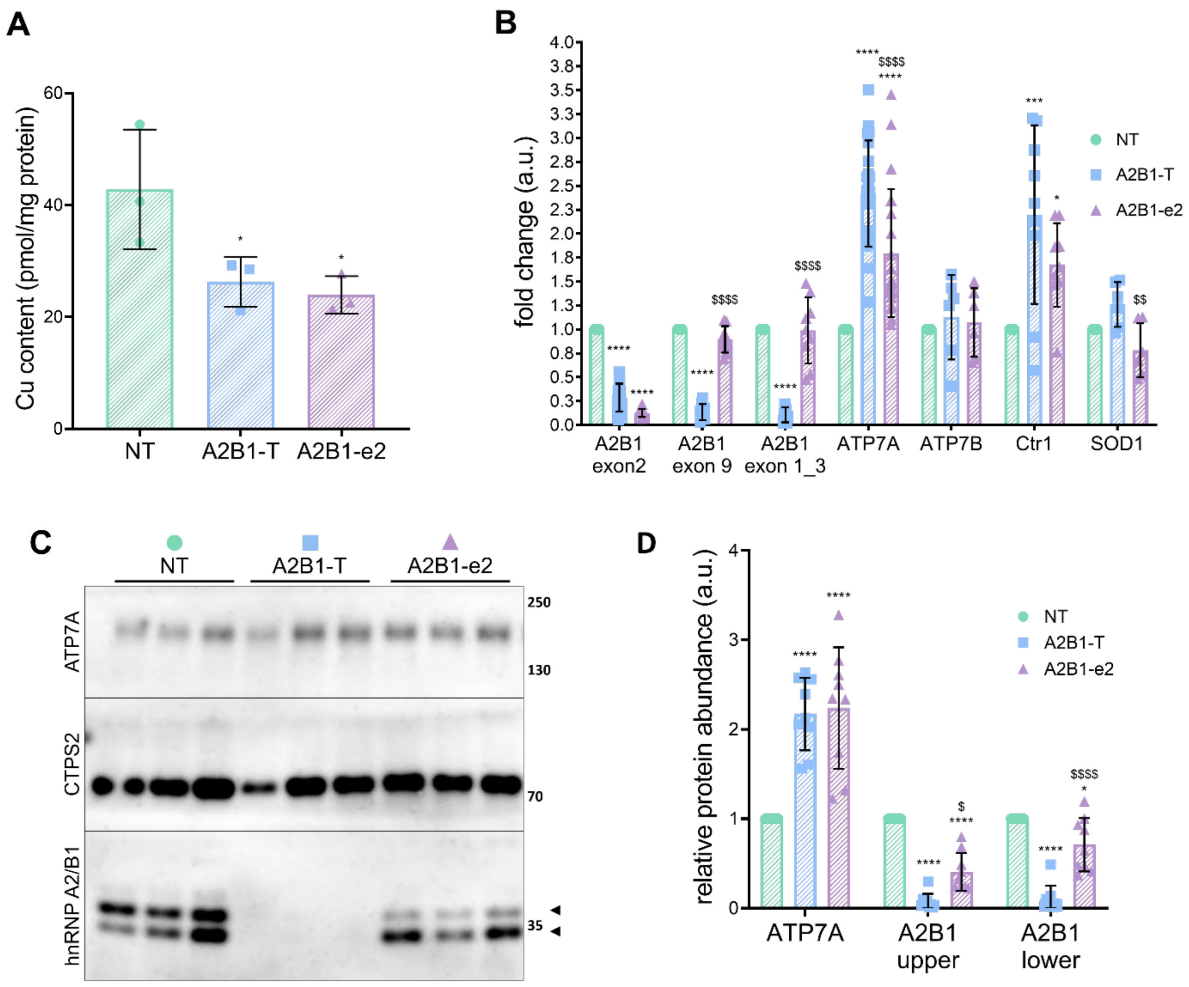

Figure 3.2. Downregulation of the hnRNP A2/B1 B-isoforms in HeLa cells results in an increase in the abundance of ATP7A.

Non-targeting (NT), all 4 isoforms (A2B1-T), and B-isoforms only (A2B1-e2) knockdown conditions were compared. **(A)** Cellular Cu levels following hnRNP A2/B1 downregulation. Values normalized to protein content and NT. *n*=3. **(B)** Changes in mRNA abundance of various Cu machinery in response to hnRNP A2/B1 downregulation. Values normalized to hS18 and NT, the values of which were taken as 1. A2B1 exon 2 *n*=15; A2B1 exon 9, A2B1 exon 1_3, and Ctr1 *n*=9; ATP7A *n*=21; ATP7B and SOD1 *n*=6. **(C, D)** Changes in hnRNP A2/B1 and ATP7A protein abundance in response to hnRNP A2/B1 downregulation. Two distinct isoforms of hnRNP A2/B1 are indicated by black arrows. Values normalized to CTPS2 and NT, the values of which were taken as 1. *n*=9. All values are reported as means ± SD. Significance was determined by two-way ANOVA; * $p<0.05$, *** $p<0.001$, **** $p<0.0001$ compared to NT and $ $p<0.05$, $$ $p<0.01$, $$$ $p<0.001$, $$$$ $p<0.0001$ compared to A2B1-T.

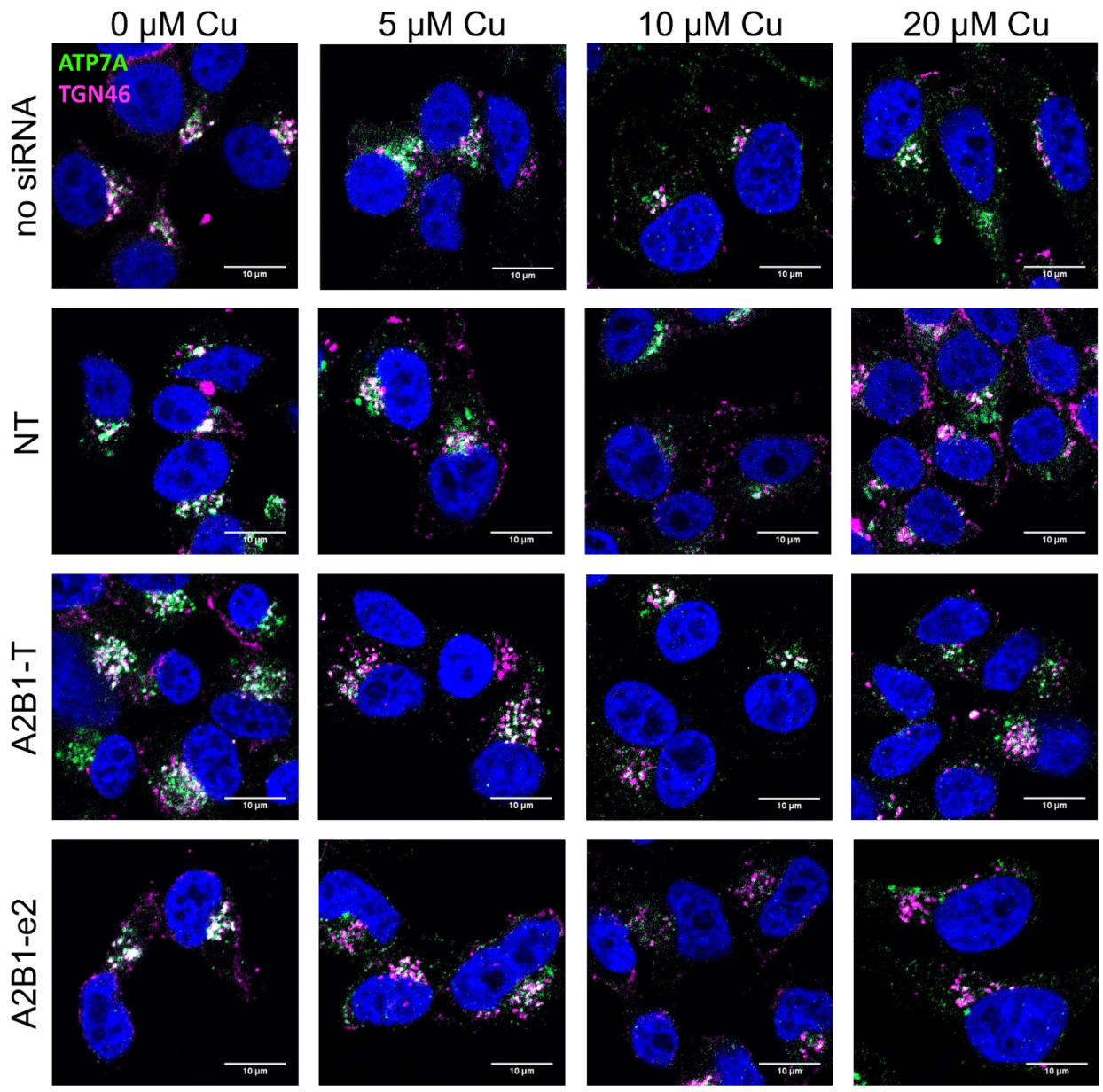

Figure 3.3. hnRNP A2/B1 downregulation in HeLa cells does not affect ATP7A trafficking in response to Cu.

No siRNA, NT, A2B1-T knockdown, and A2B1-e2 knockdown conditions were compared. Cells were treated with the indicated concentrations of Cu for 4 h. ATP7A is in green, TGN marker TGN46 in magenta, and the nucleus (DAPI) in blue. Co-localization between ATP7A and TGN46 is indicated by white coloration. *n*=3.

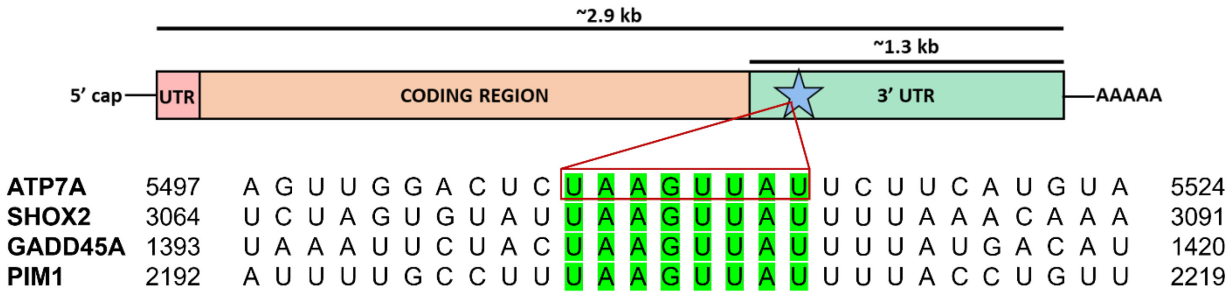

Figure 3.4. ATP7A 3' UTR contains one copy of an 8-nt motif known to direct hnRNP A2/B1-mediated decay of transcripts.

Top, cartoon representation of the ATP7A transcript with the 5' UTR indicated in pink, the coding region in orange, the 3' UTR in green, and the 8-nt motif with a blue star. Box length is indicative of the relative size of these features within the transcript. *Bottom*, aligned sequences of four transcripts, including ATP7A, that contain the 8-nt motif. The motif is highlighted in green.

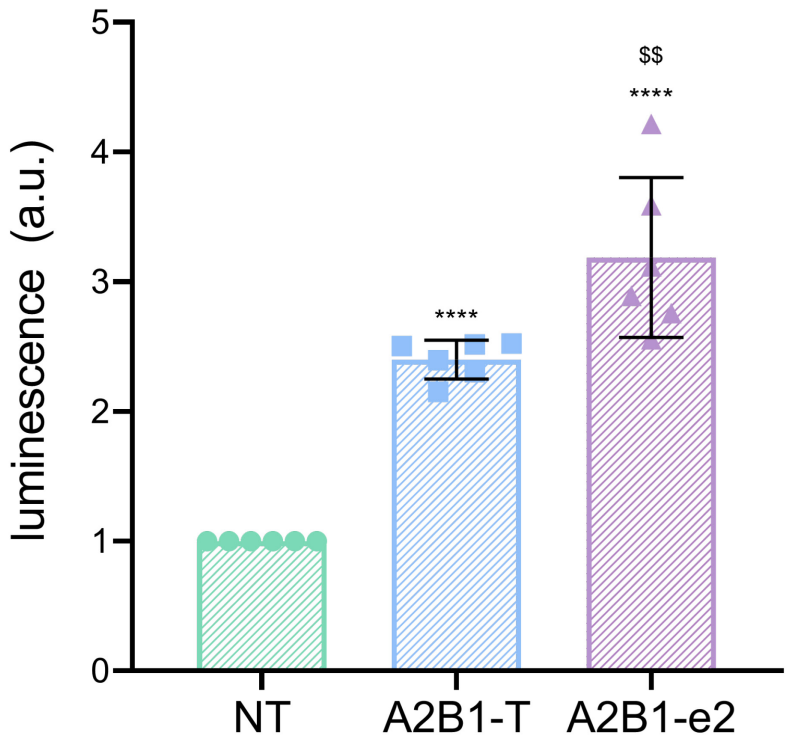

Figure 3.5. Downregulation of hnRNP A2/B1 results in an increase in the abundance of the ATP7A 3' UTR transcript.

NT, A2B1-T knockdown, and A2B1-e2 knockdown conditions were compared. Dual-luciferase assay was used to measure the luminescence of both firefly luciferase and Renilla luciferase. Values normalized to Renilla-luciferase and NT, the values of which were taken as 1. *n*=6. All values are reported as means ± SD. Significance was determined by two-way ANOVA; **** $p<0.0001$ compared to NT and $$ $p<0.01$ compared to A2B1-T.

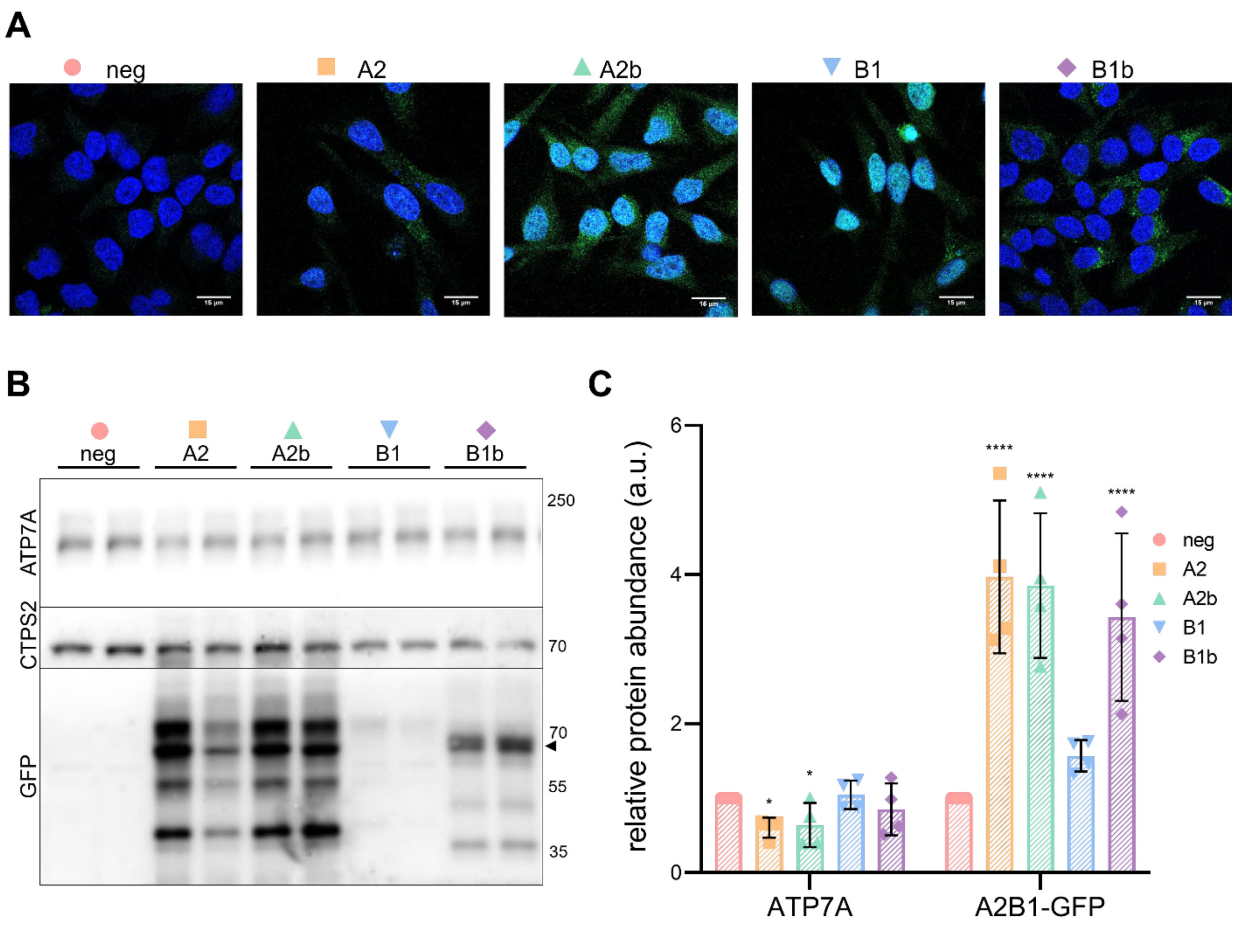

Figure 3.6. Overexpression of the 6xHis-GFP-TEV (HGT)-hnRNP A2/B1 isoforms in HeLa cells.

Cells transfected with no (neg) plasmid or the A2, A2b, B1, or B1b HGT-hnRNP A2/B1 isoform plasmids were compared. **(A)** GFP signal (green) indicating expression of the HGT-hnRNP A2/B1 isoforms in cells. **(B, C)** Protein abundance of the HGT-hnRNP A2/B1 isoforms. Suspected target hnRNP A2/B1 isoform band indicated by black arrow. Values normalized to CTPS2 and neg, the values of which were taken as 1. *n*=3. All values are reported as means ± SD. Significance was determined by two-way ANOVA; * $p<0.05$, **** $p<0.0001$ compared to neg control.

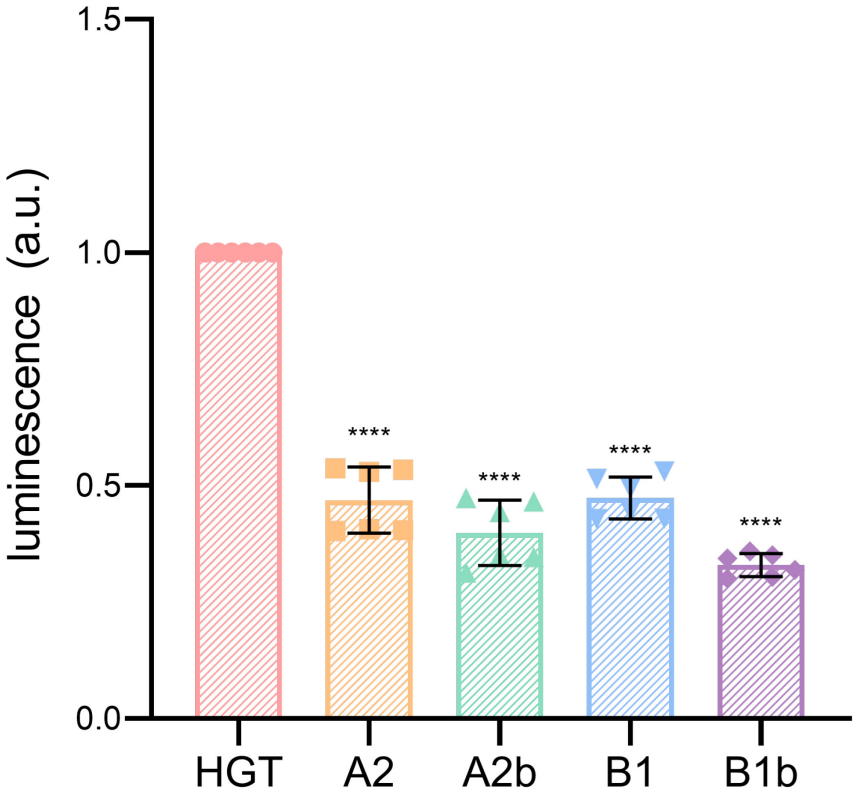

Figure 3.7. Overexpression of any of the 6xHis-GFP-TEV (HGT)-hnRNP A2/B1 isoforms results in a decrease in the abundance of the ATP7A 3' UTR transcript.

Cells transfected with the empty pSF-HGT vector (HGT) or the A2, A2b, B1, or B1b HGT-hnRNP A2/B1 isoform plasmids were compared. Dual-luciferase assay was used to measure the luminescence of both firefly luciferase and Renilla luciferase. Values normalized to Renilla-luciferase and HGT, the values of which were taken as 1. n=6. All values are reported as means ± SD. Significance was determined by two-way ANOVA; **** p<0.0001 compared to HGT control.

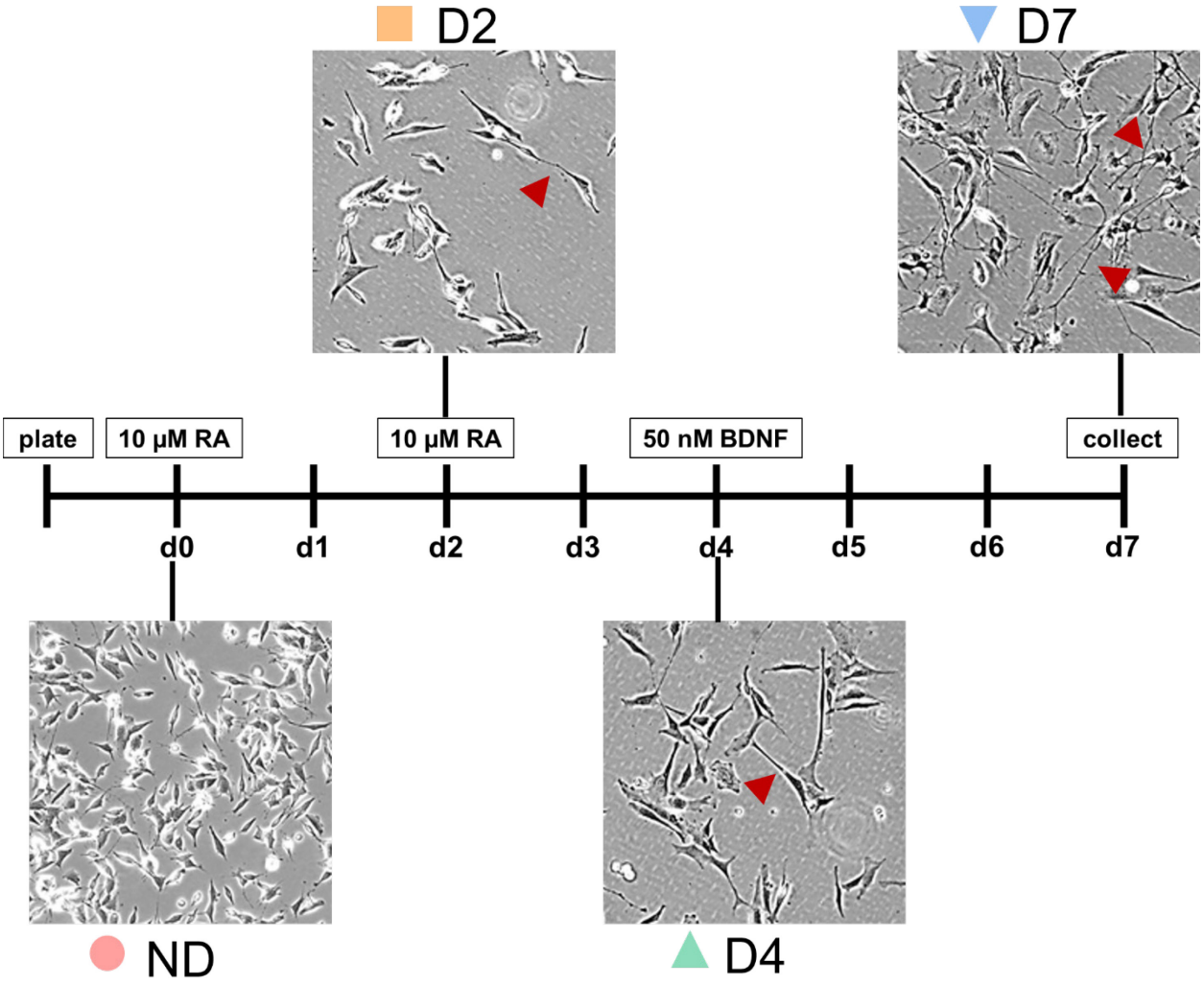

Figure 3.8. Schematic of induced differentiation in SH-SY5Y cells and accompanying morphological changes.

Retinoic acid (RA) and brain-derived neurotrophic factor (BDNF) are used to induce the differentiation of SH-SY5Y cells. SH-SY5Y neuronal glioblastoma cells were differentiated by two 2-day treatments with 10 μM RA and one 3-day treatment with BDNF. Cells were collected for analysis on days d0 (non-differentiated, ND), d2 (differentiated d2, D2), d4 (differentiated d4, D4), and d7 (differentiated d7, D7). Morphological changes in SH-SY5Y cells upon differentiation were noted, with neurites, an indication of neuronal maturation, indicated with red arrowheads.

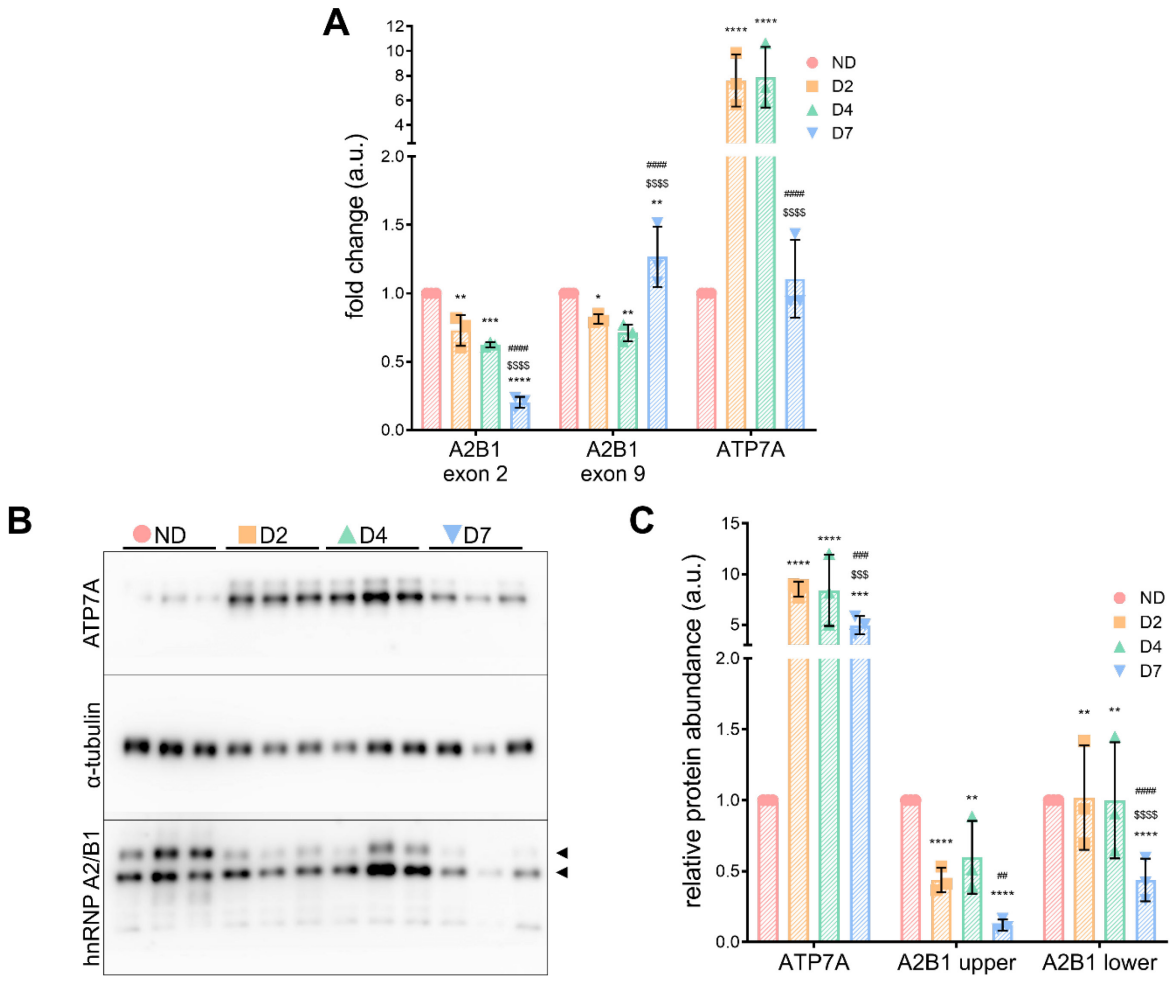

Figure 3.9. ATP7A increases and hnRNP A2/B1 decreases during neuronal differentiation in SH-SY5Y cells.

(A) ATP7A and hnRNP A2/B1 mRNA abundance during differentiation. Values normalized to hS18 and ND, the values of which were taken as 1. *n*=3. **(D, E)** ATP7A and hnRNP A2/B1 protein abundance during differentiation. Two distinct isoforms of hnRNP A2/B1 are indicated by black arrows. Values normalized to α-tubulin and ND, the values of which were taken as 1. *n*=3. All values are reported as means ± SD. Significance was determined by two-way ANOVA; * $p<0.05$, ** $p<0.01$, *** $p<0.001$, **** $p<0.0001$ compared to ND, $ $p<0.05$, $$ $p<0.01$, $$$ $p<0.001$ compared to D2, and ## $p<0.01$, #### $p<0.0001$ compared to D4.

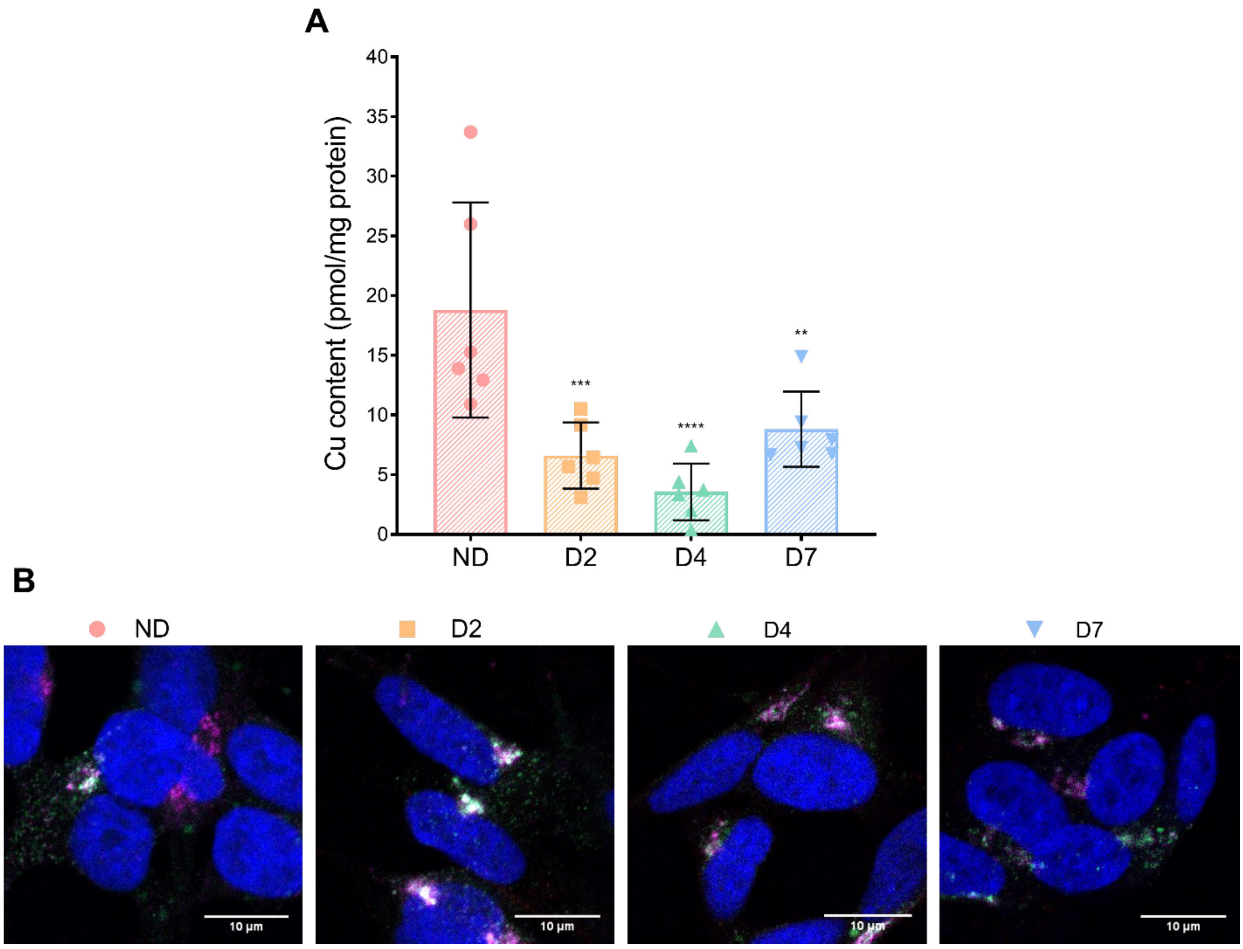

Figure 3.10. Lower levels of intracellular Cu during differentiation in SH-SY5Y cells results in TGN-localized ATP7A.

(A) Cu content decreases in SH-SY5Y cells during differentiation. Values normalized to protein content and ND. *n*=6. **(B)** ATP7A localizes mainly to the *trans*-Golgi network (TGN) during differentiation. ATP7A is in green, TGN marker TGN46 in magenta, and the nucleus (DAPI) in blue. Co-localization between ATP7A and TGN46 is indicated by white coloration. *n*=3. All values are reported as means ± SD. Significance was determined by two-way ANOVA; ** $p<0.01$, *** $p<0.001$, **** $p<0.0001$ compared to ND.

4 The nucleocytoplasmic distribution of heterogeneous nuclear ribonucleoprotein A2/B1 is altered by cellular copper content

4.1 Introduction

hnRNP A2/B1 is an RNA-binding protein (RBP) involved in the regulation of mRNA at many levels. It is known to play a role in the alternative splicing of mRNA, the packaging and trafficking of pre-mRNA, and the regulation of transcript abundance, among other processes (377,429,484,486). In order to perform these functions, hnRNP A2/B1 undergoes nucleocytoplasmic shuttling, in which the protein moves rapidly between the nucleus and cytoplasm, largely directed by the presence of a nuclear import/export signal called M9 (398,400-402,416,492). The four isoforms of hnRNP A2/B1, which arise from the alternative splicing of exons 2 and 9 (see chapter 1, **Figure 1.2**), have different nucleocytoplasmic distributions. Inclusion of exon 2 or exon 9 has been associated with a decrease in the diffusion rate of hnRNP A2/B1 proteins in the cytoplasm and nucleus, respectively, and the exclusion of exon 2 and subsequent junction of exons 1 and 3 results in a nuclear localization signal-like sequence (429). These data suggest that the isoforms may have unique nuclear and cytoplasmic targets and functions (429).

Cytoplasmic hnRNP A2/B1 can be localized to RNA granules, which are membraneless accumulations of RNA and RBPs in which many aspects of RNA processing take place (417,429). As they lack a membrane, RNA granule structure is driven by protein-protein and RNA-protein interactions among their constituents, giving them the ability to rapidly form and disperse in response to changes in intracellular conditions (417,418). These granules are classified based on content and function, and common classes include stress granules (SG), glycine- and tryptophan-rich cytoplasmic processing bodies (GW/P-bodies), and neuronal granules (418,422).

A previous study in the mouse model of Wilson disease found an increase in the nuclear abundance of hnRNP A2/B1 in response to Cu accumulation, and that the primary effect was on the exon 2-containing B-isoforms (268). However, whether this increase was due to an upregulation of hnRNP A2/B1 expression or to an increase in the nuclear localization of hnRNP A2/B1 was not clarified. In this study, we show that hnRNP A2/B1 localization is Cu-responsive in both HeLa and SH-SY5Y cells, and that Cu elevation results in an increased amount of hnRNP A2/B1 in the cytoplasm. Moreover, in response to elevated Cu, hnRNP A2/B1 is localized to cytoplasmic puncta that are negative for markers of known cytoplasmic granules, indicating that this change in hnRNP A2/B1 distribution is a novel response to Cu elevation.

4.2 Cu accumulation induces a rapid, dose-dependent change in the nucleocytoplasmic distribution of hnRNP A2/B1 in HeLa cells

hnRNP A2/B1 is a Cu-responsive protein. Its abundance is increased in the nuclei of Cu-overloaded hepatocytes from Wilson disease mouse models compared to wild type controls (268). There are two main ways in which this nuclear increase could be facilitated: (i) Cu accumulation induces an increase in the expression of hnRNP A2/B1, resulting in an overall higher abundance of the protein, or (ii) Cu accumulation triggers the nuclear retention of hnRNP A2/B1, resulting in a higher abundance in the nuclei without changing total abundance.

To determine whether Cu accumulation affects hnRNP A2/B1 expression, HeLa cells were treated with different concentrations of Cu for 4 h and then mRNA and protein levels of hnRNP A2/B1 were assessed. As seen in **Figure 4.1 A**, none of the Cu concentrations tested have a significant effect on hnRNP A2/B1 mRNA expression. This was true for all three hnRNP A2/B1 isoform probes tested: A2B1 exon 2 (0.81 ± 0.09 a.u. for 5 μM Cu, 0.92 ± 0.08 a.u. for 10 μM Cu, 0.96 ± 0.21 a.u. for 20 μM Cu, 0.90 ± 0.19 a.u. for 50 μM Cu, and 0.90 ± 0.10 a.u. for 100 μM Cu), A2B1 exon 9 (0.86 ± 0.09 a.u. for 5 μM Cu, 0.85 ± 0.12 a.u. for 10 μM Cu, 1.20 ± 0.60 a.u. for 20 μM

Cu, 0.93 ± 0.17 a.u. for 50 μM Cu, and 1.03 ± 0.19 a.u, for 100 μM Cu), and A2B1 exon 1_3 (0.98 ± 0.27 a.u. for 5 μM Cu, 1.24 ± 0.24 a.u. for 10 μM Cu, 1.14 ± 0.47 a.u. for 20 μM Cu, 1.03 ± 0.18 a.u. for 50 μM Cu, and 1.18 ± 0.21 a.u. for 100 μM Cu). Analysis of protein abundance using Western blotting and densitometric quantification also showed that Cu had little effect on protein abundance (**Figure 4.1 B, C**). Specifically, the upper hnRNP A2/B1 isoform band (~38 kDa, roughly corresponding to B1) only had a significantly different abundance at 10 μM Cu compared to all other concentrations (0.90 ± 0.29 a.u. for 5 μM Cu, 1.39 ± 0.52 a.u. for 10 μM Cu, 0.92 ± 0.10 a.u. for 20 μM Cu, 0.73 ± 0.25 a.u. for 50 μM Cu, and 0.87 ± 0.08 a.u. for 100 μM Cu). The lower band (~36 kDa, roughly corresponding to A2) was similar in that there was only one concentration at which the isoform abundance differed from that of the control—the abundance at 20 μM Cu was 40% higher than the abundance at 0 μM Cu (1.27 ± 0.09 a.u. for 5 μM Cu, 1.02 ± 0.25 a.u. for 10 μM Cu, 1.41 ± 0.05 a.u. for 20 μM Cu, 1.39 ± 0.38 a.u. for 50 μM Cu, and 1.05 ± 0.32 a.u. for 100 μM Cu).

Data described in the previous chapter demonstrate that hnRNP A2/B1 regulates the expression of the Cu-transporter ATP7A. In agreement with our data showing that Cu did not affect hnRNP A2/B1 expression, ATP7A expression was similarly unaltered upon Cu treatment. As seen in **Figure 4.1 A and B**, neither ATP7A mRNA abundance (1.09 ± 0.17 a.u. for 5 μM Cu, 1.24 ± 0.15 a.u. for 10 μM Cu, 0.99 ± 0.10 a.u. for 20 μM Cu, 1.16 ± 0.12 a.u. for 50 μM Cu, and 1.26 ± 0.39 a.u. for 100 μM Cu) nor ATP7A protein abundance (1.05 ± 0.15 a.u. for 5 μM Cu, 1.25 ± 0.33 a.u. for 10 μM Cu, 1.38 ± 0.21 a.u. for 20 μM Cu, 0.87 ± 0.14 a.u. for 50 μM Cu, and 1.09 ± 0.22 a.u. for 100 μM Cu) change significantly in response to increasing Cu concentrations. Thus, although ATP7A is directly involved in maintaining Cu homeostasis, changes in cellular Cu concentrations do not alter ATP7A expression, in agreement with previous findings (17,105).

We then examined whether Cu accumulation altered the intracellular localization of hnRNP A2/B1. hnRNP A2/B1 localizes mainly to the nucleus, but it shuttles into the cytoplasm to enable

mRNA trafficking and regulate translation (429). The previously reported increase in amounts of nuclear hnRNP A2/B1 in response to high Cu could therefore be due to alterations in the nucleocytoplasmic distribution of hnRNP A2/B1. To test whether Cu alters the retention of hnRNP A2/B1 in the nucleus, HeLa cells were treated with increasing concentrations of Cu for 4 h and the distribution of hnRNP A2/B1 was monitored by immunofluorescence. The amount of nuclear hnRNP A2/B1 signal (i.e., the green hnRNP A2/B1 signal overlapping with the blue DAPI signal) was compared to the amount of non-nuclear, or cytoplasmic, hnRNP A2/B1 signal to calculate the nuclear/cytoplasmic ratio (N/C). A higher N/C value indicated relatively more nuclear hnRNP A2/B1 compared to cytoplasmic hnRNP A2/B1, while a lower N/C value indicated relatively less.

Cu treatment significantly altered the nucleocytoplasmic distribution of hnRNP A2/B1 (**Figure 4.2 A, B**). With Cu concentrations as low as 5 μM, the N/C ratio decreased by 33% (0.67 ± 0.06 a.u.) compared to the basal control. Moreover, this effect was dose-dependent: increasing Cu concentrations resulted in decreasing N/C ratios, with the ratio at 10 μM being 43% lower, at 20 μM 51% lower, at 50 μM 62% lower, and at 100 μM 68% lower (0.57 ± 0.08 a.u., 0.49 ± 0.04 a.u., 0.38 ± 0.03 a.u., and 0.32 ± 0.02 a.u., respectively). These data suggest that increasing Cu concentrations result in more hnRNP A2/B1 outside of the nucleus, and that the higher the concentration of Cu, the more hnRNP A2/B1 will be localized to the cytoplasm.

To investigate how quickly after treatment the change in nucleocytoplasmic distribution occurs, and to determine whether this change is time-dependent, HeLa cells were treated with 20 μM Cu for 0, 1, 2, 3, 4, 6, or 8 h prior to fixing and immunostaining. As **Figure 4.3 A** shows, hnRNP A2/B1 signal was detected outside the nucleus within 1 h of treatment. In fact, the bulk of this nucleocytoplasmic redistribution occurs within this first hour, with a 47% decrease in the N/C ratio (0.52 ± 0.01 a.u.) compared to the basal control and only small changes thereafter (0.52 ± 0.31 a.u. at 2h, 0.50 ± 0.02 a.u. at 3 h, and 0.50 ± 0.03 a.u. at 4 h). After 6 h of treatment, the N/C ratio drops slightly more, with a 56% decrease compared to the basal control (0.44 ± 0.02 a.u.), and

by 8 h following treatment, the N/C ratio decreased by 61% compared to the basal control (0.39 ± 0.01 a.u.). Taken together, these data suggest that this effect is Cu-sensitive, with the change in distribution occurring at Cu concentrations as low as 5 μM and as quickly as within 1 h of treatment.

4.3 Cu accumulation induces a change in the nucleocytoplasmic distribution of hnRNP A2/B1 in SH-SY5Y cells

While HeLa cells serve as an excellent and convenient model for these experiments, the question arose as to whether this nucleocytoplasmic redistribution would occur in different cell lines. Data in the previous chapter suggested an association between changes in Cu levels and hnRNP A2/B1 abundance in SH-SY5Y neuroblastoma cells during differentiation. Non-differentiated SH-SY5Y cells were treated with 0, 5, 10, or 20 μM Cu for 4 h and the effect on the nucleocytoplasmic distribution of hnRNP A2/B1 was examined (**Figure 4.4 A)**. As in HeLa cells, Cu elevation results in an altered nucleocytoplasmic distribution of hnRNP A2/B1 (**Figure 4.4 B**). At 5 μM Cu, the N/C ratio was 19% lower than that at basal Cu level (0.81 ± 0.04 a.u.), further decreasing by 29% at 10 μM Cu (0.71 ± 0.02 a.u.) and by 34% at 20 μM Cu (0.66 ± 0.05 a.u.) compared to the basal control. The distribution of hnRNP A1, a homolog of hnRNP A2/B1 also known to undergo nucleocytoplasmic shuttling (400), was also characterized to determine whether Cu affected the distributions of this hnRNP similarly or if this phenomenon was specific to hnRNP A2/B1 (**Figure 4.4 C**). The N/C ratio of hnRNP A1 did not significantly change compared to the basal control at any Cu concentration tested (0.96 ± 0.06 a.u. at 5 μM Cu, 1.09 ± 0.04 a.u. at 10 μM Cu, 0.87 ± 0.09 a.u. at 20 μM Cu), indicating that the Cu-responsive change in nucleocytoplasmic distribution is specific to hnRNP A2/B1.

4.4 hnRNP A2/B1 localizes to unique cytoplasmic granules in response to Cu accumulation

Shuttling in and out of the nucleus is essential to the function of hnRNP A2/B1, and each of the four isoforms contain an M9 nuclear localization signal to facilitate entry into the nucleus (276,323). Under basal conditions, hnRNP A2/B1 largely localizes to the nucleus (424,484). The addition of as little as 5 μM Cu to the growth medium results in the appearance of punctate staining in the cytoplasm. Comparison of the hnRNP A2/B1 staining pattern at 0 μM Cu and 20 μM Cu (**Figure 4.5 A, B**) shows that these puncta are numerous at higher concentrations of Cu and can be quite large, some up to 300–500 nm in diameter.

It is well-known that hnRNP A2/B1 can be found in cytoplasmic RNA granules, a phenomenon that has been best characterized in oligodendrocytes during the process of myelination (380,462,493-495). Several types of RBP-containing RNA granules exist—e.g., SGs, GW/P-bodies, and U-rich small nuclear ribonucleoprotein-containing bodies (U-bodies)—and previous studies have confirmed the presence of hnRNPs in SGs and GW/P-bodies (378,418,422,423,426,496). To determine whether Cu accumulation induces the incorporation of hnRNP A2/B1 into one or more of these types of granules, cells were co-stained with antibodies against hnRNP A2/B1 and markers of various granules. As shown in **Figure 4.6 A**, hnRNP A2/B1 (green signal) does not co-localize with the SG marker (497), G3BP1 (magenta signal), at any of the tested Cu concentrations. Likewise, hnRNP A2/B1 does not appear to co-localize with either the U-body marker (498), DDX20 (**Figure 4.6 B**, magenta signal), or the GW/P-body marker (422), Dcp2 (**Figure 4.6 C**, magenta signal). These results suggest that Cu accumulation does not drive the inclusion of hnRNP A2/B1 into common RNA granules.

A previous study suggested that RNA granules may tether to lysosomes during transportation (499). Given the average lysosomal size in HeLa cells is approximately 300–400 nm—the

diameter of some of the larger hnRNP A2/B1-stained granules—and the fact that lysosomes are known to be involved in the regulation of cellular Cu balance, it seemed possible that co-localization with lysosomes could account for the hnRNP A2/B1 staining pattern (500,501). However, staining with LAMP1 (**Figure 4.6 D**, magenta signal), a lysosomal marker (500), showed that there was no co-localization with hnRNP A2/B1 at any of the tested Cu concentrations. Taken together, these results indicate that hnRNP A2/B1 localizes to potentially novel cytoplasmic granules in response to Cu elevation.

4.5 Cu-induced change in the nucleocytoplasmic distribution of hnRNP A2/B1 largely affects the B-isoforms

Burkhead, et al. showed that the increase in nuclear hnRNP A2/B1 in Cu-overloaded mouse livers was largely due to a specific retention of exon 2-containing isoforms—the B-isoforms. To determine whether these isoforms are indeed more sensitive to Cu-induced changes in localization, HeLa cells were transfected with non-targeting (NT) siRNA, siRNA against all four hnRNP A2/B1 isoforms (A2B1-T), or siRNA against the exon 2-containing isoforms (A2B1-e2) and treated with increasing concentrations of Cu for 4 h and the ratio of nuclear hnRNP A2/B1 signal to cytoplasmic hnRNP A2/B1 signal (N/C ratio) was determined **(Figure 4.7 A**). As expected, A2B1-T cells had very little hnRNP A2/B1 (green) signal, reflecting efficient downregulation. NT cells also acted as expected (**Figure 4.7 B**), with the N/C ratio decreasing by 28% at 5 μM Cu (0.72 ± 0.02 a.u.), 37% at 10 μM Cu (0.63 ± 0.06 a.u.), and 47% at 20 μM Cu (0.53 ± 0.03 a.u.) compared to 0 μM Cu, which tracks well with the N/C ratio decrease observed in non-transfected cells that underwent the same Cu treatment (**Figure 4.2**). In contrast, A2B1-e2 cells had no change in the N/C ratio at any of the tested concentrations of Cu compared to the basal control (1.05 ± 0.08 a.u. at 5 μM Cu, 1.02 ± 0.13 a.u. for 10 μM Cu, and 1.00 ± 0.15 a.u. at 20 μM Cu). This result indicates that the remaining isoforms, the A-isoforms, do not significantly

change nucleocytoplasmic distribution in response to Cu treatment, suggesting that the distribution of the B-isoforms is sensitive to elevated Cu.

4.6 Discussion

The nucleocytoplasmic shuttling of hnRNP A2/B1 is essential to its function as a regulator of mRNA processing and expression (276,323). Different aspects of RNA regulation take place in different subcellular locations—e.g., alternative splicing of transcripts occurs in the nucleus, while mRNA trafficking occurs in the cytoplasm—and loss of the ability of hnRNP A2/B1 to travel between the nucleus and cytoplasm is associated with disease (426,429,476). In this study, we identified Cu accumulation as a factor that influences the nucleocytoplasmic distribution of hnRNP A2/B1 and characterized the nature of this effect.

We found that Cu accumulation had a modest effect on hnRNP A2/B1 expression, with no significant changes in the mRNA levels of the four isoforms at any of the Cu levels tested and a small increase in the upper hnRNP A2/B1 isoform band at 10 μM Cu and the lower hnRNP A2/B1 isoform band at 20 μM Cu. Analysis of the localization of hnRNP A2/B1 showed that Cu accumulation resulted in a *decrease* in nuclear hnRNP A2/B1 levels, contrary to the finding by Burkhead, et al. in the hepatic nuclei of Wilson disease model mice. This discrepancy could be explained in part by the fact that this earlier study examined the effect of long-term Cu overload on mouse livers, while our study focused on the response of cultured cells to brief, extracellular Cu treatments performed over the span of hours (268). It may also be due in part to the fact that mouse hepatocytes express all four hnRNP A2/B1 isoforms whereas HeLa cells only express up to three—B1, A2, and A2b (268,429). Regardless, these data show that increasing Cu concentrations in the growth medium results in an increase in cytoplasmic hnRNP A2/B1 signal and that this effect was dose-dependent. Notably, this change in the distribution of hnRNP A2/B1 was observed in the presence of as little as 5 μM of Cu, and within 1 h of treatment, suggesting

that this effect is both rapid and highly sensitive. Moreover, this increase in cytoplasmic levels of hnRNP A2/B1 in response to Cu accumulation occurs in SH-SY5Y neuroblastoma cells as well, and comparison of the localization of hnRNP A2/B1 to a homologous protein, hnRNP A1, showed that this Cu-responsive change in nucleocytoplasmic distribution is specific to hnRNP A2/B1.

What drives this change in subcellular distribution? Closer observation of the cytoplasmic hnRNP A2/B1 reveals that the staining is punctate, with some of these puncta as large as 500 nm in diameter. This suggested that hnRNP A2/B1 is being incorporated into granular structures in the cytoplasm. RNA granules are hubs of RNA metabolism in which RBPs are known to localize (417,429). However, we found that these hnRNP A2/B1-containing granules did not stain positive for markers of SGs (G3BP1), U-bodies (DDX20), GW/P-bodies (Dcp2), or lysosomes (LAMP1). This suggests that the formation of these granules represents a unique response to Cu accumulation.

While it is tempting to speculate that Cu elevation induces the movement of hnRNP A2/B1 into a new type of RNA granule, it is presently unclear whether Cu triggers the assembly of hnRNP A2/B1 into cytoplasmic inclusions/granules, or hinders the ability of hnRNP A2/B1 to shuttle back into the nucleus. There are many factors that can affect the nucleocytoplasmic shuttling of hnRNPs: mutations that affect the nuclear localization signal, mutations that cause protein aggregation, viral infection, changes in metal ion concentration, induction of differentiation, and protein concentration saturation (416,476,487,488,490,502,503). In many of these cases, the hnRNPs undergo liquid-liquid phase separation (LLPS), wherein the protein separates out from the cytosol into a distinct, insoluble liquid condensate (503-505). Given that Cu concentrations as low as 10 μM were shown to induce LLPS of an aggregate-prone construct *in vitro* (503), it's possible that increasing Cu concentration alone could be sufficient to induce some level of LLPS of hnRNP A2/B1.

Han, et al. have shown that the hnRNP A2/B1 isoforms have different subcellular localizations, and have proposed that inclusion of exons 2 and 9 differentially affect the diffusion rates of the isoforms in the nucleus and cytoplasm (429). We found that cells in which the B-isoforms had been downregulated show no change in the nucleocytoplasmic distribution of hnRNP A2/B1 in response to Cu, whereas the control cells showed a dose-dependent decrease in the ratio of nuclear hnRNP A2/B1 to cytoplasmic hnRNP A2/B1. This suggests that the remaining A-isoforms, which lack exon 2, do not undergo a redistribution into the cytoplasm in response to increasing Cu levels. Moreover, it implies that the B-isoforms, which do contain exon 2, are specifically sensitive to cellular Cu content, and that inclusion of exon 2 may be responsible for this, at least in part. This implication that the B-isoforms are particularly attuned to cellular Cu levels corresponds well with our data from the previous chapter which show that the B-isoforms mediate Cu content via the regulation of ATP7A abundance.

This study has shown that Cu levels impact the subcellular localization of hnRNP A2/B1, with Cu elevation resulting in an increase in cytoplasmic hnRNP A2/B1 content. This effect occurs in both HeLa and SH-SY5Y cells and involves mainly the B-isoforms. This change in nucleocytoplasmic distribution results in the localization of hnRNP A2/B1 to cytoplasmic puncta that are negative for markers of known RNA granules, and thus could represent a novel cytoplasmic inclusion unique to changes in cellular Cu content. Further study into this phenomenon could reveal exciting new insights into Cu-mediated mechanisms of mRNA regulation and trafficking.

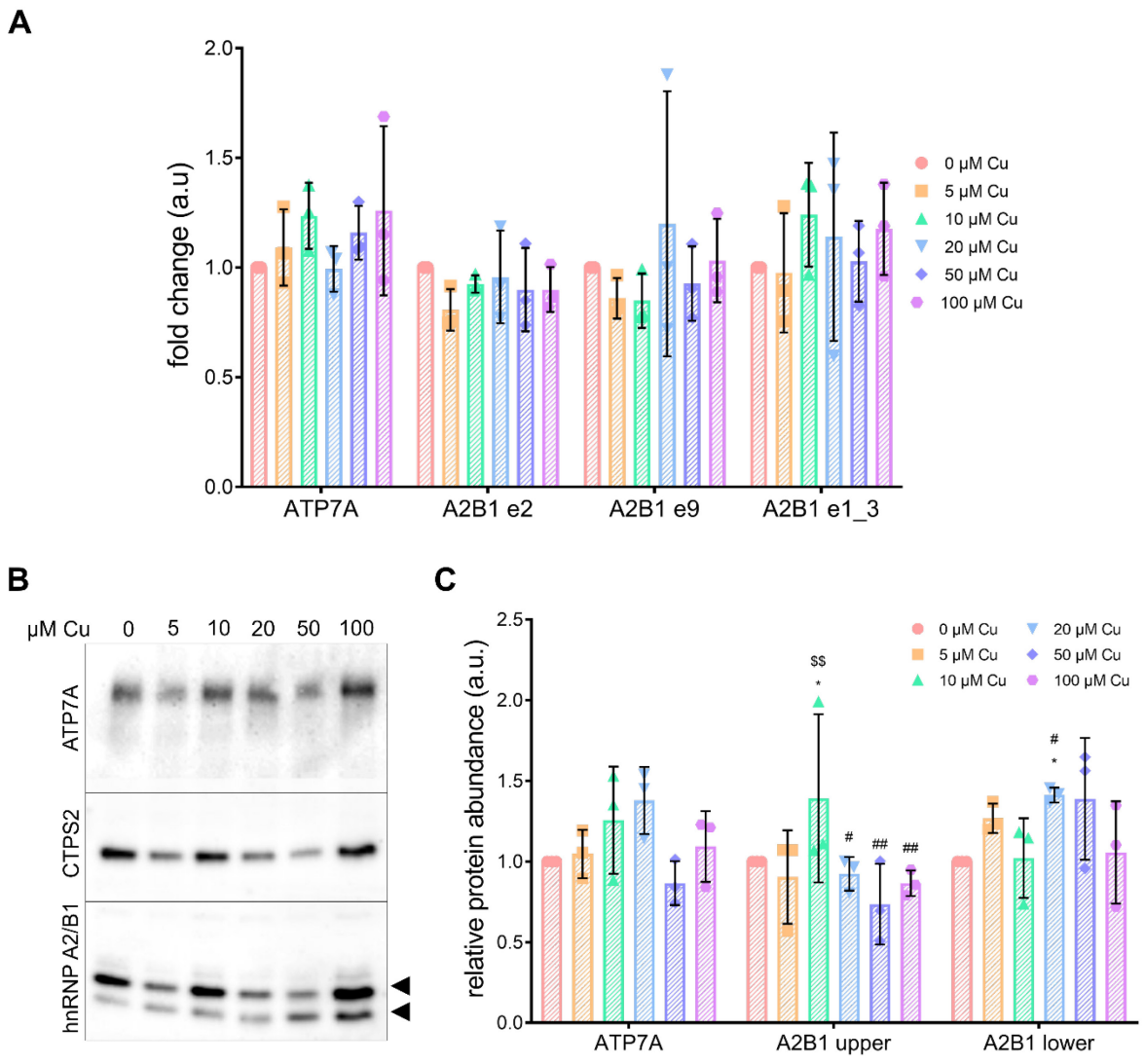

Figure 4.1. Cu accumulation does not change the expression levels of hnRNP A2/B1 or ATP7A in HeLa cells.

HeLa cells were treated with the indicated concentrations of Cu for 4 h. **(A)** ATP7A and hnRNP A2/B1 mRNA abundance in response to Cu treatment. Values normalized to hS18 and then compared to ND, the values of which were taken as 1. *n*=3. **(B, C)** ATP7A and hnRNP A2/B1 protein abundance in response to Cu treatment. Two distinct isoforms of hnRNP A2/B1 are indicated by black arrows. Values normalized to CTPS2 and ND, the values of which were taken as 1. *n*=3. All values are reported as means ± SD. Significance was determined by one-way ANOVA; * $p<0.05$ compared to 0 μM Cu; $$ $p<0.01$ compared to 5 μM Cu; # $p<0.05$, ## $p<0.01$ compared to 10 μM Cu.

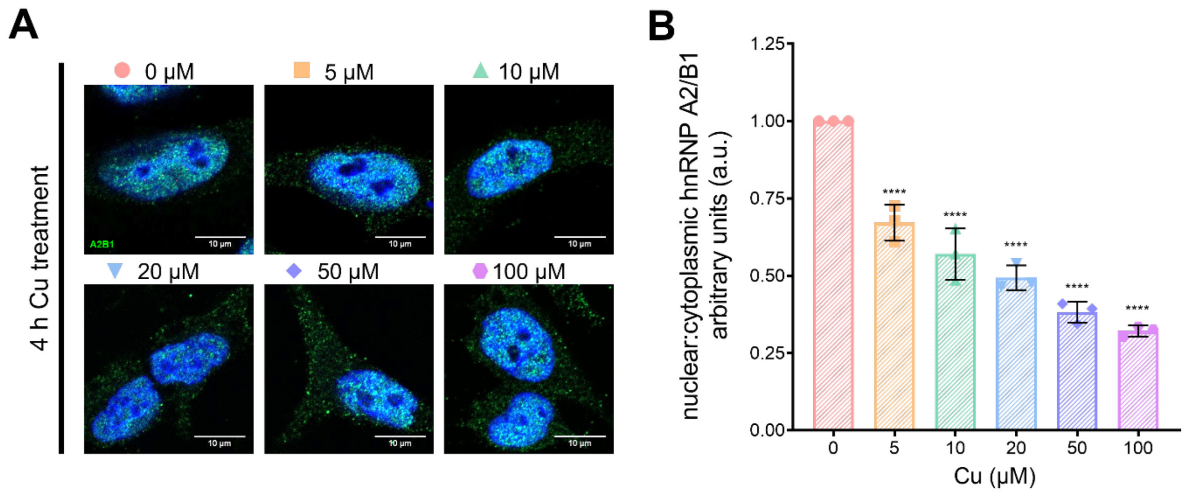

Figure 4.2. Cu accumulation results in a dose-dependent change in the nucleocytoplasmic distribution of hnRNP A2/B1 in HeLa cells.

HeLa cells were treated with the indicated concentrations of Cu for 4 h. **(A)** hnRNP A2/B1 staining in response to different concentrations of Cu. hnRNP A2/B1 is in green and nuclei (DAPI) in blue. **(B)** Quantitative analysis of the nucleocytoplasmic distribution of hnRNP A2/B1. The changes in distribution were assessed by determining the ratio of hnRNP A2/B1 signal inside the nucleus to that outside the nucleus (N/C). Values normalized to 0 μM Cu, the values of which were taken as 1. Five cells per replicate (*n*) were assessed, *n*=3. All values are reported as means ± SD. Significance was determined by one-way ANOVA; **** $p<0.0001$ compared to 0 μM Cu.

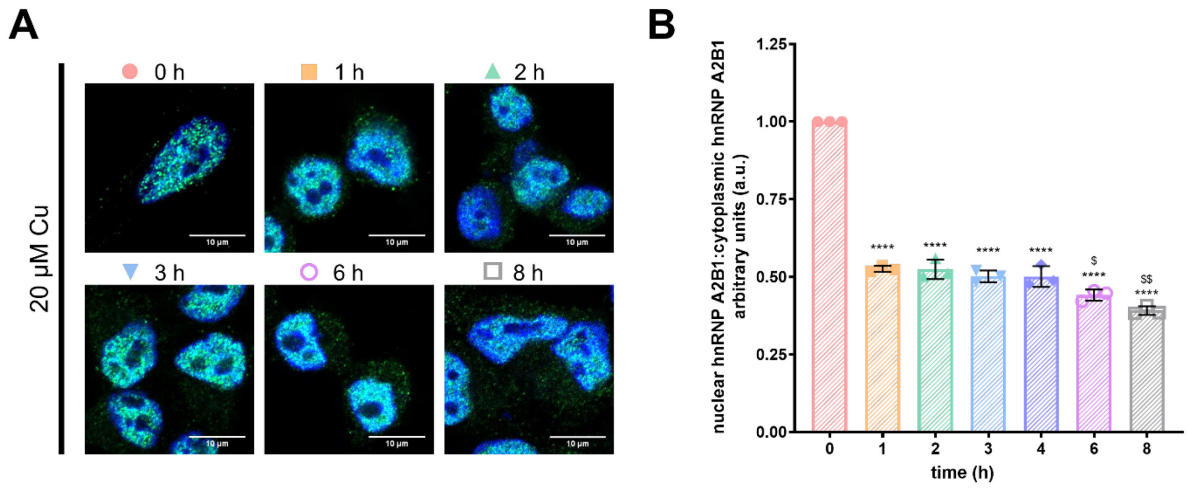

Figure 4.3. Cu accumulation results in a rapid change in the nucleocytoplasmic distribution of hnRNP A2/B1 in HeLa cells.

HeLa cells were treated with 20 µM Cu for the indicated times. **(A)** hnRNP A2B1 staining in response to different Cu treatment times. hnRNP A2/B1 is in green and nuclei (DAPI) in blue. **(B)** Quantitative analysis of the nucleocytoplasmic distribution of hnRNP A2/B1. The changes in distribution were assessed by determining the ratio of hnRNP A2/B1 signal inside the nucleus to that outside the nucleus (N/C). Values normalized to 0 h, the values of which were taken as 1. Five cells per replicate (*n*) were assessed, *n*=3. All values are reported as means ± SD. Significance was determined by one-way ANOVA; **** $p<0.0001$ compared to 0 h and $ $p<0.05$, $$ $p<0.01$ compared to 1 h.

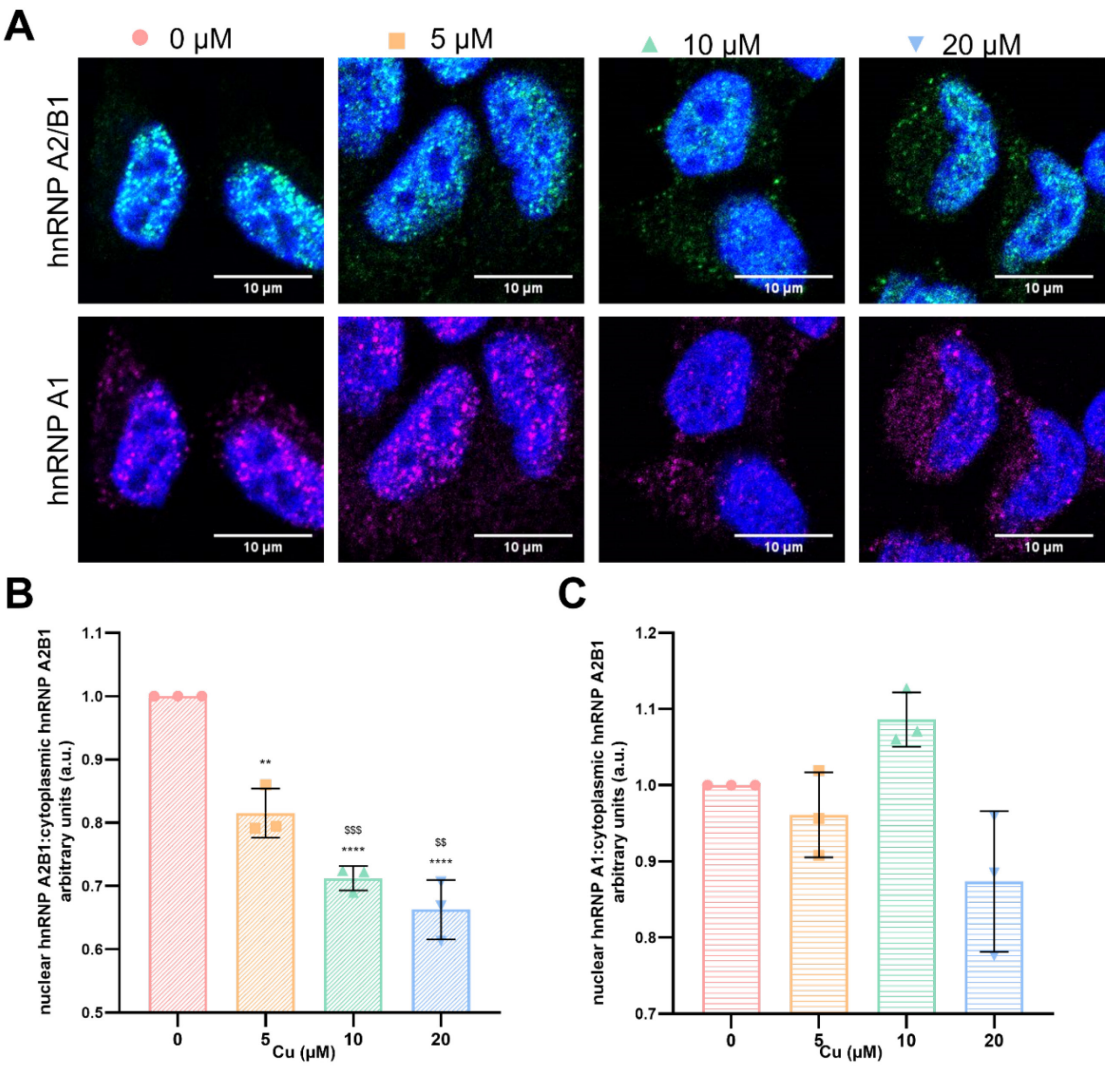

Figure 4.4. Cu accumulation results in a dose-dependent change in the nucleocytoplasmic distribution of hnRNP A2B1 in SH-SY5Y cells.

SH-SY5Y cells were treated with the indicated concentrations of Cu for 4 h. **(A)** hnRNP A2/B1 staining in response to different concentrations of Cu. hnRNP A2/B1 is in green, hnRNP A1 in magenta, and nuclei (DAPI) in blue. **(B, C)** Quantitative analysis of the nucleocytoplasmic distribution of **(B)** hnRNP A2/B1 and **(C)** hnRNP A1. The changes in distribution were assessed by determining the ratio of hnRNP A2/B1 or hnRNP A1 signal inside the nucleus to that outside the nucleus (N/C). Values normalized to 0 µM Cu, the values of which were taken as 1. Five cells per replicate (*n*) were assessed, *n*=3. All values are reported as means ± SD. Significance was determined by one-way ANOVA; ** $p<0.01$, **** $p<0.0001$ compared to 0 µM Cu and $$ $p<0.01$, $$$ $p<0.001$ compared to 5 µM Cu.

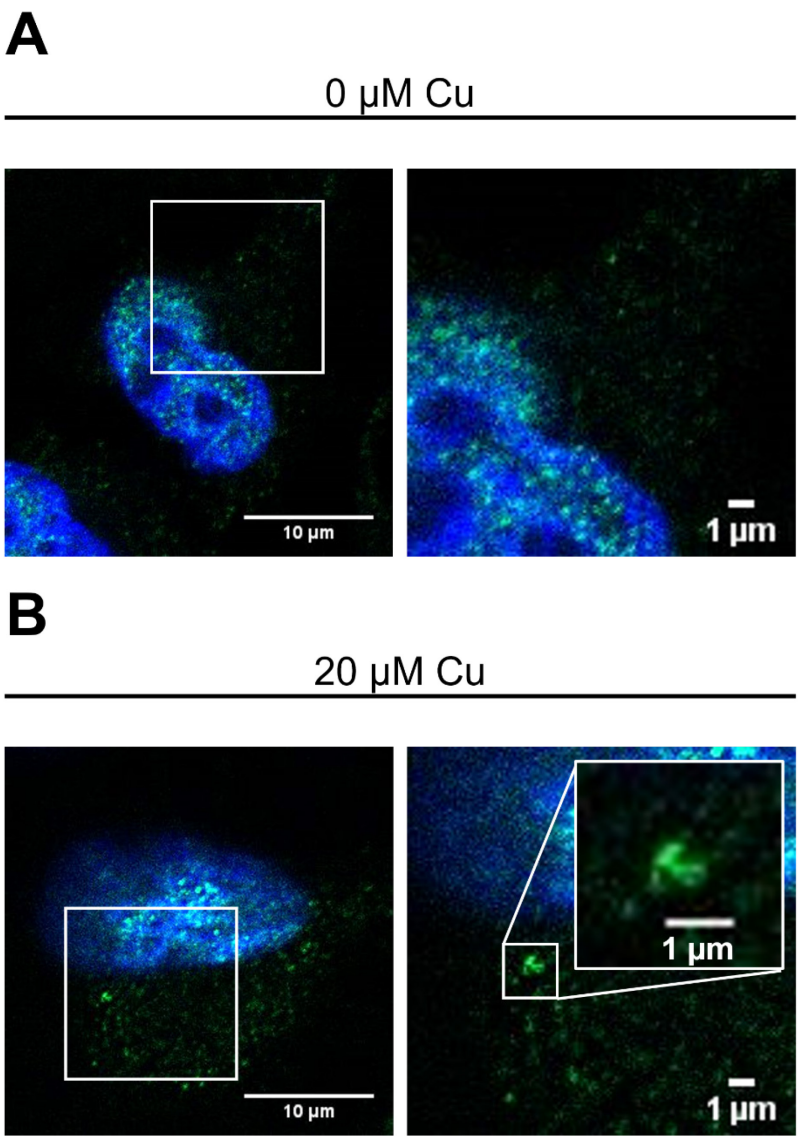

Figure 4.5. Cu accumulation induces the localization of hnRNP A2/B1 into cytoplasmic puncta.

HeLa cells were treated with the indicated concentrations of Cu 4 h and stained for hnRNP A2/B1. **(A)** 0 µM Cu. **(B)** 20 µM. hnRNP A2/B1 is in green and nuclei (DAPI) in blue. Panels on the right are 2x zooms of the indicated areas on the panels on the left, and the inset is a 10x zoom of the area indicated.

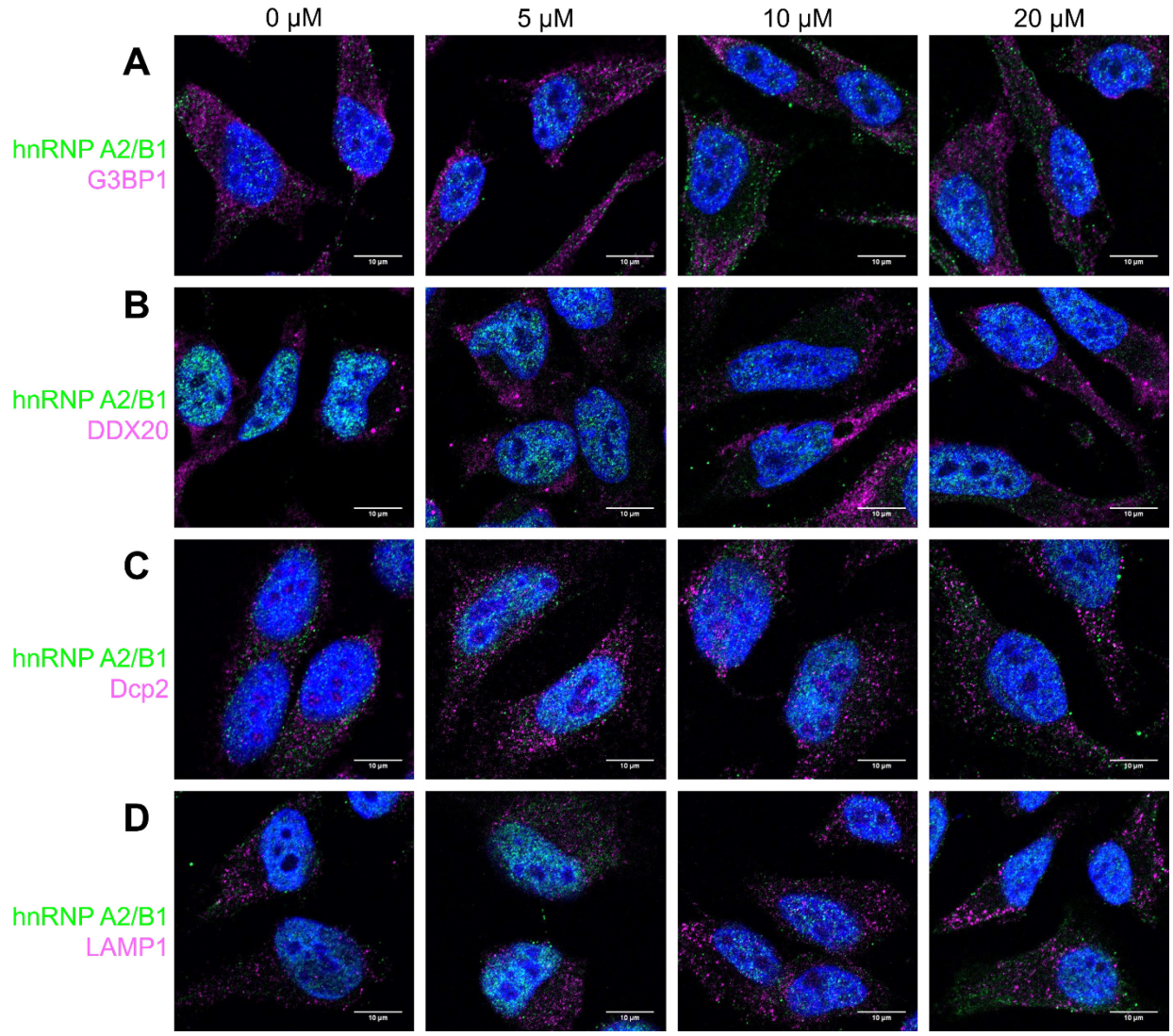

Figure 4.6. hnRNP A2/B1 localizes to unique cytoplasmic granules in response to Cu accumulation in HeLa cells.

HeLa cells were treated with the indicated concentrations of Cu for 4 h prior to staining. **(A)** Staining pattern of G3BP, a marker of stress granules. **(B)** Staining pattern of DDX20, a marker of U snRNP-containing (U) bodies. **(C)** Staining pattern of Dcp2, a marker of processing (P) bodies. **(D)** Staining pattern of LAMP1, a marker of lysosomes. hnRNP A2/B1 is in green, the nucleus (DAPI) in blue, and each marker in red. *n*=3.

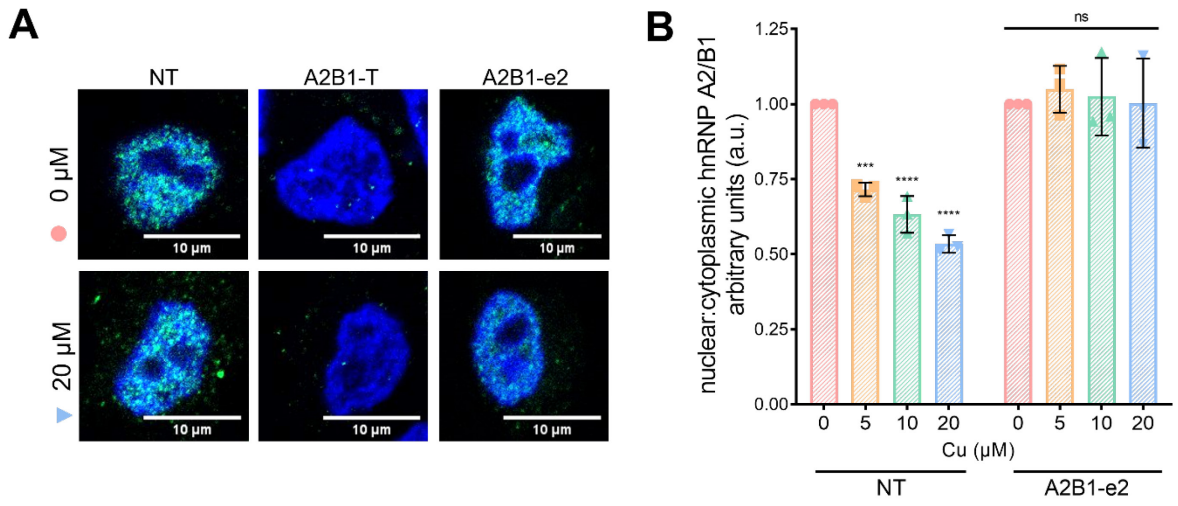

Figure 4.7. Cu accumulation does not induce significant changes in the distribution of hnRNP A2/B1 in HeLa cells with the B-isoforms downregulated.

NT, A2B1-T, and A2B1-e2 knockdown conditions were compared. Cells were treated with the indicated concentrations of Cu for 4 h prior to staining. **(A)** hnRNP A2/B1 staining in response to Cu. hnRNP A2/B1 is in green and the nucleus (DAPI) in blue. **(B)** Quantitative analysis of the nucleocytoplasmic distribution of hnRNP A2/B1. The changes in distribution were assessed by determining the ratio of hnRNP A2/B1 signal inside to outside the nucleus (N/C). Values normalized to 0 µM Cu, the values of which were taken as 1. Five cells per replicate (*n*) were assessed, *n*=3. All values are reported as means ± SD. Significance was determined by one-way ANOVA; ** $p<0.01$ and **** $p<0.0001$ compared to NT control.

5 Conclusions and Future Directions

The goal of this thesis was to better understand the regulation of Cu homeostasis, particularly on the mRNA-level. While the main players involved in Cu transport are well-characterized, comparatively less is known about factors that regulate Cu levels outside of direct Cu-binding and Cu-transport. We have identified the RBP hnRNP A2/B1 as a novel regulator of cellular Cu concentration. hnRNP A2/B1 is known to regulate many aspects of mRNA metabolism, affecting alternative splicing, mRNA stability, mRNA trafficking, and activation of translation. Our data demonstrate that hnRNP A2/B1 modulates cellular Cu levels by regulating the abundance of the Cu-exporter ATP7A on the transcript-level—specifically, hnRNP A2/B1 serves as a negative regulator of ATP7A, with decreases in hnRNP A2/B1 abundance linked to increases in ATP7A abundance and vice-versa. The observation that hnRNP A2/B1 expression decreases and ATP7A expression increases during neuronal differentiation suggests that hnRNP A2/B1-mediated regulation of ATP7A may occur in differentiating neurons.

The exact mechanism by which hnRNP A2/B1 regulates ATP7A is unknown. Our data suggest that the ATP7A 3' UTR is key for this regulation, which prompts several questions that warrant further investigation. Does hnRNP A2/B1 directly bind the 3' UTR or does it indirectly interact through a binding partner? What sequence(s) in the ATP7A 3' UTR facilitate this regulation? Is the interaction between hnRNP A2/B1 and the ATP7A 3' UTR isoform-specific? While our data indicate that hnRNP A2/B1-mediated regulation of ATP7A may occur during neuronal differentiation, whether the observed increase in ATP7A abundance and decrease in hnRNP A2/B1 abundance are linked during differentiation is unclear. Additional studies examining this relationship in neuronal cells could shed light onto a facet of how Cu levels are regulated in order to meet cellular Cu needs.

In addition to serving as a regulator of Cu levels, we have found that hnRNP A2/B1 is itself affected by Cu concentration. Our data show a change in the nucleocytoplasmic distribution of hnRNP A2/B1 in response to short-term Cu treatment: the amount of cytoplasmic hnRNP A2/B1 increases with increasing Cu. Moreover, this cytoplasmic hnRNP A2/B1 clusters into granules that do not stain for markers of common RNA granules, indicating that the formation of these granules may be a unique response to Cu elevation. Characterization of these granules could reveal more about how and why they form. The formation of typical cytoplasmic granules is dependent on their RNA and protein content. Determination of the content of these hnRNP A2/B1 granules could reveal additional information about their function. It would also be interesting to determine why these granules form. Is hnRNP A2/B1 being deliberately sequestered into these granules to serve some specific function? Or is granule formation merely the result of changes in hnRNP A2/B1 solubility in response to Cu elevation? Answering these questions could provide insight into novel cellular responses to changes in Cu that are both rapid and sensitive.

In summary, further characterization of the role hnRNP A2/B1 plays in regulation cellular Cu levels would broaden our understanding of Cu homeostasis—especially our understanding of how it is regulated post-transcriptionally. Given Cu imbalance has been identified in a number of different diseases, having a more complete knowledge of the mechanisms by which Cu levels are maintained could prove invaluable to developing therapeutic strategies to treat these diseases.

6 Appendix I: Single nucleotide polymorphisms in the human ATP7B gene modify the properties of the ATP7B protein

Courtney J. McCann, Samuel Jayakanthan, Mariacristina Siotto, Nan Yang, Maria Osipova, Rosanna Squitti, and Svetlana Lutsenko

This chapter is a slightly modified version of an article published in *Metallomics*. The published version is available online at: https://academic.oup.com/metallomics/article/11/8/1441/5921753.

6.1 Abstract

Single nucleotide polymorphisms (SNPs) are the largest source of sequence variation in the human genome. However, their functional significance is not well understood. We show that SNPs in the Wilson disease gene, ATP7B, that produce amino-acid substitutions K832R and R952K, modulate ATP7B properties in vitro and influence serum copper (Cu) status in vivo. The presence of R832 is associated with a lower ATP7B abundance and a diminished trafficking in response to elevated Cu. The K832R substitution alters surface exposure of amino acid residues in the actuator domain and increases its conformational flexibility. All SNP-related ATP7B variants (R832/R952, R832/K952, K832/K952, and K832/ R952) have Cu-transport activity. However, the activity of ATP7B-K832/K952 is lower compared to other variants. In humans, the presence of K952 is associated with a higher fraction of exchangeable Cu in serum. Thus, SNPs may modulate the properties of ATP7B and the organism Cu status.

6.2 Introduction

Copper (Cu) is an essential metal that is required in numerous cellular processes. Cu serves as a cofactor of enzymes involved in respiration, oxygen radical detoxification, iron transport, and neurotransmitter synthesis (8,111). Either insufficient or excessive Cu is detrimental; therefore, Cu homeostasis is tightly regulated through a network of Cu-transporting and Cu-utilizing proteins. ATP7B is a mammalian Cu-transporting P_{1B}-type ATPase that plays a major role in balancing Cu levels in tissues. Although ATP7B is most highly expressed in the liver, it also is expressed in the brain, intestine, heart, kidneys, lungs, mammary glands, and placenta (506). In hepatocytes, ATP7B is localized to the *trans*-Golgi network (TGN), where it facilitates the incorporation of Cu into the secreted ferroxidase ceruloplasmin (Cp), the major Cu-binding protein in the serum (507). When intracellular Cu levels in hepatocytes exceed cellular needs, ATP7B traffics from the TGN to the canalicular membrane and facilitates the export of excess Cu into the bile (508,509).

Inactivation of ATP7B causes Wilson disease (WD), a potentially fatal disorder of Cu misbalance (510). Loss of ATP7B activity is associated with intracellular Cu accumulation, impaired incorporation of Cu into Cp, and an increased proportion of labile (i.e., non-Cp bound) Cu in the serum, which serves as one of the clinical markers of WD (511). WD manifestations range from mild hepatic inflammation and tremor to cirrhosis, fulminant liver failure, depression, and psychotic episodes. The exact cause of this phenotypic variability remains poorly understood. Over 600 WD-causing mutations have been identified in *ATP7B*, and a large number of those mutations have been characterized. Studies have revealed a spectrum of biochemical and cellular effects, ranging from a complete loss of ATP7B function to potentially milder effects on ATP7B trafficking or stability. However, strong correlations between mutations and associated phenotypes have not been observed, suggesting the existence of additional, modifying factors. Furthermore, there is increasing evidence showing that altered Cu homeostasis is present in several other disorders

(e.g., Alzheimer's disease, Parkinson's disease, and non-alcoholic fatty liver disease), and the basis for altered Cu balance in these disorders remains mostly unclear.

Single nucleotide polymorphisms (SNPs) represent a rich source of variation in the genome. Approximately 800 SNPs have been identified in *ATP7B*; the vast majority of these SNPs have not been studied and are assumed to be benign (512). However, two common SNP-related substitutions (SNPRS) in ATP7B—R832 (c.2495 A>G, rs1061472) and K952 (c.2855 G>A, rs732774)—appear to be enriched in patients with Alzheimer's disease (AD). While 31% of the healthy population is homozygous for R832 and 30% for K952, 43% of AD patients are homozygous for R832 and 45% for K952 (513). The higher frequency of these variants could be significant, as the ATP7B-R832 variant has decreased Cu transport activity *in vitro* (514), and AD patients with these variants have a higher fraction of labile Cu in the serum compared to healthy controls (513,515,516). Furthermore, the presence of Arg in the *Drosophila melanogaster* Cu-ATPase at a position equivalent to that of 832 in human ATP7B results in the loss of Cu-ATPase function (517). Given these reports, we tested whether or not the SNPRS, R832 and K952, modulate the properties of ATP7B. We found that these SNPs do influence the biochemical and cellular behavior of ATP7B and, therefore, may impact Cu homeostasis in cells and tissues.

6.3 Materials and Methods

6.3.1 Human subjects and serum sample collection

All procedures involving human subjects were compliant with the ethical standards of the Committee on Human Experimentation of IRCCS Istituto Centro San Giovanni di Dio-Fatebenefratelli and the Helsinki Declaration of 1975. Blind procedures for data collection and analysis were applied. Eight-one elderly volunteers were recruited and screened for conditions known to affect copper metabolism and biological variables of oxidative and for neurological, psychiatric, and cardio-cerebro-vascular diseases. A mini-mental state examination (MMSE) test was conducted (518) Blood was drawn the morning after an overnight fast, collected in a test tube (Vacutainer® BD Thrombin) containing an activator of coagulation, quickly frozen, and stored at -80°C.

6.3.2 Genotyping and serum analysis

Genomic DNA was purified from peripheral blood using the conventional method for DNA isolation (QIAamp DNA Blood Midi kit). SNP IDs are ID_C_1919004_30 (rs1061472) and ID_C_938208_30 (rs732774). Genotyping was performed using the TaqMan allelic discrimination assay (Applied Biosystems, Inc), as previously described (515). Direct DNA bidirectional sequencing was performed for 15% of the PCR products, which were randomly selected and analyzed to confirm the genotypes.

Total serum Cu was measured using an Analyst 600 Perkin Elmer atomic absorption spectrophotometer following previously described methods (519). Cp concentration was measured with an immunoturbidimetry assay (Horiba ABX, Montpellier, France) automated on an ABX Pentra 400 (Horiba ABX, Montpellier, France), performed in duplicate. For each serum Cu

and Cp pair, the amount of Cu bound to Cp, the amount of non-Cp Cu, and Cu:Cp ratio were calculated, as previously described (520,521).

Sample subjects were stratified based on whether or not they were carriers of at least one of the alleles of interest. First, the Cu values of carriers of at least one K952 allele were compared to those from non-carriers. Second, Cu values of carriers of at least one R832 allele were compared to those from non-carriers. Lastly, Cu values of carriers of at least one R832 and one K952 allele were compared to those from non-carriers. Student's t-test was used to determine the significance of difference between the groups described above. * $p<0.05$, ** $p<0.01$.

6.3.3 Conservation analysis of the ATP7B SNPs

NCBI BLASTP (NCBI) was used to identify animal orthologs of human ATP7B (ID: XP_005266487.1). A library of 165 unique sequences from vertebrate species was assembled and 11-residue amino acid (AA) sequences centered on the SNP of interest were extracted. These sequences for each SNP were compiled into a WebLogo (522).

6.3.4 Generation of GFP-tagged ATP7B variants

The plasmid pYG7, encoding ATP7B with an N-terminal GFP tag, was used as a template (523). The four ATP7B variants—R832/R952, R832/K952, K832/K952, and K832/R952—were generated using the QuikChange XL Site-directed Mutagenesis kit (Stratagene), following the manufacturer's protocol. The primers used were as follows:
K832R 5'-GGCGATATCGTCA-GGGTGGTCCC-3', 5'-CCCAGGGACCACCCTGACGATAT-3'; *R952K* 5'-GGTGTTGT-TCAGAAATACTTTCC-3', 5'-GTTAGGAAAGTATTTCTGAACAA-3'. Presence of the correct mutations for each variant was confirmed by sequencing the entire ATPB cDNA region. The identical purity and quantity of plasmids was verified prior to transfection into cells by examining the 210-300 nm spectra.

6.3.5 Cell culture and transfection

HEK293A and skin fibroblast (YST) cells were cultured in complete medium consisting of Dulbecco's modified Eagle's medium (DMEM) supplemented with 10% fetal bovine serum (FBS) and 1% penicillin/streptomycin. Cell cultures were maintained at 37°C in a humidified chamber (5% CO_2). Cells were transfected in 6-well plates for 20 h using Lipofectamine LTX with PLUS reagent (Invitrogen), with 2 μg plasmid DNA/well, and 6 μL Lipofectamine/well, according to the manufacturer's protocol. HEK293A cells were used for determining protein abundance and trafficking; YST cells were used for determining ATP7B Cu transport activity.

6.3.6 Protein abundance of ATP7B variants

Transfected cells were lysed in 1X RIPA buffer (10X RIPA: 0.5 M tris-HCl, pH 7.0; 1.5 M NaCl; 2.5% deoxycholic acid; 10% NP-40; 10 mM EDTA; Millipore) for 30 min on ice. Centrifugation at 3000 x*g* for 15 min removed cell debris, and the supernatant was collected and used for further studies as whole cell lysates. Protein concentration was determined using BCA assay (Pierce). Thirty micrograms of protein were separated on 10% Laemmli gels and then transferred to PVDF (Millipore) membranes using CAPS, pH 11 transfer buffer. Membranes were blocked for 1 h at room temperature (RT) in 5% milk in phosphate-buffered saline (PBS), then incubated for overnight (16 h) in either 1:6000 anti-ATP7B (Abcam, ab124973) or 1:2000 anti-β-actin (Abcam, ab6276) diluted in PBS with 0.2% Tween-20 (PBST) and 0.05% sodium azide. Membranes were then incubated for 1 h at RT in either 1:10000 anti-mouse or anti-rabbit secondary antibodies (Santa Cruz) before imaging on an AlphaImager (ProteinSimple). The fluorescent intensity of protein bands was determined with Image-J (NIH) and ATP7B levels were normalized to β-actin loading control.

6.3.7 Analysis of ATP7B degradation

HEK293A cells were transfected with each of the ATP7B variants and protein synthesis was blocked 16 h post-transfection by the addition of 50 mM cycloheximide (CHX). Cells were then incubated in the presence of CHX for 0, 6, 12, or 24 h to allow for protein degradation. Cells were lysed using RIPA buffer, as described above. Five micrograms of total cell lysate were separated on an SDS-PAGE gel and ATP7B abundance was analyzed by Western blot. The blots were imaged on an AlphaImager and the fluorescent intensities of the protein bands were determined using Image-J. The 6-, 12-, and 24-hour intensities for each variant were normalized to the corresponding intensity at 0 h.

6.3.8 Modeling of the ATP7B SNPRS and adaptive Poisson–Boltzmann surface calculations

The homology model of ATP7B with K832 and R952 was used to predict potential effects of the R832 and K952 SNP-related substitutions (524). The R832 and K952 variants were modeled using the PyMOL (Schrödinger, LLC) mutagenesis feature. Structural changes were visualized by using a space-filling model. The PDB coordinates for the solution NMR structure of the ATP7B A-domain were kindly provided by Dr. Banci (University of Florence). SWISS-MODEL (525) was used to generate the R832 A-domain variant. The structures were used for Adaptive Poisson-Boltzmann Surface (APBS) calculations (70). The PDB2PQR (526-528) web server was used to prepare PQR files using the AMBER-99 (529) and PARSE (530,531) force-fields. APBS calculations were done using the APBS Tools2 plug-in (532) within pyMOL. The dielectric constants for the APBS calculations were set to 2.0 (protein) and 78.0 (solvent) with ion concentrations of 150 mM (radius of +1 = 2.0 and -1 = 1.8). The probe radius for surface tracing was 1.4 Å with a system temperature of 310 K.

6.3.9 All-atom molecular dynamics simulations setup

A-domain structural models containing the K832 and R832 SNPRS (generated as detailed above) were submitted to the CHARMM-GUI web-based server to generate the respective NAMD 2.9-based molecular dynamics system and input files (533-535). A rectangular water box was constructed around each A-domain with an edge distance of 10 Å. The system was supplemented with an ionic strength of 150 mM NaCl (48 sodium and 42 chloride ions placed in each box using the Monte Carlo method) (533). The initial equilibration was performed for 35 frames using the NVT (constant volume, constant temperature) ensemble followed by production runs for up to 200 ns (10,000 frames) using the NPT (constant pressure, constant temperature) ensemble at a constant temperature of 303.15 K. All simulations were performed on the Maryland Advanced Research Computing Core (MARCC) facility high performance blue crab cluster (http://www.marcc.jhu.edu). The resulting individual trajectory was further extracted into 200 frames using the catdcd feature (stride 500 frames) within the Visual Molecular Dynamics (VMD) program (536) for further processing using a local Linux machine.

6.3.10 Molecular dynamics simulation trajectory analysis

The root-mean-square deviation (RMSD) calculations for the individual trajectories were calculated using the VMD program (536). The solvent accessible surface area (SASA) measurements were performed using the Correl function and the SURF probe feature (RPROBE radius 1.4 Å) within the CHARMM program version 42b. The Gaussian network model (GNM) frequencies were generated using the GNM feature within the molecular dynamics analysis suite MDAnalysis (537). The secondary structure calculation was performed by analyzing secondary structure elements in the definition of secondary structure of proteins (DSSP) program using the GROMACs package (538-540). The cross-correlation of motion heat maps were also calculated with MDAnalysis using scripts kindly provided by Anu Nagarajan (NINDS, NIH). The GNM

frequencies were plotted using XMGRACE (http://plasma-gate.weizmann.ac.il/Grace/). The ribbon diagrams of the A-domain were displayed using UCSF chimera (541).

6.3.11 Tyrosinase assay for determining the Cu transport activity of ATP7B variants

YST cells were seeded on glass cover slips at a density of 1.5 x 10^6 cells per well. Cells were co-transfected with the pTyr plasmid and a SNPRS plasmid as described above. For activity measurements, the cells were washed in PBS and then fixed for 30 seconds in an acetone:methanol mixture (1:1 v/v) that was pre-chilled at -20°C. This was followed by incubation in 0.1% sodium phosphate, pH 6.8 containing 0.15% (wt/vol) levo-3,4-dihydroxyl-L-phenylalanine (L-DOPA) for 4 h at RT. Coverslips were then mounted onto slides using Fluoromount-G (Electron Microscopy Science). The formation of dark colored DOPA-chrome was examined using phase contrast microscopy. Forty pigment-containing areas per replicate were manually selected using the tracing tool within Image-J. The areas and intensities of pigmentation were quantified, and the intensities were normalized to the area.

Relative protein levels were estimated using confocal microscopy. The GFP-fluorescence was used as a proxy of ATP7B-GFP protein levels. Fluorescent intensity was quantified using Image-J and normalized to the area. Fluorescent intensity of control cells expressing the pTyr plasmid was used as a background control. Fluorescent intensity of the previously characterized TST-ATP7B was taken as 100% (542).

6.3.12 Trafficking studies

Transfected cells grown on glass coverslips were treated with either 25 μM tetra-thiomolybdate (TTM) or 100 μM $CuSO_4$ for 4 h at 37°C. The cells were then fixed in 3% paraformaldehyde (PFA) in PBS for 12 min and permeabilized and blocked in 0.5% Triton X-100 (Sigma) and 0.5% BSA in

PBS for 15 min. Cells were incubated with anti-TGN46 primary antibody (GeneTex) for 1 h at RT, and then incubated with donkey anti-sheep secondary antibody conjugated with AlexaFluor-555 (Invitrogen) for 1 h at RT. Coverslips were mounted using 3:1 Fluoromount: DAPI (Electron Microscopy Science). Stained cells were visualized using confocal microscopy (Zeiss) and images were processed using Image-J. For quantization of protein co-localization, at least 20 cells were used per each condition, and the loss co-localization between ATP7B-GFP and TGN46 was used as a measure of ATP7B trafficking to vesicles. Cells with predominantly overlapping ATP7B-GFP/TGN46 signals were categorized as having retention of ATP7B in the TGN, and cells with little to no overlap were categorized as having weak retention of ATP7B in the TGN.

6.3.13 Statistical analyses

All values are reported as means ± standard error of the mean (SEM) and plotted in GraphPad Prism (GraphPad Software, Inc). Statistical analyses were performed in GraphPad Prism using either unpaired Student's t-test or one-way ANOVA with Fisher's least significant differences (LDS) test, as indicated. * $p<0.05$, ** $p<0.01$, and **** $p<0.0001$.

6.4 Results

6.4.1 The presence of R832 and K952 correlates with changes in serum Cu indicators

The A>G SNP at c.2495 in *ATP7B* results in an Arg at position 832 (R832), and the G>A SNP at c.2855 results in a Lys at position 952 (K952). To determine whether these substitutions in ATP7B impact Cu status *in vivo*, we characterized blood serum samples from individuals with different SNP combinations. Cp is an abundant serum protein containing a tightly bound, nonexchangeable Cu. Cp is secreted predominantly by the liver. Decreases in ATP7B activity lower Cu incorporation into Cp and, subsequently, increase the fraction of non-Cp bound Cu (i.e., exchangeable Cu) in the serum (511). Consequently, to define the impact of *ATP7B* SNPs on Cu status, we measured four parameters: total serum Cu, total serum Cp, non-Cp Cu, and the Cu:Cp ratio. In this analysis, 81 healthy, elderly patients were recruited, and their demographic and biological variables pertaining to these subjects are reported in **Table 6.1**.

The indicators of Cu status were first compared for the carriers of the R832 allele and non-carriers (**Figure 6.1**). The levels of total serum Cu (13.43±0.31 μM vs. 14.06±1.00 μM) and non-Cp Cu (1.63±0.25 μM vs. 0.62±0.73 μM) did not significantly differ between the carriers and non-carriers. However, total Cp levels (24.98±0.65 mg/dL vs. 28.48±1.34 mg/dL, p = 0.022) were significantly lower in carriers of the R832 allele. Consequently, the Cu:Cp ratio (7.20±0.13 vs. 6.52±0.30, *p*=0.029) was increased in these individuals. Carriers of the K952 allele had Cu levels comparable to those of the non-carriers (13.52±0.32 μM vs. 13.69±0.96 μM). However, K952 carriers had significantly lower Cp levels (24.97±0.63 mg/dL vs. 28.55±1.49 mg/dL, *p*=0.019), significantly higher non-Cp Cu levels (1.74±0.25 mM vs. 0.21±0.67 mM, *p*=0.015), and a higher Cu:Cp ratio in the serum (7.24±0.13 vs. 6.35 ±0.27, *p*=0.003) than the non-carriers.

To determine whether the presence of both R832 and K952 had a combined effect, the Cu status was compared for R832/K952 carriers and non-carriers (K832/R952). Carriers of R832/K952 had serum readouts similar to those of K952 carriers. Although their total Cu levels were similar to those of noncarriers (13.45±0.32 μM vs. 13.86±1.13 μM), the R832/K952 carriers had significantly lower Cp levels (24.84±0.66 mg/dL vs. 28.70±1.61 mg/dL, p=0.021), higher non-Cp Cu levels (1.72±0.25 μM vs. 0.31±0.81 μM, p=0.041), and a higher Cu:Cp ratio (7.25±0.13 vs. 6.39±0.33, p=0.012). Thus, ATP7B SNPs appear to have functional consequences, as measured by Cu status in the serum. To directly test this prediction, we examined the effects of R832 and K952 on various properties of the ATP7B protein *in vitro*.

6.4.2 Substitution of a highly conserved K832 with R832 may impact the ATP7B structure

The two SNPs produce four possible amino acid (AA) combinations (**Figure 6.2 A**). To better understand their functional significance, we first examined conservation of the respective AA residues among ATP7B orthologs. Protein sequences from 165 vertebrate species were aligned with human ATP7B, and the results were compiled into an 11-AA long WebLogo (**Figure 6.2 B**). In a WebLogo, the size of the residue is indicative of the percentage of sequences in which that residue occurs at each given position (522). Lys at position 832 (K832) was present in all 165 sequences, suggesting that Lys in this position is a strongly preferred residue and substitutions of this residue may have structural and/or functional consequences. In contrast, Arg at position 952 (R952) was only observed in human ATP7B. The other ATP7B orthologs have mostly Lys at this position (K952).

To predict the potential effects of R832 and K952 on the ATP7B structure, we used an existing homology model of ATP7B23 (**Figure 6.2 C**). ATP7B is a large membrane protein with multiple domains that have distinct functions. The AA position 952 is located in the loop connecting

transmembrane (TM) segments TM3 and TM4. This region faces the lumen of the TGN, and its specific function is unknown (217,543). In the model, this region is predicted to be unstructured, and therefore the impact of R952K substitution on the ATP7B structure is difficult to evaluate (**Figure 6.2 C**, top panels). In contrast, the AA residue 832 is located in the actuator (A)-domain, a domain that is critically involved in conformational transitions of the protein (70). The side-chain of Arg at position 832 occludes a small ‘‘pocket’’ that is present in the A-domain containing K832, and this structural change could be consequential (**Figure 6.2 C**, bottom panels).

6.4.3 ATP7B-K952/K832 has a lower Cu-transport activity compared to other SNP-related variants

To evaluate the functional significance of the SNPRS we compared Cu-transport activity of all four variants by measuring ATP7Bdependent activation of tyrosinase. Tyrosinase activity requires the presence of a Cu cofactor, and cells expressing functional tyrosinase produce a dark brown pigment (542). YST cells, a fibroblast cell line lacking endogenous Cu-transporting ATPases, were co-transfected with the ATP7B-GFP variants and pTyr, a plasmid expressing apo-tyrosinase. The twin-strep tag (TST)-ATP7B construct, which contains R832/R952 and has been previously used in tyrosinase assays (542) served as a positive control.

All four variants showed Cu-transport activity, as evidenced by the presence of the pigment in cells (**Figure 6.3 A**). The pigment intensity and pigment area were measured and normalized to the area to compare Cu-transport activity between variants quantitatively (**Figure 6.3 B**). The sequences of the ATP7B region for TST-ATP7B and the R832/R952 GFP-ATP7B are identical, and very similar pigment intensities (1.90±0.03 vs. 1.89±0.03, p=0.911) confirmed their similar activity as well as the accuracy of the assay. The normalized pigment intensity of R832/K952 is also comparable to the TST-ATP7B control (1.93±0.034 vs. 1.90±0.03, p=0.649), while the pigment intensity of K832/R952 showed a small, but significant decrease compared to the control

(1.81±0.03 vs. 1.90±0.03, p=0.042). The K832/K952 variant showed the most significant change—an approximately 20% decrease in normalized pigment intensity compared to TST-ATP7B (1.459±0.0347, p<0.0001).

To ensure that this decrease in Cu-transport activity was not due to low protein expression levels of the K832/K952 variant, we measured the GFP-ATP7B fluorescence in transfected cells. The K832/K952 and K832/R952 variants were more abundant (2.797±0.339 and 1.771±0.145, respectively) than the R832/ R952 and R832/K952 variants (1.595±0.347 and 1.223±0.024, respectively; **Figure 6.3 C**). The lower transport activity of the K832/ K952 variant compared to the other variants is therefore not due to lower levels of expression.

6.4.4 Presence of R832 enhances ATP7B degradation and decreases protein abundance

To further explore whether protein abundance was influenced by the SNPRS, we expressed in HEK293A cells the GFP-tagged ATP7B with each of the possible AA combinations. Quantitative real-time PCR (qRT-PCR) confirmed that the mRNA levels were comparable among cells expressing the different ATP7B variants (data not shown). The protein abundance of the ATP7B variants was evaluated by Western blotting. Analysis of band intensity demonstrated that, similarly to findings in YST cells, the presence of R832 was associated with lower ATP7B abundance independently of the residue present at position 952 (**Figure 6.4 A, B**). The R832/R952 variant was less abundant than the K832/R952 variant (1.22±0.13 and 1.9±0.21, respectively; p=0.0258), and the R832/K952 variant was less abundant than the K832/K952 variant (1.172±0.218 and 1.795±0.236; p=0.0397). The ATP7B variant with both of the AD-associated SNPRS, R832/K952, was the least abundant (1.172±0.218).

To determine whether the difference in protein abundance was due to differences in ATP7B degradation, HEK293A cells expressing the ATP7B variants were treated with cycloheximide to block protein synthesis and then chased for 6, 12, or 24 h. Western blot analysis of cell lysates showed no significant changes in protein abundance after 6 h – for all variants (**Figure 6.4 C**). However, after 12 and 24 h the variants containing R832 showed lower protein abundances compared to the K832-containing variants (**Figure 6.4 C**). The R832/R952 variant had significant decreases in abundance after 12 and 24 h (0.621±0.032, p=0.017 and 0.580±0.051, p=0.0088, respectively), whereas the K832/R952 variant showed significant changes only at 24 h (0.917±0.216, p=0.5923 and 0.708±0.083, p=0.0636, respectively). Similarly, the abundance of the R832/K952 variant was decreased after 12 and 24 h of treatment (0.453±0.072, p=0.0008 and 0.271±0.052, p<0.0001), whereas K832/K952 showed a significant decrease only after 24 h (0.683±0.169, p=0.445). These results indicate that the ATP7B variants containing R832 are more susceptible to protein degradation than the variants containing K832, which may explain the observed differences in their abundance.

6.4.5 Residues at position 832 modulate ATP7B trafficking response to high Cu

Hepatic ATP7B is targeted primarily to the TGN under basal or low Cu conditions and traffics to vesicles when Cu is elevated (544). Therefore, the loss of ATP7B retention in the TGN can be used as a measure of protein trafficking. To compare the trafficking response of ATP7B variants, we measured their retention in the TGN under different Cu conditions. Cu depletion was achieved by treatment of HEK293A cells with the Cu chelator tetrathiomolybdate (TTM), and Cu elevation was produced by treating cells with CuSO4 (**Figure 6.5**). Under Cu-limiting conditions, all variants were predominantly localized to the TGN, except for R832/K952-ATP7B, which was found in both TGN and vesicles. Upon Cu elevation, the variants with K832 behaved as expected, i.e., they trafficked normally out of the TGN as evidenced by the loss of co-localization between ATP7B and the TGN marker, TGN46 (**Figure 6.5**). In contrast, the variants with R832 trafficked to vesicles

but remained close to the TGN and some retained an overlap with the TGN marker. Thus, the SNPRS do not disrupt ATP7B trafficking but may modulate the rate of ATP7B exit from the TGN.

6.4.6 R832 affects the conformational dynamics of the A-domain

The decrease in abundance of the R832 variant proteins, as well as the putative effect of this substitution on the ATP7B structure, suggested that Arg at position 832 may impact the structure of the A-domain, which has previously been shown to affect protein abundance (545). To test this hypothesis, we generated a model of the A-domain with R832 using the available NMR structure of the ATP7B A-domain with K83223 and compared the properties of each (**Figure 6.6 A**). Two different force-field calculations, AMBER-9927 and PARSE (530,531) both revealed a difference in the surface electrostatics of the domain depending on the residue present at position 832. The A-domain with K832 has a more positive net charge, whereas the A-domain with R832 has a more neutral net charge, with the largest difference between the domains occurring in the area immediately surrounding the residue 832.

To better understand the effect of the SNPRS on the secondary structure and biophysical properties of the A-domain, we performed all-atom molecular dynamics (MD) simulations in explicit solvent (water/sodium chloride) that mimics the intracellular milieu. The backbone root-mean-square deviation (RMSD) trajectories show that both the R832 and K832 variants equilibrate past 90 nanoseconds (**Figure 6.7 A**). To analyze the conformational motions of the domain and the existence of stable state(s), we calculated the frequencies of the eigenvalues using the Gaussian network model (GNM) (546,547). Explicit solvent calculations for up to 200 nanoseconds were used to determine the impact of R832 on the GNM frequencies, which represent the rotational and translational motions of the domain (546). This analysis showed that both the K832 and R832 variants were present largely in one conformational state. However, the R832 variant has a broader distribution of eigenvalues, indicating a higher conformational

flexibility (**Figure 6.6 B**). The increase in the intramolecular motion is also supported by the larger radius of gyration seen in the R832 variant compared to the K832 variant (53.15±0.733 Å vs. 49.81±0.751 Å, p=0.0016; **Figure 6.6 C**).

Effects of the SNPRS on the secondary structural elements of the A-domain were analyzed using a definition of secondary structure of proteins (DSSP) plot. The third β-strand—the strand in which residue 832 is located—was relatively stable throughout the simulation in both variants (**Figure 6.6 C**). At the same time, the R832 SNPRS significantly altered the solvent accessibility surface area (SASA) for some of the residues in the vicinity of position 832. While V833 (4.29 ±0.153 $Å^2$ vs. 4.63±0.140 $Å^2$, p=0.099) and V834 (87.65±0.633 $Å^2$ vs. 86.71±0.528 $Å^2$, p=0.255) were not significantly changed, both I830 (32.30±0.918 $Å^2$ vs. 45.62±0.655 $Å^2$, p<0.0001) and V831 (0.039±0.008 $Å^2$ vs. 0.099±0.020 $Å^2$, p=0.005) had an increase in SASA in the R832 variant (**Figure 6.6 D, Figure 6.7 B**).

The A-domain contains the highly conserved TGE motif. This motif facilitates the dephosphorylation of the catalytic Asp and the conformational transitions of the full-length ATP7B protein (548). Increased structural fluctuations associated with the presence of Arg at position 832 could have long-range, allosteric effects on this motif. To examine this possibility, we analyzed the SASA changes for the residues that constitute the TGE motif T858, G859, E860) and found that the surface exposure of G859 (57.01±0.638 $Å^2$ vs. 51.03±1.078 $Å^2$, p<0.0001) and E860 (83.05±1.431 $Å^2$ vs. 100.90±1.582 $Å^2$, p<0.0001) was higher in the R832-containing variant. The surface exposure of T858 was most significantly increased (45.31±2.102 $Å^2$ vs. 86.81±1.156 $Å^2$, p<0.0001) in the R832 variant compared to the K832 variant (**Figure 6.6 E, Figure 6.7 B**).

To visualize the effect of the SNPRS on residue motions within the A-domain, we calculated the correlation matrix for all 140 residues in the domain and displayed them as a two-dimensional heat map (**Figure 6.6 F**). Positive cross-correlation values (yellow) indicate a strongly correlated

motion of the residues in the same direction during the simulation. Negative values (blue) imply an anti-correlated motion of the residues, i.e., no communication between the residues. Position 832 (residue 40 on the map) lies within the segment of strong correlation for both variants. However, the long-range effects vary between the R832 and K832 variants, especially for residues 60–100 and 120–140. In the R832 variant, these regions show strong correlation; in the K832 variant, these regions have a less strong correlation. Taken together, the computational studies illustrate different MD of the A-domain between the two variants, which may contribute to the distinct properties of the corresponding ATP7B variants in cells.

6.5 Discussion

SNPs are typically considered benign, largely because they are frequently detected in the healthy population. In addition, SNPs often produce substitutions that preserve the main chemical properties of the corresponding amino acid residues, such as charge, bulk, and hydrophobicity. Our studies of two common SNP-dependent amino-acid substitutions in ATP7B have confirmed that ATP7B is active with any of the four amino acid combinations at positions 832/952. At the same time, we found that these substitutions have measurable effects on both the structure and other properties of ATP7B. The presence of R832 and K952 modulates ATP7B abundance, trafficking, and Cu-transport activity to varying degrees. Analysis of markers of Cu status in human serum appears to correlate with these *in vitro* effects, although direct comparison of the Cu:Cp values with ATP7B abundance and activity is needed to draw firm conclusions.

These findings add to accumulating evidence that ATP7B SNPs influence cellular Cu homeostasis and, in combination with other factors, may contribute to human disease. The presence of R832 and K952 in ATP7B variants has been linked to higher levels of labile Cu in the serum in AD patients (513,516,549). Previous *in vitro* studies measuring the ATP7B-driven Cu uptake in vesicles revealed that the R832 variant had lower Cu-transport activity (514). Moreover, R832 was identified as a loss-of-function SNP in *Drosophila melanogaster* ATP7, an ATP7B homolog (514,517). The *Drosophila* ATP7 protein containing Arg at the position equivalent to human R832 had lower expression levels than the control, and it was suggested that the presence of Arg in this position may promote protein degradation (517). Our studies in human cells show that R832 alters ATP7B protein dynamics, abundance, and trafficking, and that the K832/K952 variant has lower Cu-transport activity. We did not find the inhibitory effect of R832 on ATP7B Cu transport activity in cells using the tyrosinase assay. This discrepancy could be due to the lower sensitivity of this assay in comparison to direct measurements of Cu uptake.

R832 is located in the A-domain, which is involved in conformational transitions and catalysis during the ATP7B enzymatic cycle (70). In addition, ATP7B abundance and trafficking is regulated by kinase-mediated phosphorylation of key Ser resides (507,550,551). Currently, it is not known whether R832K affects the phosphorylation state of ATP7B, and further study is needed. Our computational studies demonstrate that R832 alters the local structure, surface charge distribution, and dynamics of the A-domain. A higher conformational flexibility of the domain containing R832 may explain propensity to stronger degradation and decreased protein abundance of R832 variants compared to K832 containing proteins. Although differences between the ATP7B variants are rather small, in combination with other factors (or over long period of time) they may impact the overall cellular Cu balance.

K952 is located in the lumenal loop between TM segments 5 and 6. An equivalent loop in the homologous ATP7A has been shown to function in Cu release from the ATPase (543) and the loop between TM3 and TM4 of ATP7B has been identified as a site of kinase-mediated phosphorylation (217). We observed that in cells, the K832/K952 variant had lower Cu-transport activity when compared to other ATP7B variants, which is consistent with the potential negative effect on Cu release. The decrease in activity is not very large—about 20%. However, in Wilson disease patients with this genetic background, the presence of K952 may exacerbate the effects of otherwise mild ATP7B mutations.

Both R832 and K952 are common in the general population (513,550). If these SNPs alter ATP7B structure or diminish protein function, how could they be present in high frequencies in the healthy population? Squitti, et al. have shown that healthy individuals are more likely to be heterozygous for R832 and K952, while AD patients are more likely to have both variants (513). Analysis of Cu status markers in the serum—total Cu, total Cp, and non-Cp Cu---revealed that both R832 and K952 may affect Cu homeostasis, even in healthy individuals. Although total Cu levels are comparable between the R832 and K952 carriers and non-carriers, the presence of R832 appears

to correlate with lower Cp levels, and carriers of K952 have both lower levels of Cp and higher levels of exchangeable Cu. In other words, the presence of certain SNPs results in measurable changes to Cu parameters in humans.

Both R832 and K952 have been reported in WD patients alongside known WD mutations (**Table 2.1**). In Asian populations where WD prevalence is greater than that worldwide, R832 and K952 both appear with higher frequency. For example, the Han Chinese in Beijing (CHB) population has a WD prevalence of approximately 1 in 5400, compared to the worldwide prevalence of 1 in 30 000. R832 and K952 both appear in 65% of the CHB population, compared to 50% in the Utah Residents with Northern and Western European Ancestry (CEU) and the Indian (IND) populations (550,552). We speculate that SNPs are generally benign but, in combination with a disease-causing mutation, may exacerbate the manifestation of the disease. Determining any contributory effects these SNPs have on disease mutation phenotypes could shed insight onto disease physiology and mechanism. More in depth studies of the effects of SNPs could result in novel diagnosis or treatment strategies for rare diseases.

Table 6.1. Demographic and biological variables of healthy individuals that are either carriers or non-carriers of R832 and K952.

Values reported are means and SD. Normal, healthy levels range from 16–24 μM for serum Cu and 20–40 mg/dL for serum Cp (506).

	Mean	**Standard Deviation**
Age (years)	65.19	12.857
MMSE score	28	1.91
Copper (μM)	13.5524	2.877
Ceruloplasmin (mg/dL)	25.6731	5.50615
Non-ceruloplasmin copper (μM)	1.4347	2.27155
Copper:Ceruloplasmin	7.0625	1.11833

Table 6.2. Presence of R832K and K952R in patients with Wilson disease and corresponding clinical symptoms.

Serum Cu in μg/dL, Cp in mg/dL. Abbreviations: WD, Wilson disease; SNPs, single nucleotide polymorphisms; KF ring, Kayser-Fleischer ring; Cp, ceruloplasmin.

WD mutation	ATP7B SNPs	Age	Sex	Phenotype	KF ring	Serum Cu	Cp	Source
p.A990P	p.K823R	14	F	hepatic	Y	22	5	(553)
p.P768L	p.R952K	28	M	hepatic	N	70	14	
p.G691R	p.K823R p.R952K	3	F	cirrhosis, subclinical hepatitis	Y	N/A	N/A	(554)
p.G691R	p.K823R p.R952K	12	M	cirrhosis, subclinical hepatitis	Y	N/A	N/A	
N/A	p.K823R p.R952K	9	F	trigonocephaly, biparietal widening, hypertelorism, hepatomegaly	N	26	5	(555)
N/A	p.K823R p.R952K	13	M	trigonocephaly, biparietal widening, hypertelorism, hepatomegaly	N	13.3	5	
N/A	p.K823R p.R952K	24	F	ataxia, dystonia, tremor	Y	0.111	N/A	(556)
p.T1220M	p.K823R p.R952K	N/A	N/A	hepatic	N/A	N/A	N/A	(557)
c.2008-2013 del	p.K823R	N/A	N/A	hepatic	N/A	N/A	N/A	
p.R969Q p.H1069Q	p.K823R	N/A	N/A	hepatic	N/A	N/A	N/A	
p.C985T p.I1148T	p.R952K	N/A	N/A	hepatic	N/A	N/A	N/A	

p.H1069Q	p.K823R	17	M	neurological, cirrhosis	Y	N/A	3.5	(558)
p.H1069Q	p.K823R	18	M	neurological	Y	N/A	0.9	
p.H1069Q	p.K823R	19	F	neurological	Y	N/A	2.6	
p.H1069Q	p.K823R	6	M	high ALT & AST	N	N/A	0.4	
p.H1069Q	p.K823R	7	F	high ALT & AST	N	N/A	0.1	
p.H1069Q	p.K823R	19	M	neurological	Y	N/A	1.2	
p.H1069Q	p.K823R	20	M	neurological, cirrhosis	Y	N/A	2.3	

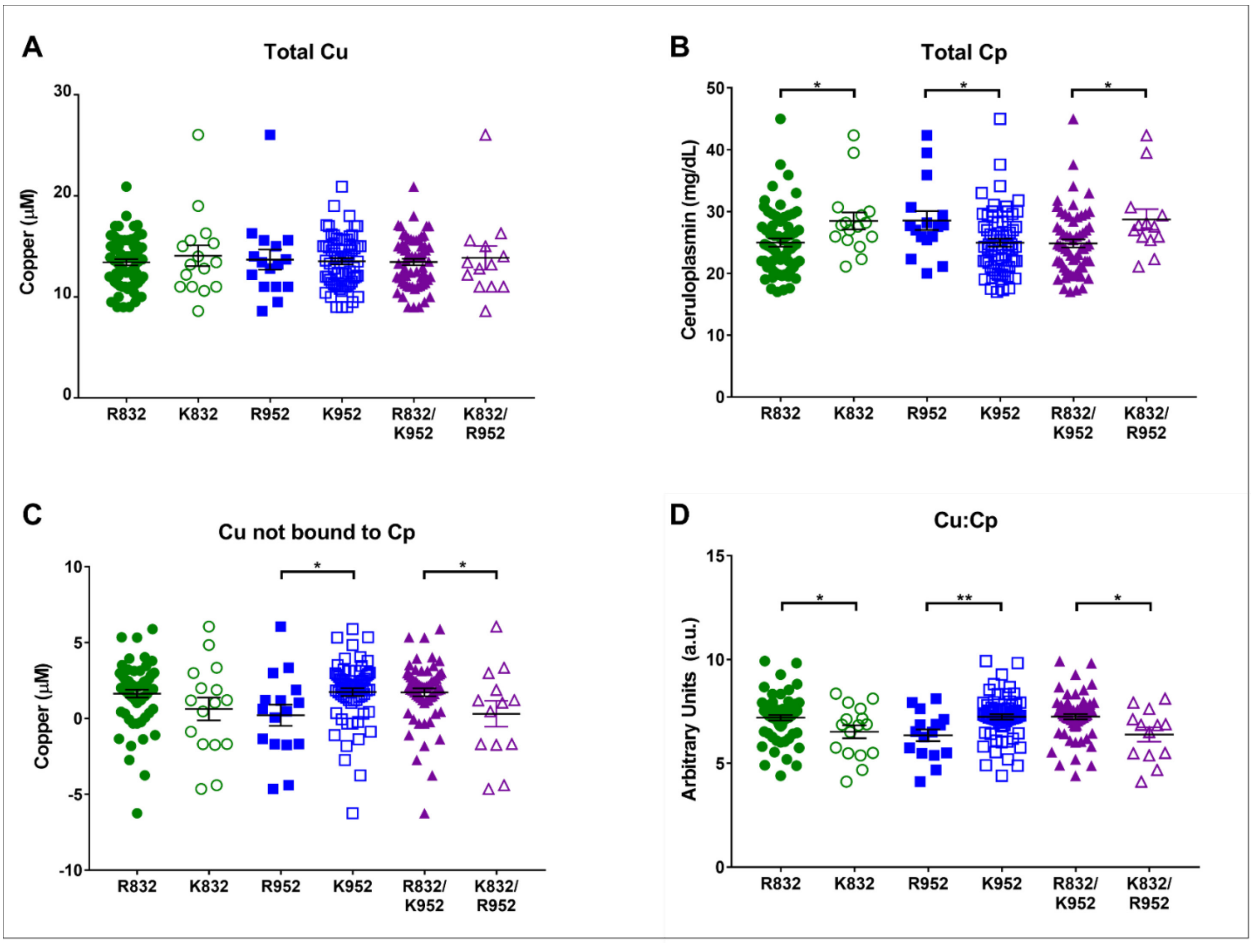

Figure 6.1. Presence of the R832 and K952 SNP-related substitutions (SNPRS) correlates with changes in serum Cu markers.

(A) Total Cu concentration, µM, in the serum samples of healthy individuals carrying ATP7B with indicated SNP-related amino acid substitutions. **(B)** Total serum Cp, mg/dL. **(C)** Non-Cp bound Cu, µM. **(D)** Ratio of total Cu to total Cp in the serum. (Normal, healthy range for Cu is 16-24 µM (559), for CP - 20-40 mg/dL (559), 0.07–2.19 µM for non-Cp Cu (560), and the Cu:CP ratio is 6.8 (560). *n*=16 for R832, *n*=65 for K832, *n*=16 for R952, *n*=65 for K952, *n*=13 for K832/R952, and *n*=62 for R832/K952. Values are reported as means ± SEM; significance was determined by Student's t-test, * $p<0.05$, ** $p<0.01$.

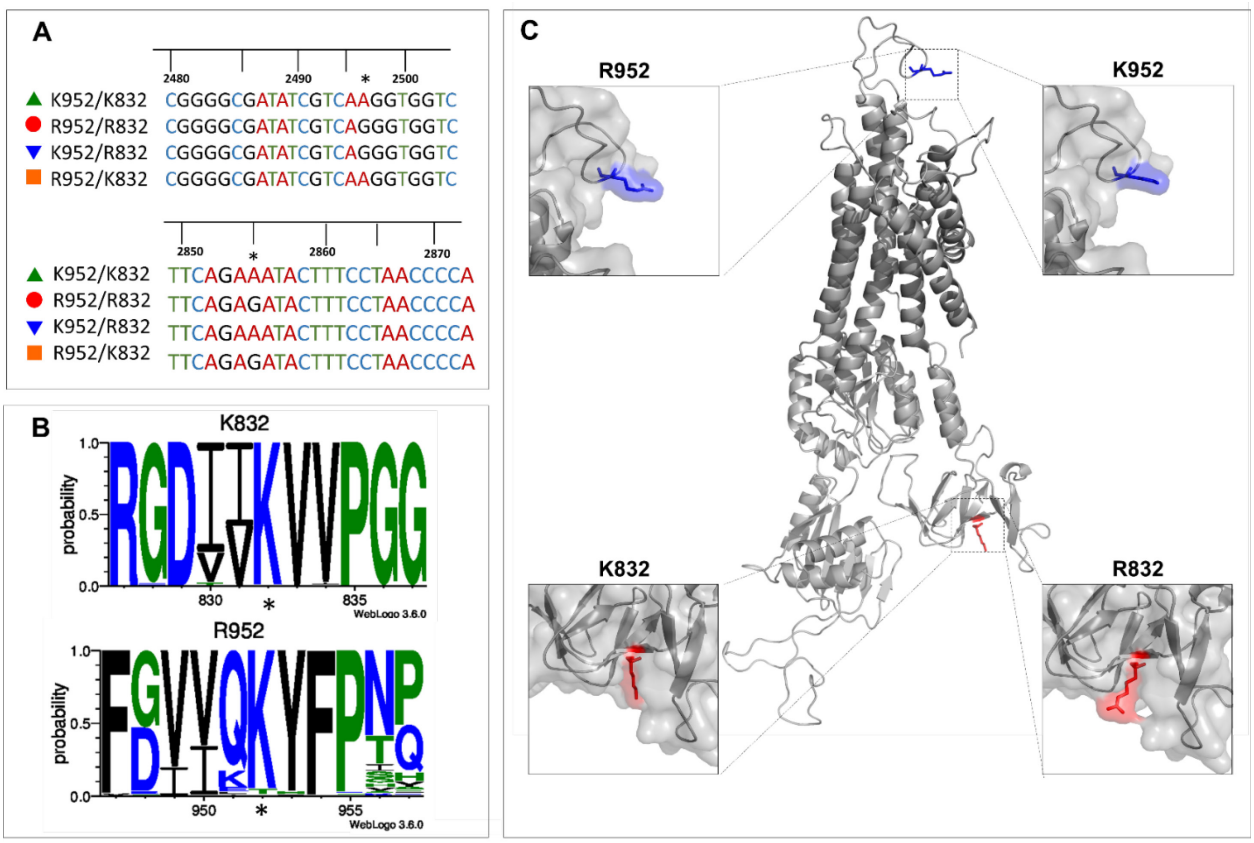

Figure 6.2. Location, conservation, and potential impact of SNP-related substitutions (SNPRS) on ATP7B structure.

(A) Sequence analysis of the ATP7B plasmids shows either an adenine (encoding Lys) or a guanine (encoding Arg) at positions 2495 and 2855, marked by asterisks. **(B)** The K832 SNP-RAAS is well-conserved among ATP7B homologs while the R952 SNP-RAAS is human-specific. Conservation logos of 11-AA sequences centered on the two SNPRSs, K832 and R952, from 165 animal ATP7B homologs. SNPRSs are marked with asterisks. **(C)** Homology model of ATP7B based on the crystal structure of *L. pneumophila* CopA. (524) *Left panels*, effects of the R/K variants at position 832 (red) on the A-domain of ATP7B. *Right panels*, effects of the R/K variants at position 952 (blue) on the lumenal loop region of ATP7B.

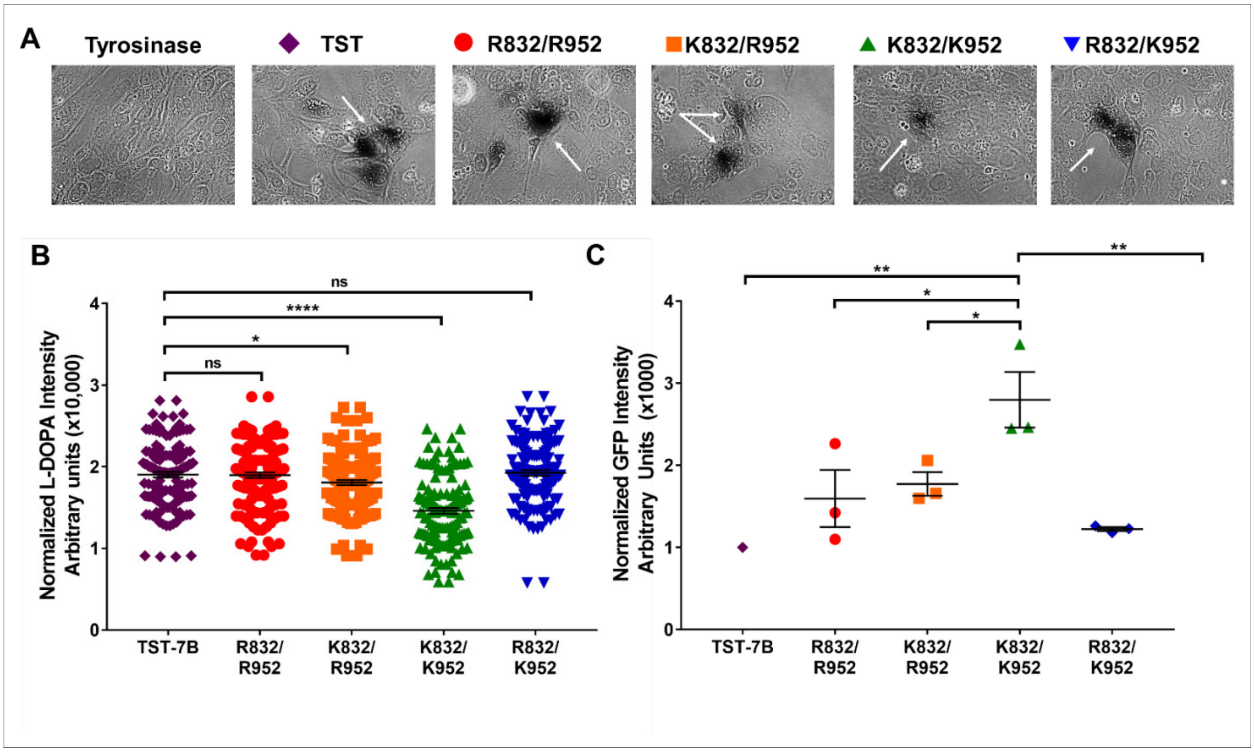

Figure 6.3. ATP7B-K952/K832 has a lower Cu-transport activity compared to other variants.

(A) Menkes fibroblasts were co-transfected with pTyrosinase (pTyr) alone or with either twin strep-tagged ATP7B (TST-ATP7B) or GFP-tagged SNP variant constructs. Activation of tyrosinase was measured as a means to evaluate Cu-transport activity of ATP7B variants. The dark brown reaction product indicates Cu-dependent tyrosinase activity (marked by white arrows). **(B)** Pigmentation intensity normalized to pigment area. TST-ATP7B in purple, R832/R952 in red, K832/R952 in orange, K832/K952 in green, and R832/K952 in blue. *n*=4, over 40 areas counted per *n*. **(C)** Quantitation of ATP7B-GFP expression in cells used in the Tyrosinase assay. GFP-ATP fluorescence were normalized to the area, the fluorescence from control cells expressing the pTyr plasmid served as a background control and the values were compared to fluorescence from cells expressing the TST-ATP7B plasmid, taken as 1 (*n*=3). All values are reported as means ± SEM; significance was determined by one-way ANOVA with Fisher's LSD test, * $p<0.05$, ** $p<0.01$, **** $p<0.0001$.

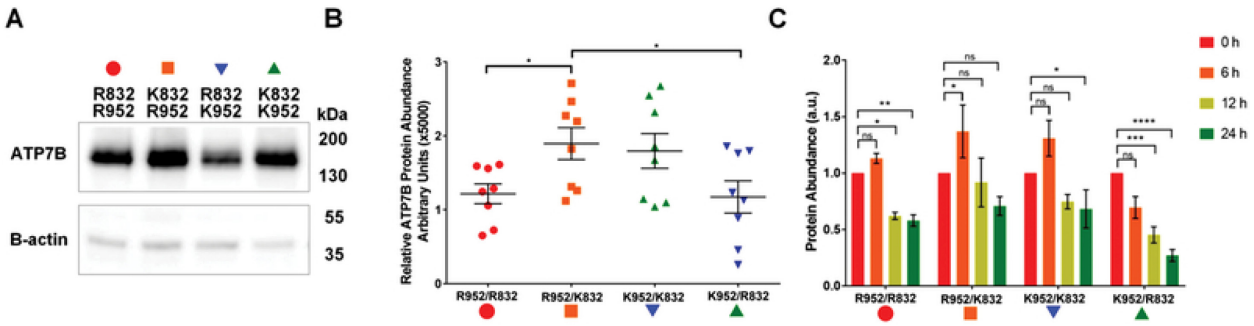

Figure 6.4. Presence of R832 is associated with lower ATP7B abundance.

(A) HEK293A cells were transfected with ATP7B-GFP variants for 20 h, whole cell lysates were prepared and run on SDS-PAGE (20 mg of protein per lane). Western blot shows the relative abundance of each ATP7B variant. β-Actin is used as a loading control. **(B)** Densitometry of Western blots, *n*=8. R832/R952 in red, K832/R952 in orange, R832/K952 in blue, and K832/ K952 in green. Intensities of ATP7B bands were normalized to β-actin and plotted. Means ± SEM are indicated by horizontal lines. Significance was determined by one-way ANOVA with Fisher's LSD test; * $p<0.05$. **(C)** The R832-containing ATP7B variants are more susceptible to degradation than K832 variants. HEK293A cells were transfected as described above, and then treated with 50 mM cycloheximide (CHX) for 0, 6, 12, or 24 h. For each time point, whole cell lysates were prepared, and equal amounts of total protein (5 mg per lane) were run on SDS-PAGE; ATP7B was visualized by Western blotting. The bars indicate the intensity of ATP7B bands at 6 h (orange), 12 h (yellow), and 24 h (green) relative to intensity at the 0h time point (red), which is taken as 1. *n*=4. Values are reported as means ± SEM. Significance was determined by one-way ANOVA with Fisher's LSD test; * $p<0.05$, ** $p<0.01$, *** $p<0.001$, and **** $p<0.0001$.

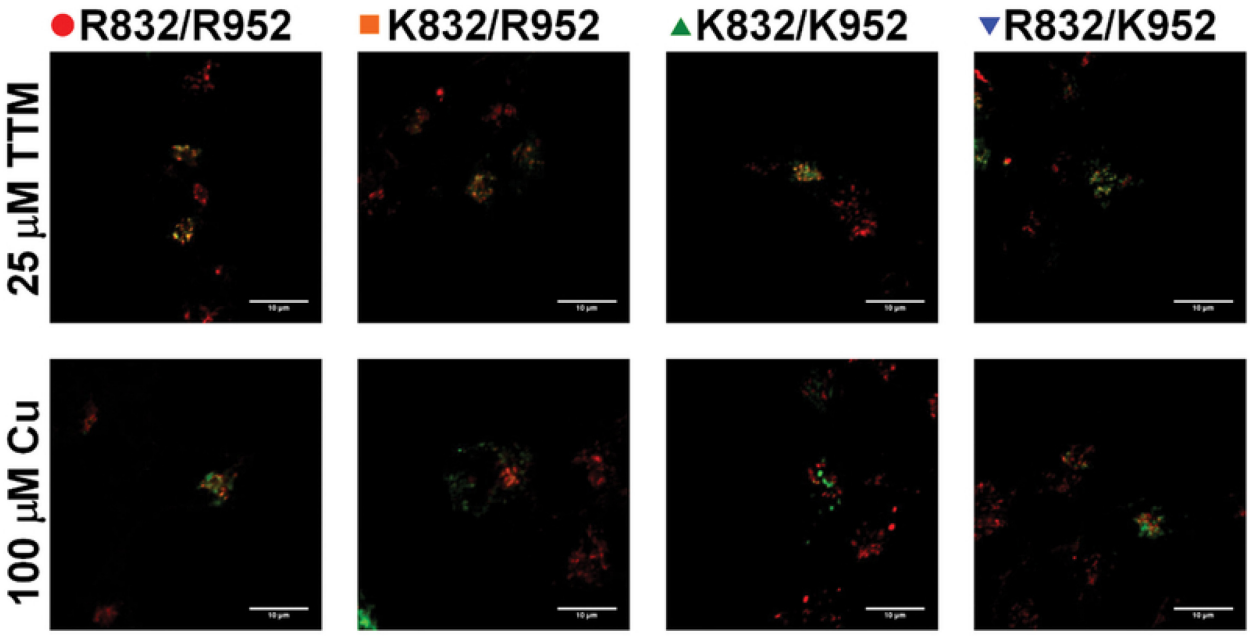

Figure 6.5. Localization of ATP7B variants in HEK293 cells in low and high copper.

HEK293 cells were transfected with one of the indicated ATP7B-GFP variant (green), cells were treated for 4 h with either 25 mM TTM (top panels) or 100 μM CuSO4 (bottom panels) and immunostained for trans Golgi network marker TGN46 (red). Co-localization is indicated by yellow; the loss of co-localization is indicative of ATP7B trafficking (*n*=4).

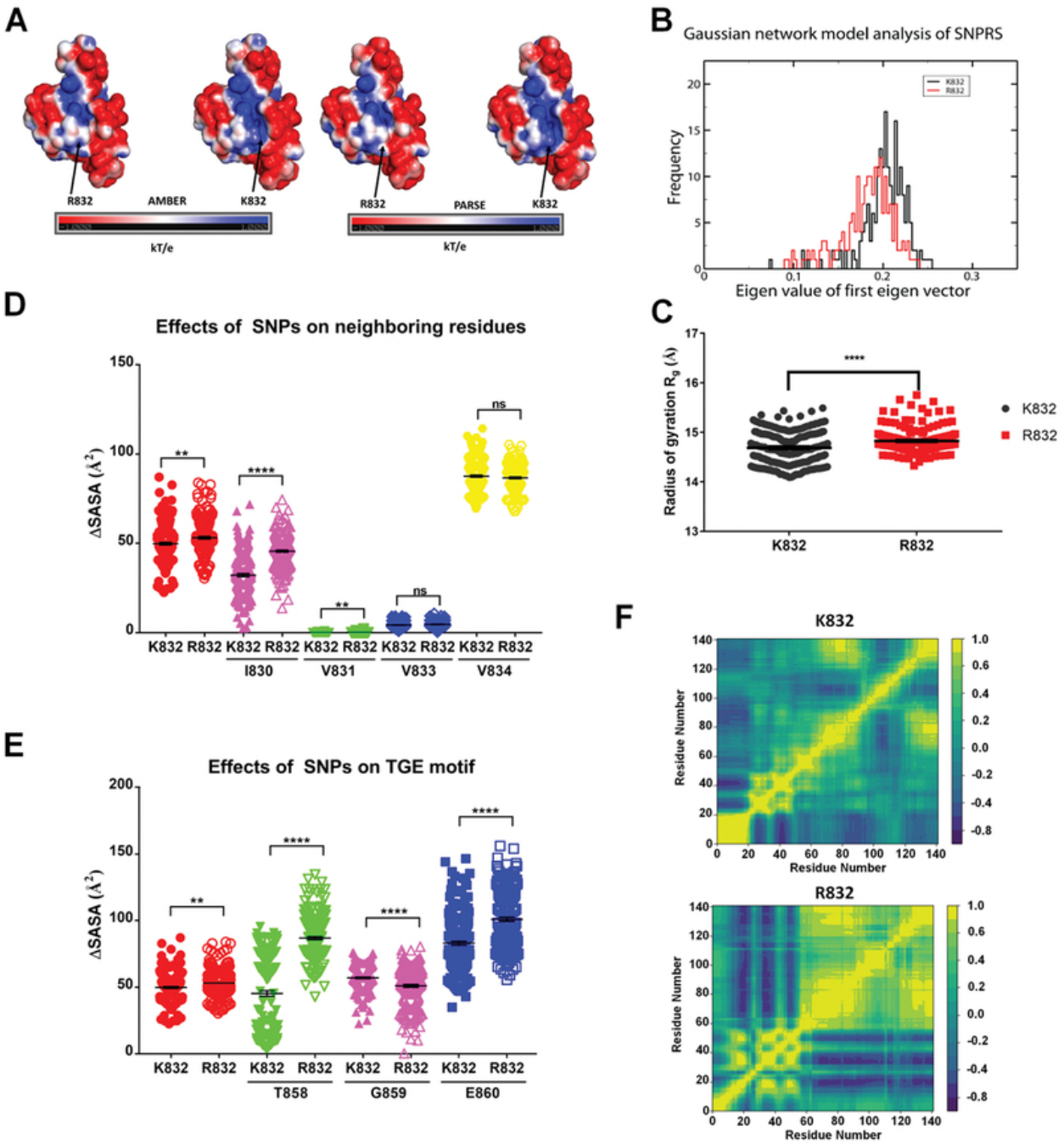

Figure 6.6. R832 increases A-domain flexibility.

(A) Surface electrostatics of the ATP7B A-domain(111) containing R832/K832 variants quantified using AMBER (left pair) or PARSE (right pair). **(B)** R832 increases the conformational flexibility of the A-domain. Gaussian network mode-based normal mode frequencies of K832 in black and R832 in red. **(C)** The radius of gyration of the A-domain containing either K832 (red) or R832 (gray). **(D)** The variation of SASA values for neighboring AA residues in β sheet 3 during 200 ns

simulation. R832 (red, filled circles), K832 (red, open circles): I830 (magenta), V831 (green), V833 (blue) and V834 (yellow). **(E)** Variation in SASA values for residues from the TGE motif in the R832 and K832 A domains: T858 (green), G859 (magenta), and E860 (blue). **(F)** Cross-correlation maps of AA motions in K832 (top) and R832 (bottom) A-domains during 200 ns simulation. Positive values (yellow) indicate motion in the same direction, whereas negative values (blue) indicate motion in the opposite direction. All values are reported as means SEM. Significance was determined by unpaired Student's t-test; ** $p<0.01$, **** $p<0.0001$.

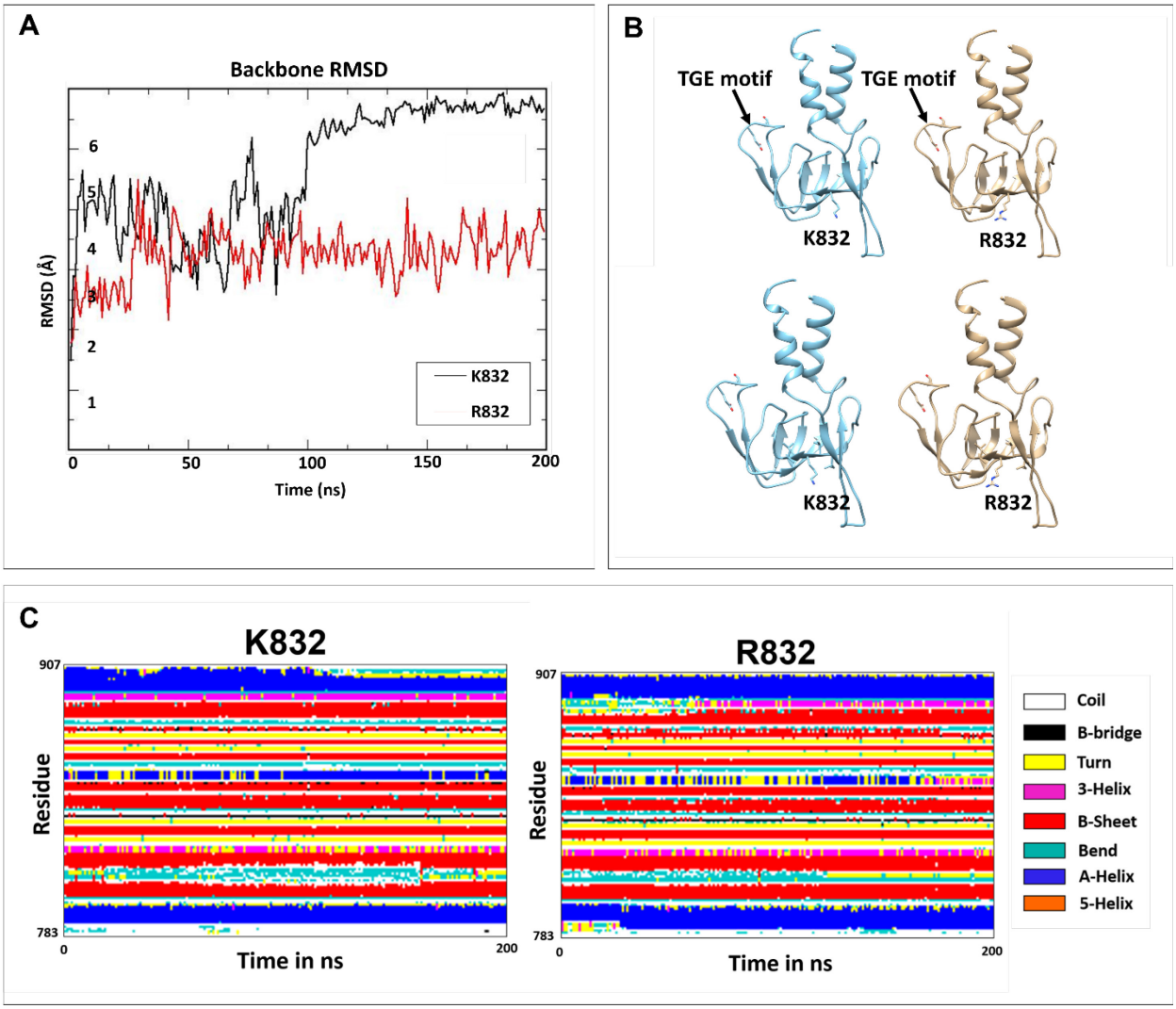

Figure 6.7. Molecular dynamics simulations of the isolated A-domain.

(A) Root mean square deviation (RMSD) differs between the domain containing K832 or R832. The backbone RMSD of the 200 nanosecond all-atom MD simulation for K832 (black) and R832 (red). **(B)** Ribbon models of the isolated K832 and R832 A-domain with the K832R residues shown as sticks. *Top panel*, residues in the TGE motif—T858, G859, E860—are shown as sticks. *Bottom panel*, residues neighboring K832R in the β-sheet 3—I830, V831, V833, and V834—highlighted as sticks. **(C)** Effects of the 832 SNPs on the secondary structure of the A-domain. The secondary structural changes on the A-domain due to K832 (left) and R832 (right), shown as a DSSP secondary structure time series diagram.

Abbreviations

A2 response element, A2 response element;

A2B1-e2 KD, hnRNP A2/B1 exon 2-specific knockdown;

A2B1-T KD, hnRNP A2/B1 total knockdown;

AA, amino acid;

AAS, atomic absorption spectrometry;

AD, Alzheimer's disease;

Ago2, argonaute-2;

ALS, amyotrophic lateral sclerosis;

AP-1, activator protein-1;

ARE; AU-rich element;

Arg, arginine;

Asn, asparagine;

Asp, aspartic acid;

Atox1, antioxidant 1 Cu chaperone;

ATP, adenosine triphosphate;

ATPase, adenosine triphosphatase;

ATP7A, copper-transporting ATPase 1;

ATP7B, copper-transporting ATPase 2;

BCA assay, bicinchoninic acid assay;

BDNF, brain-derived neurotrophic factor;

BSA, bovine serum albumin;

CAPS buffer, N-cyclohexyl-3-aminopropanesulfonic acid;

Cav-1, caveolin-1

CCO, cytochrome *c* oxidase;

CCR4-NOT, carbon catabolite repression 4-negative on TATA-less protein;

CCS, copper chaperone for superoxide dismutase;

Cd, cadmium;

C/EBP, CCAAT/enhancer-binding protein;

CHX, cycloheximide;

COMMD1, copper metabolism MURR1 domain protein 1;

Cox17, cytochrome *c* oxidase copper chaperone 17;

Cox11, cytochrome *c* oxidase copper chaperone 11;

Cp, ceruloplasmin;

CRISPR, clustered regularly interspaced short palindromic repeats;

CTPS2, CTP Synthase 2;

Ctr1, copper transporter 1;

Ctr2, copper transporter 2;

Cu, copper;

Cys, cysteine;

DAPI, 4′,6-diamidino-2-phenylindole;

Dcp1/2, decapping protein 1/2;

DDX20, DEAD-Box Helicase 20;

DMEM, Dulbecco’s Modified Eagle Medium;

DSSP plot, definition of secondary structure of proteins;

ECL, enhanced chemiluminescence;

EDTA, ethylenediaminetetraacetic acid;

eIF, eukaryotic initiation factor;

ELAV, embryonic lethal abnormal vision;

EMEM, Eagle’s Minimum Essential Medium;

FBS, fetal bovine serum;

Fe, iron;

G3BP, Ras-GAP SH3 binding protein

GDP, guanosine diphosphate;

GFP, green fluorescent protein;

Glu, glutamic acid;

Gly, glycine;

GNM, Gaussian network model;

GTP, guanosine triphosphate;

GW/P-bodies, Gly- and Trp-rich cytoplasmic processing bodies;

HGT, 6x His-GFP-TEV;

HIF-2α, hypoxia-inducible factor 2α;

His, histidine;

hnRNP, heterogeneous nuclear ribonucleoprotein;

hnRNP A2/B1, heterogeneous nuclear ribonucleoprotein A2/B1;

hnRNP A1, heterogeneous nuclear ribonucleoprotein A1;

HPLC, high-pressure liquid chromatography;

HRP, horseradish peroxide;

IRES, internal ribosome entry site;

ITAF, IRES-transactivating factors;

kb, kilobases;

KD, knockdown;

kDa, kiloDaltons;

KH domain, K-homology domain;

LAMP 1, lysosome-associated membrane protein 1;

LCD, low-complexity domain;

L-DOPA, levo-3,4-dihydroxyl-L-phenylalanine;

LLPS, liquid-liquid phase separation;

Lys, lysine;

m^6A, N6 nitrogen methylation;

MBD, metal-binding domain;

MBP, myelin basic protein;

MD, Menkes disease;

Met, methionine;

miRNA/miR, micro-RNA;

MRE, metal response element;

mRNA, messenger RNA;

MT, metallothionein;

MTF, metal-responsive transcription factor-1;

NAFLD, non-alcoholic fatty liver disease;

N/C ratio, nucleocytoplasmic ratio;

ND, non-differentiated

NLS, nuclear localization signal;

NMDA, N-methyl-D-aspartate;

ns, not significant;

nt, nucleotide;

NT KD, non-targeting knockdown;

PABP, poly(A)-binding protein;

PAS, polyadenylation site;

PBS, phosphate buffered saline;

PFA, paraformaldehyde;

PLB, passive lysis buffer;

poly(A) tail, polyadenine tail;

PrLD, prion-like domain;

qRRM, quasi-RNA recognition motif;

qRT-PCR, quantitative real-time polymerase chain reaction;

RA, retinoic acid;

Ran, Ras-related nuclear protein;

RBP, RNA-binding protein;

RGG box, Arg-Gly-Gly box;

RIPA buffer, radioimmunoprecipitation assay buffer;

RMSD, root-mean-square deviation;

RNA Pol II, RNA polymerase II;

RNP, ribonucleoprotein;

RRM, RNA recognition motif;

RT, room temperature;

SASA, solvent accessible surface area;

Sco1, synthesis of cytochrome *c* oxidase 1;

Sco2, synthesis of cytochrome *c* oxidase 2;

SDS, sodium dodecyl sulfate;

Se, selenium;

Ser, serine;

SG, stress granules;

siRNA, small interfering RNA;

SNP, single nucleotide polymorphism;

SNPRS, SNP-related substitution;

SOD1, superoxide dismutase 1;

Sp1, specificity protein 1;

SUMO, small ubiquitin-like modifier;

TAp73, transcriptional activator p73;

TF, transcription factor;

TGN, *trans*-Golgi network;

TIA, T-cell intracellular antigen;

Thr, threonine;

TM, transmembrane;

Trp, tryptophan;

TST, twin-strep tag;

TTM, tetra-thiomolybdate;

U-bodies, U-rich small nuclear ribonucleoprotein-containing bodies;

UTR, untranslated region;

WD, Wilson disease;

WT, wild type;

XIAP, X-linked inhibitor of apoptosis;

Zn, zinc

References

1. Bertinato, J., and L'Abbe, M. R. (2004) Maintaining copper homeostasis: regulation of copper-trafficking proteins in response to copper deficiency or overload. *J Nutr Biochem* **15**, 316-322
2. Uauy, R., Olivares, M., and Gonzalez, M. (1998) Essentiality of copper in humans. *Am J Clin Nutr* **67**, 952S-959S
3. Burkhead, J. L., Gogolin Reynolds, K. A., Abdel-Ghany, S. E., Cohu, C. M., and Pilon, M. (2009) Copper homeostasis. *New Phytol* **182**, 799-816
4. Lutsenko, S. (2010) Human copper homeostasis: a network of interconnected pathways. *Curr Opin Chem Biol* **14**, 211-217
5. Huster, D., Finegold, M. J., Morgan, C. T., Burkhead, J. L., Nixon, R., Vanderwerf, S. M., Gilliam, C. T., and Lutsenko, S. (2006) Consequences of copper accumulation in the livers of the Atp7b-/- (Wilson disease gene) knockout mice. *Am J Pathol* **168**, 423-434
6. Waggoner, D. J., Bartnikas, T. B., and Gitlin, J. D. (1999) The role of copper in neurodegenerative disease. *Neurobiology of Disease* **6**, 221-230
7. Kaler, S. G. (2011) ATP7A-related copper transport diseases-emerging concepts and future trends. *Nat Rev Neurol* **7**, 15-29
8. Lutsenko, S. (2016) Copper trafficking to the secretory pathway. *Metallomics* **8**, 840-852
9. Trumbo, P., Yates, A. A., Schlicker, S., and Poos, M. (2001) Dietary reference intakes: vitamin A, vitamin K, arsenic, boron, chromium, copper, iodine, iron, manganese, molybdenum, nickel, silicon, vanadium, and zinc. *J Am Diet Assoc* **101**, 294-301
10. Aigner, E., Strasser, M., Haufe, H., Sonnweber, T., Hohla, F., Stadlmayr, A., Solioz, M., Tilg, H., Patsch, W., Weiss, G., Stickel, F., and Datz, C. (2010) A role for low hepatic copper concentrations in nonalcoholic Fatty liver disease. *Am J Gastroenterol* **105**, 1978-1985
11. Tallino, S., Duffy, M., Ralle, M., Cortes, M. P., Latorre, M., and Burkhead, J. L. (2015) Nutrigenomics analysis reveals that copper deficiency and dietary sucrose up-regulate inflammation, fibrosis and lipogenic pathways in a mature rat model of nonalcoholic fatty liver disease. *J Nutr Biochem* **26**, 996-1006
12. Festa, R. A., and Thiele, D. J. (2011) Copper: an essential metal in biology. *Curr Biol* **21**, R877-883
13. Gupte, A., and Mumper, R. J. (2009) Elevated copper and oxidative stress in cancer cells as a target for cancer treatment. *Cancer Treat Rev* **35**, 32-46
14. Wee, N. K., Weinstein, D. C., Fraser, S. T., and Assinder, S. J. (2013) The mammalian copper transporters CTR1 and CTR2 and their roles in development and disease. *Int J Biochem Cell Biol* **45**, 960-963
15. Song, I. S., Chen, H. H., Aiba, I., Hossain, A., Liang, Z. D., Klomp, L. W., and Kuo, M. T. (2008) Transcription factor Sp1 plays an important role in the regulation of copper homeostasis in mammalian cells. *Mol Pharmacol* **74**, 705-713
16. Lee, J., Prohaska, J. R., and Thiele, D. J. (2001) Essential role for mammalian copper transporter Ctr1 in copper homeostasis and embryonic development. *Proc Natl Acad Sci U S A* **98**, 6842-6847
17. Nevitt, T., Ohrvik, H., and Thiele, D. J. (2012) Charting the travels of copper in eukaryotes from yeast to mammals. *Biochim Biophys Acta* **1823**, 1580-1593
18. Larson, C. A., Adams, P. L., Jandial, D. D., Blair, B. G., Safaei, R., and Howell, S. B. (2010) The role of the N-terminus of mammalian copper transporter 1 in the cellular accumulation of cisplatin. *Biochem Pharmacol* **80**, 448-454
19. Lee, J., Pena, M. M., Nose, Y., and Thiele, D. J. (2002) Biochemical characterization of the human copper transporter Ctr1. *J Biol Chem* **277**, 4380-4387

20. Klomp, A. E., Tops, B. B., Van Denberg, I. E., Berger, R., and Klomp, L. W. (2002) Biochemical characterization and subcellular localization of human copper transporter 1 (hCTR1). *Biochem J* **364**, 497-505
21. Klomp, A. E., Juijn, J. A., van der Gun, L. T., van den Berg, I. E., Berger, R., and Klomp, L. W. (2003) The N-terminus of the human copper transporter 1 (hCTR1) is localized extracellularly, and interacts with itself. *Biochem J* **370**, 881-889
22. Eisses, J. F., and Kaplan, J. H. (2002) Molecular characterization of hCTR1, the human copper uptake protein. *J Biol Chem* **277**, 29162-29171
23. Lutsenko, S., Bhattacharjee, A., and Hubbard, A. L. (2010) Copper handling machinery of the brain. *Metallomics* **2**, 596-608
24. Petris, M. J., Smith, K., Lee, J., and Thiele, D. J. (2003) Copper-stimulated endocytosis and degradation of the human copper transporter, hCtr1. *J Biol Chem* **278**, 9639-9646
25. Kuo, Y. M., Zhou, B., Cosco, D., and Gitschier, J. (2001) The copper transporter CTR1 provides an essential function in mammalian embryonic development. *Proc Natl Acad Sci U S A* **98**, 6836-6841
26. Kim, B. E., Turski, M. L., Nose, Y., Casad, M., Rockman, H. A., and Thiele, D. J. (2010) Cardiac copper deficiency activates a systemic signaling mechanism that communicates with the copper acquisition and storage organs. *Cell Metab* **11**, 353-363
27. Nose, Y., Kim, B. E., and Thiele, D. J. (2006) Ctr1 drives intestinal copper absorption and is essential for growth, iron metabolism, and neonatal cardiac function. *Cell Metab* **4**, 235-244
28. Kim, H., Son, H. Y., Bailey, S. M., and Lee, J. (2009) Deletion of hepatic Ctr1 reveals its function in copper acquisition and compensatory mechanisms for copper homeostasis. *Am J Physiol Gastrointest Liver Physiol* **296**, G356-364
29. van den Berghe, P. V., Folmer, D. E., Malingre, H. E., van Beurden, E., Klomp, A. E., van de Sluis, B., Merkx, M., Berger, R., and Klomp, L. W. (2007) Human copper transporter 2 is localized in late endosomes and lysosomes and facilitates cellular copper uptake. *Biochem J* **407**, 49-59
30. Bertinato, J., Swist, E., Plouffe, L. J., Brooks, S. P., and L'Abbe M, R. (2008) Ctr2 is partially localized to the plasma membrane and stimulates copper uptake in COS-7 cells. *Biochem J* **409**, 731-740
31. Portnoy, M. E., Schmidt, P. J., Rogers, R. S., and Culotta, V. C. (2001) Metal transporters that contribute copper to metallochaperones in Saccharomyces cerevisiae. *Mol Genet Genomics* **265**, 873-882
32. Kampfenkel, K., Kushnir, S., Babiychuk, E., Inze, D., and Van Montagu, M. (1995) Molecular characterization of a putative Arabidopsis thaliana copper transporter and its yeast homologue. *J Biol Chem* **270**, 28479-28486
33. Abada, P., and Howell, S. B. (2010) Regulation of Cisplatin cytotoxicity by cu influx transporters. *Met Based Drugs* **2010**, 317581
34. Macomber, L., and Imlay, J. A. (2009) The iron-sulfur clusters of dehydratases are primary intracellular targets of copper toxicity. *Proc Natl Acad Sci U S A* **106**, 8344-8349
35. Ladomersky, E., and Petris, M. J. (2015) Copper tolerance and virulence in bacteria. *Metallomics* **7**, 957-964
36. Gudekar, N., Shanbhag, V., Wang, Y., Ralle, M., Weisman, G. A., and Petris, M. J. (2020) Metallothioneins regulate ATP7A trafficking and control cell viability during copper deficiency and excess. *Sci Rep* **10**, 7856
37. Balamurugan, K., and Schaffner, W. (2006) Copper homeostasis in eukaryotes: teetering on a tightrope. *Biochim Biophys Acta* **1763**, 737-746
38. Hatori, Y., and Lutsenko, S. (2016) The Role of Copper Chaperone Atox1 in Coupling Redox Homeostasis to Intracellular Copper Distribution. *Antioxidants (Basel)* **5**

39. Hamza, I., Schaefer, M., Klomp, L. W., and Gitlin, J. D. (1999) Interaction of the copper chaperone HAH1 with the Wilson disease protein is essential for copper homeostasis. *Proc Natl Acad Sci U S A* **96**, 13363-13368
40. Larin, D., Mekios, C., Das, K., Ross, B., Yang, A. S., and Gilliam, T. C. (1999) Characterization of the interaction between the Wilson and Menkes disease proteins and the cytoplasmic copper chaperone, HAH1p. *J Biol Chem* **274**, 28497-28504
41. Walker, J. M., Tsivkovskii, R., and Lutsenko, S. (2002) Metallochaperone Atox1 transfers copper to the NH2-terminal domain of the Wilson's disease protein and regulates its catalytic activity. *J Biol Chem* **277**, 27953-27959
42. Hamza, I., Prohaska, J., and Gitlin, J. D. (2003) Essential role for Atox1 in the copper-mediated intracellular trafficking of the Menkes ATPase. *Proc Natl Acad Sci U S A* **100**, 1215-1220
43. Itoh, S., Kim, H. W., Nakagawa, O., Ozumi, K., Lessner, S. M., Aoki, H., Akram, K., McKinney, R. D., Ushio-Fukai, M., and Fukai, T. (2008) Novel role of antioxidant-1 (Atox1) as a copper-dependent transcription factor involved in cell proliferation. *J Biol Chem* **283**, 9157-9167
44. Hamza, I., Faisst, A., Prohaska, J., Chen, J., Gruss, P., and Gitlin, J. D. (2001) The metallochaperone Atox1 plays a critical role in perinatal copper homeostasis. *Proc Natl Acad Sci U S A* **98**, 6848-6852
45. Schmidt, P. J., Kunst, C., and Culotta, V. C. (2000) Copper activation of superoxide dismutase 1 (SOD1) in vivo. Role for protein-protein interactions with the copper chaperone for SOD1. *J Biol Chem* **275**, 33771-33776
46. Furukawa, Y., Torres, A. S., and O'Halloran, T. V. (2004) Oxygen-induced maturation of SOD1: a key role for disulfide formation by the copper chaperone CCS. *EMBO J* **23**, 2872-2881
47. Wong, P. C., Waggoner, D., Subramaniam, J. R., Tessarollo, L., Bartnikas, T. B., Culotta, V. C., Price, D. L., Rothstein, J., and Gitlin, J. D. (2000) Copper chaperone for superoxide dismutase is essential to activate mammalian Cu/Zn superoxide dismutase. *Proc Natl Acad Sci U S A* **97**, 2886-2891
48. Carroll, M. C., Girouard, J. B., Ulloa, J. L., Subramaniam, J. R., Wong, P. C., Valentine, J. S., and Culotta, V. C. (2004) Mechanisms for activating Cu- and Zn-containing superoxide dismutase in the absence of the CCS Cu chaperone. *Proc Natl Acad Sci U S A* **101**, 5964-5969
49. Subramaniam, J. R., Lyons, W. E., Liu, J., Bartnikas, T. B., Rothstein, J., Price, D. L., Cleveland, D. W., Gitlin, J. D., and Wong, P. C. (2002) Mutant SOD1 causes motor neuron disease independent of copper chaperone-mediated copper loading. *Nat Neurosci* **5**, 301-307
50. Horng, Y. C., Cobine, P. A., Maxfield, A. B., Carr, H. S., and Winge, D. R. (2004) Specific copper transfer from the Cox17 metallochaperone to both Sco1 and Cox11 in the assembly of yeast cytochrome C oxidase. *J Biol Chem* **279**, 35334-35340
51. Rees, E. M., and Thiele, D. J. (2004) From aging to virulence: forging connections through the study of copper homeostasis in eukaryotic microorganisms. *Curr Opin Microbiol* **7**, 175-184
52. Lode, A., Kuschel, M., Paret, C., and Rodel, G. (2000) Mitochondrial copper metabolism in yeast: interaction between Sco1p and Cox2p. *FEBS Lett* **485**, 19-24
53. Horng, Y. C., Leary, S. C., Cobine, P. A., Young, F. B., George, G. N., Shoubridge, E. A., and Winge, D. R. (2005) Human Sco1 and Sco2 function as copper-binding proteins. *J Biol Chem* **280**, 34113-34122
54. Inesi, G. (2017) Molecular features of copper binding proteins involved in copper homeostasis. *IUBMB Life* **69**, 211-217

55. Leary, S. C., Cobine, P. A., Kaufman, B. A., Guercin, G. H., Mattman, A., Palaty, J., Lockitch, G., Winge, D. R., Rustin, P., Horvath, R., and Shoubridge, E. A. (2007) The human cytochrome c oxidase assembly factors SCO1 and SCO2 have regulatory roles in the maintenance of cellular copper homeostasis. *Cell Metab* **5**, 9-20
56. Leary, S. C., Sasarman, F., Nishimura, T., and Shoubridge, E. A. (2009) Human SCO2 is required for the synthesis of CO II and as a thiol-disulphide oxidoreductase for SCO1. *Hum Mol Genet* **18**, 2230-2240
57. Glerum, D. M., Shtanko, A., and Tzagoloff, A. (1996) SCO1 and SCO2 act as high copy suppressors of a mitochondrial copper recruitment defect in Saccharomyces cerevisiae. *J Biol Chem* **271**, 20531-20535
58. Takahashi, Y., Kako, K., Kashiwabara, S., Takehara, A., Inada, Y., Arai, H., Nakada, K., Kodama, H., Hayashi, J., Baba, T., and Munekata, E. (2002) Mammalian copper chaperone Cox17p has an essential role in activation of cytochrome C oxidase and embryonic development. *Mol Cell Biol* **22**, 7614-7621
59. Bamji, M. (2004) *Functional characterization of the human cytochrome c oxidase factor COX11 using RNA interference.* Master of Science, McGill University
60. Barresi, V., Trovato-Salinaro, A., Spampinato, G., Musso, N., Castorina, S., Rizzarelli, E., and Condorelli, D. F. (2016) Transcriptome analysis of copper homeostasis genes reveals coordinated upregulation of SLC31A1,SCO1, and COX11 in colorectal cancer. *FEBS Open Bio* **6**, 794-806
61. Stiburek, L., Vesela, K., Hansikova, H., Hulkova, H., and Zeman, J. (2009) Loss of function of Sco1 and its interaction with cytochrome c oxidase. *Am J Physiol Cell Physiol* **296**, C1218-1226
62. Valnot, I., Osmond, S., Gigarel, N., Mehaye, B., Amiel, J., Cormier-Daire, V., Munnich, A., Bonnefont, J. P., Rustin, P., and Rotig, A. (2000) Mutations of the SCO1 gene in mitochondrial cytochrome c oxidase deficiency with neonatal-onset hepatic failure and encephalopathy. *Am J Hum Genet* **67**, 1104-1109
63. Salviati, L., Sacconi, S., Rasalan, M. M., Kronn, D. F., Braun, A., Canoll, P., Davidson, M., Shanske, S., Bonilla, E., Hays, A. P., Schon, E. A., and DiMauro, S. (2002) Cytochrome c oxidase deficiency due to a novel SCO2 mutation mimics Werdnig-Hoffmann disease. *Arch Neurol* **59**, 862-865
64. Leary, S. C., Kaufman, B. A., Pellecchia, G., Guercin, G. H., Mattman, A., Jaksch, M., and Shoubridge, E. A. (2004) Human SCO1 and SCO2 have independent, cooperative functions in copper delivery to cytochrome c oxidase. *Hum Mol Genet* **13**, 1839-1848
65. Papadopoulou, L. C., Sue, C. M., Davidson, M. M., Tanji, K., Nishino, I., Sadlock, J. E., Krishna, S., Walker, W., Selby, J., Glerum, D. M., Coster, R. V., Lyon, G., Scalais, E., Lebel, R., Kaplan, P., Shanske, S., De Vivo, D. C., Bonilla, E., Hirano, M., DiMauro, S., and Schon, E. A. (1999) Fatal infantile cardioencephalomyopathy with COX deficiency and mutations in SCO2, a COX assembly gene. *Nat Genet* **23**, 333-337
66. Jaksch, M., Ogilvie, I., Yao, J., Kortenhaus, G., Bresser, H. G., Gerbitz, K. D., and Shoubridge, E. A. (2000) Mutations in SCO2 are associated with a distinct form of hypertrophic cardiomyopathy and cytochrome c oxidase deficiency. *Hum Mol Genet* **9**, 795-801
67. McCord, J. M., and Fridovich, I. (1969) Superoxide dismutase. An enzymic function for erythrocuprein (hemocuprein). *J Biol Chem* **244**, 6049-6055
68. Banci, L., Bertini, I., Cantini, F., Kozyreva, T., Massagni, C., Palumaa, P., Rubino, J. T., and Zovo, K. (2012) Human superoxide dismutase 1 (hSOD1) maturation through interaction with human copper chaperone for SOD1 (hCCS). *Proc Natl Acad Sci U S A* **109**, 13555-13560
69. Seo, S. J., Kim, H. T., Cho, G., Rho, H. M., and Jung, G. (1996) Sp1 and C/EBP-related factor regulate the transcription of human Cu/Zn SOD gene. *Gene* **178**, 177-185

70. Banci, L., Bertini, I., Cantini, F., Migliardi, M., Natile, G., Nushi, F., and Rosato, A. (2009) Solution structures of the actuator domain of ATP7A and ATP7B, the Menkes and Wilson disease proteins. *Biochemistry* **48**, 7849-7855
71. Parge, H. E., Getzoff, E. D., Scandella, C. S., Hallewell, R. A., and Tainer, J. A. (1986) Crystallographic characterization of recombinant human CuZn superoxide dismutase. *J Biol Chem* **261**, 16215-16218
72. Forman, H. J., and Fridovich, I. (1973) On the stability of bovine superoxide dismutase. The effects of metals. *J Biol Chem* **248**, 2645-2649
73. Roe, J. A., Butler, A., Scholler, D. M., Valentine, J. S., Marky, L., and Breslauer, K. J. (1988) Differential scanning calorimetry of Cu,Zn-superoxide dismutase, the apoprotein, and its zinc-substituted derivatives. *Biochemistry* **27**, 950-958
74. Arnesano, F., Banci, L., Bertini, I., Martinelli, M., Furukawa, Y., and O'Halloran, T. V. (2004) The unusually stable quaternary structure of human Cu,Zn-superoxide dismutase 1 is controlled by both metal occupancy and disulfide status. *J Biol Chem* **279**, 47998-48003
75. Tainer, J. A., Getzoff, E. D., Beem, K. M., Richardson, J. S., and Richardson, D. C. (1982) Determination and analysis of the 2 A-structure of copper, zinc superoxide dismutase. *J Mol Biol* **160**, 181-217
76. Andersen, P. M. (2001) Genetics of sporadic ALS. *Amyotroph Lateral Scler Other Motor Neuron Disord* **2 Suppl 1**, S37-41
77. Rosen, D. R., Siddique, T., Patterson, D., Figlewicz, D. A., Sapp, P., Hentati, A., Donaldson, D., Goto, J., O'Regan, J. P., Deng, H. X., and et al. (1993) Mutations in Cu/Zn superoxide dismutase gene are associated with familial amyotrophic lateral sclerosis. *Nature* **362**, 59-62
78. Nishida, C. R., Gralla, E. B., and Valentine, J. S. (1994) Characterization of three yeast copper-zinc superoxide dismutase mutants analogous to those coded for in familial amyotrophic lateral sclerosis. *Proc Natl Acad Sci U S A* **91**, 9906-9910
79. Duan, W., Guo, M., Yi, L., Liu, Y., Li, Z., Ma, Y., Zhang, G., Liu, Y., Bu, H., Song, X., and Li, C. (2020) The deletion of mutant SOD1 via CRISPR/Cas9/sgRNA prolongs survival in an amyotrophic lateral sclerosis mouse model. *Gene Ther* **27**, 157-169
80. Banci, L., Bertini, I., Cantini, F., D'Onofrio, M., and Viezzoli, M. S. (2002) Structure and dynamics of copper-free SOD: The protein before binding copper. *Protein Sci* **11**, 2479-2492
81. Gurney, M. E., Liu, R., Althaus, J. S., Hall, E. D., and Becker, D. A. (1998) Mutant CuZn superoxide dismutase in motor neuron disease. *J Inherit Metab Dis* **21**, 587-597
82. Gurney, M. E., Pu, H., Chiu, A. Y., Dal Canto, M. C., Polchow, C. Y., Alexander, D. D., Caliendo, J., Hentati, A., Kwon, Y. W., Deng, H. X., and et al. (1994) Motor neuron degeneration in mice that express a human Cu,Zn superoxide dismutase mutation. *Science* **264**, 1772-1775
83. Ripps, M. E., Huntley, G. W., Hof, P. R., Morrison, J. H., and Gordon, J. W. (1995) Transgenic mice expressing an altered murine superoxide dismutase gene provide an animal model of amyotrophic lateral sclerosis. *Proc Natl Acad Sci U S A* **92**, 689-693
84. Bruijn, L. I., Becher, M. W., Lee, M. K., Anderson, K. L., Jenkins, N. A., Copeland, N. G., Sisodia, S. S., Rothstein, J. D., Borchelt, D. R., Price, D. L., and Cleveland, D. W. (1997) ALS-linked SOD1 mutant G85R mediates damage to astrocytes and promotes rapidly progressive disease with SOD1-containing inclusions. *Neuron* **18**, 327-338
85. Bruijn, L. I., Houseweart, M. K., Kato, S., Anderson, K. L., Anderson, S. D., Ohama, E., Reaume, A. G., Scott, R. W., and Cleveland, D. W. (1998) Aggregation and motor neuron toxicity of an ALS-linked SOD1 mutant independent from wild-type SOD1. *Science* **281**, 1851-1854

86. Williamson, T. L., Corson, L. B., Huang, L., Burlingame, A., Liu, J., Bruijn, L. I., and Cleveland, D. W. (2000) Toxicity of ALS-linked SOD1 mutants. *Science* **288**, 399
87. Taylor, J. P., Brown, R. H., Jr., and Cleveland, D. W. (2016) Decoding ALS: from genes to mechanism. *Nature* **539**, 197-206
88. Calvo, J., Jung, H., and Meloni, G. (2017) Copper metallothioneins. *IUBMB Life* **69**, 236-245
89. Thirumoorthy, N., Manisenthil Kumar, K. T., Shyam Sundar, A., Panayappan, L., and Chatterjee, M. (2007) Metallothionein: an overview. *World J Gastroenterol* **13**, 993-996
90. Coyle, P., Philcox, J. C., Carey, L. C., and Rofe, A. M. (2002) Metallothionein: the multipurpose protein. *Cell Mol Life Sci* **59**, 627-647
91. Vasak, M. (2005) Advances in metallothionein structure and functions. *J Trace Elem Med Biol* **19**, 13-17
92. Thornalley, P. J., and Vasak, M. (1985) Possible role for metallothionein in protection against radiation-induced oxidative stress. Kinetics and mechanism of its reaction with superoxide and hydroxyl radicals. *Biochim Biophys Acta* **827**, 36-44
93. Vasak, M. (2011) Metallothioneins: chemical and biological challenges. *J Biol Inorg Chem* **16**, 975-976
94. Carpene, E., Andreani, G., and Isani, G. (2007) Metallothionein functions and structural characteristics. *J Trace Elem Med Biol* **21 Suppl 1**, 35-39
95. Koh, J. Y., and Lee, S. J. (2020) Metallothionein-3 as a multifunctional player in the control of cellular processes and diseases. *Mol Brain* **13**, 116
96. Ogra, Y., Aoyama, M., and Suzuki, K. T. (2006) Protective role of metallothionein against copper depletion. *Arch Biochem Biophys* **451**, 112-118
97. Kelly, E. J., and Palmiter, R. D. (1996) A murine model of Menkes disease reveals a physiological function of metallothionein. *Nat Genet* **13**, 219-222
98. Yang, L., Li, H., Yu, T., Zhao, H., Cherian, M. G., Cai, L., and Liu, Y. (2008) Polymorphisms in metallothionein-1 and -2 genes associated with the risk of type 2 diabetes mellitus and its complications. *Am J Physiol Endocrinol Metab* **294**, E987-992
99. Erickson, J. C., Hollopeter, G., Thomas, S. A., Froelick, G. J., and Palmiter, R. D. (1997) Disruption of the metallothionein-III gene in mice: analysis of brain zinc, behavior, and neuron vulnerability to metals, aging, and seizures. *J Neurosci* **17**, 1271-1281
100. Coyle, P., Hubert, C. A., Philcox, J. C., and Rofe, A. M. (2001) Importance of storage conditions for the stability of zinc- and cadmium-induced metallothionein. *Biol Trace Elem Res* **81**, 269-278
101. Miyazaki, I., Sogawa, C. A., Asanuma, M., Higashi, Y., Tanaka, K. I., Nakanishi, T., and Ogawa, N. (2000) Expression of metallothionein-III mRNA and its regulation by levodopa in the basal ganglia of hemi-parkinsonian rats. *Neurosci Lett* **293**, 65-68
102. Uchida, Y., Takio, K., Titani, K., Ihara, Y., and Tomonaga, M. (1991) The growth inhibitory factor that is deficient in the Alzheimer's disease brain is a 68 amino acid metallothionein-like protein. *Neuron* **7**, 337-347
103. Gupta, A., Das, S., and Ray, K. (2018) A glimpse into the regulation of the Wilson disease protein, ATP7B, sheds light on the complexity of mammalian apical trafficking pathways. *Metallomics* **10**, 378-387
104. La Fontaine, S., and Mercer, J. F. (2007) Trafficking of the copper-ATPases, ATP7A and ATP7B: role in copper homeostasis. *Arch Biochem Biophys* **463**, 149-167
105. Chun, H., Catterton, T., Kim, H., Lee, J., and Kim, B. E. (2017) Organ-specific regulation of ATP7A abundance is coordinated with systemic copper homeostasis. *Sci Rep* **7**, 12001
106. Linz, R., and Lutsenko, S. (2007) Copper-transporting ATPases ATP7A and ATP7B: cousins, not twins. *J Bioenerg Biomembr* **39**, 403-407
107. Nyasae, L., Bustos, R., Braiterman, L., Eipper, B., and Hubbard, A. (2007) Dynamics of endogenous ATP7A (Menkes protein) in intestinal epithelial cells: copper-dependent

redistribution between two intracellular sites. *Am J Physiol Gastrointest Liver Physiol* **292**, G1181-1194
108. Kaler, S. G. (1998) Diagnosis and therapy of Menkes syndrome, a genetic form of copper deficiency. *Am J Clin Nutr* **67**, 1029S-1034S
109. Morrell, A., Tallino, S., Yu, L., and Burkhead, J. L. (2017) The role of insufficient copper in lipid synthesis and fatty-liver disease. *IUBMB Life* **69**, 263-270
110. Tang, Z., Gasperkova, D., Xu, J., Baillie, R., Lee, J. H., and Clarke, S. D. (2000) Copper deficiency induces hepatic fatty acid synthase gene transcription in rats by increasing the nuclear content of mature sterol regulatory element binding protein 1. *J Nutr* **130**, 2915-2921
111. van den Berghe, P. V., and Klomp, L. W. (2009) New developments in the regulation of intestinal copper absorption. *Nutr Rev* **67**, 658-672
112. Camakaris, J., Voskoboinik, I., and Mercer, J. F. (1999) Molecular mechanisms of copper homeostasis. *Biochem Biophys Res Commun* **261**, 225-232
113. DiDonato, M., and Sarkar, B. (1997) Copper transport and its alterations in Menkes and Wilson diseases. *Biochim Biophys Acta* **1360**, 3-16
114. Harris, E. D. (2003) Basic and clinical aspects of copper. *Crit Rev Clin Lab Sci* **40**, 547-586
115. Voskoboinik, I., and Camakaris, J. (2002) Menkes copper-translocating P-type ATPase (ATP7A): biochemical and cell biology properties, and role in Menkes disease. *J Bioenerg Biomembr* **34**, 363-371
116. Heffern, M. C., Park, H. M., Au-Yeung, H. Y., Van de Bittner, G. C., Ackerman, C. M., Stahl, A., and Chang, C. J. (2016) In vivo bioluminescence imaging reveals copper deficiency in a murine model of nonalcoholic fatty liver disease. *Proc Natl Acad Sci U S A* **113**, 14219-14224
117. Lei, K. Y. (1983) Alterations in plasma lipid, lipoprotein and apolipoprotein concentrations in copper-deficient rats. *J Nutr* **113**, 2178-2183
118. Yang, H., Ralle, M., Wolfgang, M. J., Dhawan, N., Burkhead, J. L., Rodriguez, S., Kaplan, J. H., Wong, G. W., Haughey, N., and Lutsenko, S. (2018) Copper-dependent amino oxidase 3 governs selection of metabolic fuels in adipocytes. *PLoS Biol* **16**, e2006519
119. McCann, C. J., Jayakanthan, S., Siotto, M., Yang, N., Osipova, M., Squitti, R., and Lutsenko, S. (2019) Single nucleotide polymorphisms in the human ATP7B gene modify the properties of the ATP7B protein. *Metallomics* **11**, 1128-1139
120. Pierson, H., Muchenditsi, A., Kim, B. E., Ralle, M., Zachos, N., Huster, D., and Lutsenko, S. (2018) The Function of ATPase Copper Transporter ATP7B in Intestine. *Gastroenterology* **154**, 168-180 e165
121. Roelofsen, H., Wolters, H., Van Luyn, M. J., Miura, N., Kuipers, F., and Vonk, R. J. (2000) Copper-induced apical trafficking of ATP7B in polarized hepatoma cells provides a mechanism for biliary copper excretion. *Gastroenterology* **119**, 782-793
122. Prohaska, J. R., and Gybina, A. A. (2004) Intracellular copper transport in mammals. *J Nutr* **134**, 1003-1006
123. Wijmenga, C., and Klomp, L. W. (2004) Molecular regulation of copper excretion in the liver. *Proc Nutr Soc* **63**, 31-39
124. Suzuki, M., and Gitlin, J. D. (1999) Intracellular localization of the Menkes and Wilson's disease proteins and their role in intracellular copper transport. *Pediatr Int* **41**, 436-442
125. Vanderwerf, S. M., Cooper, M. J., Stetsenko, I. V., and Lutsenko, S. (2001) Copper specifically regulates intracellular phosphorylation of the Wilson's disease protein, a human copper-transporting ATPase. *J Biol Chem* **276**, 36289-36294
126. Elferink, R. O., and Groen, A. K. (2002) Genetic defects in hepatobiliary transport. *Biochim Biophys Acta* **1586**, 129-145

127. Lutsenko, S., Efremov, R. G., Tsivkovskii, R., and Walker, J. M. (2002) Human copper-transporting ATPase ATP7B (the Wilson's disease protein): biochemical properties and regulation. *J Bioenerg Biomembr* **34**, 351-362
128. Haywood, S. (1985) Copper toxicosis and tolerance in the rat. I--Changes in copper content of the liver and kidney. *J Pathol* **145**, 149-158
129. Brewer, G. J., and Askari, F. K. (2005) Wilson's disease: clinical management and therapy. *J Hepatol* **42 Suppl**, S13-21
130. Muchenditsi, A., Yang, H., Hamilton, J. P., Koganti, L., Housseau, F., Aronov, L., Fan, H., Pierson, H., Bhattacharjee, A., Murphy, R., Sears, C., Potter, J., Wooton-Kee, C. R., and Lutsenko, S. (2017) Targeted inactivation of copper transporter Atp7b in hepatocytes causes liver steatosis and obesity in mice. *Am J Physiol Gastrointest Liver Physiol* **313**, G39-G49
131. Muchenditsi, A., Talbot, C. C., Jr., Gottlieb, A., Yang, H., Kang, B., Boronina, T., Cole, R., Wang, L., Dev, S., Hamilton, J. P., and Lutsenko, S. (2021) Systemic deletion of Atp7b modifies the hepatocytes' response to copper overload in the mouse models of Wilson disease. *Sci Rep* **11**, 5659
132. Niciu, M. J., Ma, X. M., El Meskini, R., Pachter, J. S., Mains, R. E., and Eipper, B. A. (2007) Altered ATP7A expression and other compensatory responses in a murine model of Menkes disease. *Neurobiol Dis* **27**, 278-291
133. Linz, R., Barnes, N. L., Zimnicka, A. M., Kaplan, J. H., Eipper, B., and Lutsenko, S. (2008) Intracellular targeting of copper-transporting ATPase ATP7A in a normal and Atp7b-/- kidney. *Am J Physiol Renal Physiol* **294**, F53-61
134. Furukawa, T., Komatsu, M., Ikeda, R., Tsujikawa, K., and Akiyama, S. (2008) Copper transport systems are involved in multidrug resistance and drug transport. *Curr Med Chem* **15**, 3268-3278
135. Muller, P., van Bakel, H., van de Sluis, B., Holstege, F., Wijmenga, C., and Klomp, L. W. (2007) Gene expression profiling of liver cells after copper overload in vivo and in vitro reveals new copper-regulated genes. *J Biol Inorg Chem* **12**, 495-507
136. Balamurugan, K., Egli, D., Selvaraj, A., Zhang, B., Georgiev, O., and Schaffner, W. (2004) Metal-responsive transcription factor (MTF-1) and heavy metal stress response in Drosophila and mammalian cells: a functional comparison. *Biol Chem* **385**, 597-603
137. Tavera-Montanez, C., Hainer, S. J., Cangussu, D., Gordon, S. J. V., Xiao, Y., Reyes-Gutierrez, P., Imbalzano, A. N., Navea, J. G., Fazzio, T. G., and Padilla-Benavides, T. (2019) The classic metal-sensing transcription factor MTF1 promotes myogenesis in response to copper. *FASEB J* **33**, 14556-14574
138. Gunther, V., Lindert, U., and Schaffner, W. (2012) The taste of heavy metals: gene regulation by MTF-1. *Biochim Biophys Acta* **1823**, 1416-1425
139. Selvaraj, A., Balamurugan, K., Yepiskoposyan, H., Zhou, H., Egli, D., Georgiev, O., Thiele, D. J., and Schaffner, W. (2005) Metal-responsive transcription factor (MTF-1) handles both extremes, copper load and copper starvation, by activating different genes. *Genes Dev* **19**, 891-896
140. Heuchel, R., Radtke, F., Georgiev, O., Stark, G., Aguet, M., and Schaffner, W. (1994) The transcription factor MTF-1 is essential for basal and heavy metal-induced metallothionein gene expression. *EMBO J* **13**, 2870-2875
141. Zhang, B., Egli, D., Georgiev, O., and Schaffner, W. (2001) The Drosophila homolog of mammalian zinc finger factor MTF-1 activates transcription in response to heavy metals. *Mol Cell Biol* **21**, 4505-4514
142. Giedroc, D. P., Chen, X., and Apuy, J. L. (2001) Metal response element (MRE)-binding transcription factor-1 (MTF-1): structure, function, and regulation. *Antioxid Redox Signal* **3**, 577-596

143. Bellingham, S. A., Coleman, L. A., Masters, C. L., Camakaris, J., and Hill, A. F. (2009) Regulation of prion gene expression by transcription factors SP1 and metal transcription factor-1. *J Biol Chem* **284**, 1291-1301
144. Qin, K., Zhao, L., Ash, R. D., McDonough, W. F., and Zhao, R. Y. (2009) ATM-mediated transcriptional elevation of prion in response to copper-induced oxidative stress. *J Biol Chem* **284**, 4582-4593
145. O'Connor, L., Gilmour, J., and Bonifer, C. (2016) The Role of the Ubiquitously Expressed Transcription Factor Sp1 in Tissue-specific Transcriptional Regulation and in Disease. *Yale J Biol Med* **89**, 513-525
146. Yuan, S., Chen, S., Xi, Z., and Liu, Y. (2017) Copper-finger protein of Sp1: the molecular basis of copper sensing. *Metallomics* **9**, 1169-1175
147. Liang, Z. D., Tsai, W. B., Lee, M. Y., Savaraj, N., and Kuo, M. T. (2012) Specificity protein 1 (sp1) oscillation is involved in copper homeostasis maintenance by regulating human high-affinity copper transporter 1 expression. *Mol Pharmacol* **81**, 455-464
148. Muller, P. A., and Klomp, L. W. (2009) ATOX1: a novel copper-responsive transcription factor in mammals? *Int J Biochem Cell Biol* **41**, 1233-1236
149. Bauerly, K. A., Kelleher, S. L., and Lonnerdal, B. (2004) Functional and molecular responses of suckling rat pups and human intestinal Caco-2 cells to copper treatment. *J Nutr Biochem* **15**, 155-162
150. Bauerly, K. A., Kelleher, S. L., and Lonnerdal, B. (2005) Effects of copper supplementation on copper absorption, tissue distribution, and copper transporter expression in an infant rat model. *Am J Physiol Gastrointest Liver Physiol* **288**, G1007-1014
151. van den Berghe, P. V., and Klomp, L. W. (2010) Posttranslational regulation of copper transporters. *J Biol Inorg Chem* **15**, 37-46
152. Kuo, Y. M., Gybina, A. A., Pyatskowit, J. W., Gitschier, J., and Prohaska, J. R. (2006) Copper transport protein (Ctr1) levels in mice are tissue specific and dependent on copper status. *J Nutr* **136**, 21-26
153. Lee, J., Prohaska, J. R., Dagenais, S. L., Glover, T. W., and Thiele, D. J. (2000) Isolation of a murine copper transporter gene, tissue specific expression and functional complementation of a yeast copper transport mutant. *Gene* **254**, 87-96
154. Pourvali, K., Matak, P., Latunde-Dada, G. O., Solomou, S., Mastrogiannaki, M., Peyssonnaux, C., and Sharp, P. A. (2012) Basal expression of copper transporter 1 in intestinal epithelial cells is regulated by hypoxia-inducible factor 2alpha. *FEBS Lett* **586**, 2423-2427
155. Hasan, N. M., and Lutsenko, S. (2012) Regulation of copper transporters in human cells. *Curr Top Membr* **69**, 137-161
156. Wang, Y., Zhu, S., Hodgkinson, V., Prohaska, J. R., Weisman, G. A., Gitlin, J. D., and Petris, M. J. (2012) Maternofetal and neonatal copper requirements revealed by enterocyte-specific deletion of the Menkes disease protein. *Am J Physiol Gastrointest Liver Physiol* **303**, G1236-1244
157. Milani, P., Gagliardi, S., Cova, E., and Cereda, C. (2011) SOD1 Transcriptional and Posttranscriptional Regulation and Its Potential Implications in ALS. *Neurol Res Int* **2011**, 458427
158. Afonso, V., Santos, G., Collin, P., Khatib, A. M., Mitrovic, D. R., Lomri, N., Leitman, D. C., and Lomri, A. (2006) Tumor necrosis factor-alpha down-regulates human Cu/Zn superoxide dismutase 1 promoter via JNK/AP-1 signaling pathway. *Free Radic Biol Med* **41**, 709-721
159. Minc, E., de Coppet, P., Masson, P., Thiery, L., Dutertre, S., Amor-Gueret, M., and Jaulin, C. (1999) The human copper-zinc superoxide dismutase gene (SOD1) proximal promoter is regulated by Sp1, Egr-1, and WT1 via non-canonical binding sites. *J Biol Chem* **274**, 503-509

160. Cao, X. M., Guy, G. R., Sukhatme, V. P., and Tan, Y. H. (1992) Regulation of the Egr-1 gene by tumor necrosis factor and interferons in primary human fibroblasts. *J Biol Chem* **267**, 1345-1349
161. Chaudhary, L. R., Cheng, S. L., and Avioli, L. V. (1996) Induction of early growth response-1 gene by interleukin-1 beta and tumor necrosis factor-alpha in normal human bone marrow stromal an osteoblastic cells: regulation by a protein kinase C inhibitor. *Mol Cell Biochem* **156**, 69-77
162. Haq, F., Mahoney, M., and Koropatnick, J. (2003) Signaling events for metallothionein induction. *Mutat Res* **533**, 211-226
163. Palmiter, R. D. (1994) Regulation of metallothionein genes by heavy metals appears to be mediated by a zinc-sensitive inhibitor that interacts with a constitutively active transcription factor, MTF-1. *Proc Natl Acad Sci U S A* **91**, 1219-1223
164. Naruse, S., Igarashi, S., Furuya, T., Kobayashi, H., Miyatake, T., and Tsuji, S. (1994) Structures of the human and mouse growth inhibitory factor-encoding genes. *Gene* **144**, 283-287
165. Tang, C. M., Westling, J., and Seto, E. (1999) trans repression of the human metallothionein IIA gene promoter by PZ120, a novel 120-kilodalton zinc finger protein. *Mol Cell Biol* **19**, 680-689
166. Krezel, A., and Maret, W. (2017) The Functions of Metamorphic Metallothioneins in Zinc and Copper Metabolism. *Int J Mol Sci* **18**
167. Palmiter, R. D. (1998) The elusive function of metallothioneins. *Proc Natl Acad Sci U S A* **95**, 8428-8430
168. Paynter, J. A., Grimes, A., Lockhart, P., and Mercer, J. F. (1994) Expression of the Menkes gene homologue in mouse tissues lack of effect of copper on the mRNA levels. *FEBS Lett* **351**, 186-190
169. Tomasini, R., Tsuchihara, K., Wilhelm, M., Fujitani, M., Rufini, A., Cheung, C. C., Khan, F., Itie-Youten, A., Wakeham, A., Tsao, M. S., Iovanna, J. L., Squire, J., Jurisica, I., Kaplan, D., Melino, G., Jurisicova, A., and Mak, T. W. (2008) TAp73 knockout shows genomic instability with infertility and tumor suppressor functions. *Genes Dev* **22**, 2677-2691
170. Amelio, I., Antonov, A. A., Catani, M. V., Massoud, R., Bernassola, F., Knight, R. A., Melino, G., and Rufini, A. (2014) TAp73 promotes anabolism. *Oncotarget* **5**, 12820-12934
171. Marini, A., Rotblat, B., Sbarrato, T., Niklison-Chirou, M. V., Knight, J. R. P., Dudek, K., Jones, C., Bushell, M., Knight, R. A., Amelio, I., Willis, A. E., and Melino, G. (2018) TAp73 contributes to the oxidative stress response by regulating protein synthesis. *Proc Natl Acad Sci U S A* **115**, 6219-6224
172. Lopriore, P., Capitanio, N., Panatta, E., Di Daniele, N., Gambacurta, A., Melino, G., and Amelio, I. (2018) TAp73 regulates ATP7A: possible implications for ageing-related diseases. *Aging (Albany NY)* **10**, 3745-3760
173. Collins, J. F., Franck, C. A., Kowdley, K. V., and Ghishan, F. K. (2005) Identification of differentially expressed genes in response to dietary iron deprivation in rat duodenum. *Am J Physiol Gastrointest Liver Physiol* **288**, G964-971
174. Ravia, J. J., Stephen, R. M., Ghishan, F. K., and Collins, J. F. (2005) Menkes Copper ATPase (Atp7a) is a novel metal-responsive gene in rat duodenum, and immunoreactive protein is present on brush-border and basolateral membrane domains. *J Biol Chem* **280**, 36221-36227
175. Xie, L., and Collins, J. F. (2011) Transcriptional regulation of the Menkes copper ATPase (Atp7a) gene by hypoxia-inducible factor (HIF2{alpha}) in intestinal epithelial cells. *Am J Physiol Cell Physiol* **300**, C1298-1305

176. Xie, L., and Collins, J. F. (2013) Transcription factors Sp1 and Hif2alpha mediate induction of the copper-transporting ATPase (Atp7a) gene in intestinal epithelial cells during hypoxia. *J Biol Chem* **288**, 23943-23952
177. Bohlken, A., Cheung, B. B., Bell, J. L., Koach, J., Smith, S., Sekyere, E., Thomas, W., Norris, M., Haber, M., Lovejoy, D. B., Richardson, D. R., and Marshall, G. M. (2009) ATP7A is a novel target of retinoic acid receptor beta2 in neuroblastoma cells. *Br J Cancer* **100**, 96-105
178. Hardman, B., Michalczyk, A., Greenough, M., Camakaris, J., Mercer, J. F., and Ackland, M. L. (2007) Hormonal regulation of the Menkes and Wilson copper-transporting ATPases in human placental Jeg-3 cells. *Biochem J* **402**, 241-250
179. Stalke, A., Pfister, E. D., Baumann, U., Illig, T., Reischl, E., Sandbothe, M., Vajen, B., Huge, N., Schlegelberger, B., von Neuhoff, N., and Skawran, B. (2020) MTF1 binds to metal-responsive element e within the ATP7B promoter and is a strong candidate in regulating the ATP7B expression. *Ann Hum Genet* **84**, 195-200
180. Gross, C., Kelleher, M., Iyer, V. R., Brown, P. O., and Winge, D. R. (2000) Identification of the copper regulon in Saccharomyces cerevisiae by DNA microarrays. *J Biol Chem* **275**, 32310-32316
181. De Freitas, J. M., Kim, J. H., Poynton, H., Su, T., Wintz, H., Fox, T., Holman, P., Loguinov, A., Keles, S., van der Laan, M., and Vulpe, C. (2004) Exploratory and confirmatory gene expression profiling of mac1Delta. *J Biol Chem* **279**, 4450-4458
182. van Bakel, H., Strengman, E., Wijmenga, C., and Holstege, F. C. (2005) Gene expression profiling and phenotype analyses of S. cerevisiae in response to changing copper reveals six genes with new roles in copper and iron metabolism. *Physiol Genomics* **22**, 356-367
183. Bird, A. J. (2008) Metallosensors, the ups and downs of gene regulation. *Adv Microb Physiol* **53**, 231-267
184. Kim, B. E., Nevitt, T., and Thiele, D. J. (2008) Mechanisms for copper acquisition, distribution and regulation. *Nat Chem Biol* **4**, 176-185
185. Guo, Y., Smith, K., Lee, J., Thiele, D. J., and Petris, M. J. (2004) Identification of methionine-rich clusters that regulate copper-stimulated endocytosis of the human Ctr1 copper transporter. *J Biol Chem* **279**, 17428-17433
186. Molloy, S. A., and Kaplan, J. H. (2009) Copper-dependent recycling of hCTR1, the human high affinity copper transporter. *J Biol Chem* **284**, 29704-29713
187. Hardman, B., Manuelpillai, U., Wallace, E. M., Monty, J. F., Kramer, D. R., Kuo, Y. M., Mercer, J. F., and Ackland, M. L. (2006) Expression, localisation and hormone regulation of the human copper transporter hCTR1 in placenta and choriocarcinoma Jeg-3 cells. *Placenta* **27**, 968-977
188. Maryon, E. B., Molloy, S. A., and Kaplan, J. H. (2007) O-linked glycosylation at threonine 27 protects the copper transporter hCTR1 from proteolytic cleavage in mammalian cells. *J Biol Chem* **282**, 20376-20387
189. Bertinato, J., and L'Abbe, M. R. (2003) Copper modulates the degradation of copper chaperone for Cu,Zn superoxide dismutase by the 26 S proteosome. *J Biol Chem* **278**, 35071-35078
190. West, E. C., and Prohaska, J. R. (2004) Cu,Zn-superoxide dismutase is lower and copper chaperone CCS is higher in erythrocytes of copper-deficient rats and mice. *Exp Biol Med (Maywood)* **229**, 756-764
191. Bertinato, J., Iskandar, M., and L'Abbe, M. R. (2003) Copper deficiency induces the upregulation of the copper chaperone for Cu/Zn superoxide dismutase in weanling male rats. *J Nutr* **133**, 28-31
192. Prohaska, J. R., Broderius, M., and Brokate, B. (2003) Metallochaperone for Cu,Zn-superoxide dismutase (CCS) protein but not mRNA is higher in organs from copper-deficient mice and rats. *Arch Biochem Biophys* **417**, 227-234

193. Caruano-Yzermans, A. L., Bartnikas, T. B., and Gitlin, J. D. (2006) Mechanisms of the copper-dependent turnover of the copper chaperone for superoxide dismutase. *J Biol Chem* **281**, 13581-13587
194. Mufti, A. R., Burstein, E., and Duckett, C. S. (2007) XIAP: cell death regulation meets copper homeostasis. *Arch Biochem Biophys* **463**, 168-174
195. Mufti, A. R., Burstein, E., Csomos, R. A., Graf, P. C., Wilkinson, J. C., Dick, R. D., Challa, M., Son, J. K., Bratton, S. B., Su, G. L., Brewer, G. J., Jakob, U., and Duckett, C. S. (2006) XIAP Is a copper binding protein deregulated in Wilson's disease and other copper toxicosis disorders. *Mol Cell* **21**, 775-785
196. Brady, G. F., Galban, S., Liu, X., Basrur, V., Gitlin, J. D., Elenitoba-Johnson, K. S., Wilson, T. E., and Duckett, C. S. (2010) Regulation of the copper chaperone CCS by XIAP-mediated ubiquitination. *Mol Cell Biol* **30**, 1923-1936
197. Tsang, C. K., Liu, Y., Thomas, J., Zhang, Y., and Zheng, X. F. (2014) Superoxide dismutase 1 acts as a nuclear transcription factor to regulate oxidative stress resistance. *Nat Commun* **5**, 3446
198. Tsang, C. K., Chen, M., Cheng, X., Qi, Y., Chen, Y., Das, I., Li, X., Vallat, B., Fu, L. W., Qian, C. N., Wang, H. Y., White, E., Burley, S. K., and Zheng, X. F. S. (2018) SOD1 Phosphorylation by mTORC1 Couples Nutrient Sensing and Redox Regulation. *Mol Cell* **70**, 502-515 e508
199. Hjornevik, L. V., Fismen, L., Young, F. M., Solstad, T., and Fladmark, K. E. (2012) Nodularin exposure induces SOD1 phosphorylation and disrupts SOD1 co-localization with actin filaments. *Toxins (Basel)* **4**, 1482-1499
200. Banci, L., Bertini, I., Boca, M., Calderone, V., Cantini, F., Girotto, S., and Vieru, M. (2009) Structural and dynamic aspects related to oligomerization of apo SOD1 and its mutants. *Proc Natl Acad Sci U S A* **106**, 6980-6985
201. Banks, C. J., and Andersen, J. L. (2019) Mechanisms of SOD1 regulation by post-translational modifications. *Redox Biol* **26**, 101270
202. Rasouli, S., Abdolvahabi, A., Croom, C. M., Plewman, D. L., Shi, Y., Ayers, J. I., and Shaw, B. F. (2017) Lysine acylation in superoxide dismutase-1 electrostatically inhibits formation of fibrils with prion-like seeding. *J Biol Chem* **292**, 19366-19380
203. Kaliszewski, M., Kennedy, A. K., Blaes, S. L., Shaffer, R. S., Knott, A. B., Song, W., Hauser, H. A., Bossy, B., Huang, T. T., and Bossy-Wetzel, E. (2016) SOD1 Lysine 123 Acetylation in the Adult Central Nervous System. *Front Cell Neurosci* **10**, 287
204. Antinone, S. E., Ghadge, G. D., Ostrow, L. W., Roos, R. P., and Green, W. N. (2017) S-acylation of SOD1, CCS, and a stable SOD1-CCS heterodimer in human spinal cords from ALS and non-ALS subjects. *Sci Rep* **7**, 41141
205. Lin, C., Zeng, H., Lu, J., Xie, Z., Sun, W., Luo, C., Ding, J., Yuan, S., Geng, M., and Huang, M. (2015) Acetylation at lysine 71 inactivates superoxide dismutase 1 and sensitizes cancer cells to genotoxic agents. *Oncotarget* **6**, 20578-20591
206. Marin, E. P., Derakhshan, B., Lam, T. T., Davalos, A., and Sessa, W. C. (2012) Endothelial cell palmitoylproteomic identifies novel lipid-modified targets and potential substrates for protein acyl transferases. *Circ Res* **110**, 1336-1344
207. Banks, C. J., Rodriguez, N. W., Gashler, K. R., Pandya, R. R., Mortenson, J. B., Whited, M. D., Soderblom, E. J., Thompson, J. W., Moseley, M. A., Reddi, A. R., Tessem, J. S., Torres, M. P., Bikman, B. T., and Andersen, J. L. (2017) Acylation of Superoxide Dismutase 1 (SOD1) at K122 Governs SOD1-Mediated Inhibition of Mitochondrial Respiration. *Mol Cell Biol* **37**
208. Fei, E., Jia, N., Yan, M., Ying, Z., Sun, Q., Wang, H., Zhang, T., Ma, X., Ding, H., Yao, X., Shi, Y., and Wang, G. (2006) SUMO-1 modification increases human SOD1 stability and aggregation. *Biochem Biophys Res Commun* **347**, 406-412

209. Niikura, T., Kita, Y., and Abe, Y. (2014) SUMO3 modification accelerates the aggregation of ALS-linked SOD1 mutants. *PLoS One* **9**, e101080
210. Kabuta, T., Suzuki, Y., and Wada, K. (2006) Degradation of amyotrophic lateral sclerosis-linked mutant Cu,Zn-superoxide dismutase proteins by macroautophagy and the proteasome. *J Biol Chem* **281**, 30524-30533
211. Bosco, D. A., Morfini, G., Karabacak, N. M., Song, Y., Gros-Louis, F., Pasinelli, P., Goolsby, H., Fontaine, B. A., Lemay, N., McKenna-Yasek, D., Frosch, M. P., Agar, J. N., Julien, J. P., Brady, S. T., and Brown, R. H., Jr. (2010) Wild-type and mutant SOD1 share an aberrant conformation and a common pathogenic pathway in ALS. *Nat Neurosci* **13**, 1396-1403
212. Wilcox, K. C., Zhou, L., Jordon, J. K., Huang, Y., Yu, Y., Redler, R. L., Chen, X., Caplow, M., and Dokholyan, N. V. (2009) Modifications of superoxide dismutase (SOD1) in human erythrocytes: a possible role in amyotrophic lateral sclerosis. *J Biol Chem* **284**, 13940-13947
213. Rakhit, R., Cunningham, P., Furtos-Matei, A., Dahan, S., Qi, X. F., Crow, J. P., Cashman, N. R., Kondejewski, L. H., and Chakrabartty, A. (2002) Oxidation-induced misfolding and aggregation of superoxide dismutase and its implications for amyotrophic lateral sclerosis. *J Biol Chem* **277**, 47551-47556
214. Rakhit, R., Crow, J. P., Lepock, J. R., Kondejewski, L. H., Cashman, N. R., and Chakrabartty, A. (2004) Monomeric Cu,Zn-superoxide dismutase is a common misfolding intermediate in the oxidation models of sporadic and familial amyotrophic lateral sclerosis. *J Biol Chem* **279**, 15499-15504
215. Kabashi, E., Valdmanis, P. N., Dion, P., and Rouleau, G. A. (2007) Oxidized/misfolded superoxide dismutase-1: the cause of all amyotrophic lateral sclerosis? *Ann Neurol* **62**, 553-559
216. Veldhuis, N. A., Gaeth, A. P., Pearson, R. B., Gabriel, K., and Camakaris, J. (2009) The multi-layered regulation of copper translocating P-type ATPases. *Biometals* **22**, 177-190
217. Bartee, M. Y., Ralle, M., and Lutsenko, S. (2009) The loop connecting metal-binding domains 3 and 4 of ATP7B is a target of a kinase-mediated phosphorylation. *Biochemistry* **48**, 5573-5581
218. Veldhuis, N. A., Valova, V. A., Gaeth, A. P., Palstra, N., Hannan, K. M., Michell, B. J., Kelly, L. E., Jennings, I., Kemp, B. E., Pearson, R. B., Robinson, P. J., and Camakaris, J. (2009) Phosphorylation regulates copper-responsive trafficking of the Menkes copper transporting P-type ATPase. *Int J Biochem Cell Biol* **41**, 2403-2412
219. Pilankatta, R., Lewis, D., Adams, C. M., and Inesi, G. (2009) High yield heterologous expression of wild-type and mutant Cu+-ATPase (ATP7B, Wilson disease protein) for functional characterization of catalytic activity and serine residues undergoing copper-dependent phosphorylation. *J Biol Chem* **284**, 21307-21316
220. Pilankatta, R., Lewis, D., and Inesi, G. (2011) Involvement of protein kinase D in expression and trafficking of ATP7B (copper ATPase). *J Biol Chem* **286**, 7389-7396
221. Liu, Y., Pilankatta, R., Hatori, Y., Lewis, D., and Inesi, G. (2010) Comparative features of copper ATPases ATP7A and ATP7B heterologously expressed in COS-1 cells. *Biochemistry* **49**, 10006-10012
222. Yu, C. H., Dolgova, N. V., and Dmitriev, O. Y. (2017) Dynamics of the metal binding domains and regulation of the human copper transporters ATP7B and ATP7A. *IUBMB Life* **69**, 226-235
223. Inesi, G., Pilankatta, R., and Tadini-Buoninsegni, F. (2014) Biochemical characterization of P-type copper ATPases. *Biochem J* **463**, 167-176
224. de Bie, P., van de Sluis, B., Burstein, E., van de Berghe, P. V., Muller, P., Berger, R., Gitlin, J. D., Wijmenga, C., and Klomp, L. W. (2007) Distinct Wilson's disease mutations

in ATP7B are associated with enhanced binding to COMMD1 and reduced stability of ATP7B. *Gastroenterology* **133**, 1316-1326
225. Sudhahar, V., Okur, M. N., Bagi, Z., O'Bryan, J. P., Hay, N., Makino, A., Patel, V. S., Phillips, S. A., Stepp, D., Ushio-Fukai, M., and Fukai, T. (2018) Akt2 (Protein Kinase B Beta) Stabilizes ATP7A, a Copper Transporter for Extracellular Superoxide Dismutase, in Vascular Smooth Muscle: Novel Mechanism to Limit Endothelial Dysfunction in Type 2 Diabetes Mellitus. *Arterioscler Thromb Vasc Biol* **38**, 529-541
226. Sudhahar, V., Okur, M. N., O'Bryan, J. P., Minshall, R. D., Fulton, D., Ushio-Fukai, M., and Fukai, T. (2020) Caveolin-1 stabilizes ATP7A, a copper transporter for extracellular SOD, in vascular tissue to maintain endothelial function. *Am J Physiol Cell Physiol* **319**, C933-C944
227. Yu, C. H., Yang, N., Bothe, J., Tonelli, M., Nokhrin, S., Dolgova, N. V., Braiterman, L., Lutsenko, S., and Dmitriev, O. Y. (2017) The metal chaperone Atox1 regulates the activity of the human copper transporter ATP7B by modulating domain dynamics. *J Biol Chem* **292**, 18169-18177
228. Banci, L., Bertini, I., Cantini, F., Della-Malva, N., Migliardi, M., and Rosato, A. (2007) The different intermolecular interactions of the soluble copper-binding domains of the menkes protein, ATP7A. *J Biol Chem* **282**, 23140-23146
229. Maine, G. N., and Burstein, E. (2007) COMMD proteins and the control of the NF kappa B pathway. *Cell Cycle* **6**, 672-676
230. van de Sluis, B., Muller, P., Duran, K., Chen, A., Groot, A. J., Klomp, L. W., Liu, P. P., and Wijmenga, C. (2007) Increased activity of hypoxia-inducible factor 1 is associated with early embryonic lethality in Commd1 null mice. *Mol Cell Biol* **27**, 4142-4156
231. Phillips-Krawczak, C. A., Singla, A., Starokadomskyy, P., Deng, Z., Osborne, D. G., Li, H., Dick, C. J., Gomez, T. S., Koenecke, M., Zhang, J. S., Dai, H., Sifuentes-Dominguez, L. F., Geng, L. N., Kaufmann, S. H., Hein, M. Y., Wallis, M., McGaughran, J., Gecz, J., Sluis, B., Billadeau, D. D., and Burstein, E. (2015) COMMD1 is linked to the WASH complex and regulates endosomal trafficking of the copper transporter ATP7A. *Mol Biol Cell* **26**, 91-103
232. Materia, S., Cater, M. A., Klomp, L. W., Mercer, J. F., and La Fontaine, S. (2011) Clusterin (apolipoprotein J), a molecular chaperone that facilitates degradation of the copper-ATPases ATP7A and ATP7B. *J Biol Chem* **286**, 10073-10083
233. Materia, S., Cater, M. A., Klomp, L. W., Mercer, J. F., and La Fontaine, S. (2012) Clusterin and COMMD1 independently regulate degradation of the mammalian copper ATPases ATP7A and ATP7B. *J Biol Chem* **287**, 2485-2499
234. Stewart, D. J., Short, K. K., Maniaci, B. N., and Burkhead, J. L. (2019) COMMD1 and PtdIns(4,5)P2 interaction maintain ATP7B copper transporter trafficking fidelity in HepG2 cells. *J Cell Sci* **132**
235. Schlief, M. L., Craig, A. M., and Gitlin, J. D. (2005) NMDA receptor activation mediates copper homeostasis in hippocampal neurons. *J Neurosci* **25**, 239-246
236. White, C., Kambe, T., Fulcher, Y. G., Sachdev, S. W., Bush, A. I., Fritsche, K., Lee, J., Quinn, T. P., and Petris, M. J. (2009) Copper transport into the secretory pathway is regulated by oxygen in macrophages. *J Cell Sci* **122**, 1315-1321
237. Burkhead, J. L., Reynolds, K. A., Abdel-Ghany, S. E., Cohu, C. M., and Pilon, M. (2009) Copper homeostasis. *New Phytol* **182**, 799-816
238. Waldron, K. J., Rutherford, J. C., Ford, D., and Robinson, N. J. (2009) Metalloproteins and metal sensing. *Nature* **460**, 823-830
239. Giorgi, C., and Moore, M. J. (2007) The nuclear nurture and cytoplasmic nature of localized mRNPs. *Semin Cell Dev Biol* **18**, 186-193
240. Moore, M. J., and Proudfoot, N. J. (2009) Pre-mRNA processing reaches back to transcription and ahead to translation. *Cell* **136**, 688-700

241. Zhou, B., and Gitschier, J. (1997) hCTR1: a human gene for copper uptake identified by complementation in yeast. *Proc Natl Acad Sci U S A* **94**, 7481-7486
242. Sherman, L., Levanon, D., Lieman-Hurwitz, J., Dafni, N., and Groner, Y. (1984) Human Cu/Zn superoxide dismutase gene: molecular characterization of its two mRNA species. *Nucleic Acids Res* **12**, 9349-9365
243. Kilk, A., Laan, M., and Torp, A. (1995) Human CuZn superoxide dismutase enzymatic activity in cells is regulated by the length of the mRNA. *FEBS Lett* **362**, 323-327
244. Groner, Y., Lieman-Hurwitz, J., Dafni, N., Sherman, L., Levanon, D., Bernstein, Y., Danciger, E., and Elroy-Stein, O. (1985) Molecular structure and expression of the gene locus on chromosome 21 encoding the Cu/Zn superoxide dismutase and its relevance to Down syndrome. *Ann N Y Acad Sci* **450**, 133-156
245. Milani, P., Amadio, M., Laforenza, U., Dell'Orco, M., Diamanti, L., Sardone, V., Gagliardi, S., Govoni, S., Ceroni, M., Pascale, A., and Cereda, C. (2013) Posttranscriptional regulation of SOD1 gene expression under oxidative stress: Potential role of ELAV proteins in sporadic ALS. *Neurobiol Dis* **60**, 51-60
246. Sadhu, C., and Gedamu, L. (1989) Metal-specific posttranscriptional control of human metallothionein genes. *Mol Cell Biol* **9**, 5738-5741
247. Vasconcelos, M. H., Tam, S. C., Beattie, J. H., and Hesketh, J. E. (1996) Evidence for differences in the post-transcriptional regulation of rat metallothionein isoforms. *Biochem J* **315 (Pt 2)**, 665-671
248. Miles, A. T., Hawksworth, G. M., Beattie, J. H., and Rodilla, V. (2000) Induction, regulation, degradation, and biological significance of mammalian metallothioneins. *Crit Rev Biochem Mol Biol* **35**, 35-70
249. Lin, Y. J., Ho, T. J., Lin, T. H., Hsu, W. Y., Huang, S. M., Liao, C. C., Lai, C. H., Liu, X., Tsang, H., Lai, C. C., and Tsai, F. J. (2015) P-coumaric acid regulates exon 12 splicing of the ATP7B gene by modulating hnRNP A1 protein expressions. *Biomedicine (Taipei)* **5**, 10
250. Vest, K. E., Paskavitz, A. L., Lee, J. B., and Padilla-Benavides, T. (2018) Dynamic changes in copper homeostasis and post-transcriptional regulation of Atp7a during myogenic differentiation. *Metallomics* **10**, 309-322
251. Tian, B., and Manley, J. L. (2017) Alternative polyadenylation of mRNA precursors. *Nat Rev Mol Cell Biol* **18**, 18-30
252. Beaudoing, E., Freier, S., Wyatt, J. R., Claverie, J. M., and Gautheret, D. (2000) Patterns of variant polyadenylation signal usage in human genes. *Genome Res* **10**, 1001-1010
253. Edwalds-Gilbert, G., Veraldi, K. L., and Milcarek, C. (1997) Alternative poly(A) site selection in complex transcription units: means to an end? *Nucleic Acids Res* **25**, 2547-2561
254. Colgan, D. F., and Manley, J. L. (1997) Mechanism and regulation of mRNA polyadenylation. *Genes Dev* **11**, 2755-2766
255. Reddy, M. C., and Harris, E. D. (1998) Multiple transcripts coding for the menkes gene: evidence for alternative splicing of Menkes mRNA. *Biochem J* **334 (Pt 1)**, 71-77
256. Reddy, M. C., Majumdar, S., and Harris, E. D. (2000) Evidence for a Menkes-like protein with a nuclear targeting sequence. *Biochem J* **350 Pt 3**, 855-863
257. Leung, A. K., Young, A. G., Bhutkar, A., Zheng, G. X., Bosson, A. D., Nielsen, C. B., and Sharp, P. A. (2011) Genome-wide identification of Ago2 binding sites from mouse embryonic stem cells with and without mature microRNAs. *Nat Struct Mol Biol* **18**, 237-244
258. Mukherjee, N., Corcoran, D. L., Nusbaum, J. D., Reid, D. W., Georgiev, S., Hafner, M., Ascano, M., Jr., Tuschl, T., Ohler, U., and Keene, J. D. (2011) Integrative regulatory mapping indicates that the RNA-binding protein HuR couples pre-mRNA processing and mRNA stability. *Mol Cell* **43**, 327-339

259. Yao, C., Biesinger, J., Wan, J., Weng, L., Xing, Y., Xie, X., and Shi, Y. (2012) Transcriptome-wide analyses of CstF64-RNA interactions in global regulation of mRNA alternative polyadenylation. *Proc Natl Acad Sci U S A* **109**, 18773-18778
260. Pilon, M. (2017) The copper microRNAs. *New Phytol* **213**, 1030-1035
261. Yamasaki, H., Abdel-Ghany, S. E., Cohu, C. M., Kobayashi, Y., Shikanai, T., and Pilon, M. (2007) Regulation of copper homeostasis by micro-RNA in Arabidopsis. *J Biol Chem* **282**, 16369-16378
262. Abdel-Ghany, S. E., and Pilon, M. (2008) MicroRNA-mediated systemic down-regulation of copper protein expression in response to low copper availability in Arabidopsis. *J Biol Chem* **283**, 15932-15945
263. Lu, T. X., and Rothenberg, M. E. (2018) MicroRNA. *J Allergy Clin Immunol* **141**, 1202-1207
264. Wang, Q., Wang, Y., Minto, A. W., Wang, J., Shi, Q., Li, X., and Quigg, R. J. (2008) MicroRNA-377 is up-regulated and can lead to increased fibronectin production in diabetic nephropathy. *FASEB J* **22**, 4126-4135
265. Xiao, F., Li, Y., Wan, Y., and Xue, M. (2018) MircroRNA-139 sensitizes ovarian cancer cell to cisplatin-based chemotherapy through regulation of ATP7A/B. *Cancer Chemother Pharmacol* **81**, 935-947
266. Xiao, F., Xiao, S., and Xue, M. (2019) miR-139 Controls Viability Of Ovarian Cancer Cells Through Apoptosis Induction And Exosome Shedding Inhibition By Targeting ATP7A. *Onco Targets Ther* **12**, 10727-10737
267. Yu, Z., Cao, W., Ren, Y., Zhang, Q., and Liu, J. (2020) ATPase copper transporter A, negatively regulated by miR-148a-3p, contributes to cisplatin resistance in breast cancer cells. *Clin Transl Med* **10**, 57-73
268. Burkhead, J. L., Ralle, M., Wilmarth, P., David, L., and Lutsenko, S. (2011) Elevated copper remodels hepatic RNA processing machinery in the mouse model of Wilson's disease. *J Mol Biol* **406**, 44-58
269. Malinouski, M., Hasan, N. M., Zhang, Y., Seravalli, J., Lin, J., Avanesov, A., Lutsenko, S., and Gladyshev, V. N. (2014) Genome-wide RNAi ionomics screen reveals new genes and regulation of human trace element metabolism. *Nat Commun* **5**, 3301
270. Bentley, D. L. (2014) Coupling mRNA processing with transcription in time and space. *Nat Rev Genet* **15**, 163-175
271. Darnell, J. E., Jr. (1982) Variety in the level of gene control in eukaryotic cells. *Nature* **297**, 365-371
272. Nevins, J. R. (1983) The pathway of eukaryotic mRNA formation. *Annu Rev Biochem* **52**, 441-466
273. Dreyfuss, G., Matunis, M. J., Pinol-Roma, S., and Burd, C. G. (1993) hnRNP proteins and the biogenesis of mRNA. *Annu Rev Biochem* **62**, 289-321
274. Dreyfuss, G., Swanson, M. S., and Pinol-Roma, S. (1988) Heterogeneous nuclear ribonucleoprotein particles and the pathway of mRNA formation. *Trends Biochem Sci* **13**, 86-91
275. Mili, S., Shu, H. J., Zhao, Y., and Pinol-Roma, S. (2001) Distinct RNP complexes of shuttling hnRNP proteins with pre-mRNA and mRNA: candidate intermediates in formation and export of mRNA. *Mol Cell Biol* **21**, 7307-7319
276. Han, S. P., Tang, Y. H., and Smith, R. (2010) Functional diversity of the hnRNPs: past, present and perspectives. *Biochem J* **430**, 379-392
277. Gorlach, M., Burd, C. G., Portman, D. S., and Dreyfuss, G. (1993) The hnRNP proteins. *Mol Biol Rep* **18**, 73-78
278. Kamma, H., Portman, D. S., and Dreyfuss, G. (1995) Cell type-specific expression of hnRNP proteins. *Exp Cell Res* **221**, 187-196

279. Chaudhury, A., Chander, P., and Howe, P. H. (2010) Heterogeneous nuclear ribonucleoproteins (hnRNPs) in cellular processes: Focus on hnRNP E1's multifunctional regulatory roles. *RNA* **16**, 1449-1462
280. Dreyfuss, G., Kim, V. N., and Kataoka, N. (2002) Messenger-RNA-binding proteins and the messages they carry. *Nat Rev Mol Cell Biol* **3**, 195-205
281. Weighardt, F., Biamonti, G., and Riva, S. (1996) The roles of heterogeneous nuclear ribonucleoproteins (hnRNP) in RNA metabolism. *Bioessays* **18**, 747-756
282. Swanson, M. S. (1995) Functions of Nuclear Pre-mRNA/mRNA Binding Proteins. in *Pre-mRNA Processing*, Springer, Berlin, Heidelberg. pp 17-33
283. Pinol-Roma, S., Choi, Y. D., Matunis, M. J., and Dreyfuss, G. (1988) Immunopurification of heterogeneous nuclear ribonucleoprotein particles reveals an assortment of RNA-binding proteins. *Genes Dev* **2**, 215-227
284. Wurtz, T., Kiseleva, E., Nacheva, G., Alzhanova-Ericcson, A., Rosen, A., and Daneholt, B. (1996) Identification of two RNA-binding proteins in Balbiani ring premessenger ribonucleoprotein granules and presence of these proteins in specific subsets of heterogeneous nuclear ribonucleoprotein particles. *Mol Cell Biol* **16**, 1425-1435
285. Singh, R., and Valcarcel, J. (2005) Building specificity with nonspecific RNA-binding proteins. *Nat Struct Mol Biol* **12**, 645-653
286. Query, C. C., Bentley, R. C., and Keene, J. D. (1989) A common RNA recognition motif identified within a defined U1 RNA binding domain of the 70K U1 snRNP protein. *Cell* **57**, 89-101
287. Hofmann, Y., and Wirth, B. (2002) hnRNP-G promotes exon 7 inclusion of survival motor neuron (SMN) via direct interaction with Htra2-beta1. *Hum Mol Genet* **11**, 2037-2049
288. Birney, E., Kumar, S., and Krainer, A. R. (1993) Analysis of the RNA-recognition motif and RS and RGG domains: conservation in metazoan pre-mRNA splicing factors. *Nucleic Acids Res* **21**, 5803-5816
289. Maris, C., Dominguez, C., and Allain, F. H. (2005) The RNA recognition motif, a plastic RNA-binding platform to regulate post-transcriptional gene expression. *FEBS J* **272**, 2118-2131
290. Dominguez, C., and Allain, F. H. (2006) NMR structure of the three quasi RNA recognition motifs (qRRMs) of human hnRNP F and interaction studies with Bcl-x G-tract RNA: a novel mode of RNA recognition. *Nucleic Acids Res* **34**, 3634-3645
291. Kiledjian, M., and Dreyfuss, G. (1992) Primary structure and binding activity of the hnRNP U protein: binding RNA through RGG box. *EMBO J* **11**, 2655-2664
292. Christensen, M. E., and Fuxa, K. P. (1988) The nucleolar protein, B-36, contains a glycine and dimethylarginine-rich sequence conserved in several other nuclear RNA-binding proteins. *Biochem Biophys Res Commun* **155**, 1278-1283
293. Siomi, H., Matunis, M. J., Michael, W. M., and Dreyfuss, G. (1993) The pre-mRNA binding K protein contains a novel evolutionarily conserved motif. *Nucleic Acids Res* **21**, 1193-1198
294. Liu, Y., and Shi, S. L. (2021) The roles of hnRNP A2/B1 in RNA biology and disease. *Wiley Interdiscip Rev RNA* **12**, e1612
295. Thibault, P. A., Ganesan, A., Kalyaanamoorthy, S., Clarke, J. W. E., Salapa, H. E., and Levin, M. C. (2021) hnRNP A/B Proteins: An Encyclopedic Assessment of Their Roles in Homeostasis and Disease. *Biology (Basel)* **10**
296. Michael, W. M., Eder, P. S., and Dreyfuss, G. (1997) The K nuclear shuttling domain: a novel signal for nuclear import and nuclear export in the hnRNP K protein. *EMBO J* **16**, 3587-3598
297. Siomi, H., and Dreyfuss, G. (1995) A nuclear localization domain in the hnRNP A1 protein. *J Cell Biol* **129**, 551-560

298. Michael, W. M., Choi, M., and Dreyfuss, G. (1995) A nuclear export signal in hnRNP A1: a signal-mediated, temperature-dependent nuclear protein export pathway. *Cell* **83**, 415-422
299. Izaurralde, E., Jarmolowski, A., Beisel, C., Mattaj, I. W., Dreyfuss, G., and Fischer, U. (1997) A role for the M9 transport signal of hnRNP A1 in mRNA nuclear export. *J Cell Biol* **137**, 27-35
300. Karn, J., Vidali, G., Boffa, L. C., and Allfrey, V. G. (1977) Characterization of the non-histone nuclear proteins associated with rapidly labeled heterogeneous nuclear RNA. *J Biol Chem* **252**, 7307-7322
301. Mayrand, S. H., Dwen, P., and Pederson, T. (1993) Serine/threonine phosphorylation regulates binding of C hnRNP proteins to pre-mRNA. *Proc Natl Acad Sci U S A* **90**, 7764-7768
302. Habelhah, H., Shah, K., Huang, L., Ostareck-Lederer, A., Burlingame, A. L., Shokat, K. M., Hentze, M. W., and Ronai, Z. (2001) ERK phosphorylation drives cytoplasmic accumulation of hnRNP-K and inhibition of mRNA translation. *Nat Cell Biol* **3**, 325-330
303. Ostareck-Lederer, A., Ostareck, D. H., Cans, C., Neubauer, G., Bomsztyk, K., Superti-Furga, G., and Hentze, M. W. (2002) c-Src-mediated phosphorylation of hnRNP K drives translational activation of specifically silenced mRNAs. *Mol Cell Biol* **22**, 4535-4543
304. Buxade, M., Parra, J. L., Rousseau, S., Shpiro, N., Marquez, R., Morrice, N., Bain, J., Espel, E., and Proud, C. G. (2005) The Mnks are novel components in the control of TNF alpha biosynthesis and phosphorylate and regulate hnRNP A1. *Immunity* **23**, 177-189
305. Cobianchi, F., Calvio, C., Stoppini, M., Buvoli, M., and Riva, S. (1993) Phosphorylation of human hnRNP protein A1 abrogates in vitro strand annealing activity. *Nucleic Acids Res* **21**, 949-955
306. Zhang, S., Schlott, B., Gorlach, M., and Grosse, F. (2004) DNA-dependent protein kinase (DNA-PK) phosphorylates nuclear DNA helicase II/RNA helicase A and hnRNP proteins in an RNA-dependent manner. *Nucleic Acids Res* **32**, 1-10
307. Leffers, H., Dejgaard, K., and Celis, J. E. (1995) Characterisation of two major cellular poly(rC)-binding human proteins, each containing three K-homologous (KH) domains. *Eur J Biochem* **230**, 447-453
308. Wilk, H. E., Werr, H., Friedrich, D., Kiltz, H. H., and Schafer, K. P. (1985) The core proteins of 35S hnRNP complexes. Characterization of nine different species. *Eur J Biochem* **146**, 71-81
309. Dreyfuss, G., Choi, Y. D., and Adam, S. A. (1984) Characterization of heterogeneous nuclear RNA-protein complexes in vivo with monoclonal antibodies. *Mol Cell Biol* **4**, 1104-1114
310. Holcomb, E. R., and Friedman, D. L. (1984) Phosphorylation of the C-proteins of HeLa cell hnRNP particles. Involvement of a casein kinase II-type enzyme. *J Biol Chem* **259**, 31-40
311. Kim, S., Merrill, B. M., Rajpurohit, R., Kumar, A., Stone, K. L., Papov, V. V., Schneiders, J. M., Szer, W., Wilson, S. H., Paik, W. K., and Williams, K. R. (1997) Identification of N(G)-methylarginine residues in human heterogeneous RNP protein A1: Phe/Gly-Gly-Gly-Arg-Gly-Gly-Gly/Phe is a preferred recognition motif. *Biochemistry* **36**, 5185-5192
312. Beyer, A. L., Christensen, M. E., Walker, B. W., and LeStourgeon, W. M. (1977) Identification and characterization of the packaging proteins of core 40S hnRNP particles. *Cell* **11**, 127-138
313. Chen, Y., Zhou, X., Liu, N., Wang, C., Zhang, L., Mo, W., and Hu, G. (2008) Arginine methylation of hnRNP K enhances p53 transcriptional activity. *FEBS Lett* **582**, 1761-1765
314. Shen, E. C., Henry, M. F., Weiss, V. H., Valentini, S. R., Silver, P. A., and Lee, M. S. (1998) Arginine methylation facilitates the nuclear export of hnRNP proteins. *Genes Dev* **12**, 679-691

315. Friend, L. R., Landsberg, M. J., Nouwens, A. S., Wei, Y., Rothnagel, J. A., and Smith, R. (2013) Arginine methylation of hnRNP A2 does not directly govern its subcellular localization. *PLoS One* **8**, e75669
316. Yu, M. C. (2011) The Role of Protein Arginine Methylation in mRNP Dynamics. *Mol Biol Int* **2011**, 163827
317. Li, T., Evdokimov, E., Shen, R. F., Chao, C. C., Tekle, E., Wang, T., Stadtman, E. R., Yang, D. C., and Chock, P. B. (2004) Sumoylation of heterogeneous nuclear ribonucleoproteins, zinc finger proteins, and nuclear pore complex proteins: a proteomic analysis. *Proc Natl Acad Sci U S A* **101**, 8551-8556
318. Lee, S. W., Lee, M. H., Park, J. H., Kang, S. H., Yoo, H. M., Ka, S. H., Oh, Y. M., Jeon, Y. J., and Chung, C. H. (2012) SUMOylation of hnRNP-K is required for p53-mediated cell-cycle arrest in response to DNA damage. *EMBO J* **31**, 4441-4452
319. Richard, P., Vethantham, V., and Manley, J. L. (2017) Roles of Sumoylation in mRNA Processing and Metabolism. *Adv Exp Med Biol* **963**, 15-33
320. Vassileva, M. T., and Matunis, M. J. (2004) SUMO modification of heterogeneous nuclear ribonucleoproteins. *Mol Cell Biol* **24**, 3623-3632
321. Villarroya-Beltri, C., Gutierrez-Vazquez, C., Sanchez-Cabo, F., Perez-Hernandez, D., Vazquez, J., Martin-Cofreces, N., Martinez-Herrera, D. J., Pascual-Montano, A., Mittelbrunn, M., and Sanchez-Madrid, F. (2013) Sumoylated hnRNPA2B1 controls the sorting of miRNAs into exosomes through binding to specific motifs. *Nat Commun* **4**, 2980
322. Vethantham, V., Rao, N., and Manley, J. L. (2007) Sumoylation modulates the assembly and activity of the pre-mRNA 3' processing complex. *Mol Cell Biol* **27**, 8848-8858
323. Geuens, T., Bouhy, D., and Timmerman, V. (2016) The hnRNP family: insights into their role in health and disease. *Hum Genet* **135**, 851-867
324. Caceres, J. F., Stamm, S., Helfman, D. M., and Krainer, A. R. (1994) Regulation of alternative splicing in vivo by overexpression of antagonistic splicing factors. *Science* **265**, 1706-1709
325. Chou, M. Y., Rooke, N., Turck, C. W., and Black, D. L. (1999) hnRNP H is a component of a splicing enhancer complex that activates a c-src alternative exon in neuronal cells. *Mol Cell Biol* **19**, 69-77
326. Kessler, M. M., Henry, M. F., Shen, E., Zhao, J., Gross, S., Silver, P. A., and Moore, C. L. (1997) Hrp1, a sequence-specific RNA-binding protein that shuttles between the nucleus and the cytoplasm, is required for mRNA 3'-end formation in yeast. *Genes Dev* **11**, 2545-2556
327. Gallouzi, I. E., and Steitz, J. A. (2001) Delineation of mRNA export pathways by the use of cell-permeable peptides. *Science* **294**, 1895-1901
328. Carson, J. H., Cui, H., Krueger, W., Schlepchenko, B., Brumwell, C., and Barbarese, E. (2001) RNA trafficking in oligodendrocytes. *Results Probl Cell Differ* **34**, 69-81
329. Xu, K., Yen, T., and Geczy, C. L. (2001) Il-10 up-regulates macrophage expression of the S100 protein S100A8. *J Immunol* **166**, 6358-6366
330. Wang, Y., Liu, J., Huang, B. O., Xu, Y. M., Li, J., Huang, L. F., Lin, J., Zhang, J., Min, Q. H., Yang, W. M., and Wang, X. Z. (2015) Mechanism of alternative splicing and its regulation. *Biomed Rep* **3**, 152-158
331. Black, D. L. (2003) Mechanisms of alternative pre-messenger RNA splicing. *Annu Rev Biochem* **72**, 291-336
332. Bruun, G. H., Doktor, T. K., Borch-Jensen, J., Masuda, A., Krainer, A. R., Ohno, K., and Andresen, B. S. (2016) Global identification of hnRNP A1 binding sites for SSO-based splicing modulation. *BMC Biol* **14**, 54
333. Mayeda, A., Munroe, S. H., Caceres, J. F., and Krainer, A. R. (1994) Function of conserved domains of hnRNP A1 and other hnRNP A/B proteins. *EMBO J* **13**, 5483-5495

334. Ding, J., Hayashi, M. K., Zhang, Y., Manche, L., Krainer, A. R., and Xu, R. M. (1999) Crystal structure of the two-RRM domain of hnRNP A1 (UP1) complexed with single-stranded telomeric DNA. *Genes Dev* **13**, 1102-1115
335. Martinez-Contreras, R., Fisette, J. F., Nasim, F. U., Madden, R., Cordeau, M., and Chabot, B. (2006) Intronic binding sites for hnRNP A/B and hnRNP F/H proteins stimulate pre-mRNA splicing. *PLoS Biol* **4**, e21
336. Gautrey, H., Jackson, C., Dittrich, A. L., Browell, D., Lennard, T., and Tyson-Capper, A. (2015) SRSF3 and hnRNP H1 regulate a splicing hotspot of HER2 in breast cancer cells. *RNA Biol* **12**, 1139-1151
337. Soulard, M., Della Valle, V., Siomi, M. C., Pinol-Roma, S., Codogno, P., Bauvy, C., Bellini, M., Lacroix, J. C., Monod, G., Dreyfuss, G., and et al. (1993) hnRNP G: sequence and characterization of a glycosylated RNA-binding protein. *Nucleic Acids Res* **21**, 4210-4217
338. Nasim, M. T., Chernova, T. K., Chowdhury, H. M., Yue, B. G., and Eperon, I. C. (2003) HnRNP G and Tra2beta: opposite effects on splicing matched by antagonism in RNA binding. *Hum Mol Genet* **12**, 1337-1348
339. Patton, J. G., Mayer, S. A., Tempst, P., and Nadal-Ginard, B. (1991) Characterization and molecular cloning of polypyrimidine tract-binding protein: a component of a complex necessary for pre-mRNA splicing. *Genes Dev* **5**, 1237-1251
340. Xue, Y., Zhou, Y., Wu, T., Zhu, T., Ji, X., Kwon, Y. S., Zhang, C., Yeo, G., Black, D. L., Sun, H., Fu, X. D., and Zhang, Y. (2009) Genome-wide analysis of PTB-RNA interactions reveals a strategy used by the general splicing repressor to modulate exon inclusion or skipping. *Mol Cell* **36**, 996-1006
341. Expert-Bezancon, A., Le Caer, J. P., and Marie, J. (2002) Heterogeneous nuclear ribonucleoprotein (hnRNP) K is a component of an intronic splicing enhancer complex that activates the splicing of the alternative exon 6A from chicken beta-tropomyosin pre-mRNA. *J Biol Chem* **277**, 16614-16623
342. Cao, W., Razanau, A., Feng, D., Lobo, V. G., and Xie, J. (2012) Control of alternative splicing by forskolin through hnRNP K during neuronal differentiation. *Nucleic Acids Res* **40**, 8059-8071
343. Hung, L. H., Heiner, M., Hui, J., Schreiner, S., Benes, V., and Bindereif, A. (2008) Diverse roles of hnRNP L in mammalian mRNA processing: a combined microarray and RNAi analysis. *RNA* **14**, 284-296
344. Melton, A. A., Jackson, J., Wang, J., and Lynch, K. W. (2007) Combinatorial control of signal-induced exon repression by hnRNP L and PSF. *Mol Cell Biol* **27**, 6972-6984
345. Lleres, D., Denegri, M., Biggiogera, M., Ajuh, P., and Lamond, A. I. (2010) Direct interaction between hnRNP-M and CDC5L/PLRG1 proteins affects alternative splice site choice. *EMBO Rep* **11**, 445-451
346. Mourelatos, Z., Abel, L., Yong, J., Kataoka, N., and Dreyfuss, G. (2001) SMN interacts with a novel family of hnRNP and spliceosomal proteins. *EMBO J* **20**, 5443-5452
347. Vu, N. T., Park, M. A., Shultz, J. C., Goehe, R. W., Hoeferlin, L. A., Shultz, M. D., Smith, S. A., Lynch, K. W., and Chalfant, C. E. (2013) hnRNP U enhances caspase-9 splicing and is modulated by AKT-dependent phosphorylation of hnRNP L. *J Biol Chem* **288**, 8575-8584
348. Danckwardt, S., Hentze, M. W., and Kulozik, A. E. (2008) 3' end mRNA processing: molecular mechanisms and implications for health and disease. *EMBO J* **27**, 482-498
349. Ryan, K., Calvo, O., and Manley, J. L. (2004) Evidence that polyadenylation factor CPSF-73 is the mRNA 3' processing endonuclease. *RNA* **10**, 565-573
350. Dominski, Z., Yang, X. C., and Marzluff, W. F. (2005) The polyadenylation factor CPSF-73 is involved in histone-pre-mRNA processing. *Cell* **123**, 37-48

351. Mandel, C. R., Kaneko, S., Zhang, H., Gebauer, D., Vethantham, V., Manley, J. L., and Tong, L. (2006) Polyadenylation factor CPSF-73 is the pre-mRNA 3'-end-processing endonuclease. *Nature* **444**, 953-956
352. Moreira, A., Wollerton, M., Monks, J., and Proudfoot, N. J. (1995) Upstream sequence elements enhance poly(A) site efficiency of the C2 complement gene and are phylogenetically conserved. *EMBO J* **14**, 3809-3819
353. Moreira, A., Takagaki, Y., Brackenridge, S., Wollerton, M., Manley, J. L., and Proudfoot, N. J. (1998) The upstream sequence element of the C2 complement poly(A) signal activates mRNA 3' end formation by two distinct mechanisms. *Genes Dev* **12**, 2522-2534
354. Danckwardt, S., Kaufmann, I., Gentzel, M., Foerstner, K. U., Gantzert, A. S., Gehring, N. H., Neu-Yilik, G., Bork, P., Keller, W., Wilm, M., Hentze, M. W., and Kulozik, A. E. (2007) Splicing factors stimulate polyadenylation via USEs at non-canonical 3' end formation signals. *EMBO J* **26**, 2658-2669
355. Hall-Pogar, T., Liang, S., Hague, L. K., and Lutz, C. S. (2007) Specific trans-acting proteins interact with auxiliary RNA polyadenylation elements in the COX-2 3'-UTR. *RNA* **13**, 1103-1115
356. Mikula, M., Bomsztyk, K., Goryca, K., Chojnowski, K., and Ostrowski, J. (2013) Heterogeneous nuclear ribonucleoprotein (HnRNP) K genome-wide binding survey reveals its role in regulating 3'-end RNA processing and transcription termination at the early growth response 1 (EGR1) gene through XRN2 exonuclease. *J Biol Chem* **288**, 24788-24798
357. Krecic, A. M., and Swanson, M. S. (1999) hnRNP complexes: composition, structure, and function. *Curr Opin Cell Biol* **11**, 363-371
358. Arhin, G. K., Boots, M., Bagga, P. S., Milcarek, C., and Wilusz, J. (2002) Downstream sequence elements with different affinities for the hnRNP H/H' protein influence the processing efficiency of mammalian polyadenylation signals. *Nucleic Acids Res* **30**, 1842-1850
359. Bagga, P. S., Arhin, G. K., and Wilusz, J. (1998) DSEF-1 is a member of the hnRNP H family of RNA-binding proteins and stimulates pre-mRNA cleavage and polyadenylation in vitro. *Nucleic Acids Res* **26**, 5343-5350
360. Honore, B., Baandrup, U., and Vorum, H. (2004) Heterogeneous nuclear ribonucleoproteins F and H/H' show differential expression in normal and selected cancer tissues. *Exp Cell Res* **294**, 199-209
361. Veraldi, K. L., Arhin, G. K., Martincic, K., Chung-Ganster, L. H., Wilusz, J., and Milcarek, C. (2001) hnRNP F influences binding of a 64-kilodalton subunit of cleavage stimulation factor to mRNA precursors in mouse B cells. *Mol Cell Biol* **21**, 1228-1238
362. Hsu, M. C., Pan, M. R., Chu, P. Y., Tsai, Y. L., Tsai, C. H., Shan, Y. S., Chen, L. T., and Hung, W. C. (2018) Protein Arginine Methyltransferase 3 Enhances Chemoresistance in Pancreatic Cancer by Methylating hnRNPA1 to Increase ABCG2 Expression. *Cancers (Basel)* **11**
363. Henics, T., Sanfridson, A., Hamilton, B. J., Nagy, E., and Rigby, W. F. (1994) Enhanced stability of interleukin-2 mRNA in MLA 144 cells. Possible role of cytoplasmic AU-rich sequence-binding proteins. *J Biol Chem* **269**, 5377-5383
364. Hamilton, B. J., Burns, C. M., Nichols, R. C., and Rigby, W. F. (1997) Modulation of AUUUA response element binding by heterogeneous nuclear ribonucleoprotein A1 in human T lymphocytes. The roles of cytoplasmic location, transcription, and phosphorylation. *J Biol Chem* **272**, 28732-28741
365. Hamilton, B. J., Nagy, E., Malter, J. S., Arrick, B. A., and Rigby, W. F. (1993) Association of heterogeneous nuclear ribonucleoprotein A1 and C proteins with reiterated AUUUA sequences. *J Biol Chem* **268**, 8881-8887

366. Caput, D., Beutler, B., Hartog, K., Thayer, R., Brown-Shimer, S., and Cerami, A. (1986) Identification of a common nucleotide sequence in the 3'-untranslated region of mRNA molecules specifying inflammatory mediators. *Proc Natl Acad Sci U S A* **83**, 1670-1674
367. Geissler, R., Simkin, A., Floss, D., Patel, R., Fogarty, E. A., Scheller, J., and Grimson, A. (2016) A widespread sequence-specific mRNA decay pathway mediated by hnRNPs A1 and A2/B1. *Genes Dev* **30**, 1070-1085
368. Fialcowitz, E. J., Brewer, B. Y., Keenan, B. P., and Wilson, G. M. (2005) A hairpin-like structure within an AU-rich mRNA-destabilizing element regulates trans-factor binding selectivity and mRNA decay kinetics. *J Biol Chem* **280**, 22406-22417
369. Skalweit, A., Doller, A., Huth, A., Kahne, T., Persson, P. B., and Thiele, B. J. (2003) Posttranscriptional control of renin synthesis: identification of proteins interacting with renin mRNA 3'-untranslated region. *Circ Res* **92**, 419-427
370. Wang, Z., Day, N., Trifillis, P., and Kiledjian, M. (1999) An mRNA stability complex functions with poly(A)-binding protein to stabilize mRNA in vitro. *Mol Cell Biol* **19**, 4552-4560
371. Fukuda, T., Naiki, T., Saito, M., and Irie, K. (2009) hnRNP K interacts with RNA binding motif protein 42 and functions in the maintenance of cellular ATP level during stress conditions. *Genes Cells* **14**, 113-128
372. Zaidi, S. H., and Malter, J. S. (1995) Nucleolin and heterogeneous nuclear ribonucleoprotein C proteins specifically interact with the 3'-untranslated region of amyloid protein precursor mRNA. *J Biol Chem* **270**, 17292-17298
373. Ostareck, D. H., Ostareck-Lederer, A., Wilm, M., Thiele, B. J., Mann, M., and Hentze, M. W. (1997) mRNA silencing in erythroid differentiation: hnRNP K and hnRNP E1 regulate 15-lipoxygenase translation from the 3' end. *Cell* **89**, 597-606
374. Ostareck, D. H., Ostareck-Lederer, A., Shatsky, I. N., and Hentze, M. W. (2001) Lipoxygenase mRNA silencing in erythroid differentiation: The 3'UTR regulatory complex controls 60S ribosomal subunit joining. *Cell* **104**, 281-290
375. Fan, X., Xiong, H., Wei, J., Gao, X., Feng, Y., Liu, X., Zhang, G., He, Q. Y., Xu, J., and Liu, L. (2015) Cytoplasmic hnRNPK interacts with GSK3beta and is essential for the osteoclast differentiation. *Sci Rep* **5**, 17732
376. Guil, S., and Caceres, J. F. (2007) The multifunctional RNA-binding protein hnRNP A1 is required for processing of miR-18a. *Nat Struct Mol Biol* **14**, 591-596
377. Shan, J., Munro, T. P., Barbarese, E., Carson, J. H., and Smith, R. (2003) A molecular mechanism for mRNA trafficking in neuronal dendrites. *J Neurosci* **23**, 8859-8866
378. Guil, S., Long, J. C., and Caceres, J. F. (2006) hnRNP A1 relocalization to the stress granules reflects a role in the stress response. *Mol Cell Biol* **26**, 5744-5758
379. Cammas, A., Pileur, F., Bonnal, S., Lewis, S. M., Leveque, N., Holcik, M., and Vagner, S. (2007) Cytoplasmic relocalization of heterogeneous nuclear ribonucleoprotein A1 controls translation initiation of specific mRNAs. *Mol Biol Cell* **18**, 5048-5059
380. Kosturko, L. D., Maggipinto, M. J., Korza, G., Lee, J. W., Carson, J. H., and Barbarese, E. (2006) Heterogeneous nuclear ribonucleoprotein (hnRNP) E1 binds to hnRNP A2 and inhibits translation of A2 response element mRNAs. *Mol Biol Cell* **17**, 3521-3533
381. Huang, M., Rech, J. E., Northington, S. J., Flicker, P. F., Mayeda, A., Krainer, A. R., and LeStourgeon, W. M. (1994) The C-protein tetramer binds 230 to 240 nucleotides of pre-mRNA and nucleates the assembly of 40S heterogeneous nuclear ribonucleoprotein particles. *Mol Cell Biol* **14**, 518-533
382. Swanson, M. S., Nakagawa, T. Y., LeVan, K., and Dreyfuss, G. (1987) Primary structure of human nuclear ribonucleoprotein particle C proteins: conservation of sequence and domain structures in heterogeneous nuclear RNA, mRNA, and pre-rRNA-binding proteins. *Mol Cell Biol* **7**, 1731-1739

383. McCloskey, A., Taniguchi, I., Shinmyozu, K., and Ohno, M. (2012) hnRNP C tetramer measures RNA length to classify RNA polymerase II transcripts for export. *Science* **335**, 1643-1646
384. Miau, L. H., Chang, C. J., Shen, B. J., Tsai, W. H., and Lee, S. C. (1998) Identification of heterogeneous nuclear ribonucleoprotein K (hnRNP K) as a repressor of C/EBPbeta-mediated gene activation. *J Biol Chem* **273**, 10784-10791
385. Bi, H. S., Yang, X. Y., Yuan, J. H., Yang, F., Xu, D., Guo, Y. J., Zhang, L., Zhou, C. C., Wang, F., and Sun, S. H. (2013) H19 inhibits RNA polymerase II-mediated transcription by disrupting the hnRNP U-actin complex. *Biochim Biophys Acta* **1830**, 4899-4906
386. Lynch, M., Chen, L., Ravitz, M. J., Mehtani, S., Korenblat, K., Pazin, M. J., and Schmidt, E. V. (2005) hnRNP K binds a core polypyrimidine element in the eukaryotic translation initiation factor 4E (eIF4E) promoter, and its regulation of eIF4E contributes to neoplastic transformation. *Mol Cell Biol* **25**, 6436-6453
387. Stains, J. P., Lecanda, F., Towler, D. A., and Civitelli, R. (2005) Heterogeneous nuclear ribonucleoprotein K represses transcription from a cytosine/thymidine-rich element in the osteocalcin promoter. *Biochem J* **385**, 613-623
388. Pont, A. R., Sadri, N., Hsiao, S. J., Smith, S., and Schneider, R. J. (2012) mRNA decay factor AUF1 maintains normal aging, telomere maintenance, and suppression of senescence by activation of telomerase transcription. *Mol Cell* **47**, 5-15
389. Fukuda, A., Nakadai, T., Shimada, M., and Hisatake, K. (2009) Heterogeneous nuclear ribonucleoprotein R enhances transcription from the naturally configured c-fos promoter in vitro. *J Biol Chem* **284**, 23472-23480
390. Clarke, J. P., Thibault, P. A., Salapa, H. E., and Levin, M. C. (2021) A Comprehensive Analysis of the Role of hnRNP A1 Function and Dysfunction in the Pathogenesis of Neurodegenerative Disease. *Front Mol Biosci* **8**, 659610
391. Ostareck-Lederer, A., Ostareck, D. H., and Hentze, M. W. (1998) Cytoplasmic regulatory functions of the KH-domain proteins hnRNPs K and E1/E2. *Trends Biochem Sci* **23**, 409-411
392. Pickering, B. M., Mitchell, S. A., Spriggs, K. A., Stoneley, M., and Willis, A. E. (2004) Bag-1 internal ribosome entry segment activity is promoted by structural changes mediated by poly(rC) binding protein 1 and recruitment of polypyrimidine tract binding protein 1. *Mol Cell Biol* **24**, 5595-5605
393. Bushell, M., Stoneley, M., Kong, Y. W., Hamilton, T. L., Spriggs, K. A., Dobbyn, H. C., Qin, X., Sarnow, P., and Willis, A. E. (2006) Polypyrimidine tract binding protein regulates IRES-mediated gene expression during apoptosis. *Mol Cell* **23**, 401-412
394. Mukhopadhyay, N. K., Kim, J., Cinar, B., Ramachandran, A., Hager, M. H., Di Vizio, D., Adam, R. M., Rubin, M. A., Raychaudhuri, P., De Benedetti, A., and Freeman, M. R. (2009) Heterogeneous nuclear ribonucleoprotein K is a novel regulator of androgen receptor translation. *Cancer Res* **69**, 2210-2218
395. Lee, H. R., Kim, T. D., Kim, H. J., Jung, Y., Lee, D., Lee, K. H., Kim, D. Y., Woo, K. C., and Kim, K. T. (2015) Heterogeneous ribonucleoprotein R regulates arylalkylamine N-acetyltransferase synthesis via internal ribosomal entry site-mediated translation in a circadian manner. *J Pineal Res* **59**, 518-529
396. Bajenova, O., Stolper, E., Gapon, S., Sundina, N., Zimmer, R., and Thomas, P. (2003) Surface expression of heterogeneous nuclear RNA binding protein M4 on Kupffer cell relates to its function as a carcinoembryonic antigen receptor. *Exp Cell Res* **291**, 228-241
397. Chkheidze, A. N., and Liebhaber, S. A. (2003) A novel set of nuclear localization signals determine distributions of the alphaCP RNA-binding proteins. *Mol Cell Biol* **23**, 8405-8415
398. Pinol-Roma, S., and Dreyfuss, G. (1992) Shuttling of pre-mRNA binding proteins between nucleus and cytoplasm. *Nature* **355**, 730-732

399. Kanai, Y., Dohmae, N., and Hirokawa, N. (2004) Kinesin transports RNA: isolation and characterization of an RNA-transporting granule. *Neuron* **43**, 513-525
400. Gama-Carvalho, M., and Carmo-Fonseca, M. (2001) The rules and roles of nucleocytoplasmic shuttling proteins. *FEBS Lett* **498**, 157-163
401. Pinol-Roma, S., and Dreyfuss, G. (1993) hnRNP proteins: localization and transport between the nucleus and the cytoplasm. *Trends Cell Biol* **3**, 151-155
402. Michael, W. M., Siomi, H., Choi, M., Pinol-Roma, S., Nakielny, S., Liu, Q., and Dreyfuss, G. (1995) Signal sequences that target nuclear import and nuclear export of pre-mRNA-binding proteins. *Cold Spring Harb Symp Quant Biol* **60**, 663-668
403. Fu, X., Liang, C., Li, F., Wang, L., Wu, X., Lu, A., Xiao, G., and Zhang, G. (2018) The Rules and Functions of Nucleocytoplasmic Shuttling Proteins. *Int J Mol Sci* **19**
404. Siomi, M. C., Eder, P. S., Kataoka, N., Wan, L., Liu, Q., and Dreyfuss, G. (1997) Transportin-mediated nuclear import of heterogeneous nuclear RNP proteins. *J Cell Biol* **138**, 1181-1192
405. Cautain, B., Hill, R., de Pedro, N., and Link, W. (2015) Components and regulation of nuclear transport processes. *FEBS J* **282**, 445-462
406. Cammas, A., Lewis, S. M., Vagner, S., and Holcik, M. (2008) Post-transcriptional control of gene expression through subcellular relocalization of mRNA binding proteins. *Biochem Pharmacol* **76**, 1395-1403
407. Ma, S., Liu, G., Sun, Y., and Xie, J. (2007) Relocalization of the polypyrimidine tract-binding protein during PKA-induced neurite growth. *Biochim Biophys Acta* **1773**, 912-923
408. Knoch, K. P., Meisterfeld, R., Kersting, S., Bergert, H., Altkruger, A., Wegbrod, C., Jager, M., Saeger, H. D., and Solimena, M. (2006) cAMP-dependent phosphorylation of PTB1 promotes the expression of insulin secretory granule proteins in beta cells. *Cell Metab* **3**, 123-134
409. Xie, J., Lee, J. A., Kress, T. L., Mowry, K. L., and Black, D. L. (2003) Protein kinase A phosphorylation modulates transport of the polypyrimidine tract-binding protein. *Proc Natl Acad Sci U S A* **100**, 8776-8781
410. Roth, S., and Khalaila, I. (2017) The effect of O-GlcNAcylation on hnRNP A1 translocation and interaction with transportin1. *Exp Cell Res* **350**, 210-217
411. Roy, R., Durie, D., Li, H., Liu, B. Q., Skehel, J. M., Mauri, F., Cuorvo, L. V., Barbareschi, M., Guo, L., Holcik, M., Seckl, M. J., and Pardo, O. E. (2014) hnRNPA1 couples nuclear export and translation of specific mRNAs downstream of FGF-2/S6K2 signalling. *Nucleic Acids Res* **42**, 12483-12497
412. Wang, L., Wen, M., and Cao, X. (2019) Nuclear hnRNPA2B1 initiates and amplifies the innate immune response to DNA viruses. *Science* **365**
413. Nichols, R. C., Wang, X. W., Tang, J., Hamilton, B. J., High, F. A., Herschman, H. R., and Rigby, W. F. (2000) The RGG domain in hnRNP A2 affects subcellular localization. *Exp Cell Res* **256**, 522-532
414. Kim, J. H., Hahm, B., Kim, Y. K., Choi, M., and Jang, S. K. (2000) Protein-protein interaction among hnRNPs shuttling between nucleus and cytoplasm. *J Mol Biol* **298**, 395-405
415. Nakielny, S., Siomi, M. C., Siomi, H., Michael, W. M., Pollard, V., and Dreyfuss, G. (1996) Transportin: nuclear transport receptor of a novel nuclear protein import pathway. *Exp Cell Res* **229**, 261-266
416. Brumwell, C., Antolik, C., Carson, J. H., and Barbarese, E. (2002) Intracellular trafficking of hnRNP A2 in oligodendrocytes. *Exp Cell Res* **279**, 310-320
417. Moujaber, O., and Stochaj, U. (2018) Cytoplasmic RNA Granules in Somatic Maintenance. *Gerontology* **64**, 485-494
418. Anderson, P., and Kedersha, N. (2006) RNA granules. *J Cell Biol* **172**, 803-808

419. Kedersha, N., and Anderson, P. (2009) Regulation of translation by stress granules and processing bodies. *Prog Mol Biol Transl Sci* **90**, 155-185
420. Bley, N., Lederer, M., Pfalz, B., Reinke, C., Fuchs, T., Glass, M., Moller, B., and Huttelmaier, S. (2015) Stress granules are dispensable for mRNA stabilization during cellular stress. *Nucleic Acids Res* **43**, e26
421. Kedersha, N., and Anderson, P. (2007) Mammalian stress granules and processing bodies. *Methods Enzymol* **431**, 61-81
422. Moser, J. J., and Fritzler, M. J. (2010) Cytoplasmic ribonucleoprotein (RNP) bodies and their relationship to GW/P bodies. *Int J Biochem Cell Biol* **42**, 828-843
423. Liu, J. L., and Gall, J. G. (2007) U bodies are cytoplasmic structures that contain uridine-rich small nuclear ribonucleoproteins and associate with P bodies. *Proc Natl Acad Sci U S A* **104**, 11655-11659
424. Kamma, H., Horiguchi, H., Wan, L., Matsui, M., Fujiwara, M., Fujimoto, M., Yazawa, T., and Dreyfuss, G. (1999) Molecular characterization of the hnRNP A2/B1 proteins: tissue-specific expression and novel isoforms. *Exp Cell Res* **246**, 399-411
425. Harrison, A. F., and Shorter, J. (2017) RNA-binding proteins with prion-like domains in health and disease. *Biochem J* **474**, 1417-1438
426. Kim, H. J., Kim, N. C., Wang, Y. D., Scarborough, E. A., Moore, J., Diaz, Z., MacLea, K. S., Freibaum, B., Li, S., Molliex, A., Kanagaraj, A. P., Carter, R., Boylan, K. B., Wojtas, A. M., Rademakers, R., Pinkus, J. L., Greenberg, S. A., Trojanowski, J. Q., Traynor, B. J., Smith, B. N., Topp, S., Gkazi, A. S., Miller, J., Shaw, C. E., Kottlors, M., Kirschner, J., Pestronk, A., Li, Y. R., Ford, A. F., Gitler, A. D., Benatar, M., King, O. D., Kimonis, V. E., Ross, E. D., Weihl, C. C., Shorter, J., and Taylor, J. P. (2013) Mutations in prion-like domains in hnRNPA2B1 and hnRNPA1 cause multisystem proteinopathy and ALS. *Nature* **495**, 467-473
427. Wu, B., Su, S., Patil, D. P., Liu, H., Gan, J., Jaffrey, S. R., and Ma, J. (2018) Molecular basis for the specific and multivariant recognitions of RNA substrates by human hnRNP A2/B1. *Nat Commun* **9**, 420
428. Kozu, T., Henrich, B., and Schafer, K. P. (1995) Structure and expression of the gene (HNRPA2B1) encoding the human hnRNP protein A2/B1. *Genomics* **25**, 365-371
429. Han, S. P., Friend, L. R., Carson, J. H., Korza, G., Barbarese, E., Maggipinto, M., Hatfield, J. T., Rothnagel, J. A., and Smith, R. (2010) Differential subcellular distributions and trafficking functions of hnRNP A2/B1 spliceoforms. *Traffic* **11**, 886-898
430. Nguyen, E. D., Balas, M. M., Griffin, A. M., Roberts, J. T., and Johnson, A. M. (2018) Global profiling of hnRNP A2/B1-RNA binding on chromatin highlights LncRNA interactions. *RNA Biol* **15**, 901-913
431. Zhou, H., Di Palma, S., Preisinger, C., Peng, M., Polat, A. N., Heck, A. J., and Mohammed, S. (2013) Toward a comprehensive characterization of a human cancer cell phosphoproteome. *J Proteome Res* **12**, 260-271
432. Guo, A., Gu, H., Zhou, J., Mulhern, D., Wang, Y., Lee, K. A., Yang, V., Aguiar, M., Kornhauser, J., Jia, X., Ren, J., Beausoleil, S. A., Silva, J. C., Vemulapalli, V., Bedford, M. T., and Comb, M. J. (2014) Immunoaffinity enrichment and mass spectrometry analysis of protein methylation. *Mol Cell Proteomics* **13**, 372-387
433. Steinert, P. M., Mack, J. W., Korge, B. P., Gan, S. Q., Haynes, S. R., and Steven, A. C. (1991) Glycine loops in proteins: their occurrence in certain intermediate filament chains, loricrins and single-stranded RNA binding proteins. *Int J Biol Macromol* **13**, 130-139
434. Scalabrin, M., Frasson, I., Ruggiero, E., Perrone, R., Tosoni, E., Lago, S., Tassinari, M., Palu, G., and Richter, S. N. (2017) The cellular protein hnRNP A2/B1 enhances HIV-1 transcription by unfolding LTR promoter G-quadruplexes. *Sci Rep* **7**, 45244

435. Hu, J., Chen, Z., Xia, D., Wu, J., Xu, H., and Ye, Z. Q. (2012) Promoter-associated small double-stranded RNA interacts with heterogeneous nuclear ribonucleoprotein A2/B1 to induce transcriptional activation. *Biochem J* **447**, 407-416
436. Carpenter, S., Aiello, D., Atianand, M. K., Ricci, E. P., Gandhi, P., Hall, L. L., Byron, M., Monks, B., Henry-Bezy, M., Lawrence, J. B., O'Neill, L. A., Moore, M. J., Caffrey, D. R., and Fitzgerald, K. A. (2013) A long noncoding RNA mediates both activation and repression of immune response genes. *Science* **341**, 789-792
437. Lemieux, B., Blanchette, M., Monette, A., Mouland, A. J., Wellinger, R. J., and Chabot, B. (2015) A Function for the hnRNP A1/A2 Proteins in Transcription Elongation. *PLoS One* **10**, e0126654
438. Mattick, J. S., and Makunin, I. V. (2006) Non-coding RNA. *Hum Mol Genet* **15 Spec No 1**, R17-29
439. Shishkin, S. S., Kovalev, L. I., Pashintseva, N. V., Kovaleva, M. A., and Lisitskaya, K. (2019) Heterogeneous Nuclear Ribonucleoproteins Involved in the Functioning of Telomeres in Malignant Cells. *Int J Mol Sci* **20**
440. He, Y., and Smith, R. (2009) Nuclear functions of heterogeneous nuclear ribonucleoproteins A/B. *Cell Mol Life Sci* **66**, 1239-1256
441. Kamma, H., Fujimoto, M., Fujiwara, M., Matsui, M., Horiguchi, H., Hamasaki, M., and Satoh, H. (2001) Interaction of hnRNP A2/B1 isoforms with telomeric ssDNA and the in vitro function. *Biochem Biophys Res Commun* **280**, 625-630
442. McKay, S. J., and Cooke, H. (1992) hnRNP A2/B1 binds specifically to single stranded vertebrate telomeric repeat TTAGGGn. *Nucleic Acids Res* **20**, 6461-6464
443. Wang, T. H., Chen, C. C., Hsiao, Y. C., Lin, Y. H., Pi, W. C., Huang, P. R., Wang, T. V., and Chen, C. Y. (2019) Heterogeneous Nuclear Ribonucleoproteins A1 and A2 Function in Telomerase-Dependent Maintenance of Telomeres. *Cancers (Basel)* **11**
444. Moran-Jones, K., Wayman, L., Kennedy, D. D., Reddel, R. R., Sara, S., Snee, M. J., and Smith, R. (2005) hnRNP A2, a potential ssDNA/RNA molecular adapter at the telomere. *Nucleic Acids Res* **33**, 486-496
445. Guha, M., Pan, H., Fang, J. K., and Avadhani, N. G. (2009) Heterogeneous nuclear ribonucleoprotein A2 is a common transcriptional coactivator in the nuclear transcription response to mitochondrial respiratory stress. *Mol Biol Cell* **20**, 4107-4119
446. Guha, M., Fang, J. K., Monks, R., Birnbaum, M. J., and Avadhani, N. G. (2010) Activation of Akt is essential for the propagation of mitochondrial respiratory stress signaling and activation of the transcriptional coactivator heterogeneous ribonucleoprotein A2. *Mol Biol Cell* **21**, 3578-3589
447. Huelga, S. C., Vu, A. Q., Arnold, J. D., Liang, T. Y., Liu, P. P., Yan, B. Y., Donohue, J. P., Shiue, L., Hoon, S., Brenner, S., Ares, M., Jr., and Yeo, G. W. (2012) Integrative genome-wide analysis reveals cooperative regulation of alternative splicing by hnRNP proteins. *Cell Rep* **1**, 167-178
448. Moran-Jones, K., Grindlay, J., Jones, M., Smith, R., and Norman, J. C. (2009) hnRNP A2 regulates alternative mRNA splicing of TP53INP2 to control invasive cell migration. *Cancer Res* **69**, 9219-9227
449. Zubovic, L., Baralle, M., and Baralle, F. E. (2012) Mutually exclusive splicing regulates the Nav 1.6 sodium channel function through a combinatorial mechanism that involves three distinct splicing regulatory elements and their ligands. *Nucleic Acids Res* **40**, 6255-6269
450. Martinez, F. J., Pratt, G. A., Van Nostrand, E. L., Batra, R., Huelga, S. C., Kapeli, K., Freese, P., Chun, S. J., Ling, K., Gelboin-Burkhart, C., Fijany, L., Wang, H. C., Nussbacher, J. K., Broski, S. M., Kim, H. J., Lardelli, R., Sundararaman, B., Donohue, J. P., Javaherian, A., Lykke-Andersen, J., Finkbeiner, S., Bennett, C. F., Ares, M., Jr., Burge, C. B., Taylor, J. P., Rigo, F., and Yeo, G. W. (2016) Protein-RNA Networks Regulated by

Normal and ALS-Associated Mutant HNRNPA2B1 in the Nervous System. *Neuron* **92**, 780-795
451. Brooks, S. A., and Rigby, W. F. (2000) Characterization of the mRNA ligands bound by the RNA binding protein hnRNP A2 utilizing a novel in vivo technique. *Nucleic Acids Res* **28**, E49
452. Griffin, M. E., Hamilton, B. J., Roy, K. M., Du, M., Willson, A. M., Keenan, B. J., Wang, X. W., and Nichols, R. C. (2004) Post-transcriptional regulation of glucose transporter-1 by an AU-rich element in the 3'UTR and by hnRNP A2. *Biochem Biophys Res Commun* **318**, 977-982
453. Chen, C. Y., and Shyu, A. B. (1995) AU-rich elements: characterization and importance in mRNA degradation. *Trends Biochem Sci* **20**, 465-470
454. Geissler, R., and Grimson, A. (2016) A position-specific 3'UTR sequence that accelerates mRNA decay. *RNA Biol* **13**, 1075-1077
455. Alarcon, C. R., Goodarzi, H., Lee, H., Liu, X., Tavazoie, S., and Tavazoie, S. F. (2015) HNRNPA2B1 Is a Mediator of m(6)A-Dependent Nuclear RNA Processing Events. *Cell* **162**, 1299-1308
456. Dominissini, D., Moshitch-Moshkovitz, S., Schwartz, S., Salmon-Divon, M., Ungar, L., Osenberg, S., Cesarkas, K., Jacob-Hirsch, J., Amariglio, N., Kupiec, M., Sorek, R., and Rechavi, G. (2012) Topology of the human and mouse m6A RNA methylomes revealed by m6A-seq. *Nature* **485**, 201-206
457. Meyer, K. D., Saletore, Y., Zumbo, P., Elemento, O., Mason, C. E., and Jaffrey, S. R. (2012) Comprehensive analysis of mRNA methylation reveals enrichment in 3' UTRs and near stop codons. *Cell* **149**, 1635-1646
458. Hung, C. Y., Wang, Y. C., Chuang, J. Y., Young, M. J., Liaw, H., Chang, W. C., and Hung, J. J. (2017) Nm23-H1-stabilized hnRNPA2/B1 promotes internal ribosomal entry site (IRES)-mediated translation of Sp1 in the lung cancer progression. *Sci Rep* **7**, 9166
459. Jung, Y., Seo, J. Y., Ryu, H. G., Kim, D. Y., Lee, K. H., and Kim, K. T. (2020) BDNF-induced local translation of GluA1 is regulated by HNRNP A2/B1. *Sci Adv* **6**
460. Kwon, S., Barbarese, E., and Carson, J. H. (1999) The cis-acting RNA trafficking signal from myelin basic protein mRNA and its cognate trans-acting ligand hnRNP A2 enhance cap-dependent translation. *J Cell Biol* **147**, 247-256
461. Hoek, K. S., Kidd, G. J., Carson, J. H., and Smith, R. (1998) hnRNP A2 selectively binds the cytoplasmic transport sequence of myelin basic protein mRNA. *Biochemistry* **37**, 7021-7029
462. Ainger, K., Avossa, D., Diana, A. S., Barry, C., Barbarese, E., and Carson, J. H. (1997) Transport and localization elements in myelin basic protein mRNA. *J Cell Biol* **138**, 1077-1087
463. Makeyev, A. V., and Liebhaber, S. A. (2002) The poly(C)-binding proteins: a multiplicity of functions and a search for mechanisms. *RNA* **8**, 265-278
464. Munro, T. P., Magee, R. J., Kidd, G. J., Carson, J. H., Barbarese, E., Smith, L. M., and Smith, R. (1999) Mutational analysis of a heterogeneous nuclear ribonucleoprotein A2 response element for RNA trafficking. *J Biol Chem* **274**, 34389-34395
465. Gao, L. B., Zhu, X. L., Shi, J. X., Yang, L., Xu, Z. Q., and Shi, S. L. (2021) HnRNPA2B1 promotes the proliferation of breast cancer MCF-7 cells via the STAT3 pathway. *J Cell Biochem* **122**, 472-484
466. Jiang, F., Tang, X., Tang, C., Hua, Z., Ke, M., Wang, C., Zhao, J., Gao, S., Jurczyszyn, A., Janz, S., Beksac, M., Zhan, F., Gu, C., and Yang, Y. (2021) HNRNPA2B1 promotes multiple myeloma progression by increasing AKT3 expression via m6A-dependent stabilization of ILF3 mRNA. *J Hematol Oncol* **14**, 54
467. Tang, J., Chen, Z., Wang, Q., Hao, W., Gao, W. Q., and Xu, H. (2021) hnRNPA2B1 Promotes Colon Cancer Progression via the MAPK Pathway. *Front Genet* **12**, 666451

468. Tockman, M. S., Mulshine, J. L., Piantadosi, S., Erozan, Y. S., Gupta, P. K., Ruckdeschel, J. C., Taylor, P. R., Zhukov, T., Zhou, W. H., Qiao, Y. L., and Yao, S. X. (1997) Prospective detection of preclinical lung cancer: results from two studies of heterogeneous nuclear ribonucleoprotein A2/B1 overexpression. *Clin Cancer Res* **3**, 2237-2246
469. Zhou, J., Nong, L., Wloch, M., Cantor, A., Mulshine, J. L., and Tockman, M. S. (2001) Expression of early lung cancer detection marker: hnRNP-A2/B1 and its relation to microsatellite alteration in non-small cell lung cancer. *Lung Cancer* **34**, 341-350
470. Satoh, H., Ishikawa, H., Kamma, H., Fujiwara, M., Homma, S., Kagohashi, K., Ohtsuka, M., and Sekizawa, K. (2004) Expression of hnRNP A2/B1 proteins in small airway epithelial cells. *Int J Mol Med* **14**, 605-608
471. Satoh, H., Kamma, H., Ishikawa, H., Horiguchi, H., Fujiwara, M., Yamashita, Y. T., Ohtsuka, M., and Sekizawa, K. (2000) Expression of hnRNP A2/B1 proteins in human cancer cell lines. *Int J Oncol* **16**, 763-767
472. He, Y., Brown, M. A., Rothnagel, J. A., Saunders, N. A., and Smith, R. (2005) Roles of heterogeneous nuclear ribonucleoproteins A and B in cell proliferation. *J Cell Sci* **118**, 3173-3183
473. Berson, A., Barbash, S., Shaltiel, G., Goll, Y., Hanin, G., Greenberg, D. S., Ketzef, M., Becker, A. J., Friedman, A., and Soreq, H. (2012) Cholinergic-associated loss of hnRNP-A/B in Alzheimer's disease impairs cortical splicing and cognitive function in mice. *EMBO Mol Med* **4**, 730-742
474. Kolisnyk, B., Al-Onaizi, M. A., Xu, J., Parfitt, G. M., Ostapchenko, V. G., Hanin, G., Soreq, H., Prado, M. A., and Prado, V. F. (2016) Cholinergic Regulation of hnRNPA2/B1 Translation by M1 Muscarinic Receptors. *J Neurosci* **36**, 6287-6296
475. Purice, M. D., and Taylor, J. P. (2018) Linking hnRNP Function to ALS and FTD Pathology. *Front Neurosci* **12**, 326
476. Paul, K. R., Molliex, A., Cascarina, S., Boncella, A. E., Taylor, J. P., and Ross, E. D. (2017) Effects of Mutations on the Aggregation Propensity of the Human Prion-Like Protein hnRNPA2B1. *Mol Cell Biol* **37**
477. Bampton, A., Gittings, L. M., Fratta, P., Lashley, T., and Gatt, A. (2020) The role of hnRNPs in frontotemporal dementia and amyotrophic lateral sclerosis. *Acta Neuropathol* **140**, 599-623
478. Romero-Garcia, S., Prado-Garcia, H., and Lopez-Gonzalez, J. S. (2014) Transcriptional analysis of hnRNPA0, A1, A2, B1, and A3 in lung cancer cell lines in response to acidosis, hypoxia, and serum deprivation conditions. *Exp Lung Res* **40**, 12-21
479. Hatori, Y., Yan, Y., Schmidt, K., Furukawa, E., Hasan, N. M., Yang, N., Liu, C. N., Sockanathan, S., and Lutsenko, S. (2016) Neuronal differentiation is associated with a redox-regulated increase of copper flow to the secretory pathway. *Nat Commun* **7**, 10640
480. Waggoner, D. J., Bartnikas, T. B., and Gitlin, J. D. (1999) The role of copper in neurodegenerative disease. *Neurobiol Dis* **6**, 221-230
481. Petris, M. J., Voskoboinik, I., Cater, M., Smith, K., Kim, B. E., Llanos, R. M., Strausak, D., Camakaris, J., and Mercer, J. F. (2002) Copper-regulated trafficking of the Menkes disease copper ATPase is associated with formation of a phosphorylated catalytic intermediate. *J Biol Chem* **277**, 46736-46742
482. Harris, E. D., Reddy, M. C., Majumdar, S., and Cantera, M. (2003) Pretranslational control of Menkes disease gene expression. *Biometals* **16**, 55-61
483. Song, L., Li, Y., Li, W., Wu, S., and Li, Z. (2014) miR-495 enhances the sensitivity of non-small cell lung cancer cells to platinum by modulation of copper-transporting P-type adenosine triphosphatase A (ATP7A). *J Cell Biochem* **115**, 1234-1242
484. Friend, L. R., Han, S. P., Rothnagel, J. A., and Smith, R. (2008) Differential subnuclear localisation of hnRNPs A/B is dependent on transcription and cell cycle stage. *Biochim Biophys Acta* **1783**, 1972-1980

485. Zhou, J., Allred, D. C., Avis, I., Martinez, A., Vos, M. D., Smith, L., Treston, A. M., and Mulshine, J. L. (2001) Differential expression of the early lung cancer detection marker, heterogeneous nuclear ribonucleoprotein-A2/B1 (hnRNP-A2/B1) in normal breast and neoplastic breast cancer. *Breast Cancer Res Treat* **66**, 217-224
486. He, Y., Rothnagel, J. A., Epis, M. R., Leedman, P. J., and Smith, R. (2009) Downstream targets of heterogeneous nuclear ribonucleoprotein A2 mediate cell proliferation. *Mol Carcinog* **48**, 167-179
487. Molliex, A., Temirov, J., Lee, J., Coughlin, M., Kanagaraj, A. P., Kim, H. J., Mittag, T., and Taylor, J. P. (2015) Phase separation by low complexity domains promotes stress granule assembly and drives pathological fibrillization. *Cell* **163**, 123-133
488. Monette, A., and Mouland, A. J. (2020) Zinc and Copper Ions Differentially Regulate Prion-Like Phase Separation Dynamics of Pan-Virus Nucleocapsid Biomolecular Condensates. *Viruses* **12**
489. Miller, N. P., Berg, J. C., and O'Brien, R. W. (1992) The electrophoretic mobility of a porous aggregate. *Journal of Colloid and Interface Science* **153**, 237-243
490. Choi, H. S., Lee, H. M., Jang, Y. J., Kim, C. H., and Ryu, C. J. (2013) Heterogeneous nuclear ribonucleoprotein A2/B1 regulates the self-renewal and pluripotency of human embryonic stem cells via the control of the G1/S transition. *Stem Cells* **31**, 2647-2658
491. Liang, Y., Shi, S. L., Li, Q. F., Chen, L. Y., Jing, G. J., Tan, G. W., Wang, S. Y., and Wu, F. Y. (2011) The localization of hnRNP A2/B1 in nuclear matrix and the aberrant expression during the RA-induced differentiation of human neuroblastoma SK-N-SH cells. *J Cell Biochem* **112**, 1722-1729
492. Pollard, V. W., Michael, W. M., Nakielny, S., Siomi, M. C., Wang, F., and Dreyfuss, G. (1996) A novel receptor-mediated nuclear protein import pathway. *Cell* **86**, 985-994
493. Ainger, K., Avossa, D., Morgan, F., Hill, S. J., Barry, C., Barbarese, E., and Carson, J. H. (1993) Transport and localization of exogenous myelin basic protein mRNA microinjected into oligodendrocytes. *J Cell Biol* **123**, 431-441
494. Barbarese, E., Koppel, D. E., Deutscher, M. P., Smith, C. L., Ainger, K., Morgan, F., and Carson, J. H. (1995) Protein translation components are colocalized in granules in oligodendrocytes. *J Cell Sci* **108 (Pt 8)**, 2781-2790
495. Carson, J. H., Worboys, K., Ainger, K., and Barbarese, E. (1997) Translocation of myelin basic protein mRNA in oligodendrocytes requires microtubules and kinesin. *Cell Motil Cytoskeleton* **38**, 318-328
496. Douglas, J. N., Gardner, L. A., Salapa, H. E., Lalor, S. J., Lee, S., Segal, B. M., Sawchenko, P. E., and Levin, M. C. (2016) Antibodies to the RNA-binding protein hnRNP A1 contribute to neurodegeneration in a model of central nervous system autoimmune inflammatory disease. *J Neuroinflammation* **13**, 178
497. Yang, P., Mathieu, C., Kolaitis, R. M., Zhang, P., Messing, J., Yurtsever, U., Yang, Z., Wu, J., Li, Y., Pan, Q., Yu, J., Martin, E. W., Mittag, T., Kim, H. J., and Taylor, J. P. (2020) G3BP1 Is a Tunable Switch that Triggers Phase Separation to Assemble Stress Granules. *Cell* **181**, 325-345 e328
498. Tsalikis, J., Tattoli, I., Ling, A., Sorbara, M. T., Croitoru, D. O., Philpott, D. J., and Girardin, S. E. (2015) Intracellular Bacterial Pathogens Trigger the Formation of U Small Nuclear RNA Bodies (U Bodies) through Metabolic Stress Induction. *J Biol Chem* **290**, 20904-20918
499. Liao, Y. C., Fernandopulle, M. S., Wang, G., Choi, H., Hao, L., Drerup, C. M., Patel, R., Qamar, S., Nixon-Abell, J., Shen, Y., Meadows, W., Vendruscolo, M., Knowles, T. P. J., Nelson, M., Czekalska, M. A., Musteikyte, G., Gachechiladze, M. A., Stephens, C. A., Pasolli, H. A., Forrest, L. R., St George-Hyslop, P., Lippincott-Schwartz, J., and Ward, M. E. (2019) RNA Granules Hitchhike on Lysosomes for Long-Distance Transport, Using Annexin A11 as a Molecular Tether. *Cell* **179**, 147-164 e120

500. de Araujo, M. E. G., Liebscher, G., Hess, M. W., and Huber, L. A. (2020) Lysosomal size matters. *Traffic* **21**, 60-75
501. Polishchuk, E. V., and Polishchuk, R. S. (2016) The emerging role of lysosomes in copper homeostasis. *Metallomics* **8**, 853-862
502. Zhou, F., Wan, Q., Chen, S., Chen, Y., Wang, P. H., Yao, X., and He, M. L. (2021) Attenuating innate immunity and facilitating beta-coronavirus infection by NSP1 of SARS-CoV-2 through specific redistributing hnRNP A2/B1 cellular localization. *Signal Transduct Target Ther* **6**, 371
503. Hong, K., Song, D., and Jung, Y. (2020) Behavior control of membrane-less protein liquid condensates with metal ion-induced phase separation. *Nat Commun* **11**, 5554
504. Ryan, V. H., Dignon, G. L., Zerze, G. H., Chabata, C. V., Silva, R., Conicella, A. E., Amaya, J., Burke, K. A., Mittal, J., and Fawzi, N. L. (2018) Mechanistic View of hnRNPA2 Low-Complexity Domain Structure, Interactions, and Phase Separation Altered by Mutation and Arginine Methylation. *Mol Cell* **69**, 465-479 e467
505. Ryan, V. H., Watters, S., Amaya, J., Khatiwada, B., Venditti, V., Naik, M. T., and Fawzi, N. L. (2020) Weak binding to the A2RE RNA rigidifies hnRNPA2 RRMs and reduces liquid-liquid phase separation and aggregation. *Nucleic Acids Res* **48**, 10542-10554
506. Michalczyk, A. A., Rieger, J., Allen, K. J., Mercer, J. F., and Ackland, M. L. (2000) Defective localization of the Wilson disease protein (ATP7B) in the mammary gland of the toxic milk mouse and the effects of copper supplementation. *Biochem J* **352 Pt 2**, 565-571
507. Braiterman, L. T., Gupta, A., Chaerkady, R., Cole, R. N., and Hubbard, A. L. (2015) Communication between the N and C termini is required for copper-stimulated Ser/Thr phosphorylation of Cu(I)-ATPase (ATP7B). *J Biol Chem* **290**, 8803-8819
508. Lutsenko, S., Barnes, N. L., Bartee, M. Y., and Dmitriev, O. Y. (2007) Function and regulation of human copper-transporting ATPases. *Physiol Rev* **87**, 1011-1046
509. Lalioti, V., Peiro, R., Perez-Berlanga, M., Tsuchiya, Y., Munoz, A., Villalba, T., Sanchez, C., and Sandoval, I. V. (2016) Basolateral sorting and transcytosis define the Cu+-regulated translocation of ATP7B to the bile canaliculus. *J Cell Sci* **129**, 2190-2201
510. Hamilton, J. P., Koganti, L., Muchenditsi, A., Pendyala, V. S., Huso, D., Hankin, J., Murphy, R. C., Huster, D., Merle, U., Mangels, C., Yang, N., Potter, J. J., Mezey, E., and Lutsenko, S. (2016) Activation of liver X receptor/retinoid X receptor pathway ameliorates liver disease in Atp7B(-/-) (Wilson disease) mice. *Hepatology* **63**, 1828-1841
511. James, S. A., Volitakis, I., Adlard, P. A., Duce, J. A., Masters, C. L., Cherny, R. A., and Bush, A. I. (2012) Elevated labile Cu is associated with oxidative pathology in Alzheimer disease. *Free Radic Biol Med* **52**, 298-302
512. Squitti, R., Siotto, M., Arciello, M., and Rossi, L. (2016) Non-ceruloplasmin bound copper and ATP7B gene variants in Alzheimer's disease. *Metallomics* **8**, 863-873
513. Bucossi, S., Polimanti, R., Mariani, S., Ventriglia, M., Bonvicini, C., Migliore, S., Manfellotto, D., Salustri, C., Vernieri, F., Rossini, P. M., and Squitti, R. (2012) Association of K832R and R952K SNPs of Wilson's disease gene with Alzheimer's disease. *J Alzheimers Dis* **29**, 913-919
514. Huster, D., Kuhne, A., Bhattacharjee, A., Raines, L., Jantsch, V., Noe, J., Schirrmeister, W., Sommerer, I., Sabri, O., Berr, F., Mossner, J., Stieger, B., Caca, K., and Lutsenko, S. (2012) Diverse functional properties of Wilson disease ATP7B variants. *Gastroenterology* **142**, 947-956 e945
515. Squitti, R., Polimanti, R., Bucossi, S., Ventriglia, M., Mariani, S., Manfellotto, D., Vernieri, F., Cassetta, E., Ursini, F., and Rossini, P. M. (2013) Linkage disequilibrium and haplotype analysis of the ATP7B gene in Alzheimer's disease. *Rejuvenation Res* **16**, 3-10
516. Bucossi, S., Mariani, S., Ventriglia, M., Polimanti, R., Gennarelli, M., Bonvicini, C., Pasqualetti, P., Scrascia, F., Migliore, S., Vernieri, F., Rossini, P. M., and Squitti, R. (2011)

Association between the c. 2495 A>G ATP7B Polymorphism and Sporadic Alzheimer's Disease. *Int J Alzheimers Dis* **2011**, 973692
517. Mercer, S. W., Wang, J., and Burke, R. (2017) In Vivo Modeling of the Pathogenic Effect of Copper Transporter Mutations That Cause Menkes and Wilson Diseases, Motor Neuropathy, and Susceptibility to Alzheimer's Disease. *J Biol Chem* **292**, 4113-4122
518. Folstein, M. F., Folstein, S. E., and McHugh, P. R. (1975) "Mini-mental state". A practical method for grading the cognitive state of patients for the clinician. *J Psychiatr Res* **12**, 189-198
519. Siotto, M., Simonelli, I., Pasqualetti, P., Mariani, S., Caprara, D., Bucossi, S., Ventriglia, M., Molinario, R., Antenucci, M., Rongioletti, M., Rossini, P. M., and Squitti, R. (2016) Association Between Serum Ceruloplasmin Specific Activity and Risk of Alzheimer's Disease. *J Alzheimers Dis* **50**, 1181-1189
520. Walshe, J. M., and Clinical Investigations Standing Committee of the Association of Clinical, B. (2003) Wilson's disease: the importance of measuring serum caeruloplasmin non-immunologically. *Ann Clin Biochem* **40**, 115-121
521. Twomey, P. J., Viljoen, A., House, I. M., Reynolds, T. M., and Wierzbicki, A. S. (2007) Copper:caeruloplasmin ratio. *J Clin Pathol* **60**, 441-442
522. Crooks, G. E., Hon, G., Chandonia, J. M., and Brenner, S. E. (2004) WebLogo: a sequence logo generator. *Genome Res* **14**, 1188-1190
523. Guo, Y., Nyasae, L., Braiterman, L. T., and Hubbard, A. L. (2005) NH2-terminal signals in ATP7B Cu-ATPase mediate its Cu-dependent anterograde traffic in polarized hepatic cells. *Am J Physiol Gastrointest Liver Physiol* **289**, G904-916
524. Schushan, M., Bhattacharjee, A., Ben-Tal, N., and Lutsenko, S. (2012) A structural model of the copper ATPase ATP7B to facilitate analysis of Wilson disease-causing mutations and studies of the transport mechanism. *Metallomics* **4**, 669-678
525. Guex, N., and Peitsch, M. C. (1997) SWISS-MODEL and the Swiss-PdbViewer: an environment for comparative protein modeling. *Electrophoresis* **18**, 2714-2723
526. Dolinsky, T. J., Nielsen, J. E., McCammon, J. A., and Baker, N. A. (2004) PDB2PQR: an automated pipeline for the setup of Poisson-Boltzmann electrostatics calculations. *Nucleic Acids Res* **32**, W665-667
527. Dolinsky, T. J., Czodrowski, P., Li, H., Nielsen, J. E., Jensen, J. H., Klebe, G., and Baker, N. A. (2007) PDB2PQR: expanding and upgrading automated preparation of biomolecular structures for molecular simulations. *Nucleic Acids Res* **35**, W522-525
528. Unni, S., Huang, Y., Hanson, R. M., Tobias, M., Krishnan, S., Li, W. W., Nielsen, J. E., and Baker, N. A. (2011) Web servers and services for electrostatics calculations with APBS and PDB2PQR. *J Comput Chem* **32**, 1488-1491
529. Chen, A. A., and Pappu, R. V. (2007) Parameters of monovalent ions in the AMBER-99 forcefield: assessment of inaccuracies and proposed improvements. *J Phys Chem B* **111**, 11884-11887
530. Baker, C. M., Lopes, P. E., Zhu, X., Roux, B., and Mackerell, A. D., Jr. (2010) Accurate Calculation of Hydration Free Energies using Pair-Specific Lennard-Jones Parameters in the CHARMM Drude Polarizable Force Field. *J Chem Theory Comput* **6**, 1181-1198
531. Tang, C. L., Alexov, E., Pyle, A. M., and Honig, B. (2007) Calculation of pKas in RNA: on the structural origins and functional roles of protonated nucleotides. *J Mol Biol* **366**, 1475-1496
532. Baker, N. A., Sept, D., Joseph, S., Holst, M. J., and McCammon, J. A. (2001) Electrostatics of nanosystems: application to microtubules and the ribosome. *Proc Natl Acad Sci U S A* **98**, 10037-10041
533. Lee, J., Cheng, X., Swails, J. M., Yeom, M. S., Eastman, P. K., Lemkul, J. A., Wei, S., Buckner, J., Jeong, J. C., Qi, Y., Jo, S., Pande, V. S., Case, D. A., Brooks, C. L., 3rd, MacKerell, A. D., Jr., Klauda, J. B., and Im, W. (2016) CHARMM-GUI Input Generator for

NAMD, GROMACS, AMBER, OpenMM, and CHARMM/OpenMM Simulations Using the CHARMM36 Additive Force Field. *J Chem Theory Comput* **12**, 405-413
534. Brooks, B. R., Brooks, C. L., 3rd, Mackerell, A. D., Jr., Nilsson, L., Petrella, R. J., Roux, B., Won, Y., Archontis, G., Bartels, C., Boresch, S., Caflisch, A., Caves, L., Cui, Q., Dinner, A. R., Feig, M., Fischer, S., Gao, J., Hodoscek, M., Im, W., Kuczera, K., Lazaridis, T., Ma, J., Ovchinnikov, V., Paci, E., Pastor, R. W., Post, C. B., Pu, J. Z., Schaefer, M., Tidor, B., Venable, R. M., Woodcock, H. L., Wu, X., Yang, W., York, D. M., and Karplus, M. (2009) CHARMM: the biomolecular simulation program. *J Comput Chem* **30**, 1545-1614
535. Jo, S., Kim, T., Iyer, V. G., and Im, W. (2008) CHARMM-GUI: a web-based graphical user interface for CHARMM. *J Comput Chem* **29**, 1859-1865
536. Humphrey, W., Dalke, A., and Schulten, K. (1996) VMD: visual molecular dynamics. *J Mol Graph* **14**, 33-38, 27-38
537. Michaud-Agrawal, N., Denning, E. J., Woolf, T. B., and Beckstein, O. (2011) MDAnalysis: a toolkit for the analysis of molecular dynamics simulations. *J Comput Chem* **32**, 2319-2327
538. Joosten, R. P., te Beek, T. A., Krieger, E., Hekkelman, M. L., Hooft, R. W., Schneider, R., Sander, C., and Vriend, G. (2011) A series of PDB related databases for everyday needs. *Nucleic Acids Res* **39**, D411-419
539. Kabsch, W., and Sander, C. (1983) Dictionary of protein secondary structure: pattern recognition of hydrogen-bonded and geometrical features. *Biopolymers* **22**, 2577-2637
540. Van Der Spoel, D., Lindahl, E., Hess, B., Groenhof, G., Mark, A. E., and Berendsen, H. J. (2005) GROMACS: fast, flexible, and free. *J Comput Chem* **26**, 1701-1718
541. Pettersen, E. F., Goddard, T. D., Huang, C. C., Couch, G. S., Greenblatt, D. M., Meng, E. C., and Ferrin, T. E. (2004) UCSF Chimera--a visualization system for exploratory research and analysis. *J Comput Chem* **25**, 1605-1612
542. Petris, M. J., Strausak, D., and Mercer, J. F. (2000) The Menkes copper transporter is required for the activation of tyrosinase. *Hum Mol Genet* **9**, 2845-2851
543. Barry, A. N., Otoikhian, A., Bhatt, S., Shinde, U., Tsivkovskii, R., Blackburn, N. J., and Lutsenko, S. (2011) The lumenal loop Met672-Pro707 of copper-transporting ATPase ATP7A binds metals and facilitates copper release from the intramembrane sites. *J Biol Chem* **286**, 26585-26594
544. Roelofsen, H., Wolters, H., Van Luyn, M. J. A., Miura, N., Kuipers, F., and Vonk, R. J. (2000) Copper-induced apical trafficking of ATP7B in polarized hepatoma cells provides a mechanism for biliary copper excretion. *Gastroenterology* **119**, 782-793
545. Gupta, A., Bhattacharjee, A., Dmitriev, O. Y., Nokhrin, S., Braiterman, L., Hubbard, A. L., and Lutsenko, S. (2011) Cellular copper levels determine the phenotype of the Arg875 variant of ATP7B/Wilson disease protein. *Proc Natl Acad Sci U S A* **108**, 5390-5395
546. Hall, B. A., Kaye, S. L., Pang, A., Perera, R., and Biggin, P. C. (2007) Characterization of protein conformational states by normal-mode frequencies. *J Am Chem Soc* **129**, 11394-11401
547. Bahar, I., Atilgan, A. R., and Erman, B. (1997) Direct evaluation of thermal fluctuations in proteins using a single-parameter harmonic potential. *Fold Des* **2**, 173-181
548. Tsivkovskii, R., Eisses, J. F., Kaplan, J. H., and Lutsenko, S. (2002) Functional properties of the copper-transporting ATPase ATP7B (the Wilson's disease protein) expressed in insect cells. *J Biol Chem* **277**, 976-983
549. Squitti, R., Polimanti, R., Siotto, M., Bucossi, S., Ventriglia, M., Mariani, S., Vernieri, F., Scrascia, F., Trotta, L., and Rossini, P. M. (2013) ATP7B variants as modulators of copper dyshomeostasis in Alzheimer's disease. *Neuromolecular Med* **15**, 515-522
550. Gupta, A., Maulik, M., Nasipuri, P., Chattopadhyay, I., Das, S. K., Gangopadhyay, P. K., Indian Genome Variation, C., and Ray, K. (2007) Molecular diagnosis of Wilson disease

using prevalent mutations and informative single-nucleotide polymorphism markers. *Clin Chem* **53**, 1601-1608
551. Zhang, Y., and Wu, Z.-Y. (2011) Wilson's disease in Asia. *Neurology Asia* **16**, 103-109
552. Zhang, Y., and Wu, Z. Y. (2011) Wilson's disease in Asia. *Neurol Asia* **16**, 103-109
553. Brage, A., Tome, S., Garcia, A., Carracedo, A., and Salas, A. (2007) Clinical and molecular characterization of Wilson disease in Spanish patients. *Hepatol Res* **37**, 18-26
554. Scvortova, E. (2014) Classification of mutations in ATP7B in Wilson's disease patients. *Curierul Medical* **57**
555. Cogulu, O., Onay, H., Ozgenc, F., Karaca, E., Gunduz, C., Tzetis, M., Cankaya, T., Kanavakis, E., and Ozkinay, F. (2005) Trigonocephaly and Wilson's disease in two siblings. *Clin Dysmorphol* **14**, 161-164
556. Lu, C. X., Qing, L., Huang, W. Q., and Tzeng, C. M. (2014) New mutations and polymorphisms of the ATP7B gene in sporadic Wilson disease. *Eur J Med Genet* **57**, 498-502
557. Haas, R., Gutierrez-Rivero, B., Knoche, J., Boker, K., Manns, M. P., and Schmidt, H. H. (1999) Mutation analysis in patients with Wilson disease: identification of 4 novel mutations. Mutation in brief no. 250. Online. *Hum Mutat* **14**, 88
558. Cocos, R., Sendroiu, A., Schipor, S., Bohiltea, L. C., Sendroiu, I., and Raicu, F. (2014) Genotype-phenotype correlations in a mountain population community with high prevalence of Wilson's disease: genetic and clinical homogeneity. *PLoS One* **9**, e98520
559. Brewer, G. J. (2012) Chapter 360. Wilson's Disease. in *Harrison's Principles of Internal Medicine, 18e* (Longo, D. L., Fauci, A. S., Kasper, D. L., Hauser, S. L., Jameson, J. L., and Loscalzo, J. eds.), The McGraw-Hill Companies, New York, NY. pp
560. Squitti, R., Siotto, M., Cassetta, E., El Idrissi, I. G., and Colabufo, N. A. (2017) Measurements of serum non-ceruloplasmin copper by a direct fluorescent method specific to Cu(II). *Clin Chem Lab Med* **55**, 1360-1367